谨以此论文献给我的父亲，母亲，外公，外婆，二姨，二姨父，表弟以及女朋友吴烨楠

University of Warwick

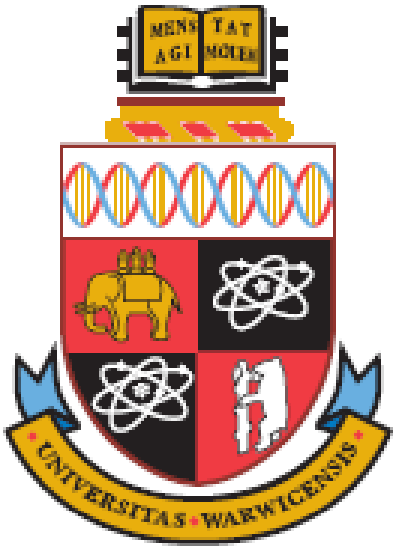

Optical Wireless MIMO Communication

by

Hao Du

Thesis

Submitted to the University of Warwick

for the degree of

Doctor of Philosophy

School of Engineering

April 2015

Table of Contents

List of Figures

List of Tables

Acknowledgements

First and foremost I offer my sincerest gratitude to my supervisor, Professor Roger Green, who has supported me though out my thesis with his patience and knowledge whilst allowing me the room to work in my own way. I attribute the level of my Ph.D degree to his encouragement and effort and without him this thesis, too, would not have been completed or written. One simply could not wish for a better or friendlier supervisor.

Secondly, Dr Yunfei Chen, as my second supervisor, has provided me with many of the research ideas, methods and insight throughout my work in this thesis as well as many others. Dr Chen has done much more than a second supervisor. Without whose encouragement and effort I could not finish the experiment and research definitely. I feel so lucky to have such a great supervisor during my Ph.D research.

In my daily work I have been blessed with a friendly and cheerful helper Professor Xiaojun Ji, a visitor form Shanghai Jiaotong University, PRC. In many ways I have learnt much from him, like circuit design, soldering, LEDs and Microcontroller selection.

The School of Engineering has provided the support and equipment I have needed to produce and complete my thesis and studies.

It is certainly that I am grateful to my parents, Weiping Du and Jingping Zhan, and all the members of my big big family, who bestowed ability and strength in me to study in University of Warwick, and complete this work. They always give me the strength and wisdom throughout my whole life. Their encouragement and concern are invaluable.

To Aunty Zhang, I deeply thank you for your advice and patience on improving my English academic writing these years.

Finally, thank you Miss Yenan Wu, thank you for everything you did for me during these years, support me by encouraging me and giving all the help you could (the happiness, the tolerance, and delicious food!) And thank everyone who loves me, my friends, no matter the ones in China, Imperial College, Nottingham University and University of Warwick. You are my courage and motivation.

Declaration

This thesis is submitted in partial fulfilment for the degree of Doctor of Philosophy under the regulations set out by the Graduate School at the University of Warwick. This thesis is solely composed of research completed by Hao Du, except where stated, under the supervision of Professor Roger Green and Dr Yunfei Chen between the dates of January 2010 and September 2013. No part of this work has been previously submitted to any institution for admission to a higher degree.

Hao Du

September 2013

Abstract

This thesis provides an in-depth investigation and evaluation of infrared optical wireless MIMO communication systems to be applied in both indoor and outdoor environment. The principle objective of the research is to demonstrate both the advantages and disadvantages of the optical wireless MIMO systems using different modulation types.

The first part provided analyses of important OW configurations using APD receivers using WMC model and SISO, MISO, SIMO and MIMO configuration. Thus, an analytical expression for 2-1 MISO, 1-2 SIMO and MIMO was successfully developed. This part also illustrates the coding gains possible using diversity schemes for APD OW systems. In the presence of strong fading, the SISO approach is rendered virtually useless, whereas diversity offers acceptable BER values. The results underpin the approach of this thesis, where indoor PIN diode based experimental measurements confirm the gains offered by diversity.

In the second part of the work, several optical wireless MIMO systems applicable for the indoor environment are developed for three different modulation types, OOK modulation, PPM modulation and SIR-RZI modulation. These modulations are used in optical MIMO systems are studied for which, mathematical models that evaluate the BER performance of the MIMO system for different axis displacement and for different distances between transmitters and receivers. Based on the results, the PPM system has been shown to present the best BER performance, including high interference-resistance capability. A group of new mathematical models have been

evaluated, which demonstrates a high level of correlation with the results derived from empirical models at 93%. Thus, the mathematical models developed and used for the specified evaluation appear to correspond reasonably well, and can be applied in future research on these aspects.

Publications

H. Du, R. J. Green, Y. Chen, "Optical wireless 2X2 indoor MIMO system based on OOK modulation", *Proc. 15th IEEE Conference on Transparent Optical Networks (ICTON)*, pp. 1-3, 2013 [3 pages].

H. Du, R. J. Green, Y. Chen, "Optical Wireless Indoor MIMO System based on OOK and PPM Modulations", submitted to IET Communications.

H. Du, R. J. Green, Y. Chen, "Infrared Indoor MIMO Communication System using 100kHz OOK and RZI Modulations", unpublished.

Chapter 1 Introduction

1.1 Overview

Optical wireless (OW) technology presents a potential application in contemporary communication systems. It also promises to supplement wireless radio-frequency (RF) technologies, which have been broadly used for commercial communication applications, such as WLAN and Bluetooth. Most important of all, the bandwidth of the OW is available worldwide, and the unlicensed OW technology does not interfere with radio frequency bands.

During the last two decades, OW technology has played the vital role for promoting high speed indoor communications as a complementary and extended scheme to the RF indoor wireless systems. The main advantages of OW communications include cost-effective, broad bandwidth access, high quality data-transmission, no interference with RF-based communication signals, and highly-secured transmissions. Consequently, the OW technology has been developed rapidly. [1]

1.2 The Indoor Optical Wireless System

Indoor optical wireless communications are mainly associated with visible light and infra-red technology applications.

1.2.1 Visible Light

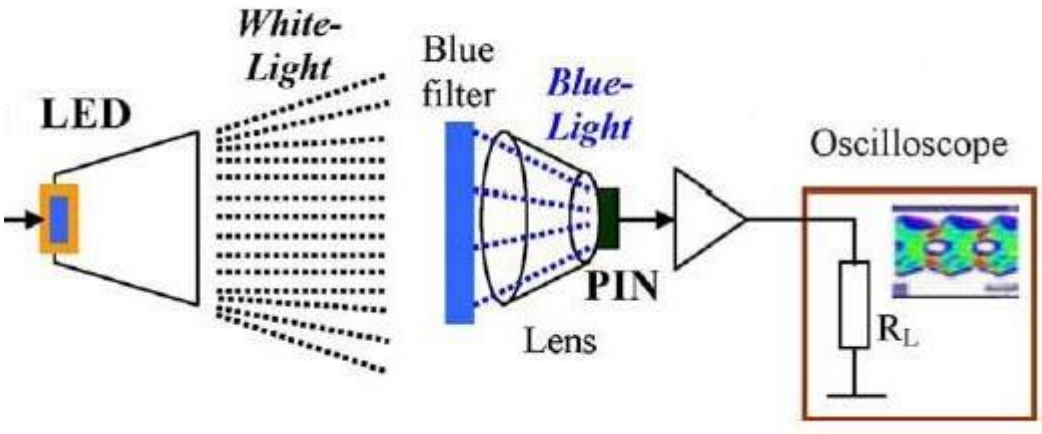

Figure 1-1 Visible Light Communication System [2]

A typical visible light communication system (VLC) using white LEDs is illustrated in Figure 1-1. In this figure, both lighting and communication link are provided by the white LED. As is mentioned in [2], the blue light used as the signal carrier can be extracted by employing the blue waveband optical filter at the receiver side to enhance the bandwidth of the system. The most important component in Figure 1-1 is the LED. In addition to pure colour LEDs, two other white LEDs are also used:

1. Red-green-blue LEDs;
2. Blue LEDs combined with yellow-coloured phosphors.

In [2], the second option is generally the preferred one for lighting because of the lower complexity in comparison with the one in three colours. One thing to be noticed is that the bandwidth of the device is between 1-10MHz, mainly due to the slow temporal response of the visible LEDs. [3, 4]

1.2.2 Infrared Light

The infrared light wireless communication system offers much higher data transmission rate than that of the visible light system because of its more powerful laser source and its wider modulation bandwidth laser source are used. Figure 1-2 shows the optical channel simulation model. In this figure, by using the collated detector, the modulated signals are received after transmitting in the free space (the simulated signal noise are added into the free space channel), and then the signals would be demodulated and output. The data are modulated by specific modulation technology, and transmitted by the transmitters; secondly, the noises are added into the channel; thirdly, the modulated signals are detected by the detectors; and finally, detected signals would be demodulated and exported.

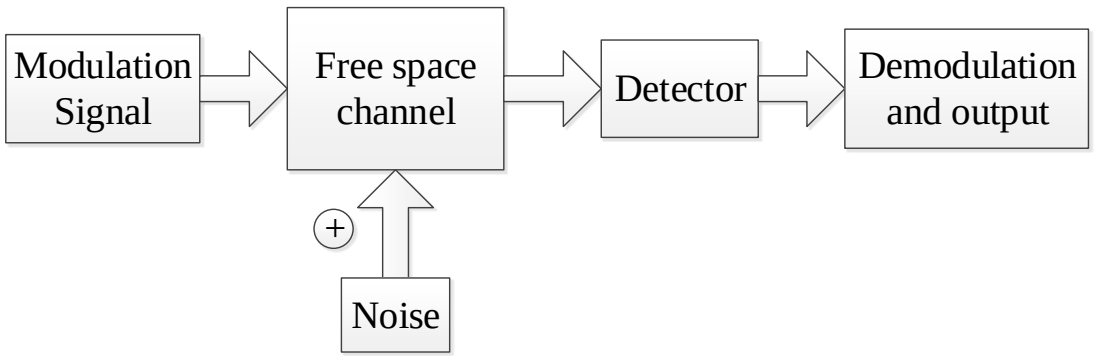

Figure 1-2 Optical Channel Simulation Model

References [2] and [5] demonstrate that in free space it is possible to achieve a data rate at the Gbps level through IR links when communicating over a distance of several km. However, it is highly recommended that the higher power transmitting within a very narrow field-of-view (FOV) is applied.

For indoor Infrared communications, there are two basic types of transmission configuration:-

1. Line of sight (LOS) transmission;
2. Non-Line of sight transmission.

Figure 1-3 illustrates the classification of infrared wireless links according to the degree of directionality of transmitters and receivers (Line of sight, Non-Line of sight and Mixed). [6]

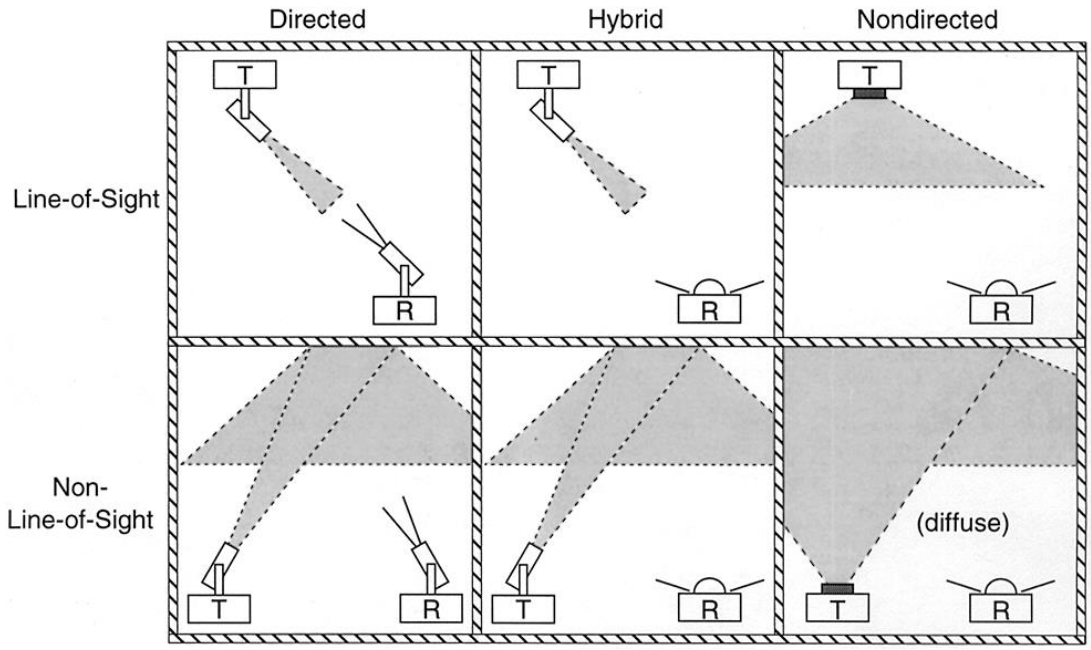

Figure 1-3 LOS and Diffuse Channel [6]

Because of the multipath induced inter-symbol interference (ISI), although more reflective in comparison with LOS links, non-LOS links offer lower bandwidth but a wider Field of Views (FOV) and a certain level of mobility (in the wireless channel, the signal multipath propagation will generate ISI. This is because with the increasing of data rate, the interval between the symbols will reduce to a certain extent which can't be distinguished by the detector, and thus results in ISI. A non-LOS OW system is discussed in [7] where parallel low speed transmission has been proposed. Reference [8] describes a high speed parallel optical wireless communication system. Haykin introduced an artificial neural network in [9] which could mitigate the multipath induced ISI in indoor OW links. However, different from non-LOS links, LOS links are capable of achieving higher power and bandwidth efficiency in high speed applications and at the same time, low signal loss and pulse dispersion from multipath. However, LOS links are limited in the area coverage related applications. In [10, 11] beam broadening is considered as an alternative technology for improving the mobility and coverage of LOS links. In summary, the infrared light systems can have better performances than the visible light systems, at the cost of more complicated designs and more compromises.

1.2.3 Challenges of Indoor Optical Wireless

The first challenge comes from the limitation of bandwidth and transmission speed. In [2], it was reported that by using a blue filter to remove the other wavelength, it is easy to achieve a high bandwidth from a visible light source. When the bandwidth is fixed, the multiple input and multiple output (MIMO) systems can offer higher data transmission (due to [5] and [6], and the transmission rate may

reach several Gbps) by transmitting data in parallel to achieve multiplexing gain. As the limiting parameter, the channel matrix can be improved by using an imaging lens system [12].

Second challenge comes from the dimming of light, mainly for the visible light system, which affects the link performance. In [3], two approaches were described to solve the specific problems of:

1. Reducing the amplitude;
2. Using pulse width modulation (PWM).

Both can help to increase the performance of the light system and can deliver desired output performance. However, the second approach will reduce the average throughput.

The third challenge comes from infrared communications. The transmission power is small due to eye safety related considerations. Consequently, infrared wireless communications are considered to be challenging due to the low power budget. In addition, it remains difficult to design and produce OW receiver with high-speed, high sensitivity and high efficiency. In [2], the typical diameter of photo-detectors is less than 100μm for transmitting data at 10Gbps, which may make it extremely challenging for the receiver to deliver accurate experiment results.

1.3 Wireless MIMO System

MIMO is broadly applied in the fourth generation mobile communication standards, such as IEEE 802.16e Worldwide Interoperability for Microwave Access (WiMAX,), Long Term Evolution (LTE), IEEE 802.11n, and the next-generation wireless LAN (WLAN) standard. MIMO also refers to spatial diversity as it uses multi antennas to perform multi-channel transmission and reception of data.

The ground-breaking work of wireless mobile communication systems by using MIMO technology was initially accomplished by the AT & T Bell laboratory in the 1990s. In 1995, in [12], Teladar demonstrated the MIMO capacity in the path-loss channel. In 1996, Foshini developed MIMO processing algorithms and revealed in Angle - Bell Labs Layered Space-Time (D-BLAST). [12] In 1998, Tarokh discussed MIMO space-time codes, while during the same year, Wolniansky used vertical - Bell Labs layered Space-Time (V-BLAST) algorithm to develop a MIMO indoor system, and tested the 20bps/MHz spectral efficiency. [13] These accomplishments attracted the worldwide attention from academia and industries. According to the number of transceivers at both ends of the antenna, other systems can be considered as a special case of MIMO, such as a Single-Input Single-Output (SISO) system, a MIMO system, a Single-Input Multiple-Output (SIMO) system, and a Multiple-Input Single-Output (MISO) system. In conclusion, MIMO systems use multiple transducers to suppress channel fading.

The development of MIMO technology maximizes the space capacity to improve the data transmitting performance, and also increases the wireless space coverage of the system. When a transmitted signal is reflected, it will produce more than one copy, and each of which is a spatial stream. The SISO system can only send or receive one spatial stream, whereas the MIMO system uses multiple antennas to send and receive multiple spatial streams, and therefore is able to distinguish different signals sent from different "transceivers". As the application of multi-antenna system allows more data to be sent, the use of multiple antennas at the transmitter or receiver can significantly reduce the channel fading effect and minimize the error rate. It is generally recognized that the diversity gain can be as high as $Nt * Nr$ (the minimum number of transmitter and receiver). Another interesting MIMO technology is related to space time coding. The primary application of space time coding is to use space and time domain encodings to achieve a certain degree of spatial and time diversity and hence reduces the bit error rate of the system.

Typically, multipath effects cause fading and hence cause undesirable impacts. However, the experiment results show that in MIMO systems, multipath can somehow be considered as a positive and desirable factor. After a space-time coding, a data stream $S(k)$ is divided into N information sub-streams $C_i(k)$, where $i = 1, ..., N$,. The N sub-streams are transmitted out by N antennas and received by M receiving antennas. The multi-antenna receivers use space time coding technology to process, separate and decode data sub-streams. In particular, N sub-streams are simultaneously sent to the channel occupying the same bandwidth to avoid the increase of bandwidth. If each channel responding between the transmitting and

receiving antenna is independent, the MIMO system can create multiple parallel spatial channels for the data transmitting through such parallel spatial channels independently, consequently, it increases data rate. Moreover, the system capacity is one of the most important parameters to characterize the communication systems, which represents the maximum transmission data rate of the communication system. As for a *N* transmit antennas and a *M* receive antennas in a MIMO system, and assuming that the channel is Rayleigh fading channel, and the *N* and *M* are large enough, the channel capacity *C* can be described approximately as below:

$$C = \min(M, N) B \log_2(\rho / 2) \tag{1.1}$$

where *B* is the signal bandwidth, ρ is the average SNR of the receiving signal, min (*M*, *N*) represents the smaller number between *M* and *N*. It is shown that when power and bandwidth are fixed, the capacity of a MIMO system increases linearly with the minimum number of antennas. As a result, MIMO has great potential for improving the capacity of a wireless communication system.

As an example, MIMO has been used in the IEEE 802.11n standard to achieve high data rate and high reliability. This standard is used to bridge users with the wireless access of user terminals in office LAN and campus networks, but the data rate can only reach 2Mbps at present. Because the data rate and transmission distance can't meet the growing demand on bandwidth, higher security of data transmission and more convenient roaming services, the IEEE group has initiated several new application standards, including the 802.11n standard.

The bandwidth of 802.11n is 2.4GHz and 5GHz, and the WLAN transmission data rate varies from 54Mbps (802.11a and 802.11g) to 108Mbps, up to 500Mbps by applying MIMO and Orthogonal Frequency Division Multiplexing (OFDM) technology. Moreover, the quality of wireless transmission is greatly enhanced.

The bandwidth of 802.11n will allow a WLAN transmission rate to be increased more than 10 times in comparison with the current transfer data rate, which can easily support high-quality music, picture voice and video transmission. Such improvement offers an opportunity for people in the office with Wi-Fi access to transmit data and communicate with other people.

The 802.11n standard also uses smart antenna technology, in which the multiple independent antenna arrays can dynamically adjust the beam to ensure that WLAN users receive stable signals and minimize interference from other signals. Consequently, the area coverage can be extended to over $1\,km^2$. This makes the application of mobile receiving instruments develop towards a broader context in the future.

1.4 Optical Wireless MIMO System

1.4.1 Categories

Due to different application ranges and channels, the optical wireless MIMO system can be divided into two categories: indoor and outdoor wireless MIMO systems. The main applications for indoor optical wireless MIMO are the indoor computer network and communication between office equipment. The indoor wireless MIMO system channel is affected by indoor room light, as well as multipath problem caused by the wall reflection, which results in the inter-symbol interference (ISI).

Outdoor wireless MIMO systems are mainly applied for free space communications such as airplane and satellite communication, which are affected by the natural background light (sun, moon, etc.), atmospheric scintillation and turbulence, also the attenuation caused by the weather (fog, rain, clouds and other natural phenomena).

1.4.2 The advantages and challenges

As having been discussed by many research groups, optical wireless technology may offer unlimited bandwidth, which has the potential to meet the high market demand on indoor wireless access applications, such as voice over IP, images, mp3 or other music data transmissions, streaming video, etc. An optical wireless system could employ both infrared and visible light indoor links by using LEDs and

corresponding photodiodes. Over the past few decades, optical wireless MIMO technology has been developed rapidly, and succeeded with substantial advantages such as offering higher data rates within the same bandwidth, license free, low or no interference as those experienced in a RF-based system (the commercial technology), and many others with potential application development. [14]

However, the main disadvantage of high data rate in the optical wireless communication is related to the limitation of transmission distances (normally less than 10m). When the transmission distances exceeds 10m, a direct light source with a narrow Angle-of-View (AOV) is highly recommended. In [13], it is explained that the optical wireless signal channels are significantly affected by large path loss and background noise such as sunlight, room light and other ambient light sources, meanwhile, the requirements for a certain signal to noise ratio (SNR) requires a limitation in bandwidth, resulting in a consequent limitation in data rate.

Comparing the two types of optical wireless transmissions, namely, the visible light link and the infrared link, the infrared wireless system has demonstrated great potential as described in [12] due to its high speed transmission and low rate of interference. Moreover, it is considered to be both cost effective and simply-designed, and the infrared wireless system provides an easier access for realization of various applications than those of fibre optic systems and radio wireless systems. The infrared wireless MIMO system is considered to be highly competitive in offering higher security, higher data rate, higher capacity and lower bit error rate.

Since 2010, the demand for high capacity data transmission increases substantially, especially on wireless communication, including optical wireless communications. As described in Section 1.3, MIMO systems have attracted great attention in the applications of radio wireless communications. As has been described in many publications, in comparison with SISO wireless system, an optical wireless MIMO system employs multiple antennas at both source and receiver end and thus, it may achieve high speed data transmission without increasing power and bandwidth. [12, 13] A typical optical MIMO system is shown in Figure 1-4: [13]

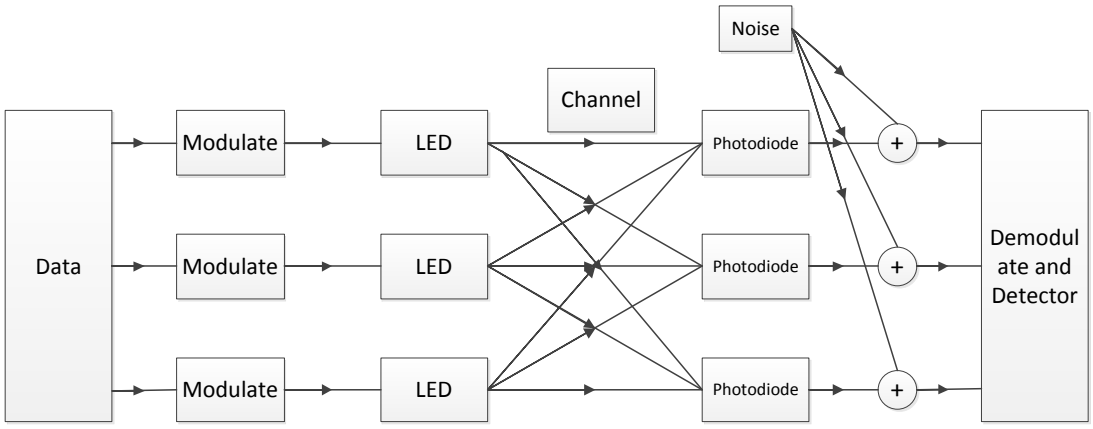

Figure 1-4 Optical MIMO System adapted from Takase et al. in [13]

As shown in [15], O'Brien et al. built a 4X4 white LED MIMO indoor optical system, in which the transmitters and receivers were arranged on two 0.2m pitches separately as shown below:

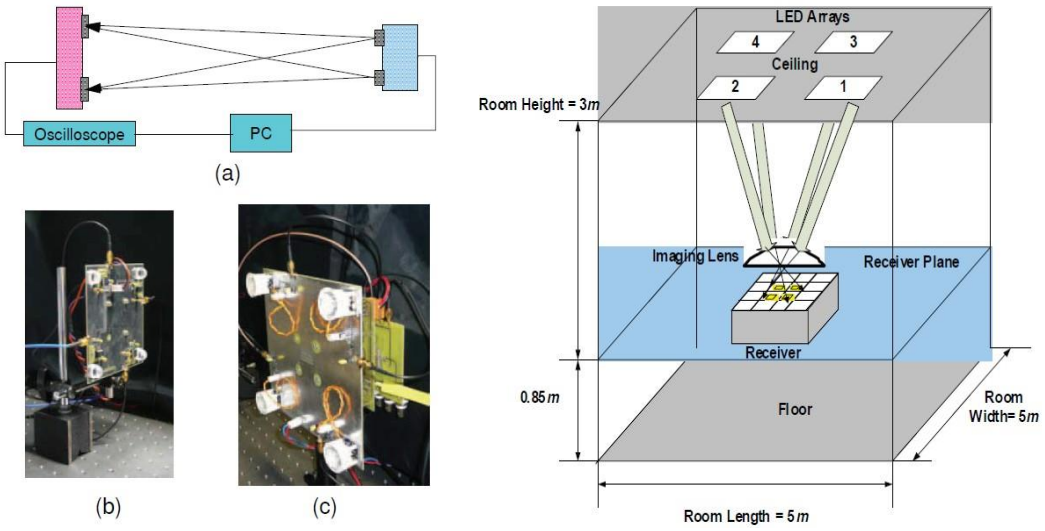

Figure 1-5 LOS MIMO system (a) Schematic (b) Receiver

(c) Transmitter (d) Schematic of imaging MIMO system adapted [15]

The can be considered as the typical non-imaging indoor wireless system model. In this system, four white LED sources are used as separate transmitters, each of which is on a 0.2m pitch. The data streams are transmitted on these 4 channels, and the resulting signal recorded. Also [15] shows the received data are correctly.

1.5 Organization of the Thesis

Most of the existed research did not incorporate any experimental results from optical wireless systems, and all their discussion and conclusion were based on the analytical models and simulation results. The novelty of this project includes the design and building of several experimental optical wireless MIMO systems and the evaluation of the relationships between BER and distance/displacement using different modulations by using curve-fitting based on BER measurements. Such

experimental systems and fitted mathematical relationships have not been obtained before.

More specifically, this project furthers studies on OW MIMO by providing three infrared MIMO experimental systems using different modulations to describe the detailed process and the experiment methodology in developing the infrared MIMO systems. On-off keying (OOK), serial infrared protocol – return to zero inverted (SIR-RZI) and pulse positon modulation (PPM) are considered. The BERs of three systems are measured and compared, and the advantage and disadvantage of these systems are illustrated and discussed. To the best of the authors' knowledge, neither the built system nor their experimental results have been published in the literature before. Moreover, using curve fitting, the experimental results of BER are fitted as functions of system parameters to derive some mathematical models that have not been studied before. The results obtained from the specified experiments indicate that the developed system is viable for indoor optical applications as verified by root mean squared error.

The contributions of this project are three-fold. Firstly, it builds three new optical wireless MIMO systems with different modulations in metal boxes. Secondly, it conducts useful experiments on the effects of several important parameters on the system performance. Thirdly, based on these experimental results, it performs curve-fitting to provide some mathematical relationships between these parameters and the performance measure.

The work in this thesis is presented in the following chapters, and each chapter has own objects and connection with all the others.

Chapter 2 represents the principle and background knowledge of the technology used in this thesis.

Chapter 3 provides analyses of important OW configurations using APD receivers. First, the WMC model was employed to analyse the SISO configuration using a large deviations approach. Then, comparison with a Gaussian approximation showed that the latter was reasonable for the parameters considered, and made for a more tractable approach. Thus, an analytical expression for 2-1 MISO was successfully developed.

Chapter 4 and 5 discuss three different hardware optical wireless MIMO systems. In the Chapter 4, the theory and design concept of the 4X4 infrared MIMO system using OOK modulation are discussed that has a working bandwidth is between 100kHz to 10MHz. Also all the designed circuits, the controller boards and experimental flow will be introduced in Chapter 4.

Chapter 5 provides a 4PPM based 4X4 infrared MIMO system, whose bandwidth is from 500kHz to 4MHz. Moreover, both SIR and FIR standards with lower working

frequency (10kHz-1MHz) for 4X4 system are built as the reference model. The design circuits and controller flow will be explained.

In Chapters 6 and 7, all the experiments using different modulation and MIMO technologies (multiplexing and diversity) are illustrated, and the fitted mathematical models are obtained using the experiment results. Chapter 8 concludes all of the work, and is showing the further research which may be investigated.

Reference Chapter 1

[1] J. Grubor, S. Randel, K. D. Langer, J. W. Walewski, "Broadband Information Broadcasting Using LED-Based Interior Lighting", IEEE Journal of Lightwave Technology, vol. 26, no. 24, 2008.

[2] H. Le Minh, Z. Ghassemlooy, D. O'Brien, G. Faulkner, "Indoor Gigabit Optical Wireless Communications - Challenges and Possibilities", *Proc. 12th IEEE Conference on Transparent Optical Networks (ICTON)*, 2010 [6 pages].

[3] H. Le Minh, D. O'Brien, G. Faulkner, L. Zeng, K. Lee, D. Jung, and Y. Oh, "High-speed visible light communications using multiple-resonant equalization", *IEEE Photonics Technology Letters*, vol. 20, no. 14, pp. 1243-1245, 2008.

[4] J. Grubor, K. D. Langer, S. C. J. Lee, T. Koonen, and J. W. Walewski, "Wireless high-speed data transmission with phosphorescent white-light LEDs", *Proc. 23rd European Conference and Exhibition of Optical Communication (ECOC)*, 2007 [2 page post deadline paper].

[5] G. Nykolak, P. F. Szajowski, G. Tourgee, and H. Presby, "2.5 Gbit/s free space

optical link over 4.4 km", *Electronics Letters*, vol.35, pp. 578-579, 1999.

[6] J. R. Barry, Wireless Infrared Communications, *Kluwer*, 1994.

[7] F. E. Alsaadi, J. M. H. Elmirghani, "Performance evaluation of 2.5Gbit/s and 5Gbit/s Optical wirelesssystems employing a two dimensional adaptive beam clustering method and imaging diversity detection", IEEE Journal on Selected Areas in Communications, vol. 27, no. 8, pp. 1507-1519, 2009.

[8] G. Ntogari, T. Kamalakis, T. Sphicopoulos, "Performance analysis of space time block codingtechniques for indoor optical wireless systems", IEEE Journal on Selected Areas in Communications, vol. 27, no. 9, pp. 1545-1552, 2009.

[9] S. Haykin, "Neural networks expand SP's horizons", IEEE Signal Processing Magazine, vol. 13, no. 2, pp. 24-49, 1996.

[10] A. Hussain, J. J. Soraghan, T. S. Durrani, "A new adaptive functional-link neural-network-based DFEfor overcoming co-channel interference", IEEE Transactions on Communications, vol. 45, no. 11, pp. 1358-1362, 1997.

[11] S. Rajbhandari, Z. Ghassemlooy, M. Angelova, "Bit error performance of diffuse indoor optical wireless channel pulse position modulation system employing artificial neural networks for channel equalisation", IET Optoelectronics, vol. 3, no. 4, pp. 169-179, 2009.

[12] D. Takase, T. Ohtsuki, "Optical Wireless MIMO Communications", *Proc. IEEE Grobal Telecommunications Conference (GLOBECOM),* vol. 2, pp. 928-932, 2004 [5 pages].

[13] D. Takase, T. Ohtsuki, "Optical Wireless MIMO (OMIMO) with Backward Spatial Filter (BSF) in Diffuse Channels", *Proc. IEEE International Conference on Communications (ICC),* vol. 2, pp. 954-958, 2007 [5 pages].

[14] R. Mesleh, R. Mehmood, H. Elgala, H. Haas, "Indoor MIMO Optical Wireless Communication Using Spatial Modulation", *Proc. IEEE International Conference on Communications (ICC)*, pp. 1-5, 2010 [5 pages].

[15] D. O'Brien, "Multi-Input Multi-Output (MIMO) Indoor Optical Wireless Communications", *Proc. 2009 Conference Record of the Forty-Third Asilomar Conference on Signals, Systems and Computers*, pp. 1636-1639. 2009 [4 pages].

Chapter 2 Literature Review

2.1 Infrared Communication Technology

2.1.1 Introduction

The infrared wavelength range varies from 0.70μm to 1mm, whereas the region of 300μm ~ 1mm is often referred as sub-millimeter. In today's infrared communication technology, the major factors affecting the quality of atmospheric infrared transmission are absorption and scattering. [1]

2.1.2 Characteristic

Infrared communication technology is considered suitable for applications in low-cost, cross-platform, point-to-point high-speed data connection of embedded systems, device interconnection, and information gateway systems. As is described in [1], infrared communication technology is recognized worldwide for its applications in wireless data transmissions and communications, which is supported by a great number of hardware and software platforms with primary application features shown as below: [1]

1. Use mutual conversion between electrical pulse and infrared light pulse for wireless data transceiver.

2. Broadly used to replace point-to-point cable connection.
3. The newly developed infrared communication standard is compatible with the existing communication standards.
4. Small angle (cone angle of 30 degrees or less), short-range, point-to-point straight line data transmission and high security.
5. High transfer rate. Fast infrared protocol (FIR) at 4Mbps has been broadly used, and Very Fast infrared protocol (VFIR) at 16Mbps has been released. A new "Gigabit-IR" standard is also undergoing trials and validation. [2]
6. An infrared signal is reflected from non-light-transmissive material, such as walls, etc. Therefore, the same infrared equipment can be used in different physical spaces.
7. Occupying lower channel resources than that of RF technology with higher security features. Eavesdropping on data within a confined space is not easy with infrared technology applications.
8. Infrared communication has excellent inter-changeability and versatility because of the optical transmission capability and limited transmitting space.
9. No harmful radiation. It has been scientifically proven that infrared is a spectrum causing no harm to human in special areas, within well-known eye safety limits. [3]

In addition, an infrared communication system is recognized to be a system with simple installation procedures, and easy maintenance.

The disadvantages of the infrared data communications technology are described as below: [1]

1. Limited transmission distance because of the line-of-sight feature.
2. The location of the communication devices have to be fixed.
3. It is not the best choice as a completely wireless network system where mobility is required, due to its point-to-point transport connection of signals.

Despite the shortcomings described above, one should not be discouraged on developing the potential application of infrared free-space communications. It has been broadly recognized that infrared technology applications have made tremendous progress in mobile phones and laptops.

2.1.3 Principles

Infrared communication uses 950nm near-infrared as the information transmission band, which is referred as the communication channel. With regard to the process of data transmission, the baseband binary signal is first modulated to a series of pulse train signals before being transmitted via an infrared launch device. With regard to the process of data reception, the infrared receiver first converts the received light pulse into an electrical current, which is then converted to a voltage and amplified. Then it is filtered with other necessary processing before the demodulation circuit is employed to convert this signal to a binary digital signal output. Generally, pulse width modulation (PWM) and pulse position modulation (PPM) can be used in such an infrared communication process. In order to take advantage of the infrared channel, the primary process of the infrared communication involves binary digital signal modulation and demodulation.

2.1.4 Standard

The infrared data association (IrDA) 1.0 standard is generally referred as an SIR, which is developed as an asynchronous communication mode based on an HP-SIR system. It uses the system of an asynchronous communication transceiver (Universal Asynchronous Receiver / Transmitter (UART)), and extends this operation to achieve the infrared data transmission from the received light signal. The highest SIR data rate is 115.2kbps. [4] In 1995, the IrDA 1.1 protocol was released, which initially referred to the FIR, and was capable of adopting 4PPM encoding and decoding signals. [5] For this, the maximum data transfer rate reached 4Mbps. During the same time period, the 1.0 standard was employed for low speed transmitting applications. According to the IrDA 1.1 standards, a higher communication rate defined in the IrDA specifications can reach 16Mbps, the VFIR standard. Moreover, the Gigabit infrared standard (Gigi-IR) defines systems which achieve 1Gbps data rate over a relatively short distance, typically up to 3m at the current time. [2]

The IrDA standard includes three basic specifications: the infrared physical layer link specification (IrPHY), the infrared link access protoco1 (IrLAP) as the infrared connection access protocol, and the infrared link management protoco1 (IrLMP) as the infrared connection management protocol. The IrPHY specification regulates the infrared communication hardware design objectives and requirements, whereas the IrLAP and IrLMP specifications are commonly considered as two software systems responsible to set up, manage and maintain the connections. According to the IrLAP

and the IrLMP specifications, when certain infrared communication applications are concerned, the IrDA generally applies on higher-level infrared protocol, such as tiny transport protocol (TinyTP), infrared object exchange protocol (IrOBEX), and Infrared Communications Protocol (IrCOMM). [6]

2.2 Mathematical Model

The input-output baseband relationship of the system can be described in a linear equation as in [7]:

$$R(x) = S(x) \otimes H(x) + n(x) \tag{2.1}$$

Where $S(x)$ is the transmitted signal, $R(x)$ is the received signal, $n(x)$ is an additive noise, $h(x)$ is the impulse response of the channel, and $\otimes$ denotes the convolution operation. If multiple transceivers are employed either at the transmitter and the receiver, then the spatial dimension may be taken into account by regarding the channel as a MIMO system. [7]

2.3 Alamouti Space Time Block Coding

2.3.1 Introduction

Alamouti developed a space time code in 1998, which offers a simple approach in developing a wireless MIMO system with two transmit and two receive antennas. [8]

Firstly, it is assumed that the transmission data sequence is defined as $\{x_1, x_2, x_3..., x_n\}$. Normally, the transmission starts at x_1 and finishes at x_n. However, by using the Alamouti space time code, two symbols are sent each time, i.e., in the first slot, x_1, x_2 are sent from the first of two antennas, whereas in the second time slot, $-x_2^*$ and x_1^* are sent from the second of the two antennas, respectively. In the following slots other symbols are sent in the same fashion, alternately. The aforementioned approach has been broadly described for use in MIMO systems, described as Alamouti STBC.

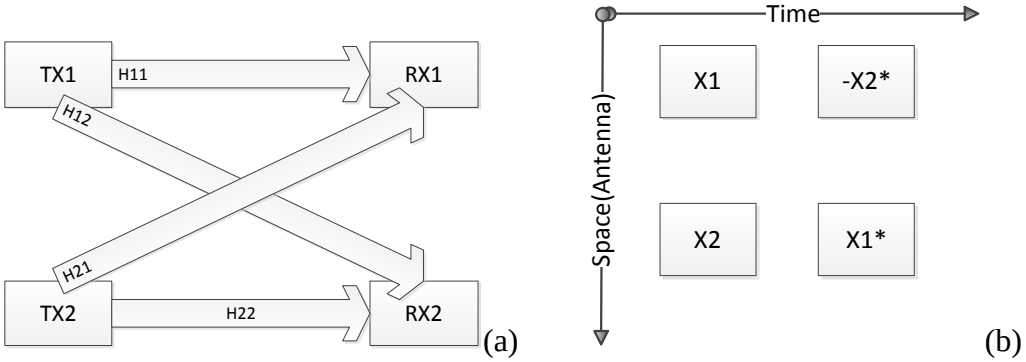

Figure 2-1: 2X2 Alamouti STBC: (a) 2X2 wireless MIMO system, and

(b) Alamouti STBC coding map.

Fig 2-1 illustrates how the MIMO system works with two transmit antennas and two receive antennas. From [9] and [10], the received signal in the first time slot is given as:

$$\begin{bmatrix} y_1^1 \\ y_2^1 \end{bmatrix} = \begin{pmatrix} h_{11} & h_{12} \\ h_{21} & h_{22} \end{pmatrix} \begin{bmatrix} x_1 \\ x_2 \end{bmatrix} + \begin{bmatrix} n_1^1 \\ n_2^1 \end{bmatrix} \tag{2.2}$$

The received signal in the second time slot is given as:

$$\begin{bmatrix} y_1^2 \\ y_2^2 \end{bmatrix} = \begin{pmatrix} h_{11} & h_{12} \\ h_{21} & h_{22} \end{pmatrix} \begin{bmatrix} -x_2^* \\ x_1^* \end{bmatrix} + \begin{bmatrix} n_1^2 \\ n_2^2 \end{bmatrix} \tag{2.3}$$

whereas $\begin{bmatrix} y_1^1 \\ y_2^1 \end{bmatrix}$ is the received information at time slot 1, $\begin{bmatrix} y_1^2 \\ y_2^2 \end{bmatrix}$ represents the data at time slot 2, h_{ij} is the channel from the i^{th} receive antenna to the j^{th} transmit antenna, and $\begin{bmatrix} n_1^1 \\ n_2^1 \end{bmatrix}, \begin{bmatrix} n_1^2 \\ n_2^2 \end{bmatrix}$ are the noise in time slot 1 and 2 respectively.

The equations are then combined at both slot 1 and 2 into the following:

$$\begin{bmatrix} y_1^1 \\ y_2^1 \\ y_1^{2*} \\ y_2^{2*} \end{bmatrix} = \begin{bmatrix} h_{11} & h_{12} \\ h_{21} & h_{22} \\ h_{12}^* & -h_{11}^* \\ h_{22}^* & -h_{21}^* \end{bmatrix} \begin{bmatrix} x_1 \\ x_2 \end{bmatrix} + \begin{bmatrix} n_1^1 \\ n_2^1 \\ n_1^{2*} \\ n_2^{2*} \end{bmatrix} \tag{2.4}$$

The transmitting channel $\begin{bmatrix} h_{11} & h_{12} \\ h_{21} & h_{22} \\ h_{12}^* & -h_{11}^* \\ h_{22}^* & -h_{21}^* \end{bmatrix}$ is defined as $\boldsymbol{H}$.

In Alamouti STBC, the estimate of the transmitted symbol is given as:

$$ES\begin{bmatrix} x_1 \\ x_2 \end{bmatrix} = (H^H H)^{-1} \begin{bmatrix} y_1^1 \\ y_2^1 \\ y_1^{2*} \\ y_2^{2*} \end{bmatrix} \tag{2.5}$$

2.3.2 Space-Time Combining

Chapter 1 has given a brief introduction on the transmission scheme of Alamouti STBC. In this chapter, the detailed of the space-time combiner is given. In [8], a classical Maximal-Ratio Combining (MRC) scheme was denoted. In this scheme, the coefficient $\alpha_{i,j}$ is considered as the path gain from transmit antenna *i* to receive antenna *j*.

h_0 represents the channel between transmitter zero and receiver zero, and the channel between the transmitter one and receiver one is denoted by h_1, and θ_0 and θ_1 denote the fading phase angles.

$$h_0 = \alpha_0 e^{j\theta_0}$$

$$h_1 = \alpha_1 e^{j\theta_1} \tag{2.6}$$

In [8], $d^2(x, y)$ is the squared Euclidean distance between signal *x* and *y*, calculated as:-

$$d^2(x, y) = (x - y)(x^* - y^*) \tag{2.7}$$

During the signal transmission, the two channels are combined as:

$$\begin{aligned} \tilde{s}_0 &= h_0^* r_0 + h_1^* r_1 \\ &= (\alpha_0^2 + \alpha_1^2) s_0 + h_0^* n_0 + h_1^* n_1 \end{aligned} \tag{2.8}$$

Similarly, S_1 can be received.

In the receiver decision scheme, s_i can be chosen if :-

$$(\alpha_0^2+\alpha_1^2)\left|s_i\right|^2-\tilde{s}_0 s_i^*-\tilde{s}_0^* s_i \le (\alpha_0^2+\alpha_1^2)\left|s_k\right|^2-\tilde{s}_0 s_k^*-\tilde{s}_0^* s_k, \forall i \ne k . \quad (2.9)$$

If the communication system uses PSK modulation, the equation is shown below:

$$\left|s_i\right|^2=\left|s_k\right|^2=E_s, \forall i \ne k . \quad (2.10)$$

Such that s_i is selected if $d^2(\tilde{s}_0, s_i) \le d^2(\tilde{s}_0, s_k), \forall i \ne k$. (2.11)

2.3.3 MIMO Cases

In [8], two MIMO cases were introduced. The first one describes the case with two transmitters and one receiver.

In a 2 x 1 system, the received signals are expressed as below: [8]

$$\begin{aligned} r_0 &= r(t) = h_0 s_0 + h_1 s_1 + n_0 \\ r_1 &= r(t+T) = -h_0 s_1^* + h_1 s_0^* + n_1 \end{aligned} \quad (2.12)$$

where r_0 and r_1 are the received signals in receiver zero and receiver one, respectively. Combining the two received signals, one has:

$$\begin{aligned} \tilde{s}_0 &= h_0^* r_0 + h_1 r_1^* \\ \tilde{s}_1 &= h_1^* r_0 - h_0 r_1^* \end{aligned} \quad (2.13)$$

By substituting the equations above:

$$\tilde{s}_0 = (\alpha_0^2 + \alpha_1^2)s_0 + h_0^* n_0 + h_1 n_1^*$$
$$\tilde{s}_1 = (\alpha_0^2 + \alpha_1^2)s_1 + h_0^* n_0 + h_1 n_1^* \quad (2.14)$$

The signals will then be sent to the maximum likelihood detector, and the combining scheme in 2.3.1 will be used.

In the second case, with two transmitters and two receivers, the received signal is denoted as below: [8]

$$r_0 = h_0 s_0 + h_1 s_1 + n_0$$
$$r_1 = -h_0 s_1^* + h_1 s_0^* + n_1$$
$$r_2 = h_2 s_0 + h_3 s_1 + n_2$$
$$r_3 = -h_2 s_1^* + h_3 s_0^* + n_3 \quad (2.15)$$

where n_i (i = 0,1,2,3) are the complex random variables representing receiver noise and interference. The combining scheme shows that the following two signals are sent to the maximum likelihood detector:

$$\tilde{s}_0 = h_0^* r_0 + h_1 r_1^* + h_2^* r_2 + h_3 r_3^*$$
$$\tilde{s}_1 = h_1^* r_0 - h_0 r_1^* + h_3^* r_2 - h_2 r_3^* \quad (2.16)$$

By substituting the equations above:

$$\tilde{s}_0 = (\alpha_0^2 + \alpha_1^2 + \alpha_2^2 + \alpha_3^2)s_0 + h_0^* n_0 + h_1 n_1^* + h_2^* n_2 + h_3 n_3^*$$
$$\tilde{s}_1 = (\alpha_0^2 + \alpha_1^2 + \alpha_2^2 + \alpha_3^2)s_1 - h_0 n_1^* + h_1^* n_0 - h_2 n_3^* + h_3^* n_2 \quad (2.17)$$

Then, S_0 and S_1 are finally sent to the maximum likelihood detector for a data decision. Similar to the 2x1 case, one may choose s_i if:-

$$d^2(\tilde{s}_0, s_i) \le d^2(\tilde{s}_0, s_k), \forall i \ne k. \quad (2.18)$$

2.4 Optical Communication System Model

The factors affecting the performance of outdoor optical wireless communication systems include free-space loss, clear-air absorption, noise scattering and scintillation induced due to atmospheric turbulence, whereas those affecting the performance of indoor optical wireless communication systems include the reflection loss and the received signals being dispersed with time due to the multipath propagation resulting in reduced pulse amplitude, increased delay spread and inter-symbol interference. [9, 10]

Consider the outdoor communication system first. The power received can be calculated by using the free-space equation shown below: [11]

$$P_r = P_t(A_{et}A_{er})\frac{1}{L^2\lambda^2} \tag{2.19}$$

where A_{et} represents the transmitting effective aperture, A_{er} represents the receiving effective aperture, Pt represents the transmitted powers, L represents the distance, and λ represents the wavelengths. The optical attenuation comes from rain, fog and gas molecules in the air. [11] Consider an indoor communication system. According to the work conducted in [10], [12] and [13], the indoor channel properties can be described by the following parameters, including free-space path loss, reflections of walls, power delay profile (PDP) and incremental angle of departures. The indoor links are mainly up against shadowing, as the transmission is affected through the high reflectivity of indoor objects such as walls. Also, due to the path/reflection loss, a large amount of transmitted power is required. The PDP gives the intensity of a

signal received through a multipath channel as a function of time delay, which is the difference in transmitting time between multipath arrivals. Additionally, in order to insure the coverage of the whole indoor area, the angle of departure has to be considered. [10]

The noise and signals are received after multiplication, while the additional system loss of the connectors are not part of the noise budget but might reduce the output signal level and have to be considered as a required system parameter. [11] References [14] and [15] give detailed reviews on the algorithms used in optical channel models, which contains the table of the comparison amongst different algorithms. The review is considered to be highly helpful in the utilization of algorithms and the relative merits of algorithms and is given in Table 2-1.

Table 2-1 Algorithms used in the normal optical channel models illustrated by Hranilovic in [15]

Parameters	Recursive Method	Statistical Model	Dustin Algorithm	Monte carlo Algorithm	Iterative Site-based Model
Computational complexity	Times calculation has to repeated	Less complex than recusive	Less complex compare to old models	Less with respect to the classical algorithm	Very less compare to recursive method
Memory required	$8N^2$ bytes	Less compare to recusive model	N^2 bytes	N^2 bytes	Less compare to recusive model
Time taken	N^k410-6 sec	Less compare to recusive	0.23 nsec per time slot less compare to recusive	Less compare to recusive DUSTIN	About 92 times faster than recursive method
Max number	Maximum	Limited no	No limits	Maximum	Up to 10

of reflection possible	3 bounce	of bounces	but restricted by emitter power	up to 40 bounce is possible	bounces are possible
Adaptation	No	No	No	Yes	Yes
Accuracy	Very less	Less	Moderate	Moderate	Moderate
Published year	1993	1997	1997	1998	2002

A practical optical channel model is described in [16]. The following illustration shows the basic structure of the model.

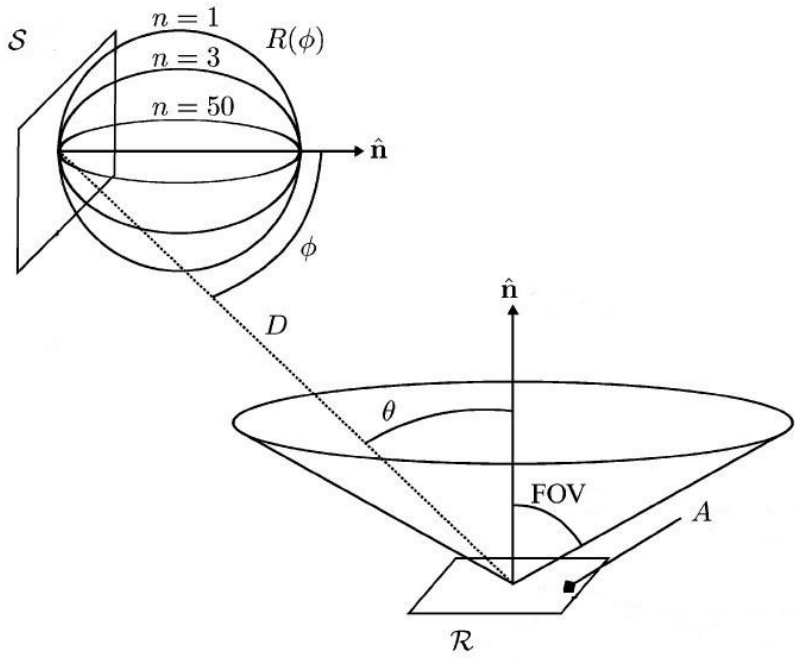

Figure 2-2 Infrared Channel Model introduced by Barry in [16]

The above model is considered to be one of the most popular optical channel models. It takes consideration of the angle between transmitter and receiver, the mode number and the distance between the source and receiver.

In the model described above, *S* represents the transmitter and *R* represents the receiver. $R(\phi)$ is expressed as below: [16]

$$R(\phi) = \frac{n+1}{2\pi} P_S \cos^n(\phi) \tag{2.20}$$

where *n* is the mode number of the radiation lobe, which specifies the directionality of the source, (n+1/2π) ensures that integrating $R(\phi)$ over the surface of a hemisphere results in the source power Ps. A mode of *n = 1* corresponds to a traditional Lambertian source. The scalar angle FOV is defined such that a receiver only detects the light where the angle of incidence is less than FOV. [16]

The impulse response of the system is given below:

$$h^{(0)}(t; S, R) = \frac{n+1}{2\pi} \cos^n(\phi) d\Omega rect(\theta / FOV) \delta(t - R/c) \tag{2.21}$$

where $d\Omega$ is the solid angle subtended by the differential area of a receiver:

$$d\Omega = \cos(\theta) A_R / R^2 \tag{2.22}$$

R is the distance between the transmitter and the receiver where:

$$R = \| r_S - r_R \| \tag{2.23}$$

θ is the angle between $\hat{n}$ and ($r_S - r_R$):

$$\cos(\theta) = \hat{n}(r_S - r_R) / R \tag{2.24}$$

ϕ is the angle between $\hat{n}$ and ($r_R - r_S$):

$$\cos(\theta) = \hat{n}(r_R - r_S) / R \tag{2.25}$$

The impulse response, *h(t)*, of the model, is as follows:

$$h^k(t; S_i, R_j) = \sum_{l=1}^{L} h^{k-1}(t; S_i, \varepsilon_l^R) * h^0(t; \varepsilon_l^S, R_j) \tag{2.26}$$

By substituting all the equations above, one has:

$$h^{(k)}(t; S, R) = \frac{n+1}{2\pi} \sum_{l=1}^{N} \frac{\rho_l \cos^n(\phi) \cos(\theta)}{R^2} rect(2\theta / \pi) h^{(k-1)}(t - R/c; S, R) \Delta A \tag{2.27}$$

It denotes the impulse response of the k^{th} bounce (power distribution). Moreover, the impulse response of the k^{th} bounce is only related to the $(k\text{-}1)^{th}$ and the first impulse responses. Meanwhile, the formula of the time domain can be transferred into that of the frequency domain, which helps to estimate the frequency response.

However, the research contains several pending issues to be verified, such as the shadowing, path loss and interference, etc. Meanwhile the number of source being employed is the only one, which implies that the MIMO system is not considered in this model. Finally, the power attenuation is defined as the multipath-induced power penalty of three bounces from one source.

2.5 Optical Wireless MIMO System

As one of the broadly-known alternative applications, indoor optical wireless systems appear to demonstrate promising potential in wireless communications,

especially those presented as the next generation communication due to the high speed and high security assurance in data transmission, facilitated by a MIMO system, which enjoys unregulated bandwidth. This section provides an in-depth discussion and analysis on the design and performance of MIMO system based on a 2X2 infrared OOK modulation and regulated bandwidth at 100kHz, 1MHz and 10MHz.

As having been described by Koonen in [17], the fibre-to-home technology may facilitate the data transmission rate up to 1Gbps at the home gateway, and has therefore attracted worldwide attention. However, as further illustrated by Ntogari et al. in [18], the application access to allocate the high rate data from fibre to customer device is considered challenging, unless the IR-based communication is of presence to proceed through the last mile. [19]

The next generation wireless communication system includes a large group of mutually-complementary technologies. As one of the important compositions, the indoor infrared communication technology may deliver the expected performance in the range of 780 – 950nm, and demonstrates many advantages for short distance transmissions, i.e., infrared emitters and detectors may accomplish high speed transmissions at much lower costs in comparison with those by radio antenna and visible light communications; in comparison with the region of radio spectrum, the infrared spectral region is much broader, and there is no need for licensing approval. However, infrared light is capable of penetrating through glass materials, but not walls or other opaque blocks. Consequently, such infrared communication can only be performed indoors. The coding and modulation of infrared transmissions can be

easily analysed by the bandwidth characteristics, as well as the coding circuit, etc. Due to the high rate and ensured security in data transmission, the new optical wireless MIMO technology based on the infrared transmitter and receiver has been previously discussed. However, it is worth noticing that the MIMO technology based on LOS has several unsettled issues to be further explored. [13, 20]

A review on various MIMO communication technologies is given below:

1. Spatial multiplexing: in comparison with SISO systems, the MIMO antenna configurations make it possible to enhance the data rate without having to increase the bandwidth, and therefore be capable of considerably enhancing the utilization of spectra. As far as transmitting is concerned, the high-rate data streams are divided into a plurality of lower rate sub-streams; whereas different sub-data streams can be transmitted on different transmit antennas in the same frequency. [21, 22, 23]

   If the antenna array of both transmitters and receivers are considerably different, i.e. providing an additional dimension of airspace outside the time domain and frequency domain, hence the transmitted signals from different transmit antennas can be distinguished from one another, and the receivers are able to distinguish the parallel sub-data streams without having to consume additional frequency or time resources. The spatial multiplexing can significantly improve the channel capacity under high SNR conditions. The Bell Labs Layered Space-Time (BLAST) is a typical example of applications from spatial multiplexing MIMO technology. Figure 2-5 illustrates a simple 2X2 MIMO spatial multiplexing

system, where the x axis is the time line, and the y axis defines the position of two transmitters and receivers.

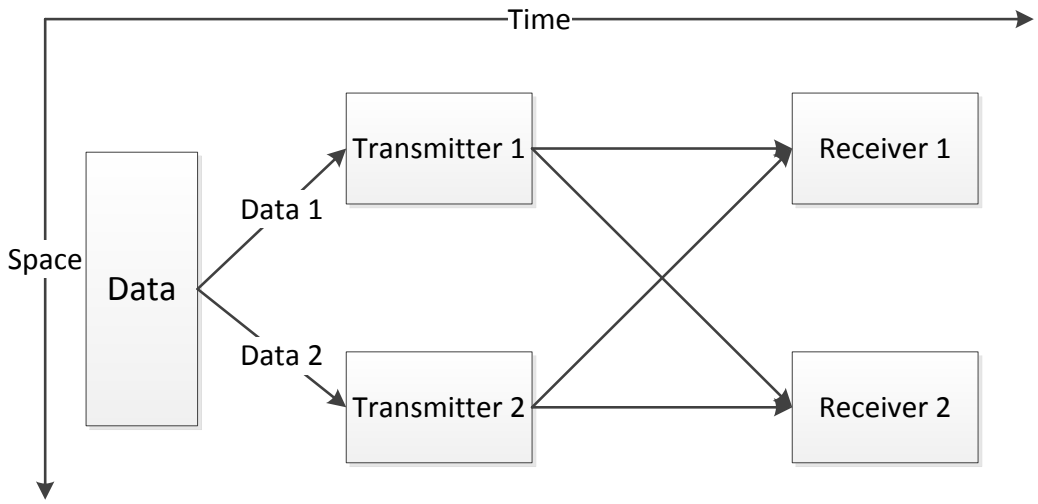

Figure 2-3 Spatial multiplexing

2. Spatial diversity: offers the opportunity to use multiple antennas to transmit or receive the same information in order to improve the quality of data significantly. [23, 24, 25]

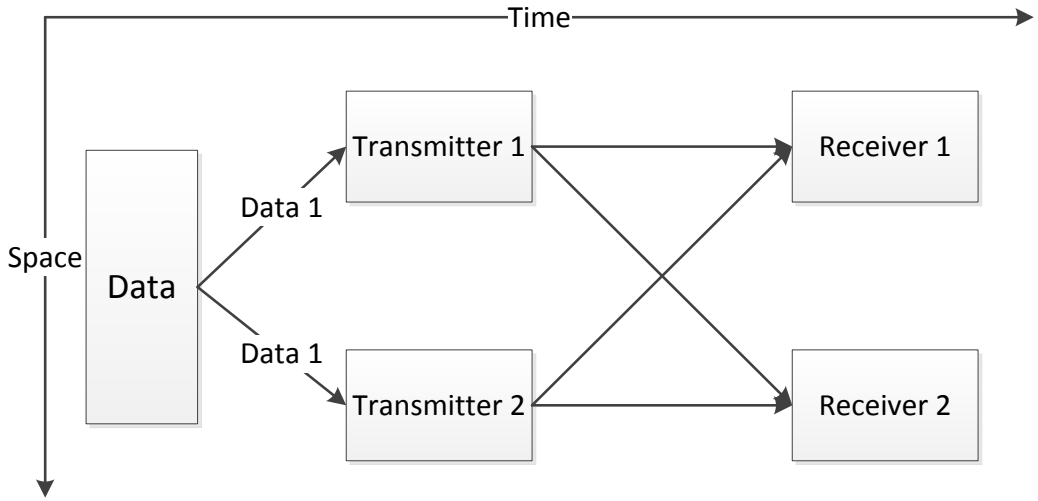

Figure 2-4 Spatial diversity

Figure 2-4 illustrates the 2X2 MIMO diversity system. The difference is two transmitters transmit same signals at the same time.

3. Beam formation: it is capable of generating a directive beam, in which the energy is concentrated in the desired direction to improve the signal quality, and minimize the impact of interference with other users. [23, 24, 26]

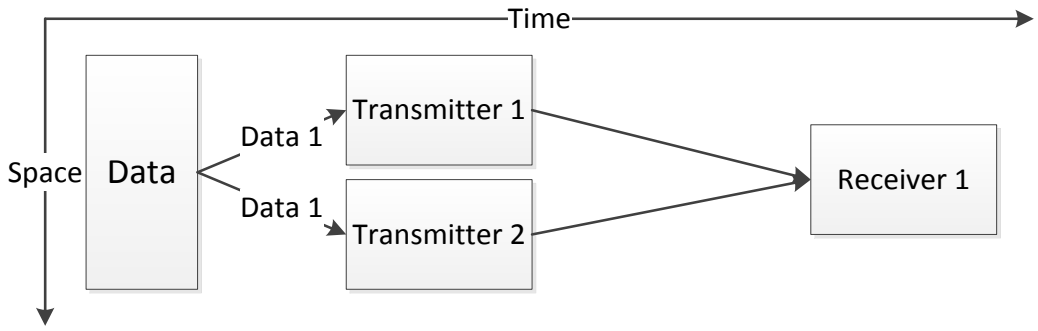

Figure 2-5 Beam formation

In Figure 2-5 Beam formation, a 2X1 MIMO system is illustrated, where beams from two transmitters are got together to improve the signal quality and reduce the interference to other users.

All the MIMO-related technologies described above are not exclusive, and can be complemented collectively with each other, i.e., a MIMO system can be integrated with the application of spatial multiplexing and diversity technology.

2.6 Optical MIMO Network

In [27], an optical MIMO network is presented, which is considered as an application for optical wireless MIMO communications.

The system provides an opportunity to establish a MIMO network by constructing repetition sensors. The Figure 2-6 describes the structure of this network, which exhibits both a fully-connected group and a partially-connected group. The illustration shows that each point (begin with point-1, and point-15 is the last point) denotes one sensor (which represents a transceiver), which receives or transmits signals.

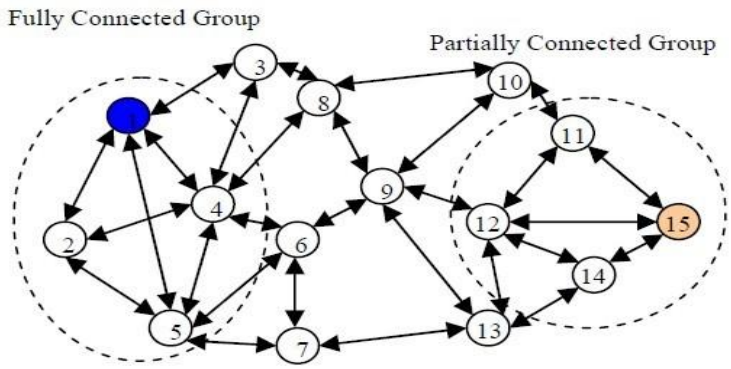

Figure 2-6 Optical MIMO Network illustrated in [27]

The Figure 2-7 describes the nodes which formulate each group. The number of 1 stands for the connected, whereas 0 represents the unconnected. For example, value between row sensor 1 and column sensor 2 is 1 means sensor 1 and 2 are connected.

$$TransmittingMatrix = \begin{bmatrix} & Sensor1 & Sensor2 & Sensor3 & Sensor4 & ...Sensor15 \\ Sensor1 & 1 & 1 & 1 & 1 & \\ Sensor2 & 1 & 1 & 0 & 1 & \\ Sensor3 & 1 & 0 & 1 & 1 & \\ Sensor4 & 1 & 1 & 1 & 1 & \\ ...Sensor15 & 0 & 0 & 0 & 0 & 1 \end{bmatrix}$$

Figure 2-7 Optical MIMO Network Transmitting Matrix adapted from [27]

The advantage of this model is that every node can change the power when it transmits different signals, and provides a promising solution to improve the data transmission quality, which could be used as the optical wireless MIMO multilayer simulation model in future research.

However, it is only an analytical model based on the Matlab simulation, and the simulation region is the radio of MIMO. More research work on lab tests needs to be carried out: firstly, difference between optical signals and radio signals should be further explored; secondly, only connections of different transceivers are demonstrated in this paper. As a result, the whole simulation channel model need to be developed, which includes the background noise, path loss and other influence factors. Thirdly, as is mentioned, this network is an analytical model, and hence further experiments using hardware optical MIMO system should be considered.

2.7 Summary

This chapter has reviewed the necessary background knowledge used in this thesis, such as infrared technology and standards for infrared communications, Alamouti space time coding for 2X2 MIMO systems, the multiplexing, diversity and beam formation technology for wireless MIMO systems, introduction of p-i-n diode based optical wireless system, and an application of optical wireless MIMO technology - optical MIMO network. Most of these aspects are used in this project, and the optical MIMO network is considered in the following research work.

References Chapter 2

[1] R. Otte, Low-Power Wireless Infrared Communications, *Springer*, 2010.

[2] H. Le Minh, Z. Ghassemlooy, D. O'Brien, and G. Faulkner, "Indoor gigabit optical wireless communications: challenges and possibilities", *Proc. IEEE 12th International Conference on Transparent Optical Networks (ICTON)*, pp.1-6, 2010 [6 pages].

[3] American National Standards Institute, American National Standard for the Safe Use of Lasers Z136.l-1993 (ANSI Z136.1-1993), pp. 31,32,41,42, 1993.

[4] Infrared Data Association, Infrared Data Association Serial Infrared Physical Layer Link Specification, Version 1.0, November, 1994.

[5] Infrared Data Association, Infrared Data Association Serial Infrared Physical Layer Link Specification, Version 1.1, November, 1995.

[6] Infrared Data Association, Infrared Data Association Serial Infrared Physical Layer Link Specification, Version 1.2, November, 1997.

[7] C. Zhang, R. R. Bitmead, "State space modeling for MIMO wireless channels", *Proc. IEEE International Conference on Communications (ICC)*, vol.2, pp. 2297-2301, 2005 [5 pages].

[8] S. M. Alamouti, "A simple transmit diversity technique for wireless communications", IEEE Journal on Select Areas in Communications, vol. 16, no. 8, pp. 1451-1458, 1998.

[9] J. B. Carruthers, J. M. Kahn, "Angle diversity for nondirected wireless infrared communication", IEEE Transactions on Communications, vol. 48, no. 6, pp. 960-969, 2000.

[10] H. Joshi, R. J. Green, M. S. Leeson, "Channel Models for Optical Wireless Communication Systems", *Proc. 11th International Conference on Transparent Optical Networks (ICTON)*, pp. 1, 2009 [1 page].

[11] K. Jastrowa, R. Miintera, R. Piesiewiczb, T. Kiimer, M. Kochd and T.Kleine-Ostmanna, "300 GHz Channel Measurement and Transmission System", *Proc. IEEE Infrared Millimeter and Terahertz Waves International Conference*, pp. 1-2, 2008 [2 pages].

[12] D. Takase, T. Ohtsuki, "Optical Wireless MIMO Communications", *Proc. IEEE Grobal Telecommunications Conference (GLOBECOM)*, vol. 2, pp. 928-932, 2004 [5 pages].

[13] D. Takase, T. Ohtsuki, "Optical Wireless MIMO (OMIMO) with Backward Spatial Filter (BSF) in Diffuse Channels", *Proc. IEEE International Conference on Communications (ICC)*, vol. 2, pp. 954-958, 2007 [5 pages].

[14] A. Sivabalan, J John, "Modeling and simulation of indoor optical wireless channels: a review", *Proc. TENCON 2003 Conference on Convergent Technologies for the Asia-Pacific Region*, Vol.3, pp. 1082-1085, 2003 [4

pages].

[15] S. Hranilovic, Wireless Optical Communication Systems, *Springer*, 2004.

[16] J. R. Barry, Wireless Infrared Communication Systems, *Kluwer*, 1994.

[17] T. Koonen, "Fiber to the home/fiber to the premises: What, where and when?", Proceedings of the IEEE, vol. 94, no. 5, pp. 911–934, 2006.

[18] G. Ntogari, T. Kamalakis, T. Sphicopoulos, "Analysis of Indoor Multiple-Input Multiple-Output Coherent Optical Wireless Systems", IEEE Journal of Lightwave Technology, vol. 30, no. 3, pp. 317-324, 2012.

[19] O. Bouchet, M. Wolf, M. E. Tabach, T. Kamalakis, F. Grahame, J. Walewski, S. Nerreter, M. Franke, J. Grubor, D. O'Brien, and K. D. Langer, "Hybrid Wireless Optics (HWO): Building the Next-Generation Home Network," *Proc. 6th International Symposium on Communication Systems, Networks and Digital Signal Processing (CNSDSP)*, pp. 283-287, 2008 [5 pages].

[20] D. C. O'Brien, S. Quasem, S. Zikic, and G. Faulkner, "Multiple input multiple output systems for optical wireless; challenges and possibilities," Proc. SPIE 6304 - Free-Space Laser Communications VI, vol. 6304, pp. 630416.1–630416.7, 2006.

[21] R. Heath, Jr. A. Paulraj, "Switching between multiplexing and diversity based on constellation distance," IEEE Transactions on Communications, vol. 53, no. 6, pp. 962-968, 2005.

[22] L. Zheng, D. N. C. Tse, "Diversity and Multiplexing: A Fundamental Tradeoff in Multiple-Antenna Channels," IEEE Transactions on Information Theory, vol. 49, no. 5, pp. 1073-1096, 2003.

[23] T. Fath, H. Haas, "Performance Comparison of MIMO Techniques for Optical Wireless Communications in Indoor Environments", IEEE Transactions on

Communications, vol. 61, no. 2, pp. 733-742, 2013.

[24] S. G. Wilson, M. Brandt-Pearce, Q. Cao, and M. Baedke, "Optical repetition MIMO transmission with multipulse PPM," IEEE Journal on Select Areas in Communications, vol. 23, no. 9, pp. 1901–1910, 2005.

[25] S. Navidpour, M. Uysal, and M. Kavehrad, "BER performance of freespace optical transmission with spatial diversity," IEEE Transactions on Wireless Communication, vol. 6, no. 8, pp. 2813–2819, 2007.

[26] L. Zeng, D. O'Brien, H. Minh, G. Faulkner, K. Lee, D. Jung, Y. Oh, and E. T. Won, "High data rate multiple input multiple output (MIMO) optical wireless communications using white LED lighting," IEEE Journal on Select Areas in Communications, vol. 27, no. 9, pp. 1654–1662, 2009.

[27] I. Mansour, J. S. Rahhal, H. Farahneh, "Two Slot MIMO Configuration for Cooperative Sensor Network", International Journal of Communications, Network and System Science, vol. 3, no. 9, pp. 750-754, 2010.

Chapter 3 Optical MIMO System Based on APD Receiver

3.1 Introduction

During the last two decades, optical wireless (OW) technology has been considered as strong candidate in applications for high speed free-space communications [1]. Its highly recognized advantages include cost-effectiveness, fast bandwidth access, high quality data transmission, no interference with RF-based communication systems and highly-secured transmissions. The development of OW technology has shown a rapid growth due to the increasing demand on systems offering high data rate and high security assurance [2]. Recently, due to high bandwidth requirements from consumers using high speed data transmission applications, multiple-input multiple-output (MIMO) systems have become established [3]. OW is no exception, with interest increasing and promising results obtained for both outdoor [4] and indoor systems [5].

Based on the specific configuration and application requirement, an OW receiver is normally designed by choosing one of two photodiodes, namely a positive intrinsic negative (P-I-N) diode or an avalanche photodiode (APD). Although the two types of receivers have similarities, the internal gain of APDs may offer benefits when correctly deployed and therefore is used for the following study [6]. In general, the noise statistics of an OW configuration utilizing an APD are intractable so here the

Webb, McIntyre and Conradi (WMC) distribution [7] is used to approximate the APD receiver output.

In this chapter, an APD receiver-based OW MIMO system model is introduced, and the numerical analysis focusing on the performance of the system is reviewed and discussed. Instead of using visible light LEDs, infrared LEDs are used to transmit optical signals so as to minimize the effect of sunlight and other possible background light. Under some special circumstances [8], however, visible light LEDs remain preferred due to the fact that they can be used for both lighting and communications, and at the same time the system can be of maximum simplicity, as desired. Visible light LEDs are considered particularly interesting because the typical bandwidth of such devices ranges between 2-8 MHz [9] , [10], and they may offer bit rates of tens of Mbps for some particular applications [11]. Their bandwidth is set by their slow temporal response, especially those using the secondary emission phosphor to cover the orange and red portion of the visible spectrum [12]. As far as the receiver is concerned, an APD photodiode-receiver can be considered because it has higher capability for longer distance transmission without having to increase the transmitter power for protecting a human eye from potential harm.

3.2 Optical MIMO

Free space optical (FSO) links offer the prospect of high speed, long distance line-of-sight transmission but suffer from atmospheric turbulence [13]. Overcoming this limitation motivates this study of MIMO FSO systems with avalanche photodiodes (APDs) in the receiver array. The key idea is that FSO MIMO

techniques can improve performance in a manner similar to RF MIMO systems [3], in this case via spatial diversity [14], while APDs help approach shot-noise-limited operation. Here, to address both challenges consideration is given to the use of (noncoherent) optical arrays, analogous to the use of antenna-array technology for microwave systems, as a means of combatting fading.

The approach here is to employ intensity-modulated separate lasers together with photodetectors assumed to be ideal noncoherent (direct-detection) receivers. The sources and detectors are in a physical arrangement so that the fading experienced between source–detector pairs is statistically independent, which delivers diversity benefits the resulting multiple-input multiple-output (MIMO) channel. Such methods have been applied with great effect in RF communications by means of transmit and receive antenna arrays combined with space–time coding [3]. Although the philosophy is the same, there are several important differences when considering optical MIMO. The MIMO channel inputs and outputs are not complex numbers but nonnegative, real intensities. Furthermore, the noise mechanisms are different since in contrast to the additive complex Gaussian noise of RF, signal-dependent shot noise becomes the limiting factor.

3.3 Noise in APDs

3.3.1 Introduction of APD Noise

The exact form of the statistics of the random gain introduced by APDs is known [15],[16] but too complicated to produce tractable analyses. An approximate analysis

of the APD receiver statistics, the Webb, McIntyre, Conradi (WMC) approach [7], yields more useable results. The fact that the WMC distribution may be obtained from the Inverse Gaussian distribution [17] delivers both its moment generating function (MGF) and cumulant generating function (CGF) that may be used in several computational methods. Following Tang and Ben Letaief [18], details of the WMC distribution and its CGF will now be presented, followed by the BER expression resulting from a large deviations approach [19] that leads to a simpler form of equation than some of the alternative possibilities such as the Modified Chernoff Bound (MCB) [20].

The primary electrons produced in the APD follow a Poisson distribution for a fixed light intensity with parameter λ_1 when a "one" is sent and λ_0 when a "zero" is sent. These Poisson rates include a dark current element λ_d, which is present in both cases. The number of secondary electrons produced in the APD, denoted by the random variable *R*, has WMC density:

$$f_R(r) = \frac{1}{\sqrt{2\pi}\sigma_k}\left[1 + \left(\frac{r - M_k}{\sigma_k \delta_k}\right)\right]^{-3/2} \exp\left\{\frac{-(r - M_k)^2}{2\sigma_k^2\left[1 + \left(\frac{r - M_k}{\sigma_k \delta_k}\right)\right]}\right\} \tag{3.1}$$

where $\delta_k = \sqrt{\lambda_k F}/(F-1)$ is the mean number of primary electrons when a one is received (k = 1) or a zero is received (k = 0), $F = \kappa G + (2 - 1/G)(1 - \kappa)$ is the excess noise factor for an ionization ratio of κ and APD gain of *G*, $M_k = \lambda_k G$ is the mean of *R* and $\sigma_k^2 = \lambda_k G^2 F$ is the variance of *R*. The CGF is given by:

$$\mu_R(s) = \delta_k^2\left(1 + \sqrt{1 - 2\frac{\sigma_k}{\delta_k}s}\right) + (M_k - \sigma_k\delta_k)s \tag{3.2}$$

3.3.2 Large Deviations Theory Approach

Following Tang and Ben Letaief [18], the probability of error for a zero (k =0) or a one (k = 1) is given by:

$$P_{ek} = \frac{e^{-I_\gamma}}{|\alpha_k^*|\sqrt{2\pi\mu_Z''(\alpha_k^*)}} \tag{3.3}$$

In (3.3), I_γ is the large deviations rate function defined as $I_\gamma \triangleq \gamma\alpha_k^* - \mu_Z(\alpha_k^*)$, where $\mu_Z(s) = \mu_R(s) + \mu_{N_T}(s)$ with $\mu_{N_T}(s) = \sigma_T^2 s^2/2$ being the CGF of the receiver thermal noise and α_k^* being the real root of the equation $\mu_Z'(s) = \gamma$.

3.4 SISO System

Firstly, a SISO free-space OW system is considered with an IR-LED and APD photodiode detector. Initially, the channel is described as in ideal conditions without fading, and the diagram of the process flow is shown in Figure 3-1 below:

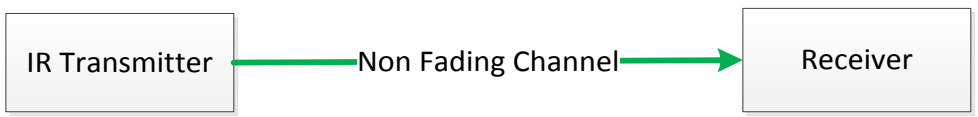

Figure 3-1 OW SISO System

The theoretical channel model can be expressed via [21]:

$$R(x) = S(x) \otimes H(x) + n(x) \tag{3.4}$$

where $R(x)$ is the received signal, *S(x)* is the transmitted signal, $H(x)$ is the channel response, and $\otimes$ represents the convolution operator; *n*(x) denotes the total channel noise. Although the type of noise associated with OW communication is commonly recognized as shot noise, the thermal noise cannot be ignored and is accounted for in the large deviations approach above so $n(x)$ is defined as the sum of both shot noise and thermal noise.

3.4.1 Results using the Parameters in [18]

A program was developed to ascertain the BER performance of the SISO link without fading and thus form a baseline case. The parameters from [18] Figure 1 were used, viz. $\lambda_d = 5; \kappa = 0.5; G = 10;\ \sigma_T^2 = 40000$; initially, the extinction ratio was assumed to be infinitive so that no photons arrived for a zero to compare with [18] but for subsequent calculations a more realistic value of 10 dB was employed meaning that, using a mean number λ of primary electrons, $\lambda_1 = \lambda + \lambda_d; \lambda_0 = \varepsilon\lambda + \lambda_d$ with ε being equal to the inverse of the numerical value of the extinction ratio. Figure 3-2 shows the BER as a function of the mean number of primary photons for the cases described.

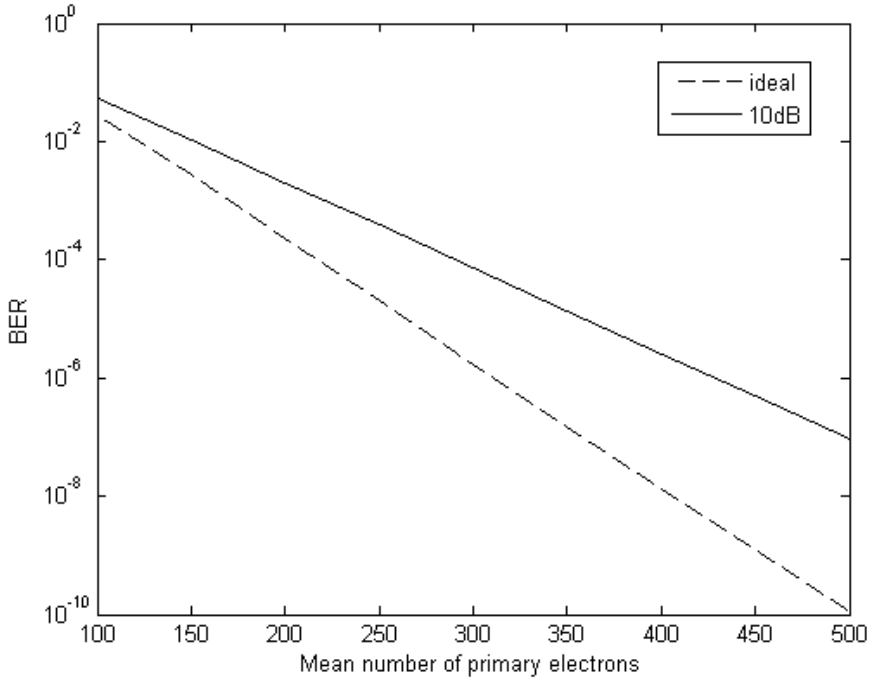

Figure 3-2 BER of SISO APD system for ideal conditions and an extinction ratio of 10 dB

3.4.2 Gaussian Approximation without Fading

For subsequent analysis, a Gaussian approximation to determine the BER was investigated. Although this may well be unsuitable in many applications of APDs [22], it has proved accurate in the modelling of FSO links when the APD gain is large (particularly for high received powers) [23]. To make the approximation, the means and variances of the APD given for the WMC distribution are taken to be the means and variances of Gaussian distributions. The total variance employed in the approximation is that of the variable Z defined for (3.3) above which includes the effect of thermal noise.

The Gaussian approximation requires a suitable decision level to distinguish between zeros and ones. The Bayesian decision rule is commonly employed in digital communication systems [24] and operates by considering the costs of information lost when a one is interpreted as a zero and vice versa. This approach leads to a ratio of the conditional probabilities for the received signal *r* thus:

$$\Lambda(r) = \frac{p(r|0)}{p(r|1)} \underset{0}{\overset{1}{\lessgtr}} \frac{C_0}{C_1}\frac{P(1)}{P(0)} \tag{3.5}$$

where $P(0)$ and $P(1)$ are the probabilities that the receiver transmits a zero and a one respectively, and the respective costs are C_0 and C_1. For a general treatment here, it is assumed that symbols are equally likely as are the costs of their loss. This reduces the receiver likelihood criterion to one of maximum likelihood, which also coincides here with maximum a posteriori probability (MAP) thus:

$$\Lambda(r) = \frac{p(r|0)}{p(r|1)} \underset{0}{\overset{1}{\lessgtr}} 1 \tag{3.6}$$

This is commonly used in a logarithmic form which becomes, for the assumptions above:

$$p(r|0) \underset{0}{\overset{1}{\lessgtr}} p(r|1) \tag{3.7}$$

The above approach may be applied to the SISO case using the Gaussian approximation, when the conditional probabilities, for means and variances of M_0 and M_1, and σ_0^2 and σ_1^2 for zeros and ones respectively, are:

$$p(r|M_1) = \frac{1}{\sqrt{2\pi}\sigma_1} \exp\left\{-\frac{1}{2\sigma_1^2}(r - M_1)^2\right\} \tag{3.8}$$

$$p(r|M_0) = \frac{1}{\sqrt{2\pi}\sigma_0} \exp\left\{-\frac{1}{2\sigma_0^2}(r - M_0)^2\right\} \tag{3.9}$$

So:

$$\Lambda(r) = \frac{\sigma_1}{\sigma_0} \exp\left\{\frac{1}{2\sigma_1^2}(r - M_1)^2 - \frac{1}{2\sigma_0^2}(r - M_0)^2\right\} \underset{0}{\overset{1}{\lessgtr}} 1 \tag{3.10}$$

As it stands, this expression is not tractable but the approach commonly taken in the case of signal dependent noise in optical amplifiers [25] may be employed here. Taking logarithms, the logarithmic ratio between the variances for ones and zeros does not vary much from zero compared to the range of the squared terms and so may be neglected. Hence,

$$\sigma_0^2(r - M_1)^2 \underset{1}{\overset{0}{\lessgtr}} \sigma_1^2(r - M_0)^2 \tag{3.11}$$

Now, consider a decision level $M_0 \leq d \leq M_1$. At the point of decision between a one and a zero, the two sides are equal but care must be taken to make the brackets on both sides positive when taking the square root to obtain *d* thus:

$$\sigma_0(M_1 - d) = \sigma_1(d - M_0)$$

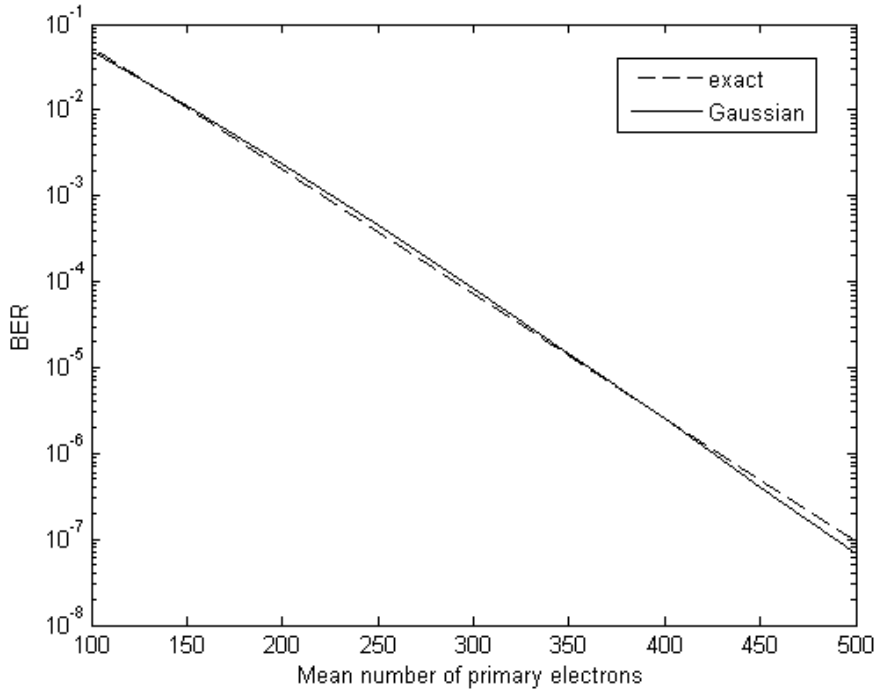

Figure 3-3 BER using large deviations and the Gaussian approximation for a 10 dB extinction ratio

$$\Rightarrow d = \frac{(\sigma_0 M_1 + \sigma_1 M_0)}{\sigma_1 + \sigma_0} \tag{3.12}$$

By substituting this into the standard Gaussian integral for the probability of error for a one or a zero which are both equal for this threshold, a BER expression for a given signal strength results thus:

$$P_{eSISO} = \frac{1}{2}\mathrm{erfc}\left[\frac{\rho}{\sqrt{2}}\right] \tag{3.13}$$

where the ratio ρ is given by $(M_1 - M_0)/(\sigma_1 + \sigma_0)$ and the means and variances of the signals for the one and zero pulses are those obtained from the WMC distribution.

Figure 3-3 shows the Gaussian approximation obtained from (3.13) and the large deviations results plotted for both the ideal case and for the 10 dB extinction ratio with the other parameters as before. It may be observed that the agreement is

generally good and leads to a tractable analysis for the later work for a small accuracy penalty. It is more conventional to display the results using a dB *x*-axis based on the mean transmitted energy employed (dBJ) [23]. This is obtained for a carrier frequency *f* and including Planck's constant thus:

$$dBJ = 10\log_{10}\{0.5(1+\varepsilon)\lambda hf\} \tag{3.14}$$

The results of this axis change using a wavelength of 1550 nm are shown in Figure 3-4 below, where it may be observed that useful performance (significantly falling BER) begins at approximately -170 dBJ, which is in line with the work in [23].

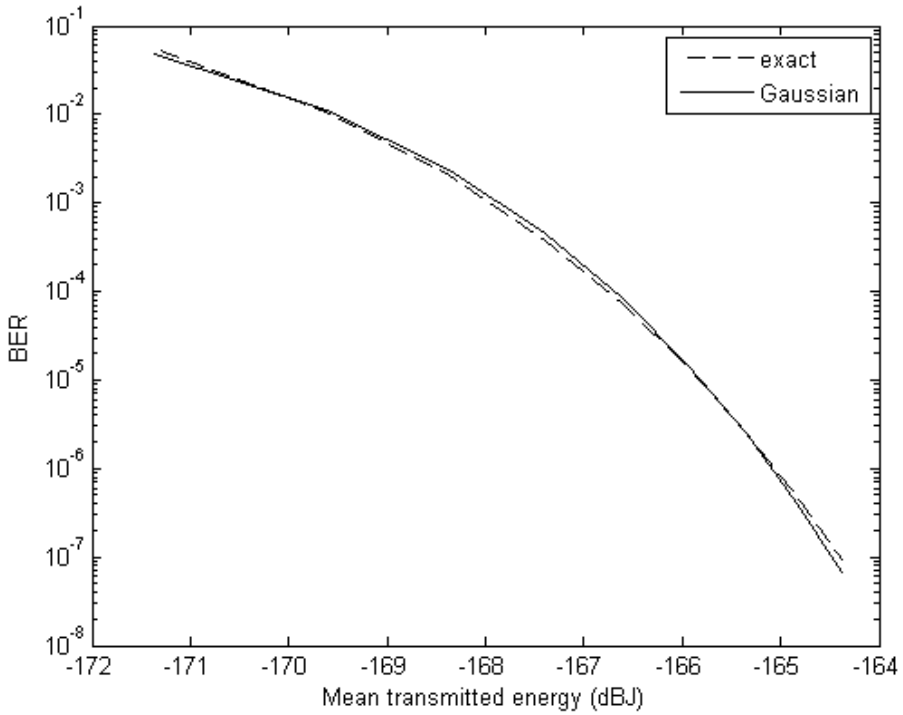

Figure 3-4 Figure 3-3 plotted using a dBJ *x*-axis

3.4.2 Gaussian Approximation with Fading

A similar analysis to that for SISO above begins with

$$p(r|I,M_1) = \frac{1}{\sqrt{2\pi}\sigma_1}\exp\left\{-\frac{1}{2\sigma_1^2}(r-IM_1)^2\right\} \tag{3.15}$$

$$p(r|I,M_0) = \frac{1}{\sqrt{2\pi}\sigma_0}\exp\left\{-\frac{1}{2\sigma_0^2}(r-IM_0)^2\right\} \tag{3.16}$$

where I is the intensity of the fade; for simplicity strong fading is assumed [26], having a PDF of:

$$p(I) = e^{-I},\ 0 \le I \le \infty \tag{3.17}$$

Thus the BER conditioned on I becomes:

$$P_{eSISO}(I) = \frac{1}{2}\mathrm{erfc}\left[\frac{I\rho}{\sqrt{2}}\right] \tag{3.18}$$

To obtain the mean BER, the expectation over all I must be taken:

$$P_{eSISO} = \frac{1}{2}\int_0^\infty \mathrm{erfc}\left[\frac{I\rho}{\sqrt{2}}\right] e^{-I} dI \tag{3.19}$$

This is amenable to integration by parts to give:

$$P_{eSISO} = \frac{1}{2}\left[1 - e^{\frac{1}{2\rho^2}}\right]\mathrm{erfc}\left[\frac{1}{\sqrt{2}\rho}\right] \tag{3.20}$$

Plotting the results for transmission with and without fading in Figure 3-5 shows that there is substantial power penalty incurred. In fact, an error floor appears at a BER value in excess of 10^{-2} making the system essentially unusable.

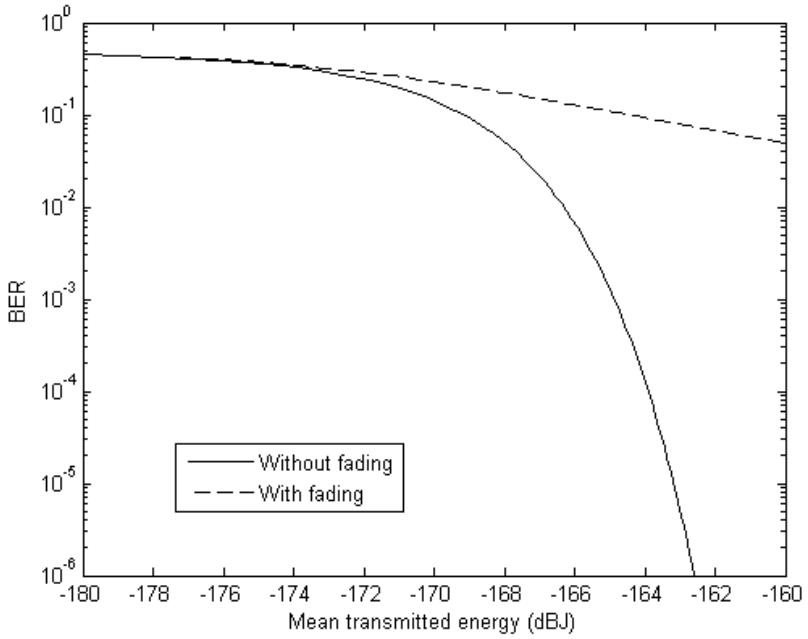

Figure 3-5 The BER results with and without fading.

3.5 OW Diversity

When using coherent receivers, the transmission of the same optical signal from multiple antennas (known as repetition coding or RC) is similar to RF in that it does not produce any diversity gain [27]. However, if the separation of the transmitters is such that they may effectively be considered as independent repetition coding, this will produce diversity gain [28], [29]. Indeed it may outperform the employment of space time (ST) codes [30] such as a modified Alamouti scheme [31]. Thus in this chapter RC is employed both because of its performance and also since it is less complex than ST coding.

3.6 Transmitter Diversity MISO (Multiple input single output) System

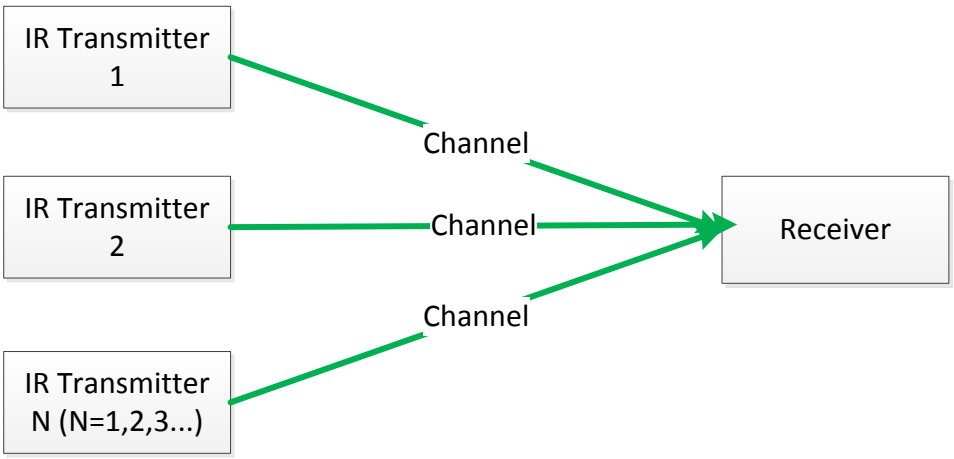

Figure 3-6 OW MISO System

The diagram flow of MISO system was shown above. Using *M* transmitters means that the results of transmission over *M* fading paths with gains I_{m} arrive at the receiver. Taking the transmitted signals here as s_1 for one and s_1 for zero, the conditional probabilities become:

$$p(r|s_1, I_m) = \frac{1}{\sqrt{2\pi}\sigma_1} \exp\left\{-\frac{1}{2\sigma_1^2}(r - s_1 \sum_{m=1}^{M} I_m)^2\right\} \tag{3.21}$$

$$p(r|s_0, I_m) = \frac{1}{\sqrt{2\pi}\sigma_0} \exp\left\{-\frac{1}{2\sigma_0^2}(r - s_0 \sum_{m=1}^{M} I_m)^2\right\} \tag{3.22}$$

The same arguments as in the previous section may be applied to the ratio of the variances and thus (3.11) for this case becomes:

$$\sigma_0^2(r - s_1 \sum_{m=1}^{M} I_m)^2 \underset{1}{\overset{0}{\lessgtr}} \sigma_1^2(r - s_0 \sum_{m=1}^{M} I_m)^2 \tag{3.23}$$

Continuing with the same logic produces a threshold:

$$d = \frac{\sum_{m=1}^{M} I_m(\sigma_0 s_1 + \sigma_1 s_0)}{\sigma_1 + \sigma_0} \tag{3.24}$$

The actual values of s_1 and s_0 must be scaled by M so that the total power of the diversity system is the same as that of the original SISO link, i.e. $s_1 = M_1/M\,; s_0 = M_0/M$. Here, substitution into the standard Gaussian integral and taking the expectation delivers:

$$P_{eMISO} = \frac{1}{2}\int_{\mathbf{I}} \operatorname{erfc}\left\{\frac{(\sum_{m=1}^{M} I_m)\rho}{\sqrt{2}M}\right\} \prod_{m=1}^{M} e^{-I_m}\, d\mathbf{I} \tag{3.25}$$

In general, this multidimensional integral will be intractable but for two transmitters it becomes:

$$P_{eMISO} = \frac{1}{2}\int_0^{\infty}\int_0^{\infty} \operatorname{erfc}\left\{(I_1 + I_1)\frac{\rho}{2\sqrt{2}}\right\} e^{-I_1} e^{-I_2} dI_1 dI_2 \tag{3.26}$$

This may again be tackled by parts and becomes, after some algebraic manipulation:

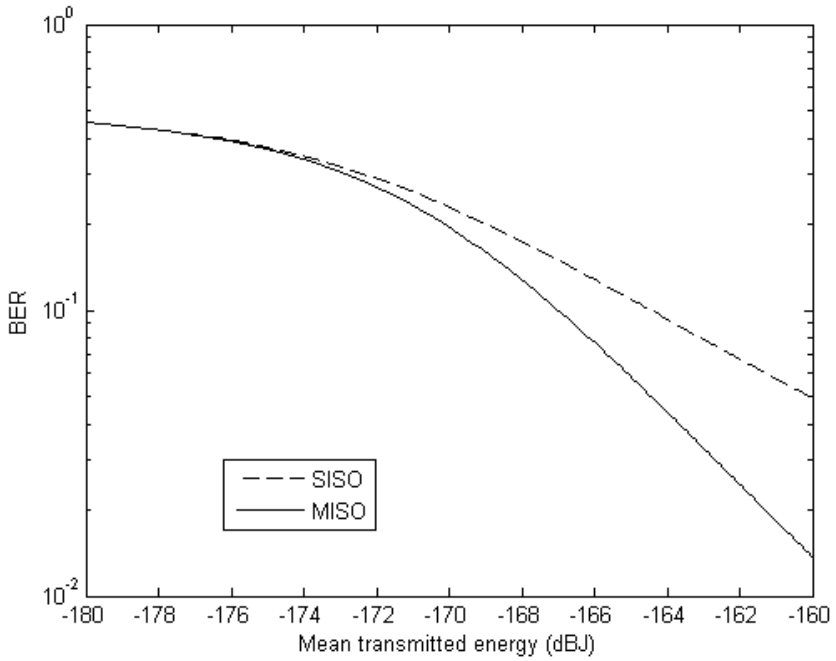

Figure 3-7 BER for SISO and 2-1 MISO

$$P_{eMISO} = \frac{1}{2}\left[1 - \frac{2}{\rho}\sqrt{\frac{2}{\pi}}\right] - \frac{1}{2} e^{\frac{2}{\rho^2}} \operatorname{erfc}\left[\frac{\sqrt{2}}{\rho}\right]\left[1 - \frac{4}{\rho^2}\right] \tag{3.27}$$

The results of the 2-1 MISO system are shown in Figure 3-xx with the SISO fading curve for comparison. It may easily be seen that the MISO approach delivers a gain of some 3-4 dB.

In general, the analytical process is too cumbersome for all but the smallest systems and so another approach to the multidimensional integral is needed. In some cases, analytical reductions to one dimension may be found [29] but in general, purely numerical approaches are needed.

3.6.1 Monte Carlo Integration

In the absence of a tractable analytical solution, it is commonplace to utilize deterministic quadrature rules (e.g. trapezoidal, Simpson's) [32] to produce a numerical approximation to the required integral. There is, however, another approach based on random samples, the Monte Carlo approach [33]. Considering the integral:

$$G = \int_a^b g(x)dx \tag{3.28}$$

This can be considered as the expectation $E[g(U)]$, where U is a random variable that is uniformly distributed $[a, b]$. An approximation to the expectation may be found by considering a sequence of random numbers $U_1, U_2, \dots, U_N$ drawn from the uniform distribution when:

$$G \approx \frac{(b-a)}{N} \sum_{n=1}^{N} g(U_n) \tag{3.29}$$

Although this method does not compete in terms of efficiency with deterministic quadrature rules, offering slow convergence needing many samples, it does come into its own for multi-dimensional integrals since the number of samples required to achieve a given accuracy is independent of the dimension of the integral. This is markedly different from deterministic quadrature rules, where the number of integration points typically increases exponentially with the dimension.

Nevertheless, the choice of randomly placed samples is not efficient since it is very likely that the majority of the contribution to a multidimensional integral is concentrated in a small region of the state space [34]. Fortunately, there is a way to speed up the process and this will now be described.

3.6.2 Importance Sampling

The problem with plain MC is that it does not sample the solution space intelligently so many of the trials will not add to the knowledge already gained (nothing interesting happens). To sharpen the tool of numerical simulation, Importance Sampling (IS) may be employed [33]. This approach may be explained beginning with an integral of the form

$$P_e = \int_{\mathbf{I}} f(\mathbf{I}) d\mathbf{I} \tag{3.30}$$

This may be rewritten as:

$$P_e = \int_{\mathbf{I}} \left[\frac{f(\mathbf{I})}{p(\mathbf{I})}\right] p(\mathbf{I}) d\mathbf{I} \tag{3.31}$$

where the function $p(\mathbf{I})$ is the joint probability distribution of the vector **I**. The integral can then be evaluated by sampling according using $p(\mathbf{I})$ and forming the sum:

$$P_{eK} = \frac{1}{K}\sum_{n=1}^{N}\left[\frac{f(\mathbf{I}_k)}{p(\mathbf{I}_k)}\right] \tag{3.32}$$

The function $p(\mathbf{I})$ should be chosen so that the chance of producing values making a large contribution to the integral is increased, and hence the variance of the estimate is reduced. In the case of (MISO) above, the form of the integral immediately suggests that $p(\mathbf{I}) = \prod_{m=1}^{M} e^{-I_m}$. This results in:

$$P_{eN} = \frac{1}{2K}\sum_{k=1}^{K}\operatorname{erfc}\left\{\frac{(\sum_{m=1}^{M} I_{mk})\rho}{\sqrt{2}M}\right\} \tag{3.33}$$

with the I_{mk} values drawn from identical unit mean exponential distributions. To illustrate the effectiveness of IS in comparison with straight MC, the MISO results from (3.27) above were simulated using MC with 10^6 sampling points and IS using just 2×10^4 points. The results are shown along with the analytical solution in Figure 3-8 below. It is apparent that IS achieves the same level of accuracy with far fewer points. In fact, the number of points could probably be reduced but was left at the value of 2×10^4 for all subsequent simulations since the running time was not prohibitive (1 second to produce the curve shown compared to in excess of 40

seconds for straight MC).

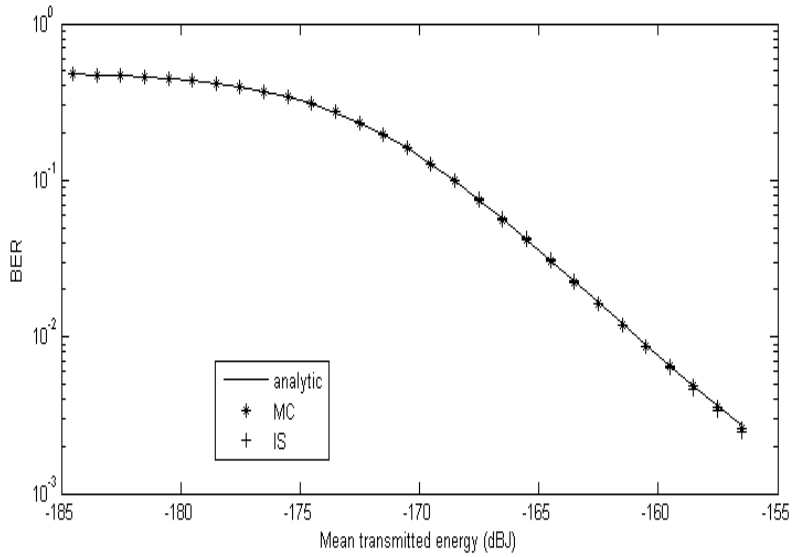

Figure 3-8 Comparison of analytical, MC and IS BER results for MISO Systems

Employing IS also facilitates extension to cases where the analytical solution would be difficult or impossible. To illustrate this, results using IS for a 4-1 MISO system are presented in Figure 3-9 along with the previous 2-1 MISO results. It may be seen that several extra dBs of gain result from the extension to more transmitters.

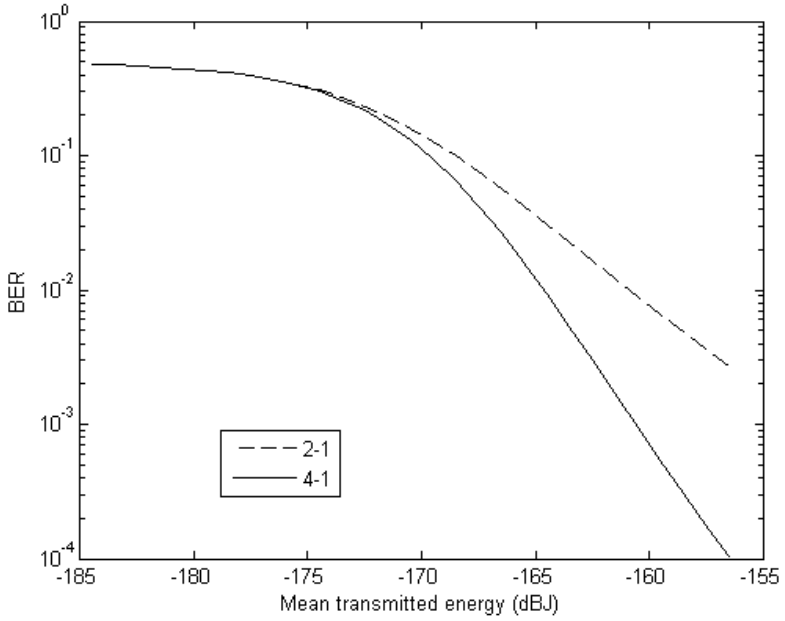

Figure 3-9 BER results for 4-1 and 2-1 MISO obtained using IS

3.7 Receiver Diversity SIMO (single input multiple output) System

It is also possible to introduce diversity at the receiver as forming a single input multiple output or SIMO system as shown in Figure 3-10.

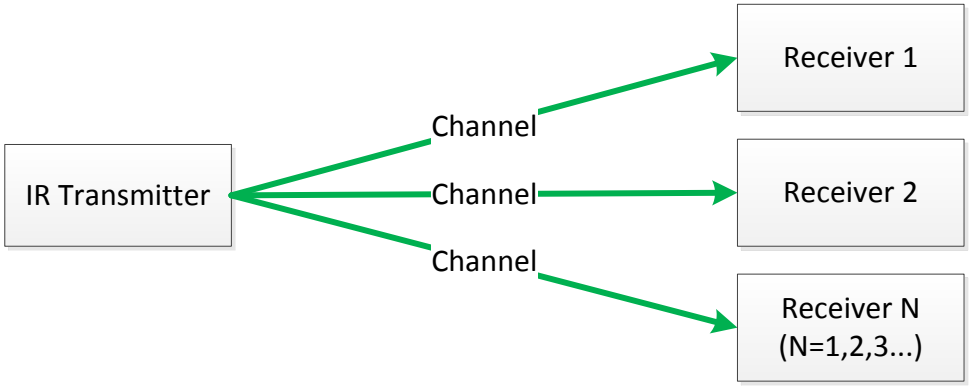

Figure 3.10 OW SIMO System

Using *N* transmitters means that the results of transmission over *N* fading paths with gains I_n arrive at the receiver. Taking the transmitted signals again as s_1 for one and s_0 for zero, the conditional probabilities become:

$$p(\mathbf{r}|s_1,\mathbf{I}) = \frac{1}{\left(\sqrt{2\pi}\sigma_1\right)^N}\exp\left\{-\frac{1}{2\sigma_1^2}\sum_{n=1}^{N}(r_n - s_1 I_n)^2\right\} \tag{3.34}$$

$$p(\mathbf{r}|s_0,\mathbf{I}) = \frac{1}{\left(\sqrt{2\pi}\sigma_0\right)^N}\exp\left\{-\frac{1}{2\sigma_0^2}\sum_{n=1}^{N}(r_n - s_0 I_n)^2\right\} \tag{3.35}$$

This time, there is a vector of **r** values and the presence of the summation over *N* means that the approach taken above will not work since there is now a sum of squared terms. To produce a tractable and straightforward solution one may consider the cause of the problem, i.e. the different variances that occur for zeros and ones. This suggests a bounding approach where an upper bound on the BER may be

obtained by setting the variance to σ_1 in both (3.34) and (3.35), taking the likelihood ratio and cancelling the common terms thus:

$$\sum_{n=1}^{N}(r_n - s_1 I_n)^2 \underset{1}{\overset{0}{\lessgtr}} \sum_{n=1}^{N}(r_n - s_0 I_n)^2 \tag{3.36}$$

By multiplying out the squares and tidying up the expression, the condition becomes:

$$\sum_{n=1}^{N} r_n I_n \underset{1}{\overset{0}{\lessgtr}} \frac{1}{2}(s_1 + s_0)\sum_{n=1}^{N} I_n^2 \tag{3.37}$$

Thus, for an error to occur when a zero arrives with a noise sample ν_n drawn from the Gaussian distribution present for ones:

$$P_{eSIMO}(0, UB|\mathbf{I}) = p\left(\sum_{n=1}^{N} r_n I_n > \frac{1}{2}(s_1 + s_0)\sum_{n=1}^{N} I_n^2 \,\middle|\, r_n = s_0 I_n + \nu_n\right)$$

$$= p\left(\sum_{n=1}^{N} I_n \nu_n > \frac{1}{2}(s_1 - s_0)\sum_{n=1}^{N} I_n^2\right) \tag{3.38}$$

The sum $\sum_{n=1}^{N} I_n \nu_n$ represents a Gaussian random variable with zero mean and variance $\sum_{n=1}^{N} I_n^2 \sigma_1^2$. Substituting this into the integral to obtain the BER produces:

$$P_{eSIMO}(0, UB|\mathbf{I}) = \frac{1}{2}\mathrm{erfc}\left[\frac{M_1 - M_0}{2\sqrt{2}N\sigma_1}\sqrt{\sum_{n=1}^{N} I_n^2}\right] \tag{3.39}$$

This time, the scaling factor of N is present to ensure that the sum of the N receiver aperture areas is the same as that of the SISO link. Repeating the process produces an identical expression for $P_{eSIMO}(1, UB|I_n)$ and so for equiprobable ones and zeros:

$$P_{eSIMO}(UB, \mathbf{I}) = \frac{1}{2}\mathrm{erfc}\left[\frac{M_1 - M_0}{2\sqrt{2}N\sigma_1}\sqrt{\sum_{n=1}^{N} I_n^2}\right] \tag{3.40}$$

Taking the variance of the zero bits, will produce

$$P_{eSIMO}(LB,\mathbf{I}) = \frac{1}{2}\text{erfc}\left[\frac{M_1-M_0}{2\sqrt{2}N\sigma_0}\sqrt{\sum_{n=1}^{N} I_n^2}\right] \tag{3.41}$$

Finally, the upper and lower bound integrals to remove the conditioning on I are:

$$P_{eSIMO}(UB) = \frac{1}{2}\int_{\mathbf{I}} \text{erfc}\left\{\frac{M_1-M_0}{2\sqrt{2}N\sigma_1}\sqrt{\sum_{n=1}^{N} I_n^2}\right\}\prod_{n=1}^{N} e^{-I_n}\, d\mathbf{I} \tag{3.42}$$

$$P_{eSIMO}(LB) = \frac{1}{2}\int_{\mathbf{I}} \text{erfc}\left\{\frac{M_1-M_0}{2\sqrt{2}N\sigma_0}\sqrt{\sum_{n=1}^{N} I_n^2}\right\}\prod_{n=1}^{N} e^{-I_n}\, d\mathbf{I} \tag{3.43}$$

These are intractable and so may be evaluated using Importance Sampling as in the case of MISO. Performing the IS simulation produces results as shown in Figure 3-11

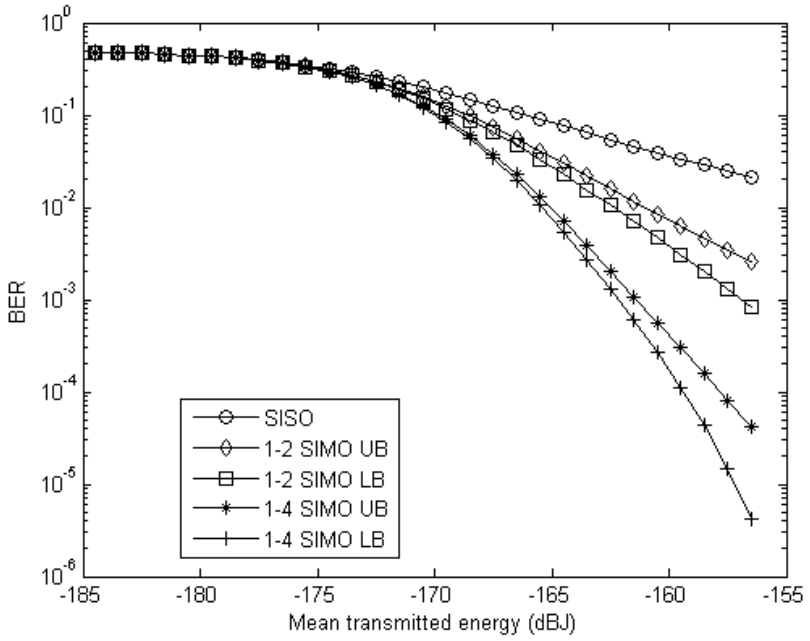

Figure 3-11 BER results for 4-1 and 2-1 SIMO obtained using IS

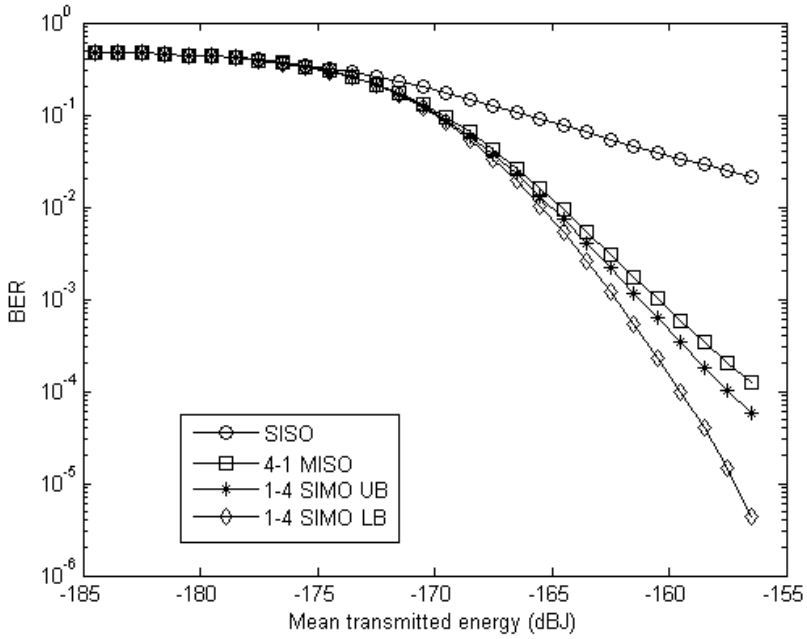

Figure 3-12 BER results for 1-4 SIMO and 4-1 MISO

It may be clearly seen in Figure 3-11 that the SIMO system offers significant gains over SISO in the fading channel. An interesting question is how SIMO compares with MISO and this is shown in Figure 3-12. It may be seen that SIMO offers a better BER performance because the transmit power is not split so the single link BER is better and there is a diversity combining gain at the receiver.

3.8 Transmitter and Receiver Diversity (MIMO System)

This case combines the previous two sections and so the analysis is much as in the case of SIMO but starting from the conditional probabilities:

$$p(\mathbf{r}|s_1,\mathbf{I}) = \frac{1}{\left(\sqrt{2\pi}\sigma_1\right)^N}\exp\left\{-\frac{1}{2\sigma_1^2}\sum_{n=1}^{N}(r_n - s_1\sum_{m=1}^{M} I_{mn})^2\right\} \tag{3.44}$$

It is also possible to introduce diversity at the receiver as forming a MIMO system as shown in Figure 3-13.

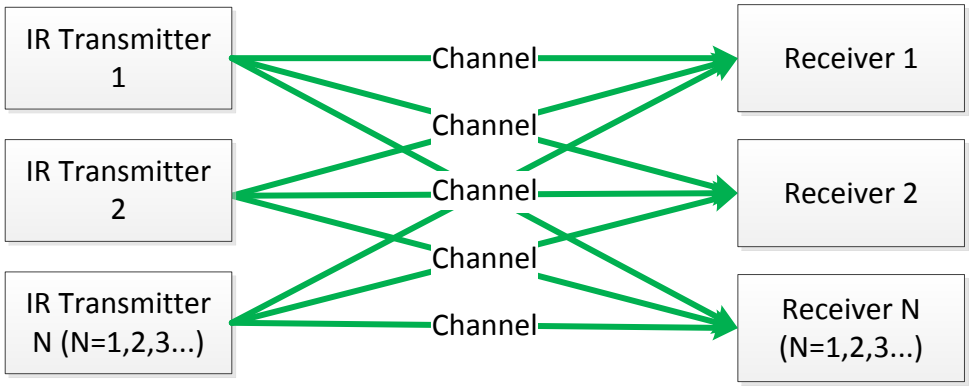

Figure 3-13 OW MIMO System

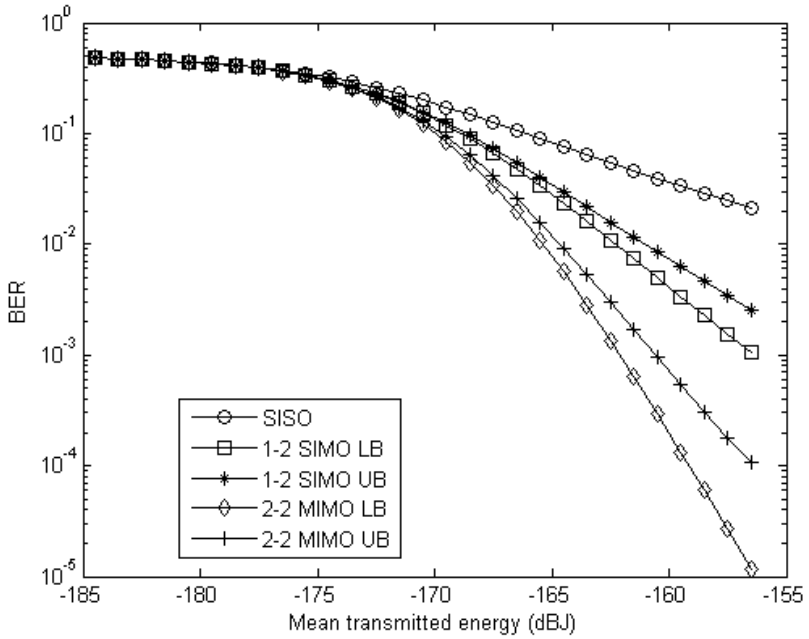

Figure 3-14 BER results for 1-2 SIMO and 2-2 MIMO

$$p(\mathbf{r}|s_0,\mathbf{I}) = \frac{1}{\left(\sqrt{2\pi}\sigma_0\right)^N}\exp\left\{-\frac{1}{2\sigma_0^2}\sum_{n=1}^{N}(r_n - s_0\sum_{m=1}^{M} I_{mn})^2\right\} \quad (3.45)$$

To produce:

$$P_{eMIMO}(UB) = \frac{1}{2}\int_{\mathbf{I}} \operatorname{erfc}\left\{\frac{M_1-M_0}{2\sqrt{2}MN\sigma_1}\sqrt{\sum_{n=1}^{N}(\sum_{m=1}^{M} I_{mn})^2}\right\}\prod_{m=1}^{M}\prod_{n=1}^{N} e^{-I_{mn}}\, d\mathbf{I} \quad (3.46)$$

$$P_{eMIMO}(LB) = \frac{1}{2}\int_{\mathbf{I}} \operatorname{erfc}\left\{\frac{M_1 - M_0}{2\sqrt{2}MN\sigma_0}\sqrt{\sum_{n=1}^{N}(\sum_{m=1}^{M} I_{mn})^2}\right\}\prod_{m=1}^{M}\prod_{n=1}^{N} e^{-I_{mn}}\, d\mathbf{I} \quad (3.45)$$

The form of these equations is similar to those derived previously and so they fit into the same framework for IS evaluation. The results for 2 by 2 and 4 by 4 MIMO are shown in Figures 3-14 and 3-15 compared with 1-2 and 1-4 SIMO since these have been established above as superior to the corresponding MISO options. It may be seen that substantial gain are provided by MIMO, particularly when employing a 4 by 4 system. The error floor is effectively removed and a gain of approximately 6 dB over SIMO results at a BER of 10^{-4}. Although the experimental results will most likely offer less than this, the promise of OW MIMO is confirmed.

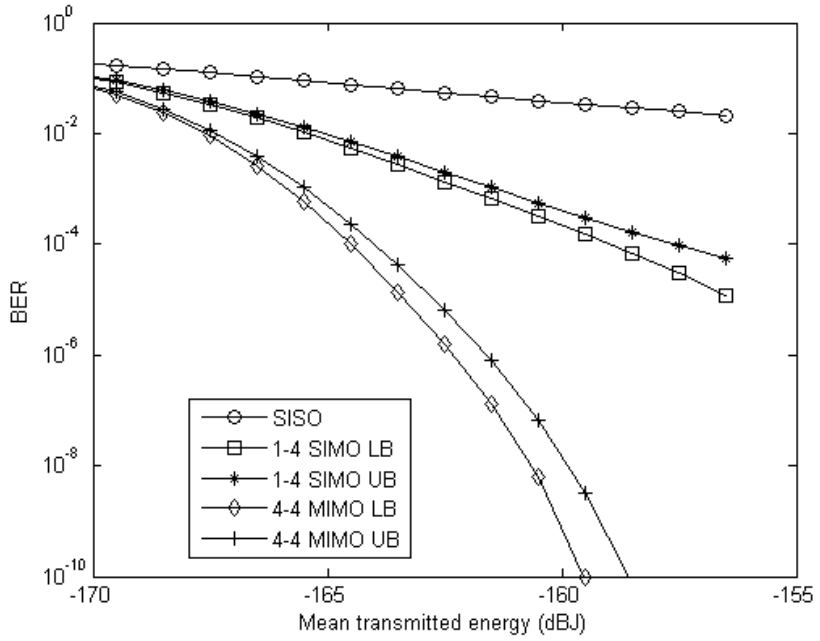

Figure 3-15 BER results for 1-4 SIMO and 4-4 MIMO

3.9 Summary

Since the WMC distribution was first introduced some 40 years ago, OW technology using APD receivers has come into existence. Looking further into long-term and sustainable applications, OW MIMO communications are a highly promising option to present a viable supplemental technology to radio frequency wireless MIMO systems. The technology is considered cost-effective; it delivers substantial bandwidth access and high quality data transmission with no interference to RF based communication signals and highly-secured transmission assurance.

This chapter has provided analyses of important OW configurations using APD receivers. First, the WMC model was employed to analyse the SISO configuration using a large deviations approach. Then, comparison with a Gaussian approximation showed that the latter was reasonable for the parameters considered, and made for a more tractable approach. Thus, an analytical expression for 2-1 MISO was successfully developed. To progress further, simulation was needed and this was implemented via using importance sampling and successfully compared to the analytical results. To complete the results for SIMO and MIMO, upper and lower bounds were introduced and the corresponding BER curves obtained from importance sampling. The chapter illustrates the coding gains possible using diversity schemes for APD OW systems. In the presence of strong fading, the SISO approach is rendered virtually useless, whereas diversity offers acceptable BER values. The results underpin the approach of this thesis, where indoor PIN diode based experimental measurements confirm the gains offered by diversity.

References for Chapter 3

[1] V. W. S. Chan , “Free-space optical communications”, IEEE/OSA Journal of Lightwave Technology, vol. 24, no. 12, pp. 4750-4762, 2006

[2] J. Grubor, S. Randel, K. Dieter Langer, and J.W. Walewski, “Broadband Information Broadcasting Using LED-Based Interior Lighting”, IEEE Journal of Lightwave Technology, vol. 26, no. 24, pp. 3883-3892, 2008.

[3] D. Gesbert, M. Shafi, D.Shiu, P. J. Smith, and A. Naguib, "From theory to practice: an overview of MIMO space-time coded wireless systems," IEEE Journal on Selected Areas in Communications, vol. 21, no. 3, pp. 281-302, 2003.

[4] M. A. Khalighi and M. Uysal, “Survey on Free Space Optical Communication: A Communication Theory Perspective”, IEEE Communications Surveys and Tutorials, vol. 16, no. 4, pp. 2231-2258, 2014.

[5] T. Fath and H. Haas, “Performance Comparison of MIMO Techniques for Optical Wireless Communications in Indoor Environments”, IEEE Transactions on Communications, vol. 61, no. 2, pp. 733- 742, 2013.

[6] S. Hranilovic, Wireless Optical Communication Systems, *Springer*, 2004.

[7] P. P. Webb, R. J. McIntyre and J. Conradi, “Properties of Avalanche Photodiodes”, RCA Review, vol. 35, pp. 234-278, 1974.

[8] H. Le Minh, Z.Ghassemlooy, D. O’Brien, G. Faulkner, “Indoor Gigabit Optical Wireless Communications - Challenges and Possibilities”, *Proc. 12th IEEE Conference on Transparent Optical Networks (ICTON)*, 2010 [6 pages].

[9] H. Le-Minh, D. O’Brien, G. Faulkner, L. Zeng, K. Lee, D. Jung, and Y. Oh, “High-speed visible light communications using multiple-resonant equalization”, *IEEE Photonics Technology Letters,* vol. 20, no. 14, pp. 1243-

1245, 2008.

[10] J. Grubor, K.-D. Langer, S. C. J. Lee, T. Koonen, and J. W. Walewski, "Wireless high-speed data transmission with phosphorescent white-light LEDs", *Proc. 23rd European Conference and Exhibition of Optical Communication (ECOC)*, 2007 [2 page post deadline paper].

[11] C. H. Yeh, Y. L. Liu and C. W. Chow, "Real-time white-light phosphor-LED visible light communication (VLC) with compact size", Optics Express, vol. 21, no. 22, pp. 26192-26197, 2013.

[12] J.-Y.Sung, C.-W. Chow and C.-H.Yeh, "Is blue optical filter necessary in high speed phosphor-based white light LED visible light communications?", Optics Express, vol. 22, no. 17, pp. 20646-20651, 2014.

[13] S.G. Wilson, M. Brandt-Pearce, Q. Cao and J. Leveque, "Free-space optical MIMO transmission with Q-ary PPM." IEEE Transactions on Communications, vol. 53, no. 8, pp. 1402-1412, 2005.

[14] S. Hranilovic, Wireless Optical Communication Systems, *Springer*, 2005.

[15] R. J. McIntyre, "The distribution of gains in uniformly multiplying avalanche photodiodes: Theory," IEEE Transactions on Electron Devices, vol. 19, no. 6, pp. 703–713, 1972.

[16] J. J. Conradi, "The distribution of gains in uniformly multiplying avalanche photodiodes: Experimental," IEEE Transactions on Electron Devices, vol. 19, no. 6, pp. 714–718, June 1972.

[17] K. R. Baker, "On the WMC density as an inverse Gaussian probability density," IEEE Transactions on Communications, vol. 44, no. 1, pp. 15–17, Jan. 1996.

[18] J. T. K. Tang and K. B. Letaief, "The use of WMC distribution for performance evaluation of APD optical communication systems", IEEE Transactions on

Communications, vol. 46, no. 2, 279-285, 1998.

[19] K. B. Letaief and J. S. Sadowsky, "Computing bit-error probabilities for avalanche photodiode receivers by large deviations theory," IEEE Transactions on Information Theory, vol. 38, no. 3, pp. 1162–1168, 1992.

[20] J. R. F. Da Rocha and J. J. O'Reilly, "Modified Chernoff bound for binary optical communication," Electronics Letters, vol. 18, no. 16, pp. 708–710, 1982.

[21] J. R. Barry, Wireless Infrared Communications, *Kluwer*, 1994.

[22] F. M. Davidson and X. Sun, "Gaussian approximation versus nearly exact performance analysis of optical communication systems with PPM signalling and APD receivers", IEEE Transactions on Communications, vol. 36, no. 11, pp.1185 -1191, 1988.

[23] N. Cvijetic, N., S. G. Wilson and M. Brandt-Pearce, "Performance Bounds for Free-Space Optical MIMO Systems with APD Receivers in Atmospheric Turbulence", IEEE Journal on Selected Areas in Communications, vol. 26, no. 3, pp. 3-12, 2008.

[24] I. A. Glover and P. M. Grant, Digital Communications, *Prentice-Hall*, 2004

[25] G. Einarsson, Principles of Lightwave Communications, *Wiley*, 1996.

[26] H.E. Nistazakis, V.D. Assimakopoulos , G.S. Tombras, "Performance estimation of free space optical links over negative exponential atmospheric turbulence channels", Optik, vol. 122, no. 24, pp. 2191–2194, 2011.

[27] J. He, R. A. Norwood, M. Brandt-Pearce, I. B. Djordjevic, M. Cvijetic, , S. Subramaniam, R. Himmelhuber, C. Reynolds, P. Blanche, B. Lynn and N. Peyghambarian, "A survey on recent advances in optical communications", Computers & Electrical Engineering, vol. 40, no. 1, pp. 216–240, 2014.

[28] E. J. Lee and V. W. S. Chan, "Part 1: optical communication over the clear turbulent atmospheric channel using diversity", IEEE Journal on Selected Areas in Communications, vol. 22, no. 9, pp. 1896-1906, 2004.

[29] S. M. Navidpour, M. Uysal, and M. Kavehrad, "BER performance of free-space optical transmission with spatial diversity," IEEE Transactions on Wireless Communications, vol. 6, no. 8, p. 2813-2819, 2007

[30] M. Safari and M. Uysal, "Do We Really Need OSTBCs for Free-Space Optical Communication with Direct Detection?", IEEE Transactions on Wireless Communications, vol. 7, no. 11, pp. 4445-4448, 2008.

[31] M. K. Simon and V. A. Vilnrotter, "Alamouti-type space-time coding for free-space optical communication with direct detection," IEEE Transactions on Wireless Communications., vol. 4, no. 1, pp. 35–39, 2005.

[32] L. M. Delves and J. L. Mohamed, Computational Methods for Integral Equations, *Cambridge University Press*, 1985.

[33] P. Brandimarte, Numerical methods in finance and economics: a MATLAB-based introduction, Hoboken, *Wiley Interscience*, 2006.

[34] D. J. C. MacKay, Information Theory, Inference, and Learning Algorithms, *Cambridge University Press*, 2003.

Chapter 4 Optical Wireless MIMO System Based on OOK Modulation

4.1 Introduction

In Chapter 3, it was concluded that the avalanche photodiode demonstrates multiple advantages in long distance transmissions. However, it proves not to be desirable as an indoor optical wireless MIMO system (the noise power increases faster than the signal power due to the gain of APDs). Consequently, under the conditions of low bandwidth and high signal power, the PIN diode is recommended as the receiver of indoor optical wireless system. This chapter describes the process of designing an infrared MIMO system using OOK modulation performing data transmission at various distances.

4.2 System Model

In the system model used to design the lab experiments, two primary parameters, namely, the diversity gain and the multiplexing gain, are considered. Initially, a typical switching criterion designed to enhance channel quality is set at 20bits, and the testing symbols are sent as pilots to each transmitter. The controller is designed

to evaluate the BER performance, and the principle data symbols (i.e. 500bits) are transmitted to those evaluated with better performance. The process is designed to generate multiplexing gains. The data rate is then doubled by using two transmitters at the same time, whereas each transmitter transmits the same data, when diversity gain can be generated.

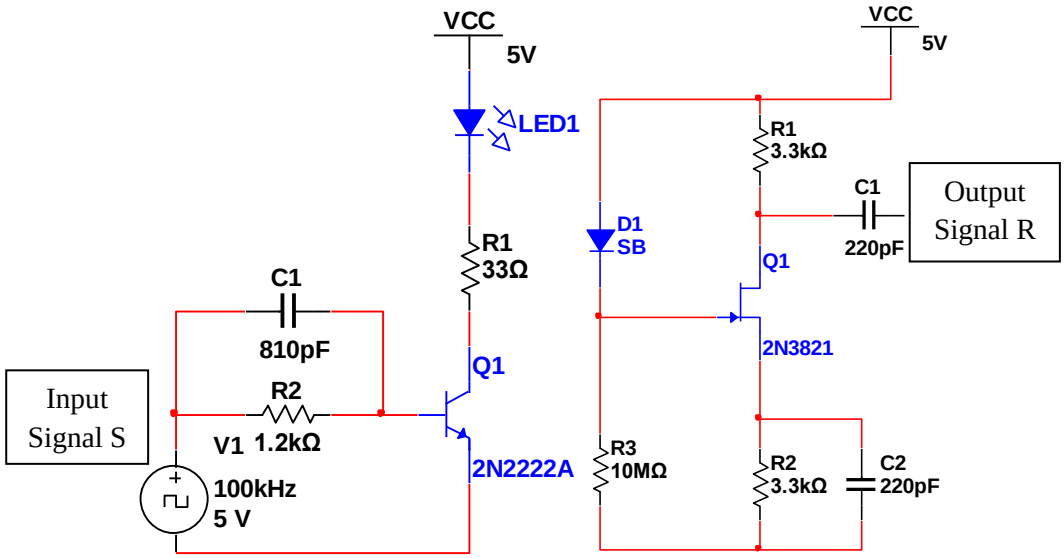

(a) (b)

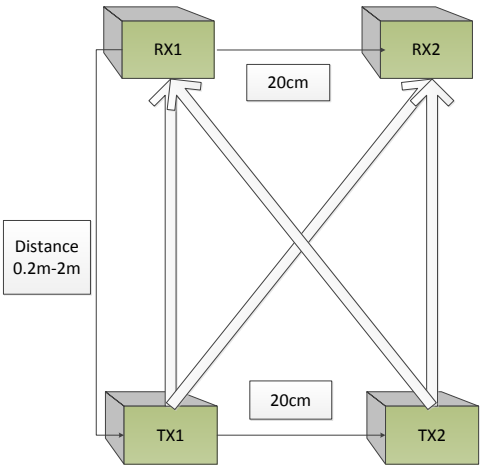

(c)

Figure 4-1 (a) Transmitter circuit; (b) Receiver circuit; (c) Indoor infrared 2X2 MIMO system schematic.

In Figure 4-1(a) and (b), the illustrations show the process of the transmitter and receiver circuit in which the receiver is only shown with the photodiode driver circuit. The receiver is designed with an amplifier and comparator to improve the performance of the data rate at 1Mbps and 10Mbps. In Figure 1(c), the schematic of the LOS system shows the configuration of the infrared LED transmitters and detectors. The infrared LEDs and photodiode are fixed at the same height, and the distance of the two LEDs is designed at 20cm apart, as are the photodiodes. The experiments are conducted under indoor lighting conditions and an ambient temperature of 25^0C. The major parameters of the LOS system are given below:

Table 4-1 Parameters of LOS System

LED Response Time	12ns
Single LED Power	320mW
Emission Angle	$\pm 13^{\circ}$
FOV of Photodiode	$\pm 60^{\circ}$
Physical area of Photodiode	$7.5mm^2$

4.3 Transmitter and Receiver design

As illustrated in Figure 4-1, the theory of the system circuit design has been developed by the research conducted in [1] and [2]. In the experimental process, the value of the resisters and capacitors are changed by taking considerations of the transmission distance and quality in the MHz area.

According to the research conducted in [1] and [2], the basic digital transmitter and receiver circuit used in the SISO system is shown in Figure 4-2. The value of R3 used for the receiver design is corresponding to the value of bandwidth used during the experiment. By taking the case of 1MHz as an example, the equation used for the calculation is shown below:

$$B = \frac{1}{2\pi RC} \tag{4.1}$$

Where B is the bandwidth response as required for the experiment, R refers to the value of $R3$ in the receiver circuit in Figure 4-2 bellow, and C represents the capacitance of the photodiode.

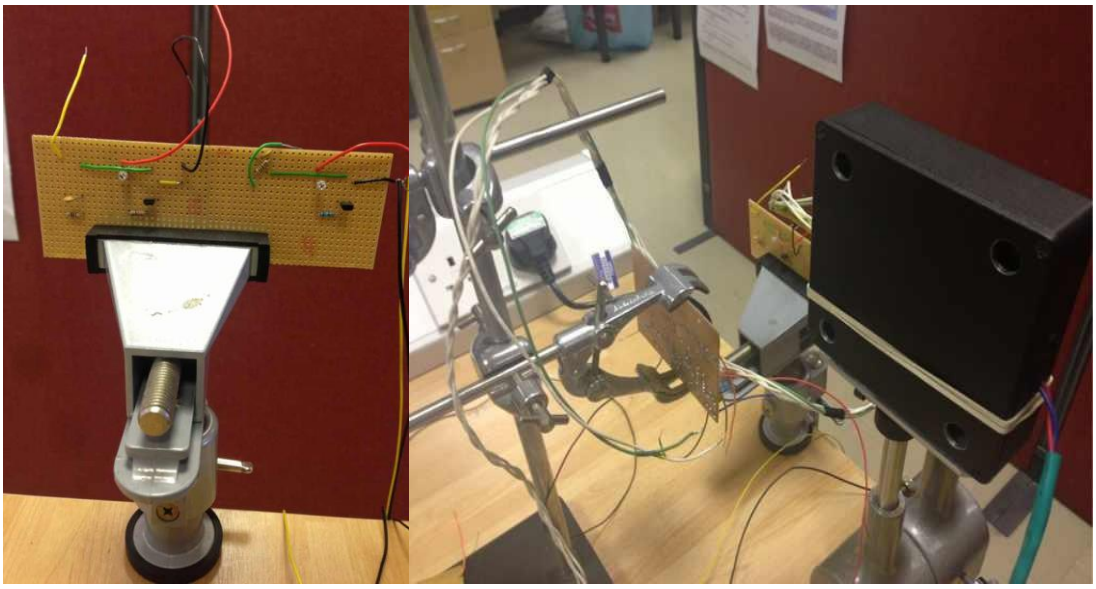

Figure 4-2 (a) Transmitter 100kHz (b) Transmitter 1MHz

In Figure 4-2, it shows the test transmitters which are designed to use a bandwidth of 100kHz and 1MHz bandwidth, first of which can transmit and receive signals of 50-500kHz clearly (these transmitters and receivers are used for test only, the formal

experiment would use PCB board system shown later in this chapter). However, the experiments are limited in using the bandwidth varied from 1MHz to 10MHz, which can't use the designed circuit directly due to the limitation of the high frequency attenuation and shot noise resulting from the configured system.

Figure 4-3 illustrates the performance of the system tested which uses the bandwidths of 100kHz or 1MHz when the transmission distance is 2m. By changing the distance and displacements of the light in the lab, the testing square wave is retained with the shape easily to be identified, hence the performance confirms on the reliability of the designed system of 100kHz. However, when 1 MHz bandwidth is used, unlike those at the lower frequency, the falling edge is unable to return at a low level current. Moreover, by increasing the transmission distance versus angle, the testing square wave declines in intensity.

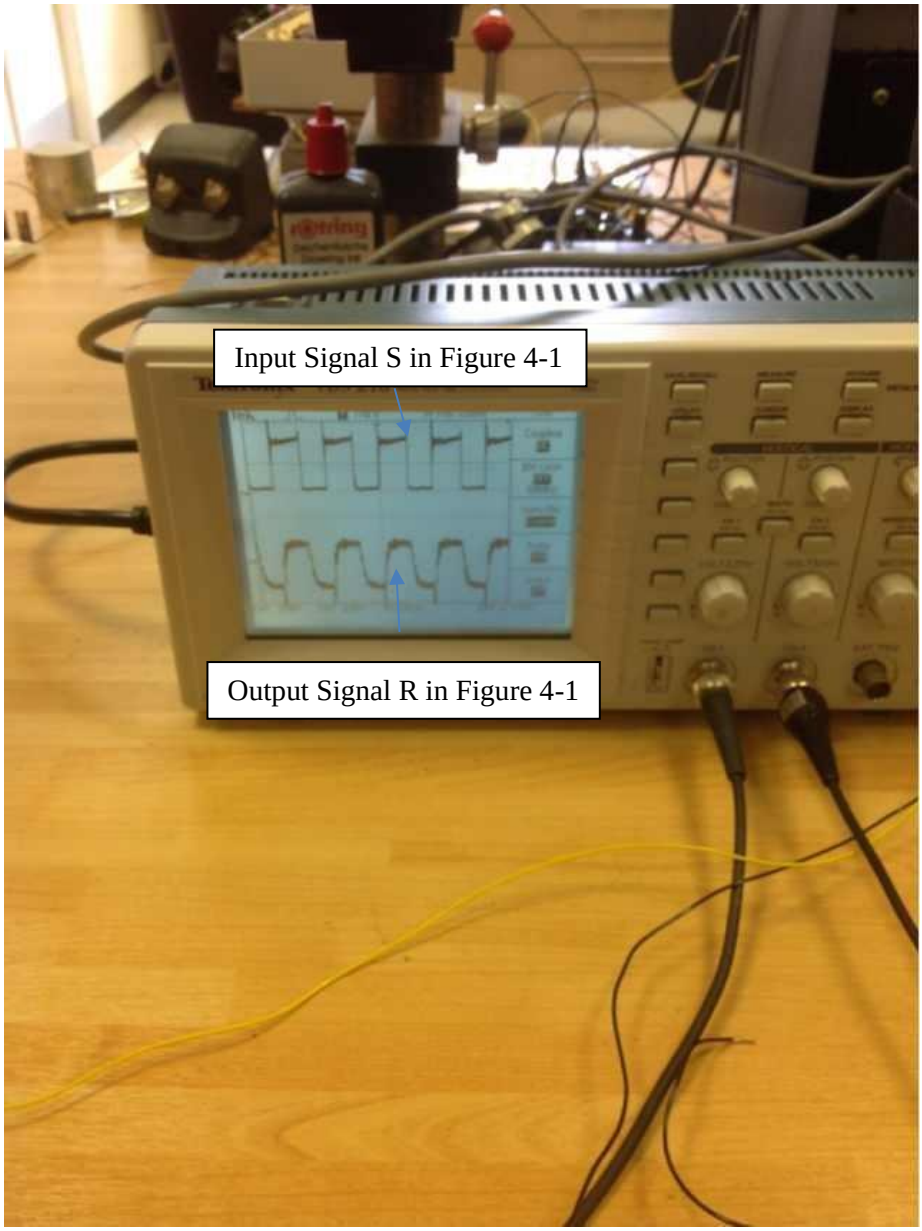

Figure 4-3 Transmitted and Received Tested Signals of 1MHz MIMO System

(Distance in 1m)

In order to solve the problem mentioned above, a new design approach is considered, in which the new values of the resister and the capacitor are estimated and used in the experiments. The results show that the infrared light decays considerably when the transmission, amplifier and comparator of a higher frequency are performed.

During the experiments at the high frequency which varies from 1MHz up to 10MHz, the transmitter is of the following design configuration:

The system shown in Figure 4-4 is capable of working at a frequency up to 1MHz bandwidth. However, as the frequency rises, the performance becomes clearly weaker. On an overall level, the system described above enables the experiments meet the objectives of the research.

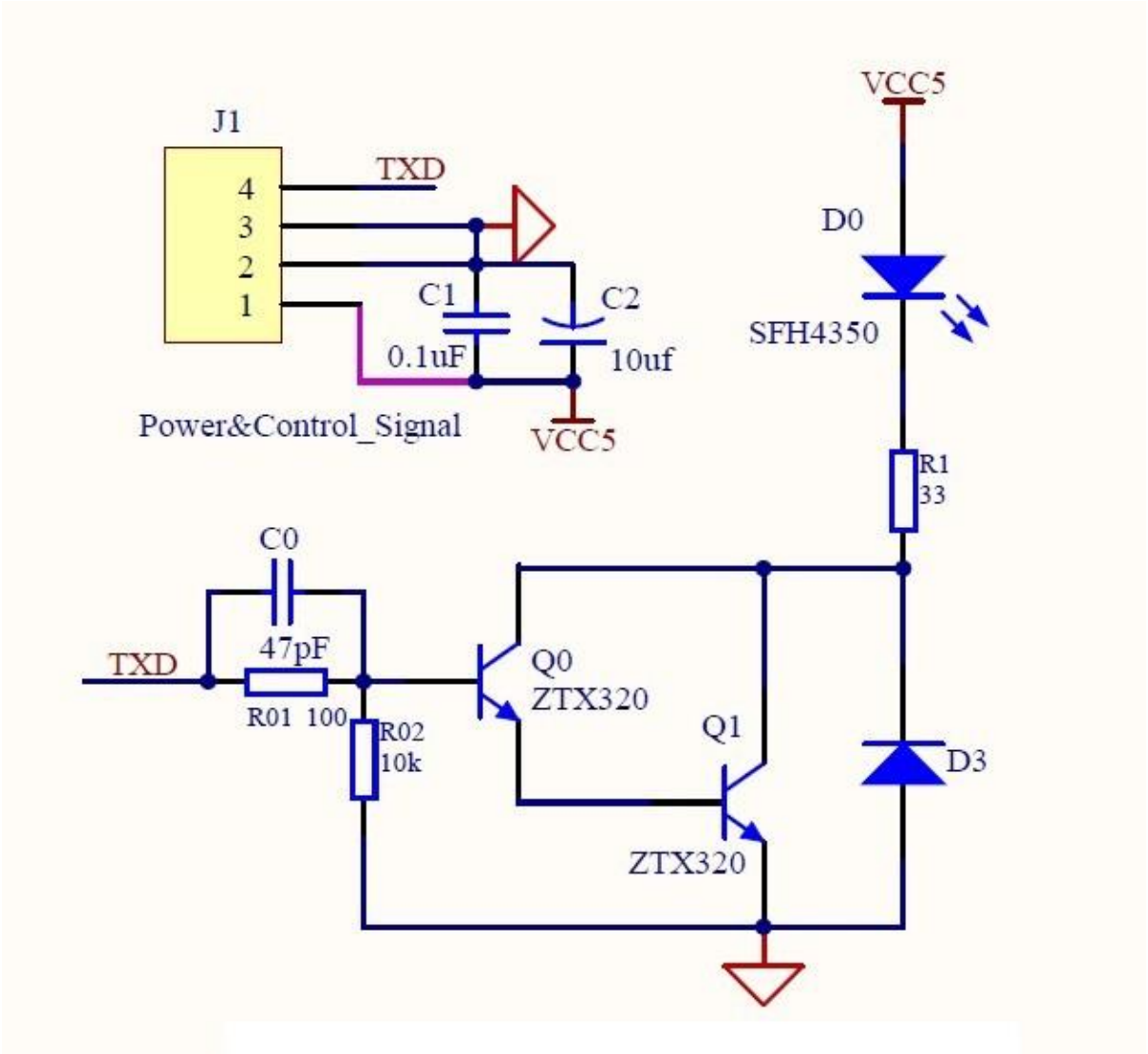

Figure 4-4 1MHz Transmitter Design

Annotations:

J1 is the power supply module used in the transmitters and receivers, where port 1 and 2 is connected with the cathode in order to stablize the voltage. Port 4 is connected to the signal controller. The transmitter at high frequency uses the Darlington circuit to increase the transmission power, whereas the gain changes within an acceptable limit, are consequently, the transmission distance will be increased.

In Figure 4-5, 4-6 and 4-7, the illustrated configurations show the high frequency receiver circuit integrated with AD8055-based amplifiers and comparator. In Figure 4-5, when the signal passes through the first amplifier, the signal voltage will be increased significantly. As shown in Figure 4-6, in order to avoid the noise being amplified, the second amplifier is equipped into the system. A 3^{rd} order Sallen-Key low pass filer is used to connect the two amplifiers, and the amplified noise is filtered out in-between the first and the second amplifier.

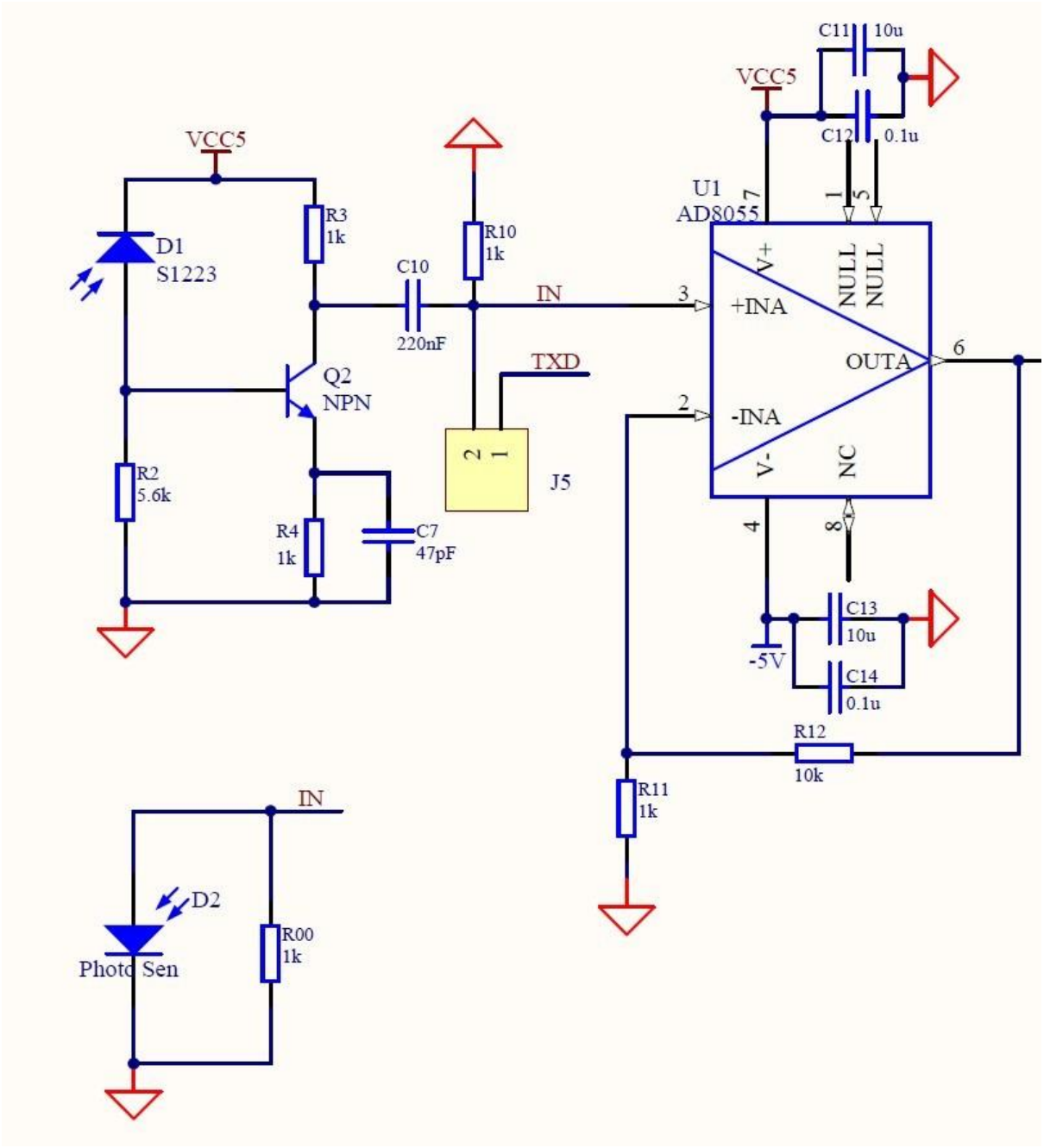

Figure 4-5 Receiver and First Amplifier

J5 is the experimental module used in the lab tests to verify the behaviour of amplifiers and comparator.

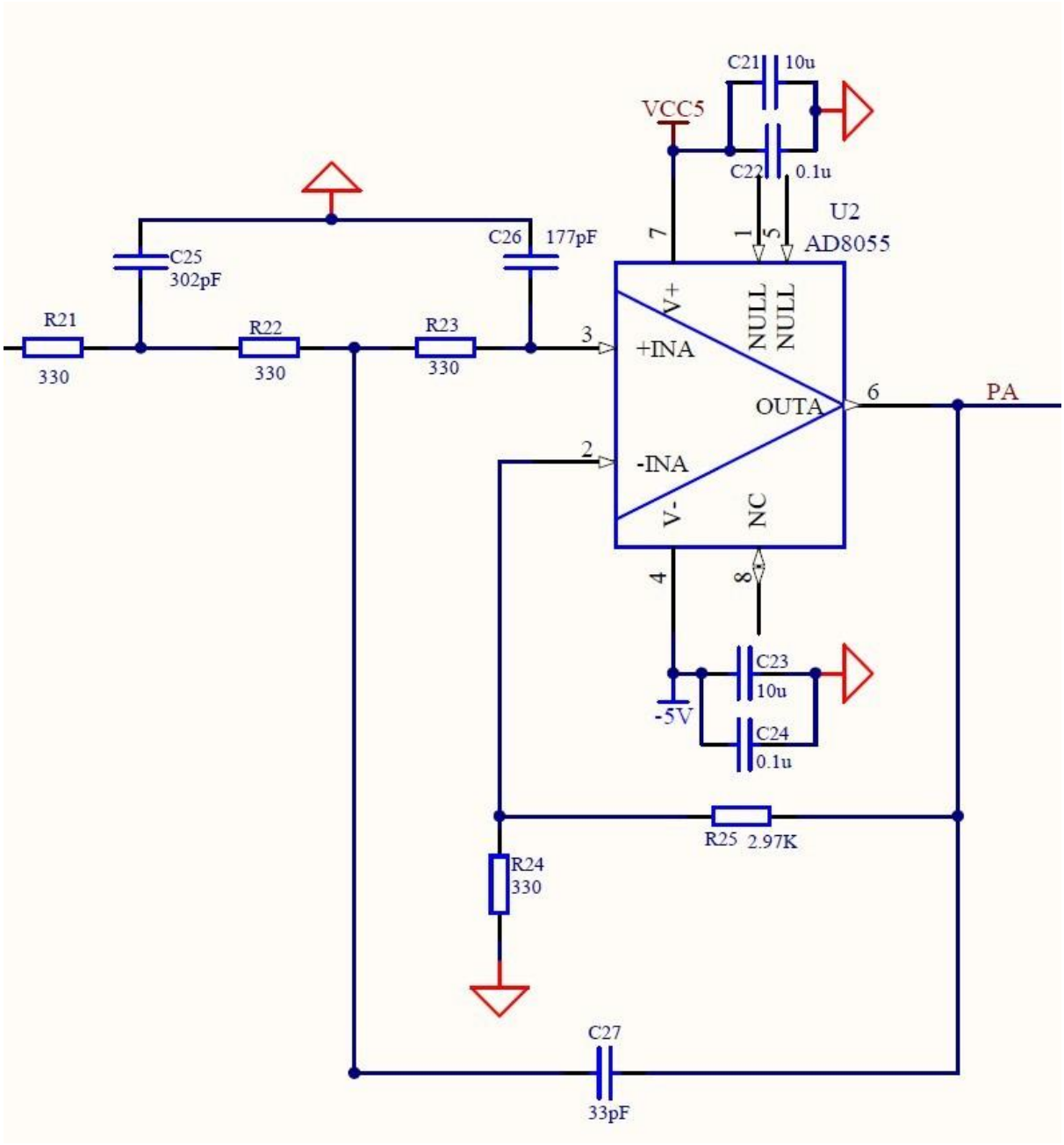

Figure 4-6 Second Amplifier

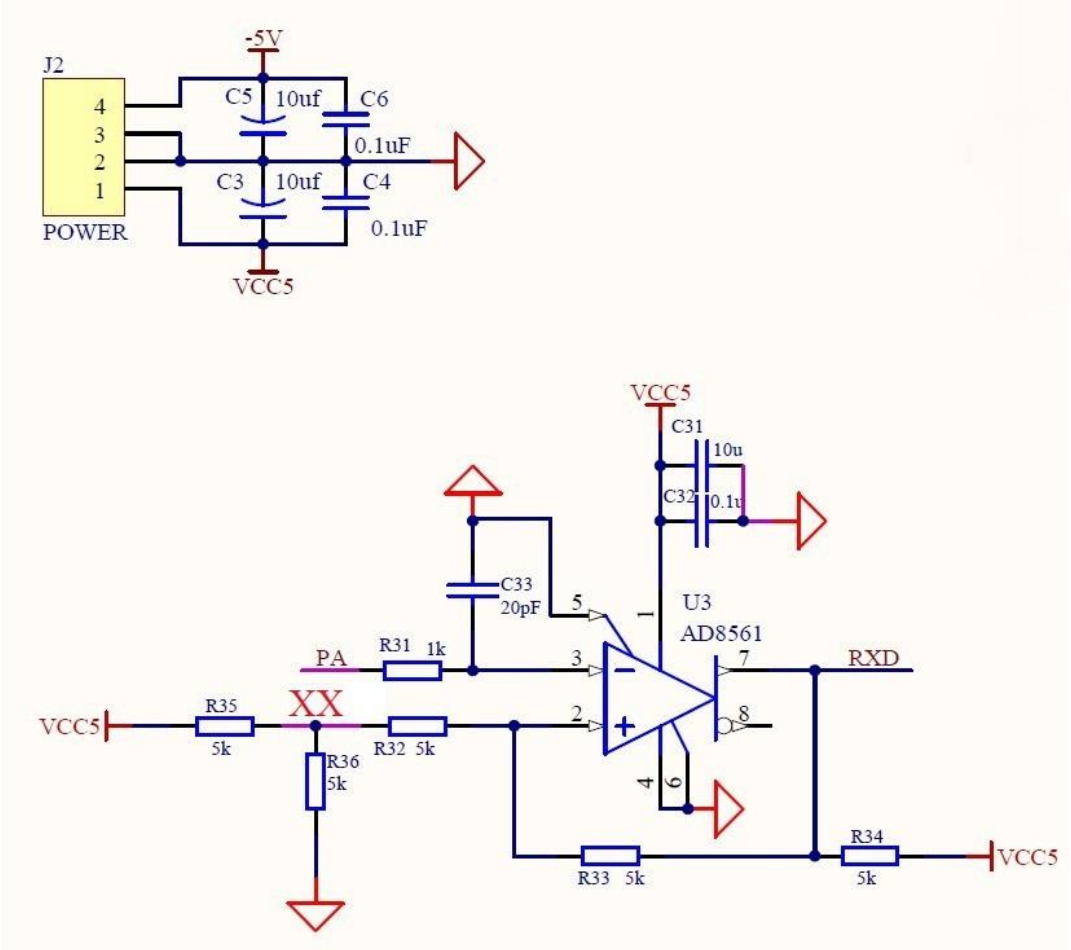

Figure 4-7 100kHz Receiver Comparator

J2 is the power supply module in the amplifiers and comparator which requires a regulated negative voltage.

The voltage of the amplified output signal from amplifier 2 is high enough to be detected by the oscilloscope. However, in order to satisfy the quality as required for the transmission, the comparator, as shown in Figure 4-8, is carried out. As can be seen, the output signal from the experiment demonstrated a square wave when the bandwidth varied from 1MHz to 10MHz. The performance of the signals during the experiments is shown in Figure 4-8(a). A random signal was generated by a signal

generator, and the output is shown as the top waveform, whereas the output waveform of the comparator is shown on the bottom. The bandwidth used to perform the experiment was 1MHz.

Figure 4-8 illustrates the 1MHz receiver with amplifiers and comparator.

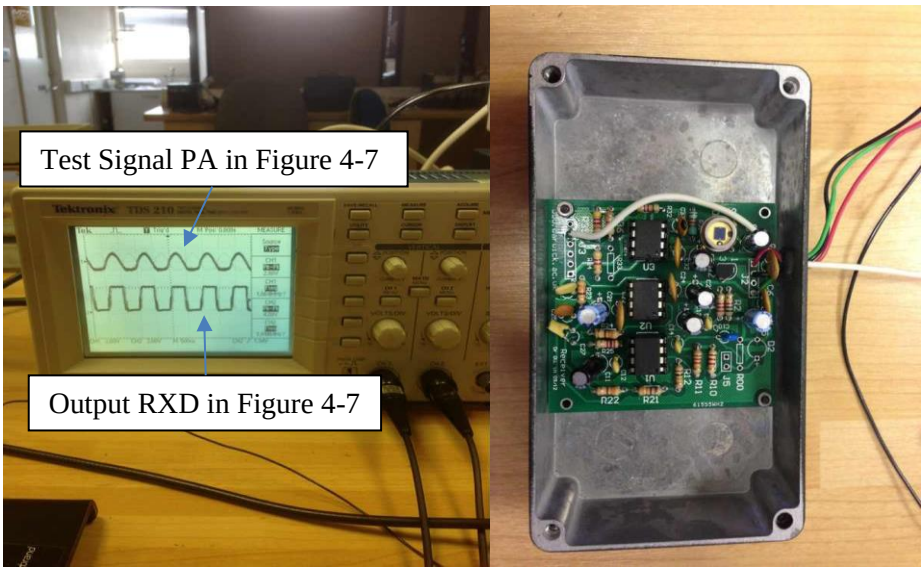

(a) (b)

Figure 4-8 (a) Performance before and after comparator (b) 1MHz receiver with amplifier and comparator model

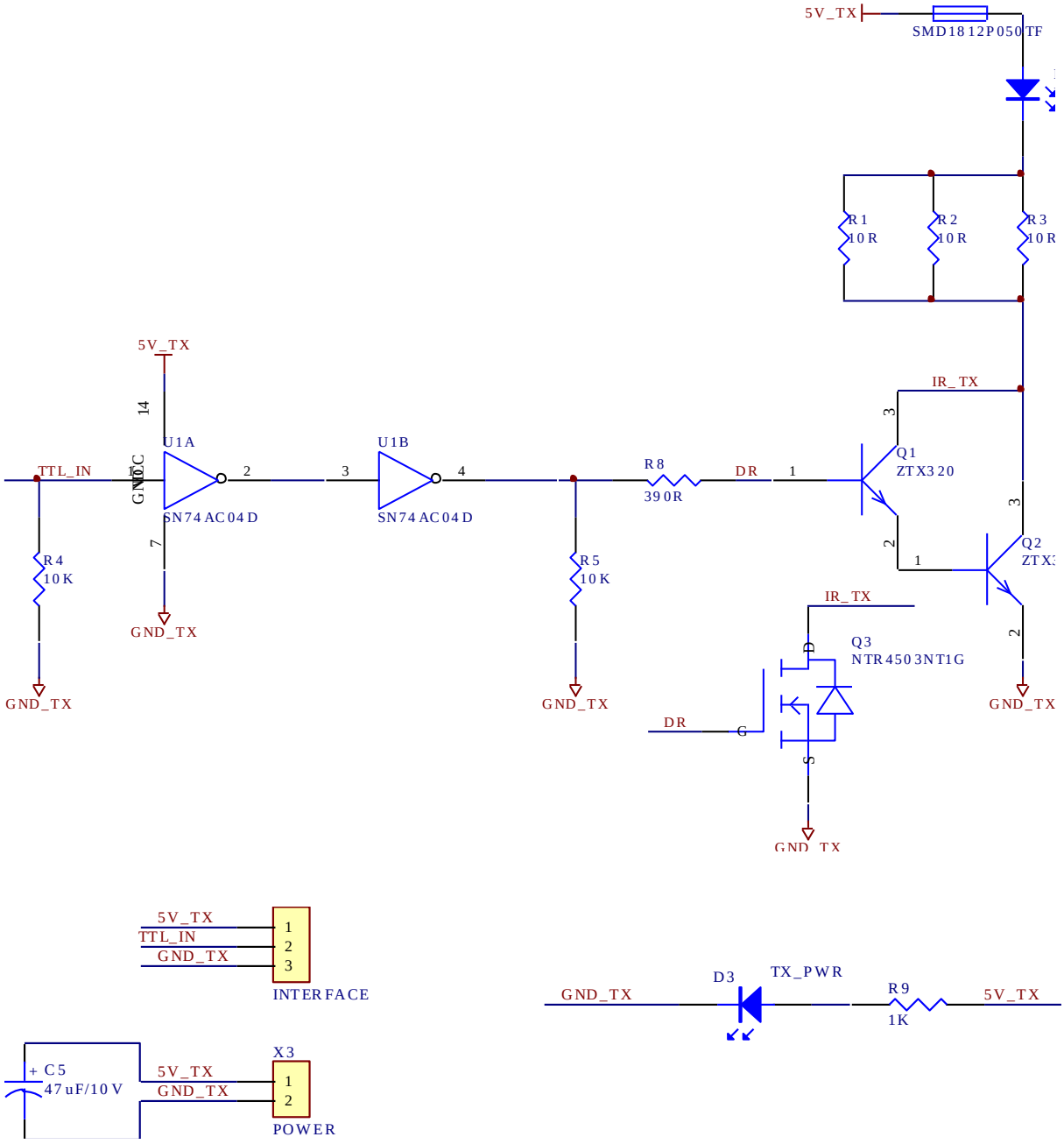

Figure 4-9 1-10MHz Transmitter Circuit

Figure 4-9 illustrates the transmitter with a designed circuit for high frequency over 1MHz. The DR is output of Schmidt trigger and is connected with two types of transistors. Due to the output performance of the transmitter, the ZTX320 is finally chosen.

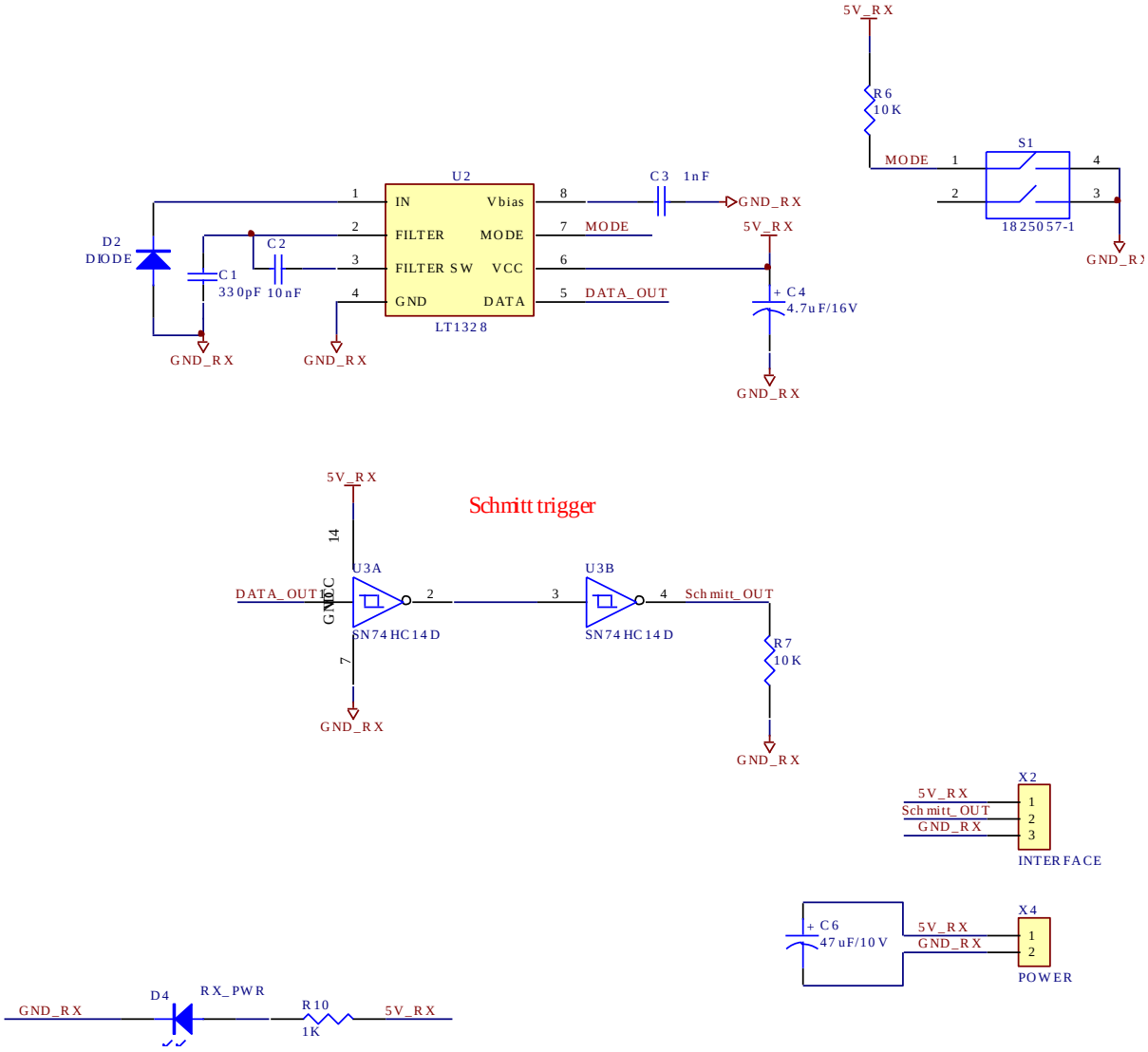

Figure 4-10 1-10MHz Receiver Circuit

Annotations of 4-10:

In order to make comparison with the transmitter designed with a lower bandwidth, two inverters designated as SN74AC04D are added to the transmitter circuit for a greater load capability. TTL_IN is the input signal sent by the I/O board from the PC. The signal voltage was 5V and drives the transistor through the two U1 inverters. Transistors Q1 and Q2 compose a Darlington circuit, and drive the LED D1. The parallel connection of resistors R1 and R3 serves to avoid the damage of the LED in the case of a long duration output.

In Figure 4-10, it shows that an infrared-received and photodiode-combined module was selected to stabilize the experiment results conducted at the frequency of 10MHz. C4 represents the external filter capacitor. According to the equation described by $f = 25/(2\pi \times 6 \times 10^4 C)$, where the f is the filtered bandwidth, and C is the corresponding capaciter, the photoelectric signal and noise below 200kHz can be filtered. C1 represents the filter capacitor at the low-speed mode. When PIN 7 (MODE) shows at a high value, LT1328 can be connected to ground, whereas C1 and C4 are arranged in a parallel connection, and the attenuation frequency falls from 200kHz to a level of 6.6kHz. The Schmitt trigger circuit is added into the system wave shaping.

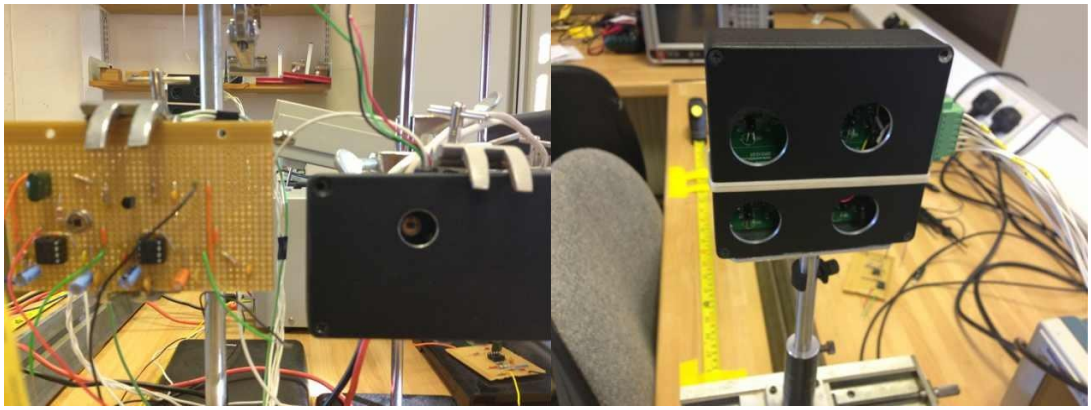

Figure 4-11 Receiver 100kHz (Left) & 1-10MHz (Right)

Figure 4-11 illustrates the receiver with 100kHz and high frequency (1-10MHz), and the system was designed according to the OOK modulation of the infrared 2X2 MIMO system. Figure 4-11 also shows the corresponding receiver circuit.

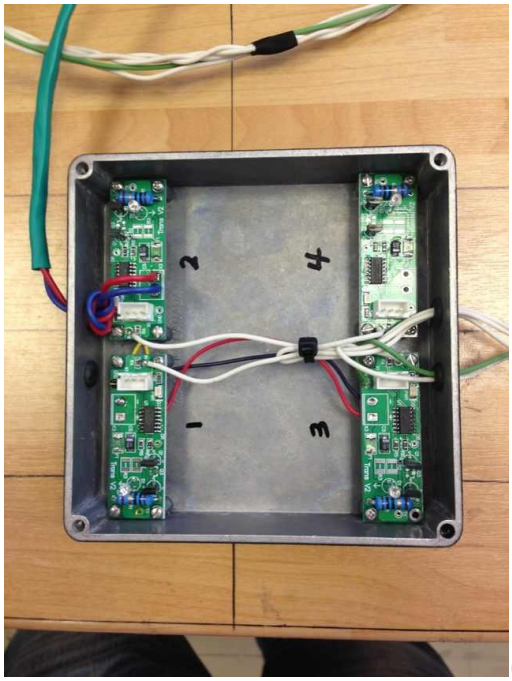

(a)

(b)

Figure 4-12 (a) Four 1-10MHz transmitters; (b) Four 1-10MHz receivers

Figure 4-12 illustrates 4 different circuits with transmitters and receivers used in experiments conducted at the frequency varied from 1 to 10MHz.

The values of the components are showed in Appendix III.

4.4 System Controller

(a)

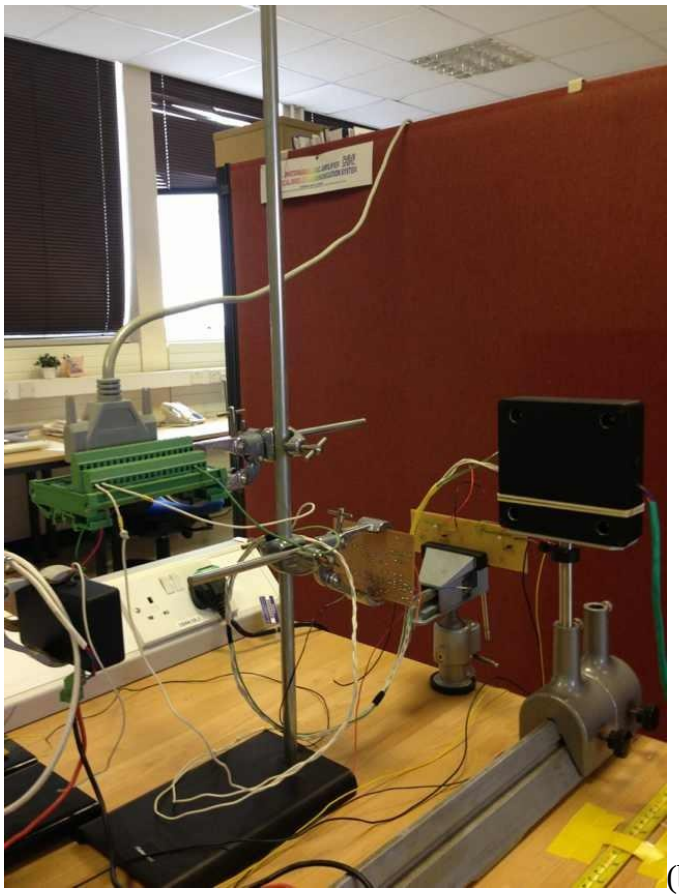

(b)

Figure 4-13 (a) PCI 7200; (b) The PCI-installed Computer connected the transmitters and receivers

Because the system is designed to work at the frequency varying from 100kHz to 10MHz, the PCI 7200 digital board with the transmission speed reaching at 12Mbps

is used as the signal generator and the received signal analyser. The BER performance was analysed by making comparisons of the transmitted and received signals in a binary system.

4.5 Research Method

4.5.1 Geometry Model

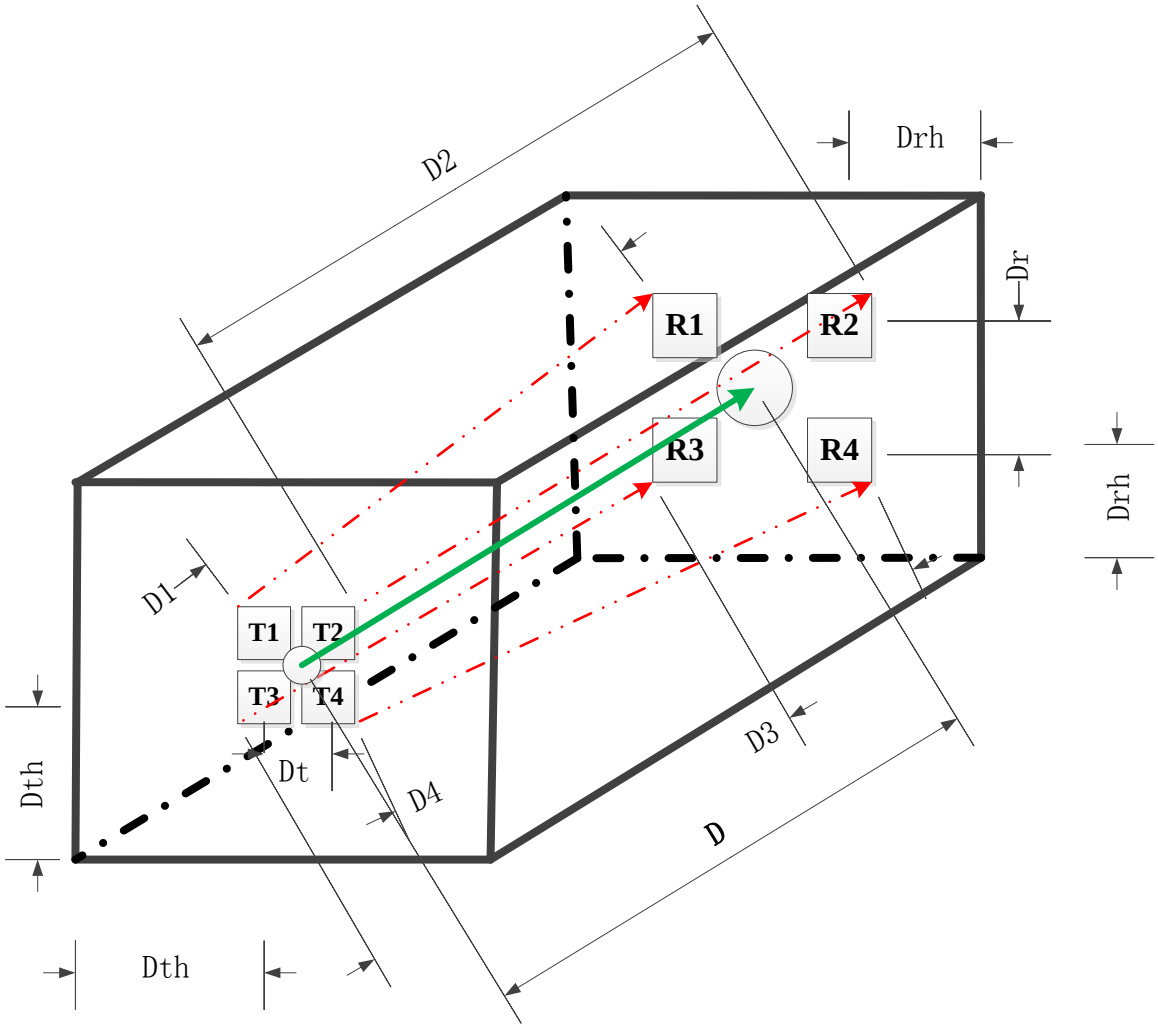

Figure 4-14 Infrared MIMO System Geometric Model

In this and the following chapters, three different systems using different modulations (OOK based, 4PPM based and SIR-RZI based) and MIMO (Multiplexing and Diversity) technologies are fully presented and illustrated. It is worth noticing that all three systems have one thing in common, that is, they have the same geometric model, as shown in Figure 4-14. As having been displayed in various diagrams, the model is designed to have transmitters and receivers fixed in two metal boxes set on a stand with a track, which allows the changes between transmitters and receivers uniformly and stably. Figure 4-14 illustrates the relationship between transmitters and receivers in the geometrical model, which has been used to perform the key experiments for delivery of the primary objectives of this research, whereas *D* represents the total length of the transmitter and receiver box (green coloured line represents the distance between central points of transmitter and receiver box). There are four transmitters/receivers placed uniformly in the metal boxes, which implies that the LEDs are placed with the same lateral and vertical distances to the edge of each box, whereas *Dth1=Dth2=Dth3=Dth4*, *Drh1=Drh2=Drh3=Drh4*, and *DthX/DrhX* represents the distance between the corresponding LED and the edge of the boxes. *Dx (x = 1, 2, 3, 4)* represents the distance between the corresponding LEDs and photodiodes, and *Dt/Dr* stands for the distance between Transmitter/Receiver 1-2, 1-3, 2-4 and 3-4. It should be noticed that the effects of both distance and background lighting conditions (switching on/off the room light) are addressed in the model.

Based on the environment for conducting the experiments as displayed in Figure 4-14, in addition to the distance and the background lighting conditions, another parameter, the angle between transmitters and receivers, is also included, with which

the geometric model is shown in Figure 4-15, whereas the transmitter array is fixed on the track, and the receiver array can be moved in parallel. As a result of this, the angle of incidence is kept changing. In the experiments with changing the angles, the effect of background lighting condition is taken into consideration for comparison references. The BER performance is evaluated in all experiments, and the differences resulted from changing distances and angles are analysed in the following sections.

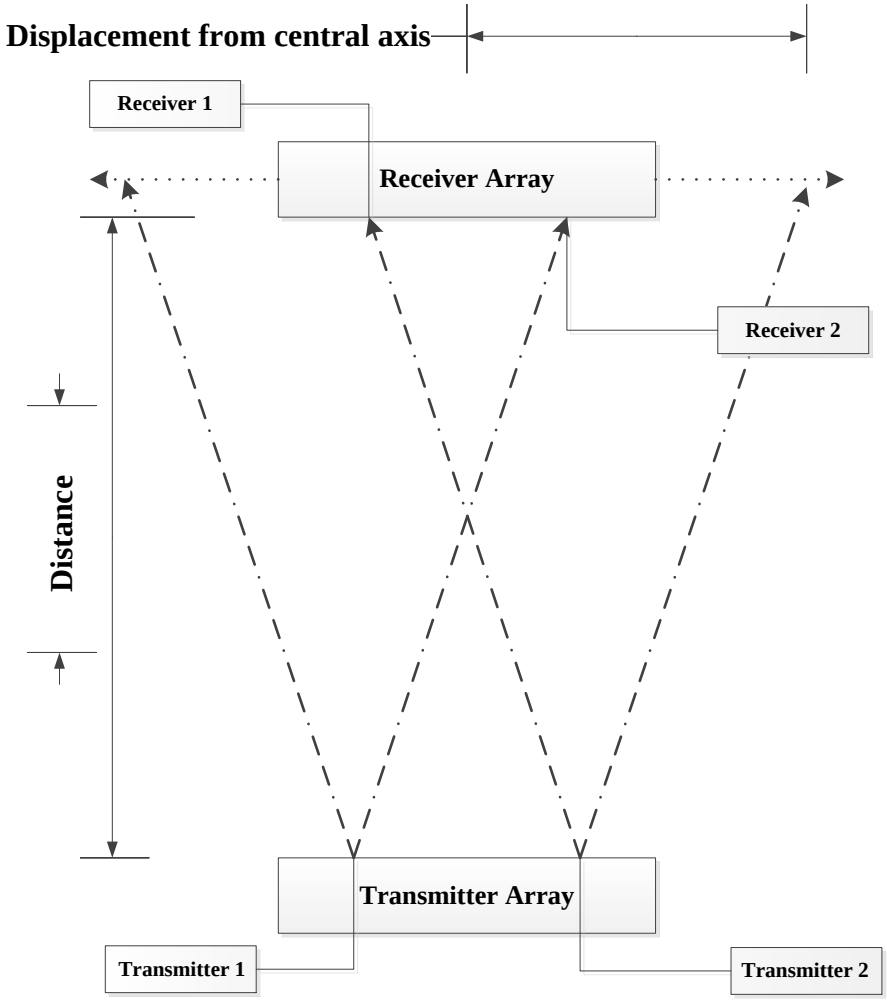

Figure 4-15 Infrared MIMO System Geometric Model Considering Displacement

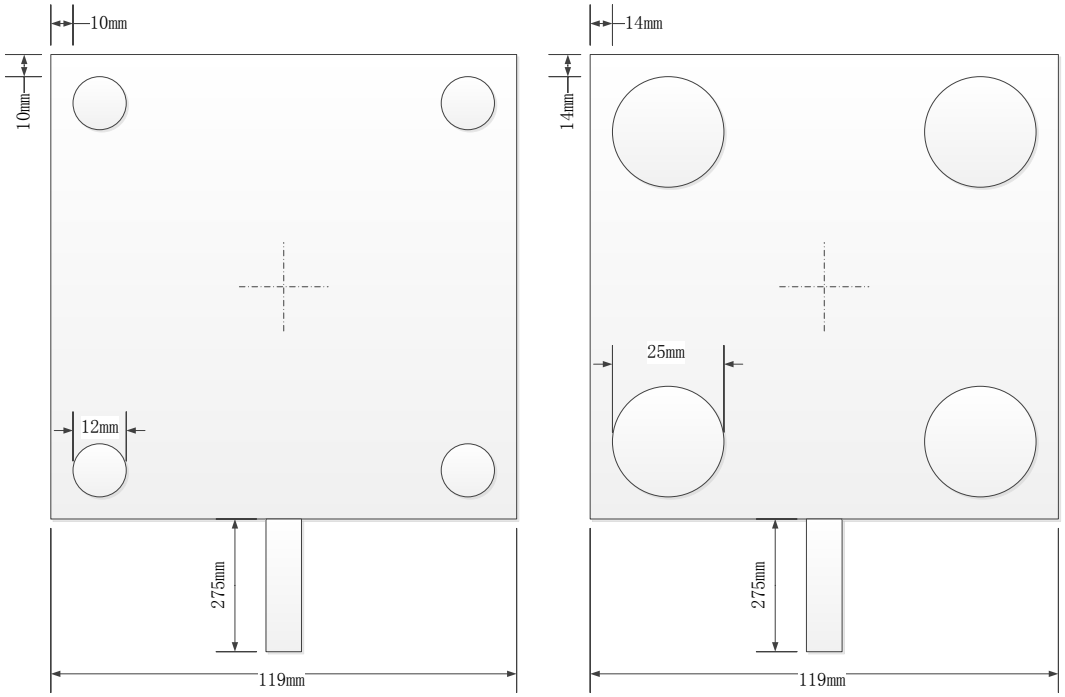

(a) (b)

Figure 4-16 (a) OOK Transmitters Stand; (b) OOK Receivers Stand

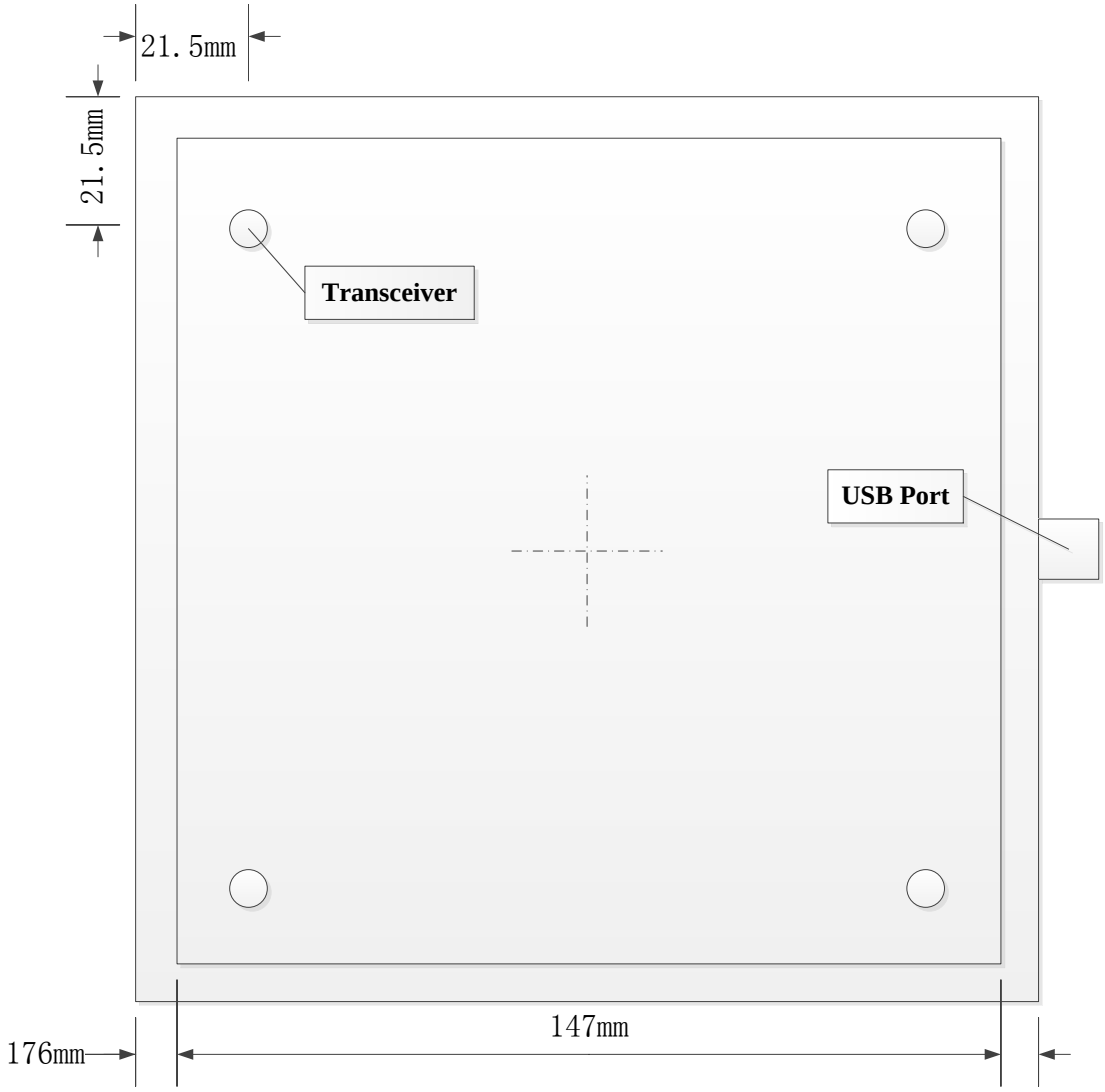

Figure 4-17 SIR/PPM Modulation Transceiver Geometric Diagram

In Figure 4-16 and 4-17, the geometric diagrams of the transmitters/receivers boxes are illustrated, which are used for experiments conducted in accordance with OOK, PPM and SIR-RZI modulations. It is worth noticing that, due to the specific requirements in the experiment of OOK modulation, and also the fact that the experiment uses the same box and box stand, the effect of height of transmitter and receiver has to be taken into consideration as well, and the same approach applies with those conducted by using the PPM and RZI modulations. In conclusion, this

research only focuses on the effect of variations in lateral distances and angles between boxes.

4.5.2 Introduction of research instruments

According to the research conducted by previous chapters, the optical transmission channel of an Alamouti Space Time Coding in a MIMO system can be analysed, whereas the distance and the angle between transmitters and receivers are considered as variable in the experiment model. Finally, the effectiveness of these variables to describe the quality of transmission performance (power attenuation, Bit-Error Rate) can be verified.

Figure 4-18 Receivers of Infrared OOK MIMO system

According to the findings from the literature review, an Infrared communication system with 4 transmitters and 4 receivers was built, and each of which was fixed on the track, whereas displacement of the receiver and transmitter stand could change from -10cm to 10cm (for the experiments of displacement). The maximum distance between the transmitter and the receiver stand can reach 2.4m (due to the signal transmission distance of the transmitters). In the experiment, four transmitters and receivers were built. Based on the results from the experiment, the transmission distance between the single transmitter-receiver pair could reach 2.4m. Figure 4-18 shows the receiver stand used in the experiment, Figure 4-19 shows the transmitter stand, and Fig 4-20 shows the completely-built transmission system.

Figure 4-19 (Up) OOK MIMO Transmitters; (Bottom) 4PPM MIMO Tranceivers

The experimental apparatus included two steel boxes which were used to fix the circuits on the stand, and the holes for installation of LEDs and photodiodes were drilled. The diameter of the holes were designed in accordance to the emission angle of LEDs and the receive range of photodiodes (diameter of the transmitter holes was designed as 1.2cm, and the diameter of receiver holes was designed as 1.7cm, which are considered by the dimensions of LEDs and photodiodes). Through the holes on the boxes, all the LEDs and photodiodes are fixed on the surface of the boxes, and hence theoretically, the optical signals can't be blocked out by the boxes placed in a distance between 0.2 to 2.4m as having demonstrated in the experiments.

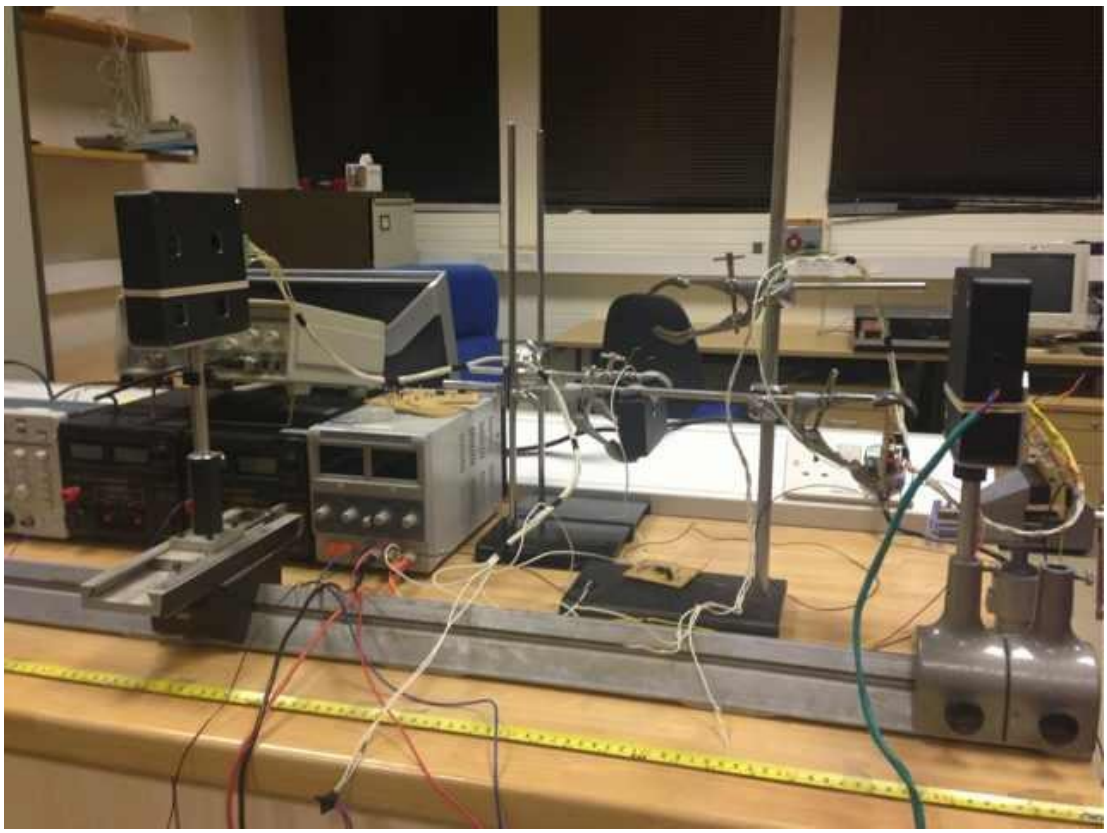

Figure 4-20 Experiment for Infrared 4x4 OOK System

A digital I/O board (PCI-7200 Multiple Input and Output) was used to control the transmitters and receivers, and the OOK signals can be coded and decode by this controller. The board generates digital signals at a specific frequency (1024kHz in this experiment), and transmits signals to the transmitters through the cable (due to the diversity gain and multiplexing gain, two different type of signals are produced, one of which allows the same signals to be transmitted to all transmitters at the same time, and in the other case the signal beam can be divided into several parts and transmitted by transmitters separately at different times).

Finally, the detected signals can be sent back to the board, and the bit-error-rate performance of each case can be analysed by making comparisons between the output and input signals that are both known in the experiments.

4.5.3 Experiment progress

When the Optical MIMO experiments are conducted according to the OOK modulation, the flow process is described below:

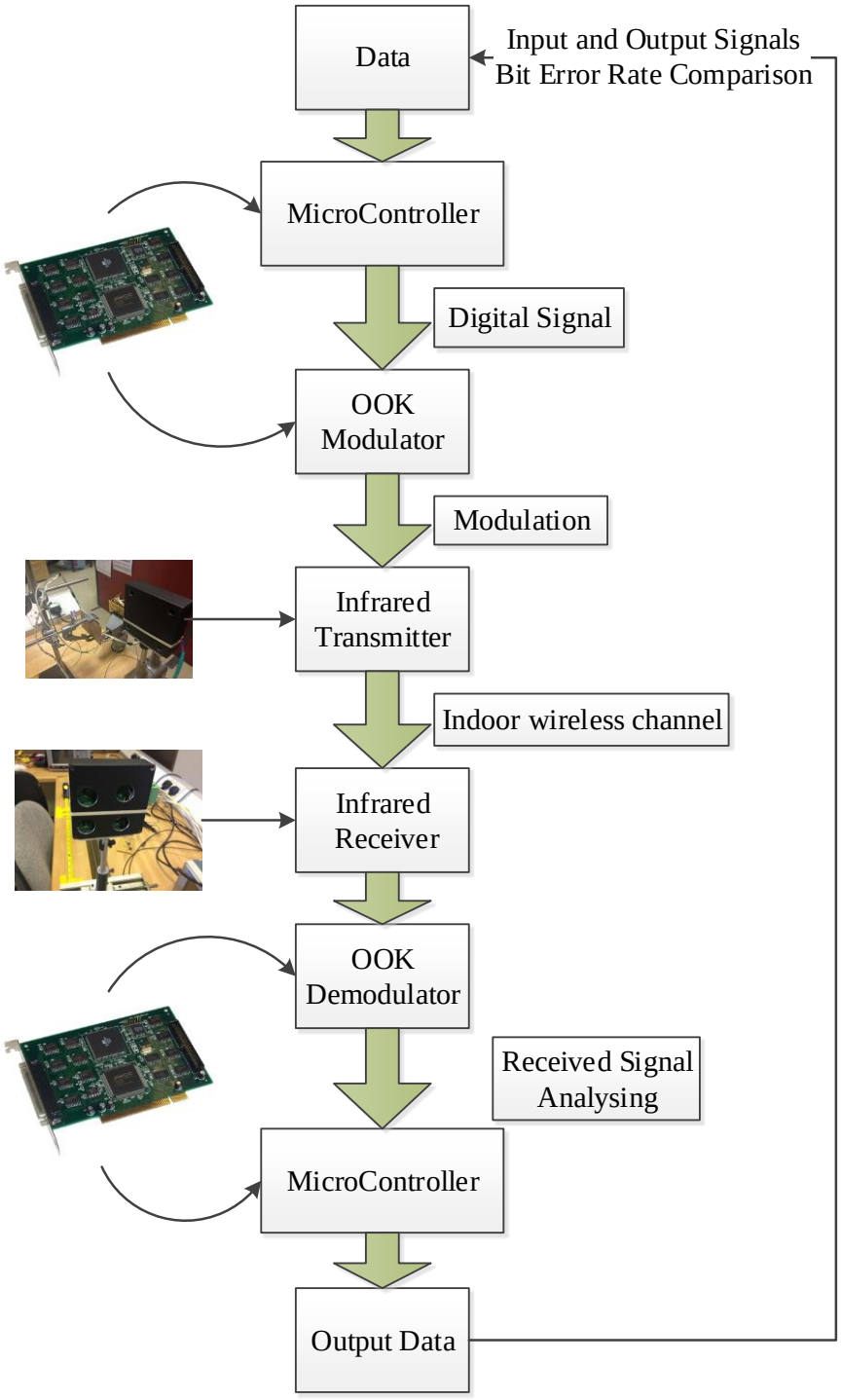

Figure 4-21 Experimental Progress

Firstly, the transmitted data can be produced and sent to the control board. Secondly, the data can be coded into OOK signals and sent to the transmitters. Thirdly, under the specific transmitting scheme, the LEDs transmit the optical signals to the receivers, and the received optical signals can be transferred into the electronic

signals and decoded by the control board. Finally, the control board analyses the decoded signals and exports the output data. In order to conduct analysis and research on the effectiveness of the transmission distance, the impact resulted from various angle and other factor on the optical data transmission, the bit-error-rate (BER) performance can be consider as an indicator. The data can be divided into several streams, and each of which can be sent separately by one of the transmitters. The following described experiments are used to conduct tests and research on the multiplexing gain of the optical MIMO.

Experiment 1: The OOK Modulation-based experiment scheme 1 is shown in Figure 4-22, where two transmitters and one receiver are applied,

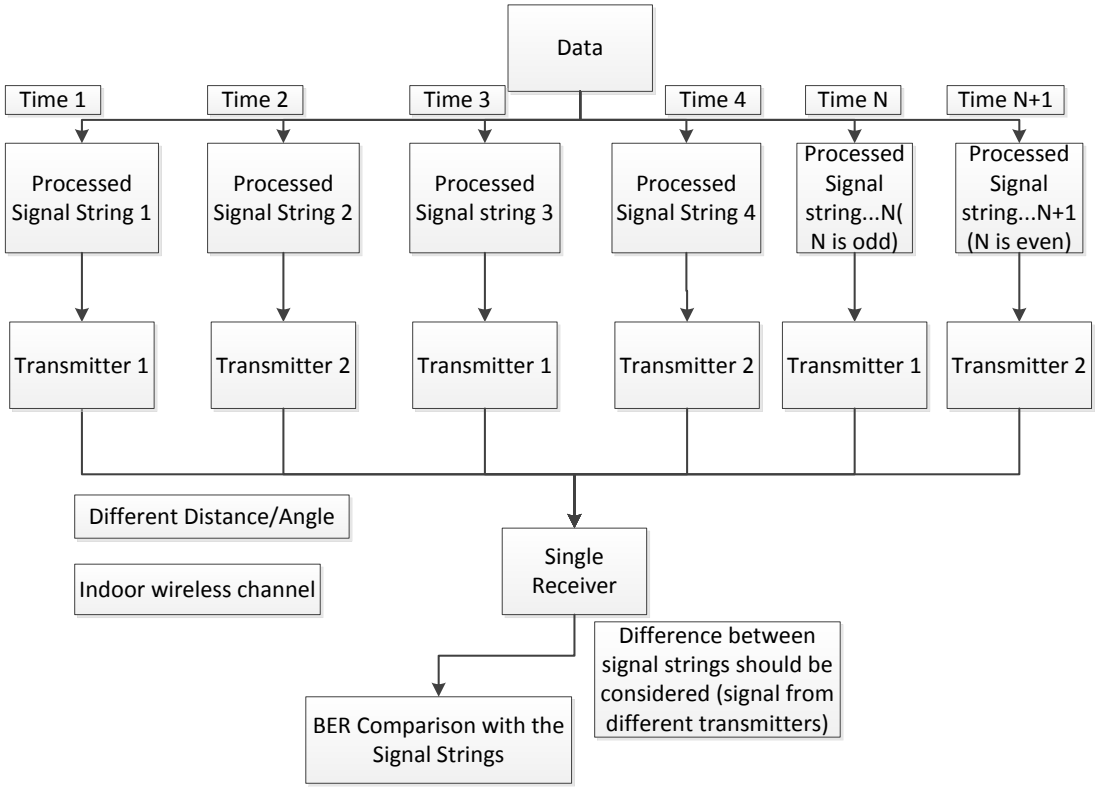

Figure 4-22 Experiment 1

The experiment process can be described as the following: At time 1, after being modulated, the first stream is assigned to Transmitter 1, which can be sent and detected; at time 2, the second stream can be progressed by Transmitter 2, and more processes follow the same fashion. The receiver can collect all of the streams, and all of which can be assembled by the control board. Finally, the PCI board decodes and exports the data. The performance of the experiments can then be analysed.

Experiment 2 uses similar approach to in Experiment 1, except that experiment 2 uses two transmitters and one receiver. However, the data are not divided, and are sent by both transmitter 1 and transmitter 2 (two transmitters can send the same data at the same time). This experiment is designed to test the diversity gain.

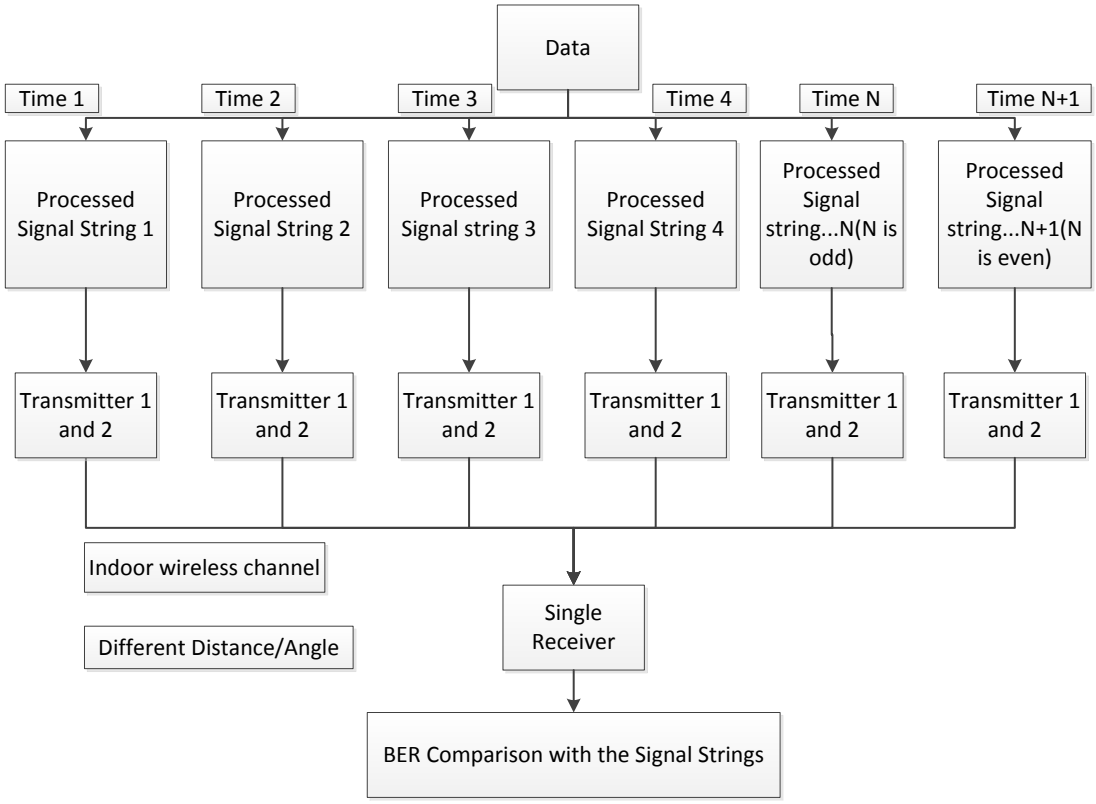

Figure 4-23 Experiment 2

In the above described experiment, from time 1 to time N+1 (the last time slot), both transmitters are used to send the same data streams, and the received signal is compared with the input data. By changing the distance, the background light intensity and the angle, different results are received and comparisons are made.

Experiment 3: The flow diagram of experiment 3 is shown in Figure 4-24. Two transmitters and two receivers are used. During this group of experiments, in order to conduct in-depth research on multiplexing gain of optical MIMO, the same experiment arrangement as used in experiment 1 is applied.

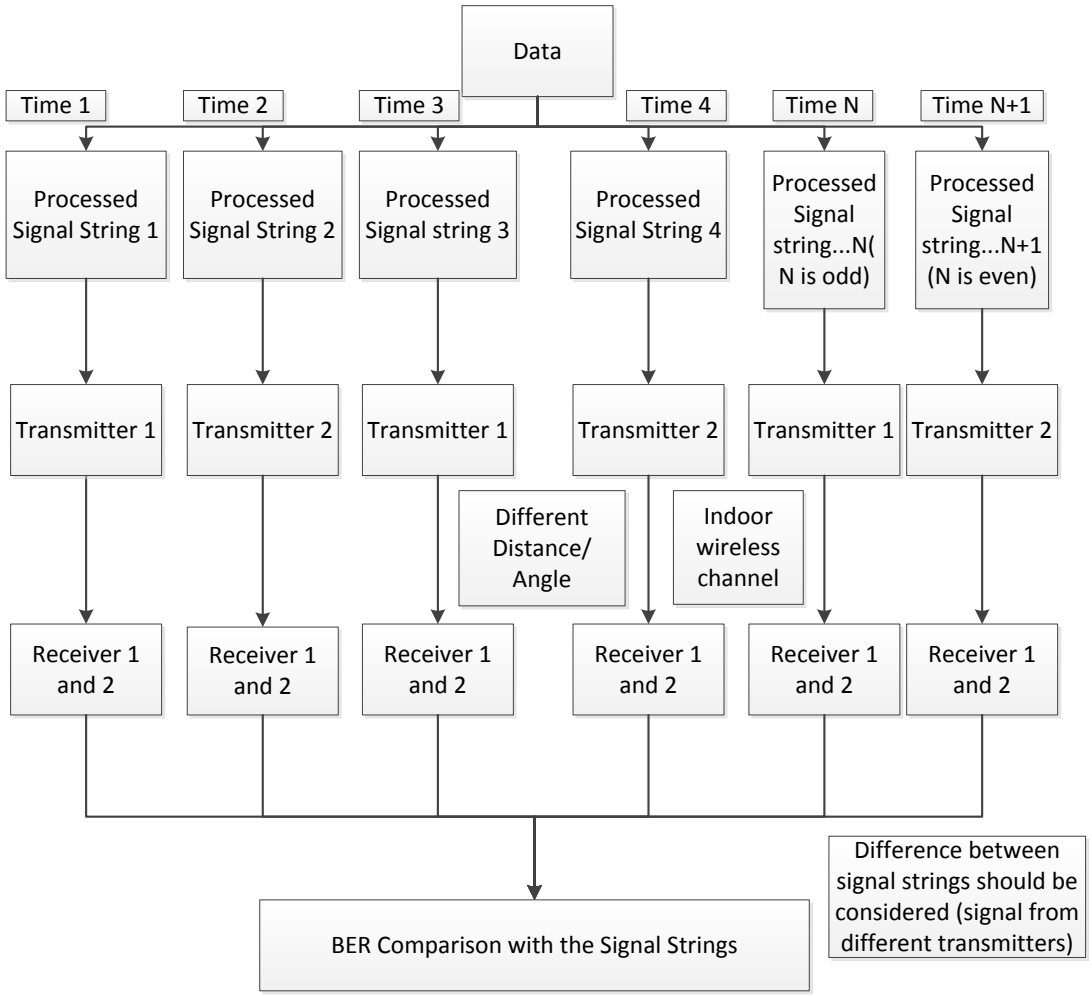

Figure 4-24 Experiment 3

During the experiments, the data are divided into multiple data streams, followed by having the OOK signal transmitted by different transmitters. At time slot 1, the data string 1 is allocated to transmitter 1 before being transmitted. Both receiver 1 and receiver 2 will detect the signals (in some specific area, only the receiver which is located in front of the transmitter can detect the signal due to the emitting angle problem). At time slot 2, the data string 2 is sent by transmitter 2 and detected. The subsequent data streams are sent in the similar fashion.

Once the PCI board collects all the received data streams, the Bit-Error-Rate calculation will start and the performance results of both receivers can be displayed. In this experiment, the performance amongst difference receivers can be analysed, and based on these, an optimized receiver is selected according to the performance evaluation. By changing the process arrangement, a new round evaluation process starts again.

Experiment 4: designed differently from experiment 3, experiment 4 is conducted to analyse the diversity gain of Optical MIMO system with two transmitters and two receivers. The flow process of the experiment is illustrated in Figure Experiment 4.

In the experiment, the data was divided into multiple streams. At time slot 1, the stream 1 is sent to both transmitters, by which the signals can be transmitted and detected. During the experiment, different frequencies are applied to test on

transmitted signal, distance, angle and background light. The results from performance evaluation on both receivers are compared.

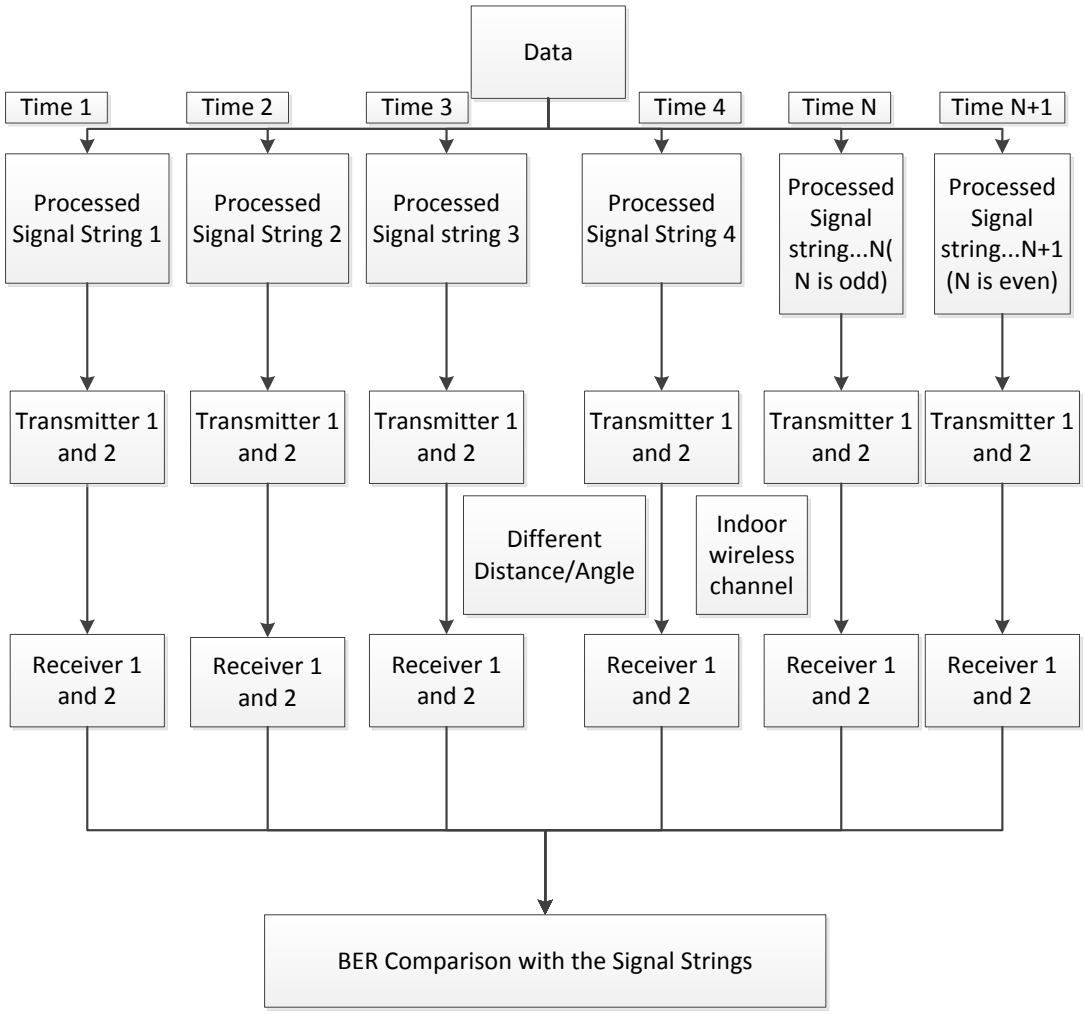

Figure 4-25 Experiment 4

Reference test: In order to make comparisons between different MIMO antenna selection systems and SISO system, a SISO (single transmitter and receiver with different distance and angle are considered) system is built and the BER (bit error rate) performance is recorded for evaluations. The flow diagram of SISO experiments is shown in Figure 4-26, where the OOK modulated signal is transmitted by the transmitter, and detected before making comparisons with the

original signals. During this experiment, the BER performance resulted from different distance, angle, background light and frequency of transmitted signals are recorded for evaluations.

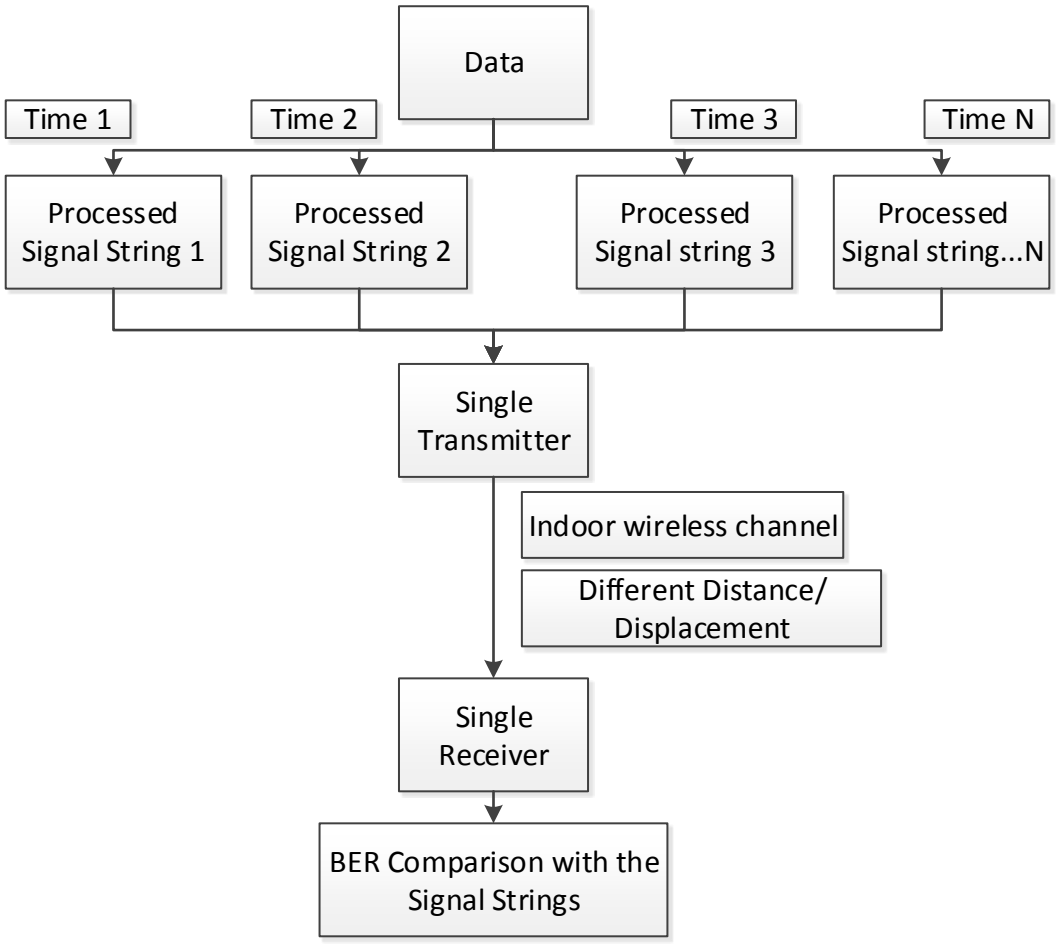

Figure 4-26 SISO Experiment

4.6 Summary

As presented in [1, 2 and 3], infrared MIMO technology has attracted worldwide attention. As far as the future indoor high speed applications are concerned, infrared MIMO technology presents a practical solution. This chapter describes the advantages of an OOK based infrared MIMO system, and making comparisons with

the SISO system, the diversity and multiplexing gain processes. It can be concluded that further research is necessary on infrared MIMO technology applications in association with issues concerning interference and background lighting. Moreover, the research method used in this thesis was introduced in detail. The whole experiment tests were concentrated on the advance of multiplexing and diversity technology, the distance, angle and background light effective were considered and the influence factors. All the theoretical and empirical results, systems designs and estimated mathematical models would be presented on the following chapters.

References Chapter 4

[1] R. R.-Iniguez, S. M. Idrus, Z. Sun, Optical wireless communications: IR for wireless connectivity, *CRC Press*, 2008.

[2] R. J. Green, M. Higgins, H. Joshi, M. Leeson, ‘‘Bandwidth Extension for Optical Wireless Receiver-Amplifiers’’, *Proc. 10th IEEE Conference on Transparent Optical Networks (ICTON)*, pp. 201-204, 2008 [4 pages].

Chapter 5 Optical Wireless MIMO System Based on PPM Modulation

5.1 Introduction

An infrared MIMO system has been discussed using OOK modulation, in Chapter 4. OOK modulation is considered as a simple but classical process of implementing the system. However, the power efficiency of the system proves to be low. In comparison with the OOK modulation, PPM modulation, another commonly-applied modulation, not only is be capable of reducing the power consumption at a considerable level, but it also increases the bandwidth. However, in the PPM modulation, the time slot and symbol synchronization becomes more difficult.

The OOK modulation scheme is considered to be the simplest optical modulation, in which 1 represents the situation when an optical transmitter sends light pulses, whereas 0 represents the situation when no light pulses are identified. In a PPM modulation scheme, an M-bit binary data group is mapped to a 2^M - slot period, where a single-pulse signal is located on one time slot, and the symbol interval is divided into the 2^M slots. If the M-bit data group is defined as $K=(m_1,m_2.....m_M)$, where the slot position is denoted as *K*, the PPM modulated mapping relationship can be expressed as:

$$p_k = m_1 + 2m_2 + ...2^{M-1}m_M \in \{0,1,2...,2^M - 1\} \quad (5.1)$$

where p_k is the pulse in kth time slot.

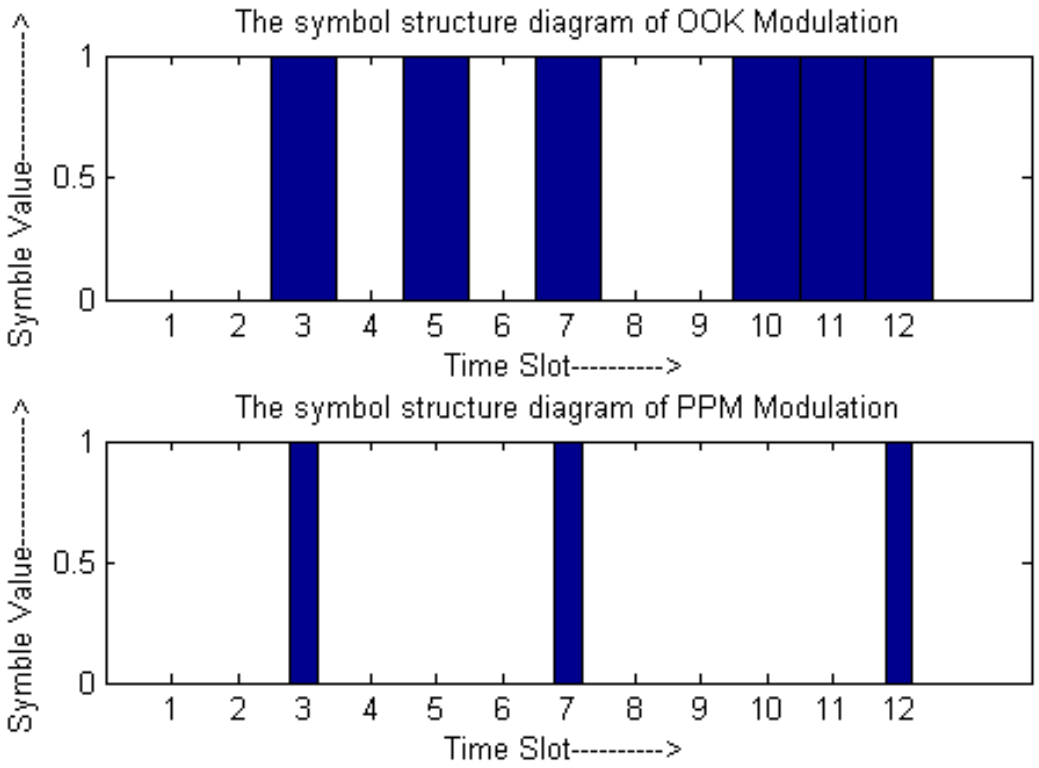

Figure 5-1 The Symbol Structure of OOK and PPM Modulation

Figure 5-1 indicates the symbol structure of both OOK and PPM modulation.

By taking consideration of the power of the two modulation schemes when transmitting the same data under the same condition, and, by assuming that the transmitting power of OOK is P_{OOK}, the transmitting power of PPM modulation P_{PPM} can be defined as:

$$P_{PPM} = \frac{2}{2^M} P_{OOK} \quad (5.2)$$

Where the M represents the number of data symbols.

In the OOK system, assume its bandwidth B_{OOK}. In a PPM system, the bandwidth is increased to $B_{PPM} = \frac{2^M}{M} B_{OOK}$, for the same bit rate. [1]

5.2 Modulation Defined by IrDA

As is introduced in Chapter 2, the data rate range in the modulation of IrDA 1.0 and IrDA 1.1 varies from 2.4kbps to 4Mbps. At the beginning of the link connection, the data rate is fixed. The IrDA 1.0 standard requires a link always initiating at 9.6kbps data rate, and, if both the transmitting and receiving parties support either higher or lower speed, the data rate can be changed as mutually agreed upon. The modulation of IrDA 1.0 uses a Return to Zero Inverted (RZI) 3/16 modulation, whereas the modulation of IrDA 1.1 uses a 4PPM. In the RZI 3/16 modulation, the IrDA links are connected with the UART, whereas the data are encoded as infrared pulses before transmitting. The reason for encoding the data before transmitting it to the UART is based on the fact that the UART and serial port uses Non-Return to Zero (NRZ) modulation, the output of NRZ modulation is maintained at the same magnitude, which results in a continuous bit stream to drive the light-emitting diodes (LEDs) arbitrarily for a long time, and a significant power consumption, which would shorten the lifetime of LEDs. On the contrary, the RZI pulse modulation can improve the situation for LEDs, by increasing the peak/average power ratio. Consequently, the RZI pulse modulation is considered to be the optimized technology for the IrDA standard. The maximum pulse width of IrDA 1.0

modulation is defined as a 3/16 bit slot. As the 16-clock divider requested by the 3/16 can be easily obtained in a number of UART modules, it is recommended that one uses the 3-clock period to encode ore receive data, and the 16- clock period to decode data.

When the IrDA 1.0 link is connected at a higher data rate (up to 4Mbps), it uses 4PPM modulation rather than a 3/16 modulation scheme at a low data rate. In 4PPM modulation, the information is obtained from the specially-positioned pulses during the transmission. In effect, the encoding scheme includes a two-digit data bits pair (DBP), which is divided into 125ns timeslots. The two-bit code is described by four statuses, namely, 00, 01, 10, and 11, to represent different positions when the pulse are placed in the 1^{st}, 2^{nd}, 3^{nd}, and 4^{th} position of the 125ns time slots. Consequently, after having locked the phase at the incoming bit stream, the decoder shall determine and select the relevant digital module by detecting the pulse position of the 500ns slots.

5.3 System Module

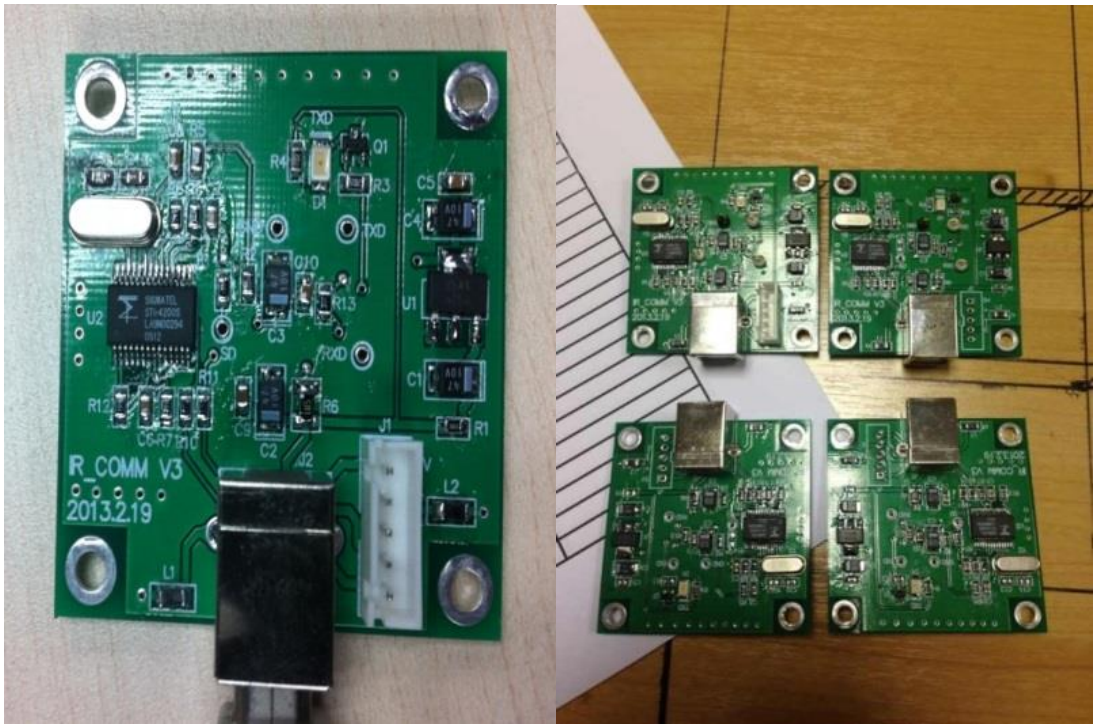

Figure 5-2 FIR-4PPM Module – Single circuit and 2X2 Module

In Figure 5-2, the circuits used for a 4PPM Module are shown. Both of the transmitter and the receiver are integrated into one circuit. It's worth noticing that due to the limitation of the IrDA 1.1 standard, the working bandwidth designed for the particular system varies from 500kHz to 1.67MHz. The bandwidth of 1MHz is used for analysing the results of the experiments. When designing the system, the cover with filter was considered for comparing the performance with/without filter, but it should be noticed that finally the transparent cover (the filter) was removed from the transceiver boxes because of the influence to the performance – the BER performance decreased significantly (over 1000 times higher than the BER without filter) and the transmission distance was shortened as well when the filter are used.

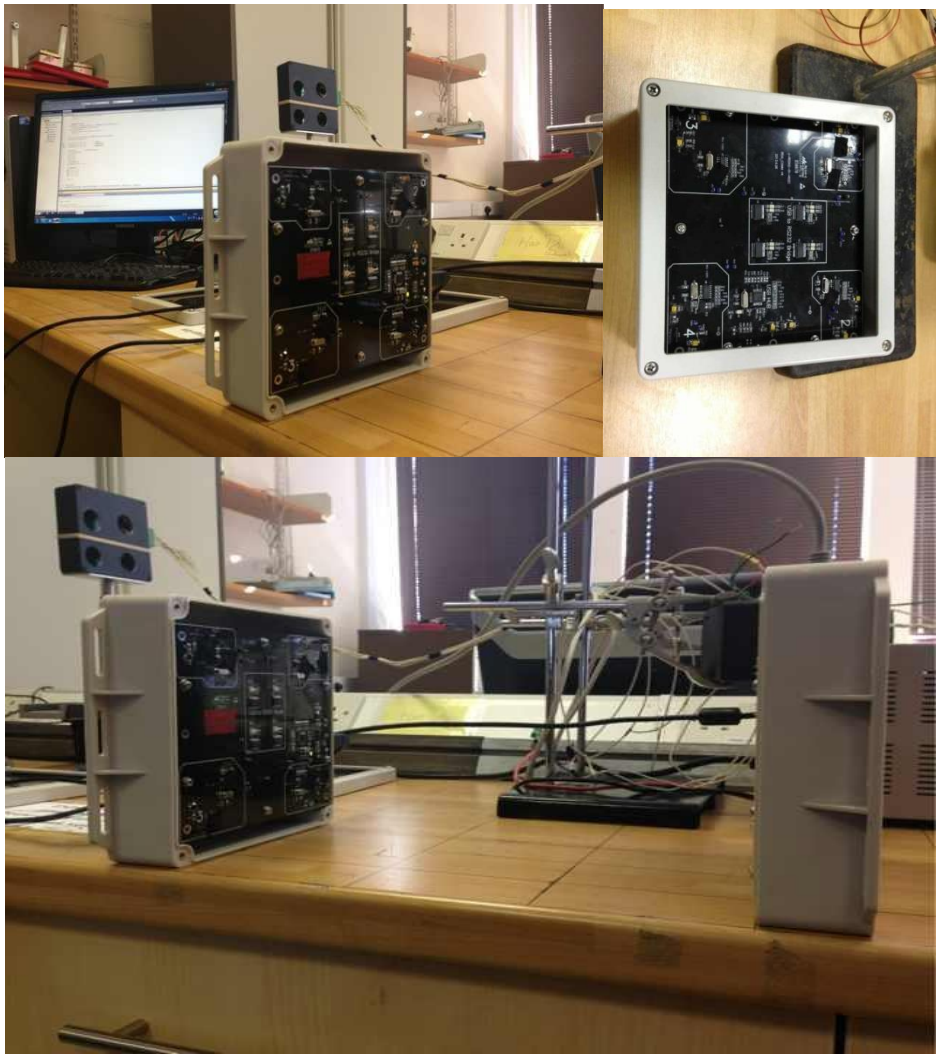

Figure 5-3 4PPM and SIR Transmitters and Receivers (4X4 Transceivers)

Figure 5-3 and Figure 5-4 illustrate the transmitters, receivers and the entire system for the SIR Model. In this particularly designed system, the working bandwidth varies from 10kHz to 115.2kHz in the experiments. The bandwidth of 100kHz is selected to comparing the 4PPM system and OOK system.

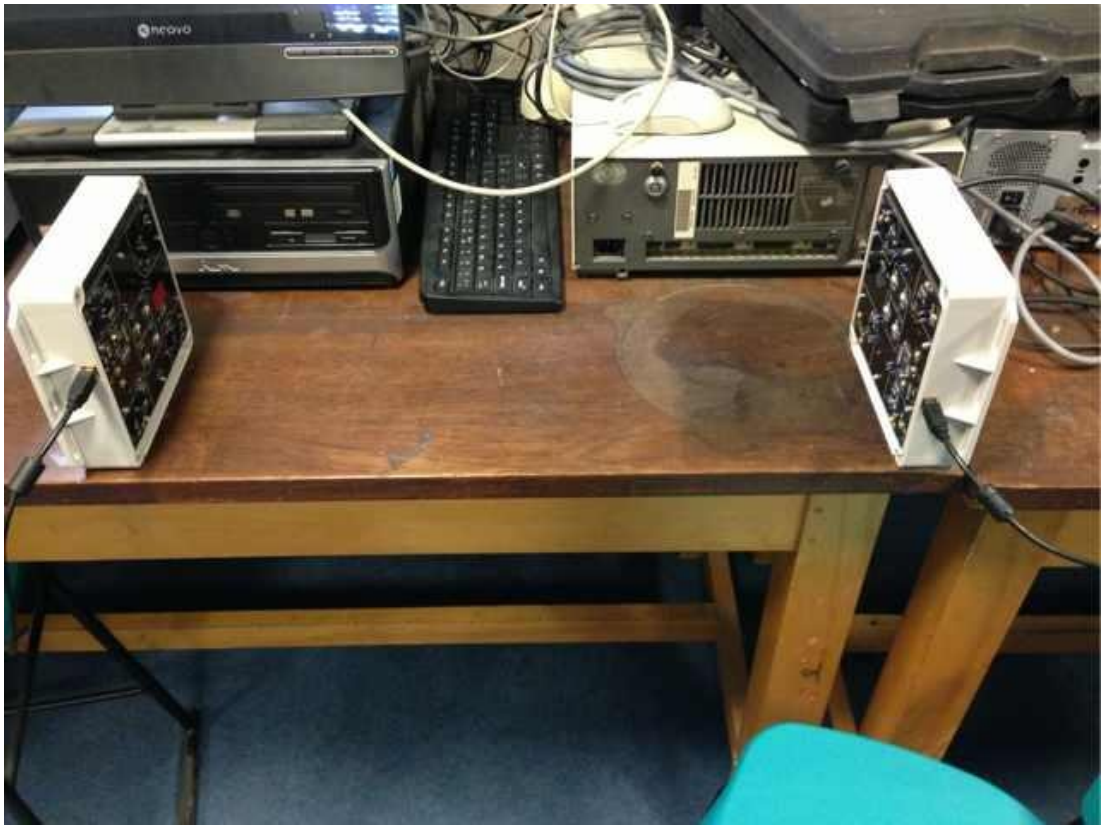

Figure 5-4 4PPM and SIR 4X4 Infrared MIMO System (same boxes)

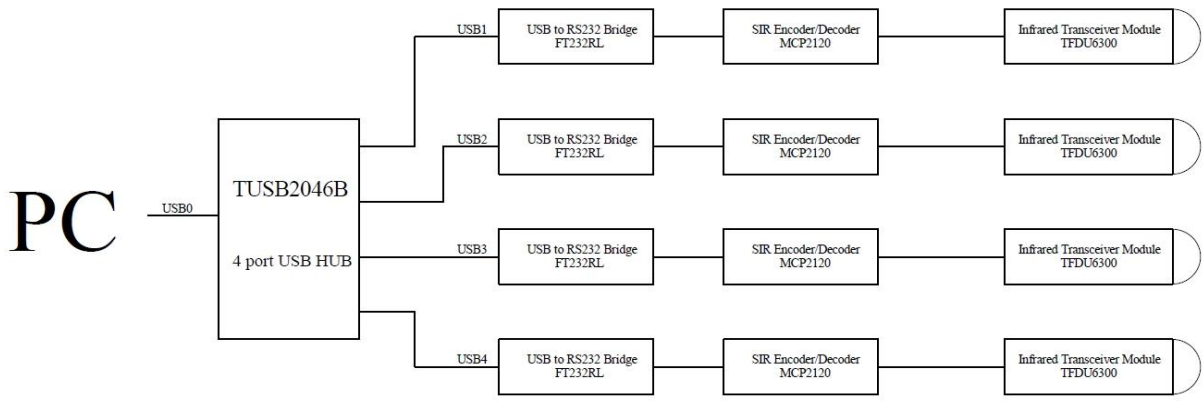

Figure 5-5 SIR System Flow

Figure 5-5 illustrates the flow diagram of the experiments. The experiment starts with the controller, or a PC. By using a program and coding (C++) system developed for the experiment, the PC sends a command to the transmitters through an USB hub port. After having assigned by the hub, the data is transmitted through the USB – RS232 bridge, and received by the MCP2120 SIR encoder, in which the data can be further 'translated' to the code in accordance to the IrDA 1.0 standard, and transmitted by the 4X4 transmitters. At the end of the experiment, by taking the considerations of the distance, the displacement and other factors, the data is detected by the transceiver module positioned on the other side. Finally, by making comparisons of the received data with the input data, the bit error rate is calculated and displayed.

Annotations:

Due to the limitation on the size of the transceiver model, the SIR experiment can not use the same track as shown in the OOK and 4PPM experiment. Consequently, the new measure method is configured. The transceiver modules were fixed on the experimental desk, where the distance, the width and the height were measured and labelled.

5.4 Transmitter and Receiver Design

5.4.1 IrDA Higher speed (1.1-1.3, FIR-4PPM)

The 4PPM system uses the STIR4200 as the main controller, which is defined as a high-speed (FIR) USB transfer infrared transceiver, and complied with the IrDA protocol. The system circuits were shown in Appendix IV.

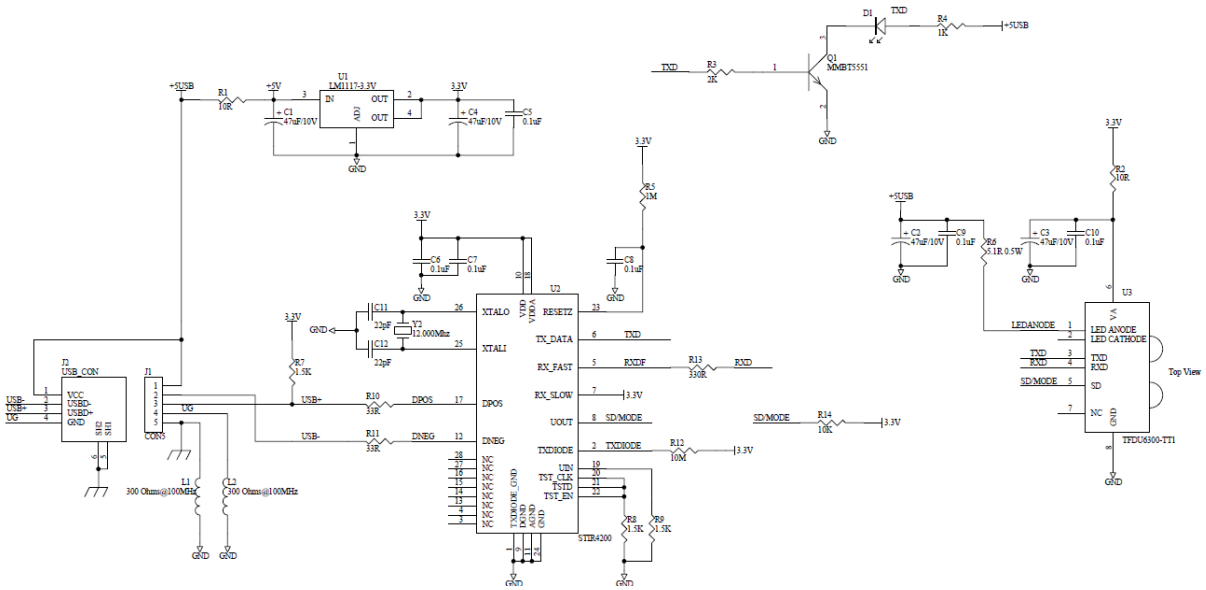

Figure 5-6 4PPM Infrared System

Figure 5-6 shows the circuit diagram of the 4PPM system. The STIR4200 module requires an external 12MHZ transistor which provides the clock source for sending and receiving signals. The DPOS and DNEG are defined as the USB data signals which are connected with the USB port. The TX_DATA and RX_FAST are defined as the infrared transceiver signals, and the signals from TX_DATA are modulated as the 4PPM codes in accordance in the STIR4200. The TFDU6300 is defined as the infrared transceiver. The U1 converts the supply power at the varied voltage from 5V to 3.3V to the STIR4200. The R5 and C8 compose a power-on reset circuit.

5.4.2 IrDA 1.0 (SIR-Pulse Modulation)

As the core model designed in the SIR system, the MCP2120 encoder/decoder is recognized with the following characteristic: (1) the micro-powered high-speed CMOS technology is used in the encoder/decoder; (2) it is designed to comply with the IrDA physical layer standard; (3) it may use any UART model and is consistent with all of the transceivers designed in accordance with the IrDA standard; (4) the baud rate rage varies from 9600bps to 115.2kbps, and reaches at 312.5kbps (maximum) when the clock frequency is set at 20MHz; (5) it can only transmit or receive data once at a time, indicating that the transmitting and receiving process will not occur asynchronously.

Figure 5-7 shows the device circuit used for the infrared transceiver modules which support the high speed FIR model. This module is also compatible with the SIR module. The reset default mode is set at the SIR mode. Moreover, when the data rate is below 115.2k, the mode is set at the SIR mode.

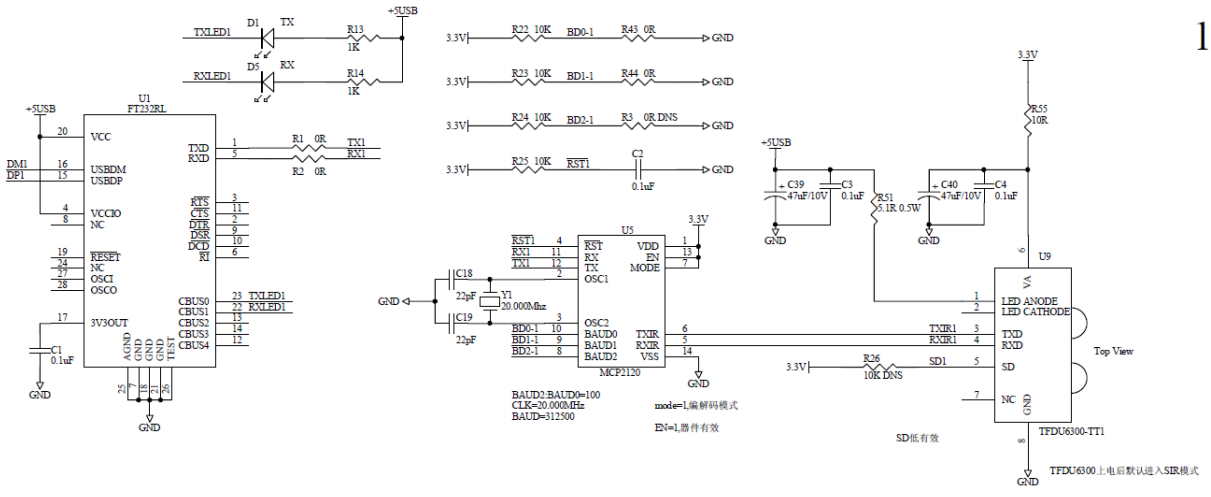

Figure 5-7 SIR Infrared System

By using the first channel as an example, the U1 (FT232R) is defined as the USB-UART conversion module, and the sent and received signal are transmitted to the U5 MCP2120 coding module through two resistors, R1 and R2. The modulations of TXLED and RXLED are employed to display the status of data transmission when the LEDs are switched on with data being transmitted. The signals ports, BD0, BD1 and BD2 transmit data through six resistors, when three 10K-ohm resistors are connected with a power supply of 3.3V. When each signal port is only connected with the 10K-resistor, the signal status is defined as 1, otherwise the signal indicates a 0. For example, the configuration of the image above can be described as BD2: BD0 = 100. TXIR and RXIR are defined as infrared transceiver signals, which are corresponding to the serial ports of TX and RX, respectively.

The TXIR signal is encoded directly and drives an infrared transceiver module of TFDU6300, whereas the coded waveform is shown below:

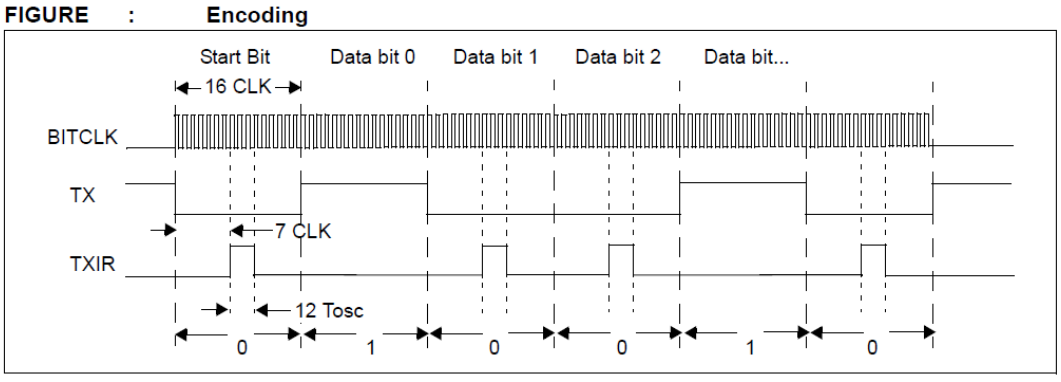

Figure 5-8 Clock

The BITCLK is defined as the clock. The TX represents signals from the serial port for which the baud rate could reach up to 312,500 (maximum 312500), and TXIR is defined as the infrared signal with its baud rate calculated by using the equation of

$(312500\times16)/3 = 1.67Mbps$ (each TX signal corresponds to 16 BITCLK, the frequency of BITCLK is $312500\times16Hz$, and the TXIR pulse width is three times to the BITCLK pulse width. In conclusion, the frequency of TXIR is 1.67Mpbs. More accurately, the 1.67Mbps is the peak data rate of TXIR.

5.5 Summary

Using same geometry model as the Infrared MIMO system based on OOK modulation, this chapter has described the theoretical approach and the circuit design of the infrared MIMO system based on a 4PPM modulation, and also a MIMO system based on the SIR pulse modulation. The comparisons are made on the SISO system, including 1X4, 2X4 and 4X4 MIMO system. Moreover, the experiment methodology is described in detail, and the experimental results and the performance analysis on various bit error rates shall be further discussed in the next chapter.

References Chapter 5

[1] Z. Ghassemlooy, S. Rajbhandari, "Performance of diffused indoor optical wireless links employing neural and adaptive linear equalizers", *Proc. IEEE 6th conference on Information, Communications and Signal Processing*, pp. 1-6, 2007 [6 pages].

Chapter 6 Performance Analysis

6.1 Introduction

Using the settings and the systems designed in the previous chapters, the varying performance of different systems is analysed.

Three different systems using OOK, SIR-RZI and PPM modulations with MIMO technologies are illustrated in this chapter. It is worth mentioning that all the systems have one thing in common, that is, they have the same geometric model as shown in Chapter 4. As having been displayed in Section 4.5, this model is designed to have transmitters and receivers fixed in two metal boxes set on a stand with a track, which makes the changes of the distances between transmitters and receivers uniform and stable. There are four transmitters/receivers placed uniformly in the metal boxes, where the LEDs are placed with the same lateral and vertical distances to the edge of each box, In the later sections, the effects of both distance and background lighting conditions (switching on/off the room light) will be examined using this model.

Based on the geometrical model in Section 4.5, in addition to the distances and the background lighting conditions, another important parameter, the displacement between transmitters and receivers, is also included as shown. The transmitters are fixed on the track, while the receivers can move in parallel. As a result, the

displacement of incidence keeps changing. The bit error rate (BER) performance is evaluated in all experiments, and the differences due to changing distances and displacements are analysed in the following sections.

In all three systems, transmitters and receivers were built, each of which was fixed on the track, whereas displacement of the receiver and transmitter stand could change from -10cm to 10cm (for the experiments on displacement). The maximum distance between the transmitter and the receiver stand can reach 2.4m (due to the transmission range of the transmitters).

6.2 Experiment Performance Analysis

6.2.1 OOK Modulation 100kHz

It is worth noticing that experimental progress has been achieved by varying the distance between transmitters and receivers from 20cm to 140cm with a step size of 10cm, but only 20cm, 50cm, 70cm, 100cm and 140cm have been illustrated in this thesis.

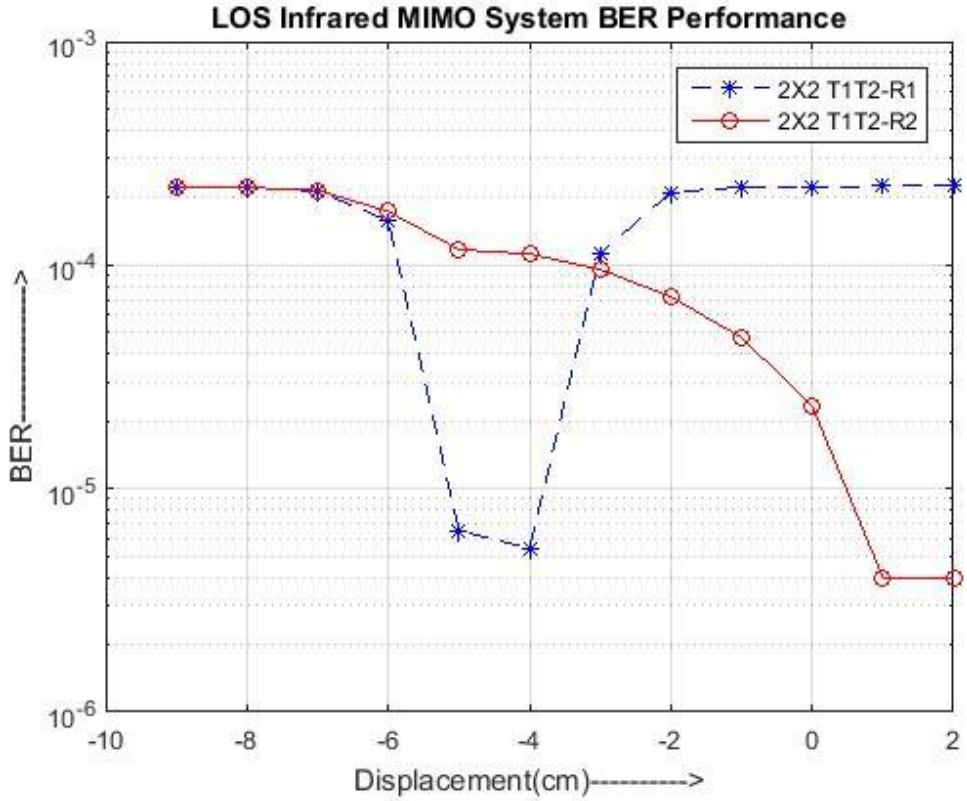

Figure 6-1 Distance = 20cm

In Figure 6-1, the result of BER-Displacement performance for distance = 20cm in the OOK 2X2 MIMO system is illustrated. The lateral coordinate is defined as displacement values, or defined as the displacement from the centre axis of the Receiver boxes, whereas the vertical coordinate is defined as the BER values.

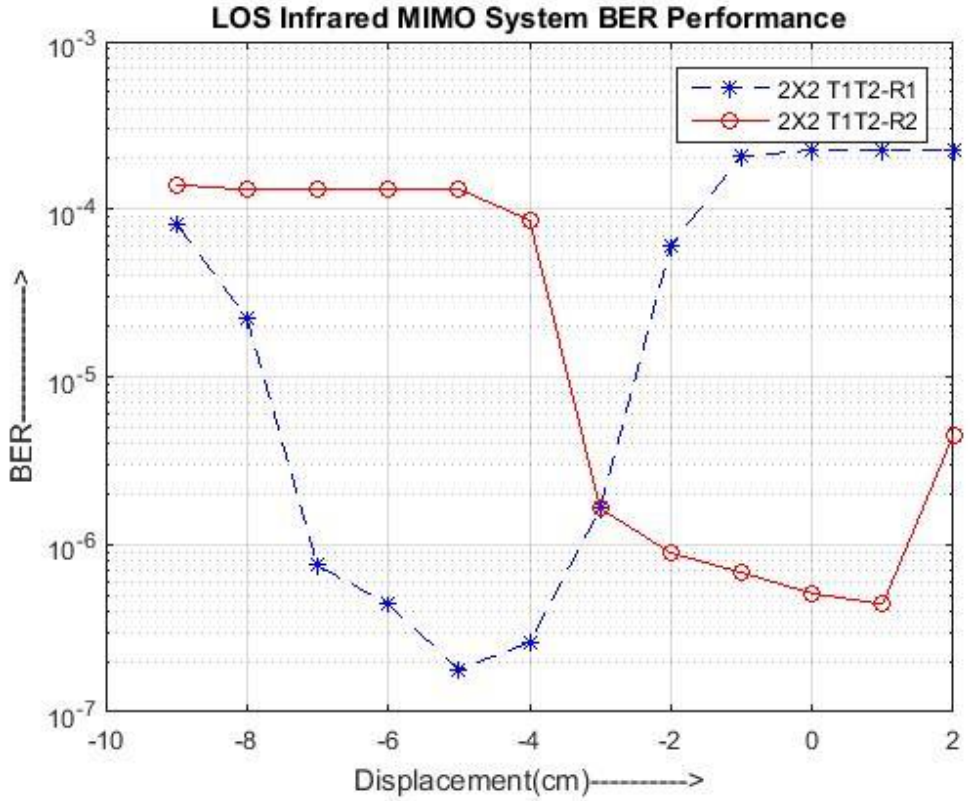

Figure 6-2 Distance = 50cm

Figure 6-2 shows the BER performance received from the experiments for distance = 50cm. In this case, the BER values received from the middle-ranged distances declines more sharply than those from the closer distances because of the increased coverage and lower power densities. The BER value of the Receiver 2 (R2) shows a gradual decline, mainly because that the transmitter box is moved to the middle where the coverage of R2 is greater.

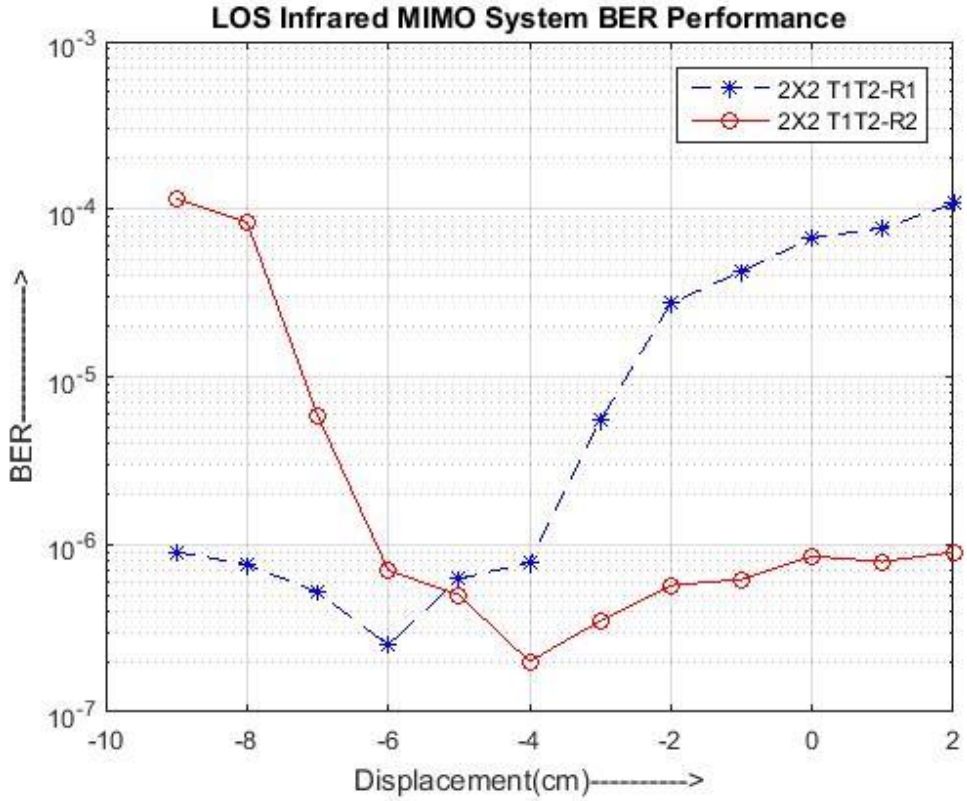

Figure 6-3 Distance = 70cm

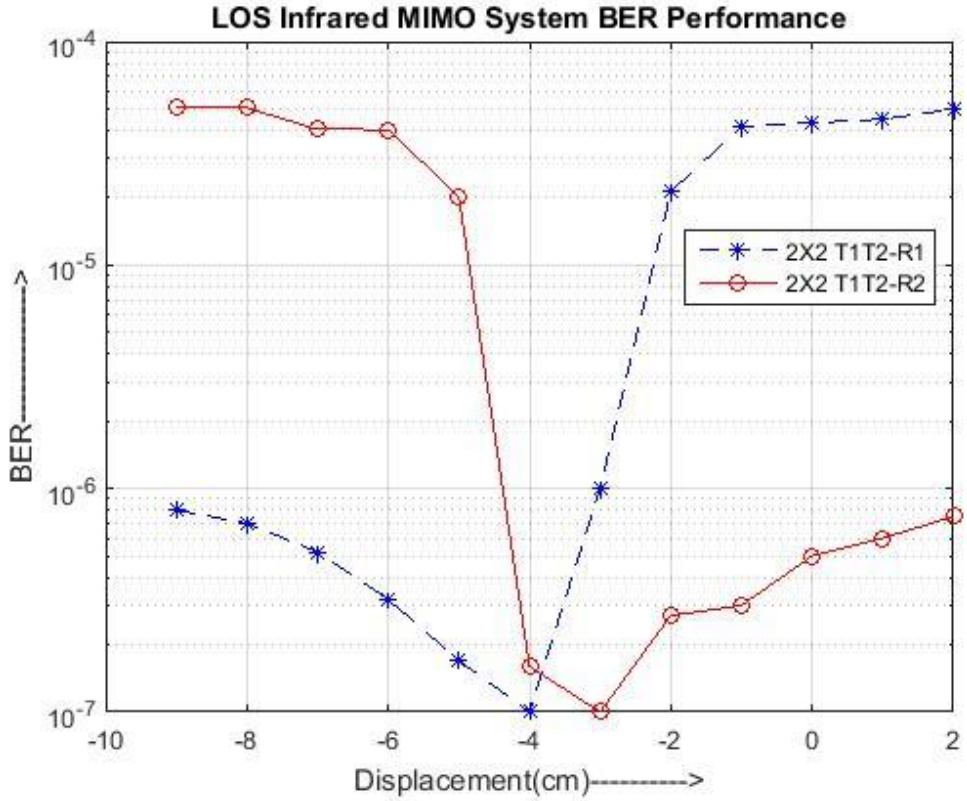

Figure 6-4 Distance = 100cm

In Figures of 6-3 and 6-4, it illustrates the BER values of the two receivers in the long-ranged distances, whereas the BER value of R1 increases while the BER value of R2 decreases when the receiver box is moved with changing distances. It can be observed that the BER performance of the two receivers is presented with symmetric features due to different angle values, but they function in the same fashion, and share the same circuit design.

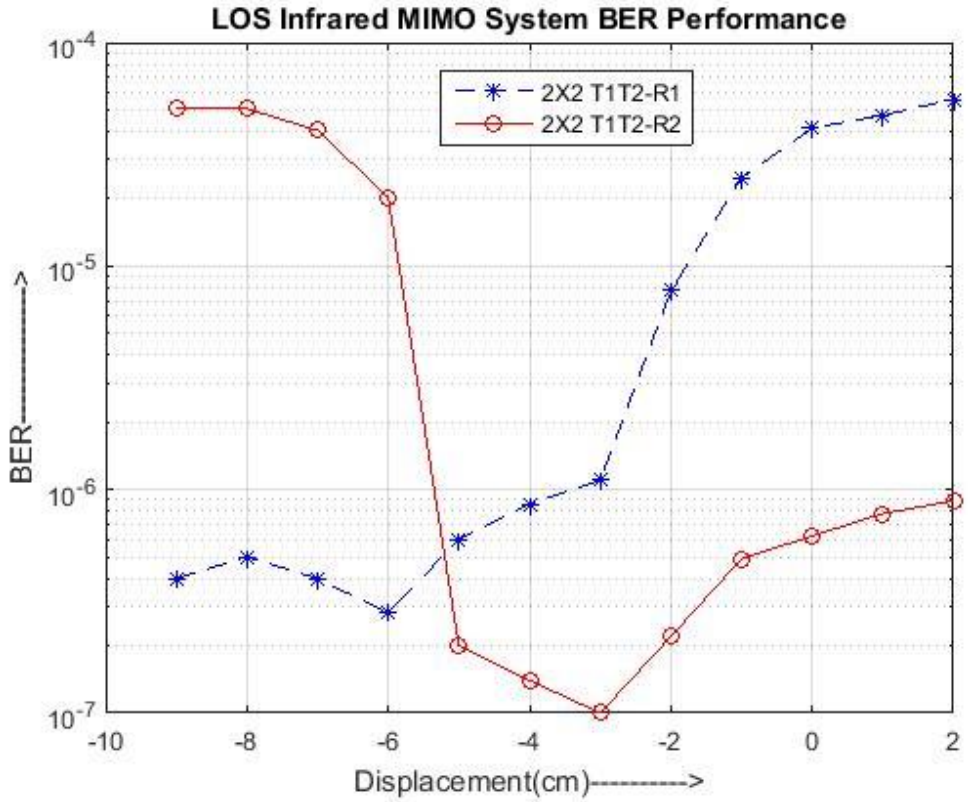

Figure 6-5 Distance = 140cm

The distance represents the lateral length measured between LEDs and photodiodes, and the displacement represents the movement from the centre axis of the Receiver boxes. The diagrams above illustrate the BER-Displacement correlations. It is worth noticing that displacement 3 is considered as the middle displacement of the receiver box. The reason for choosing 3 as the middle angle, instead of 0, is that the circuit of the receivers is so designed to avoid having the photodiodes placed in the middle of

the box. According to the diagrams illustrating the results from the experiments, the BER performance of the two receivers crosses with each other at the lower value sections with the variations in angles. When the receiver box is moved with its position from one side to the middle, Receiver R1, which was fully covered, demonstrates a highly accurate BER value, whereas the BER value of Receiver R2 is a 100 times higher than that of R1. However, the BER value of R1 becomes higher with the changes in the angle. Moreover, it is observed that the BER of R2 reduces considerably when the displacement approaches at the central axis. It is also worth noticing that, when the distances increase, the BER value is improved with increased coverage. When the distance becomes greater than 100cm, the BER value shows a decline due to the path loss.

6.2.2 OOK Modulation 1MHz

It is worth noticing that experimental progress has been achieved by varying the distance between transmitters and receivers from 20cm to 140cm with a step size of 10cm, but only 20cm, 60cm, 140cm were illustrated in this thesis.

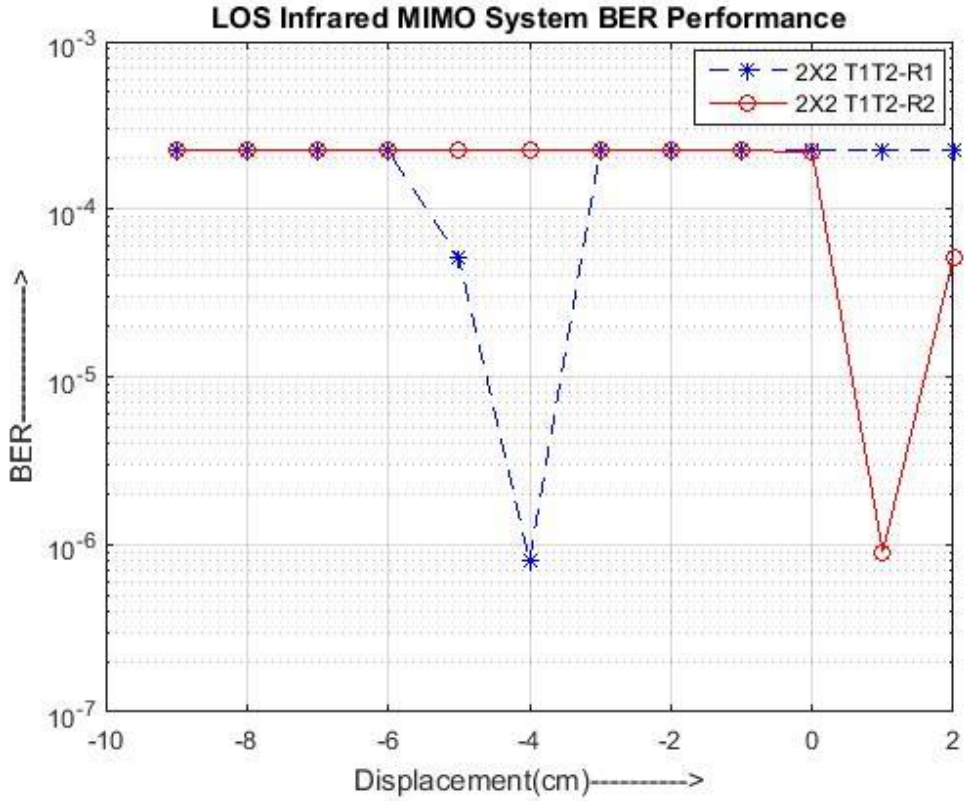

Figure 6-6 Distance = 20cm

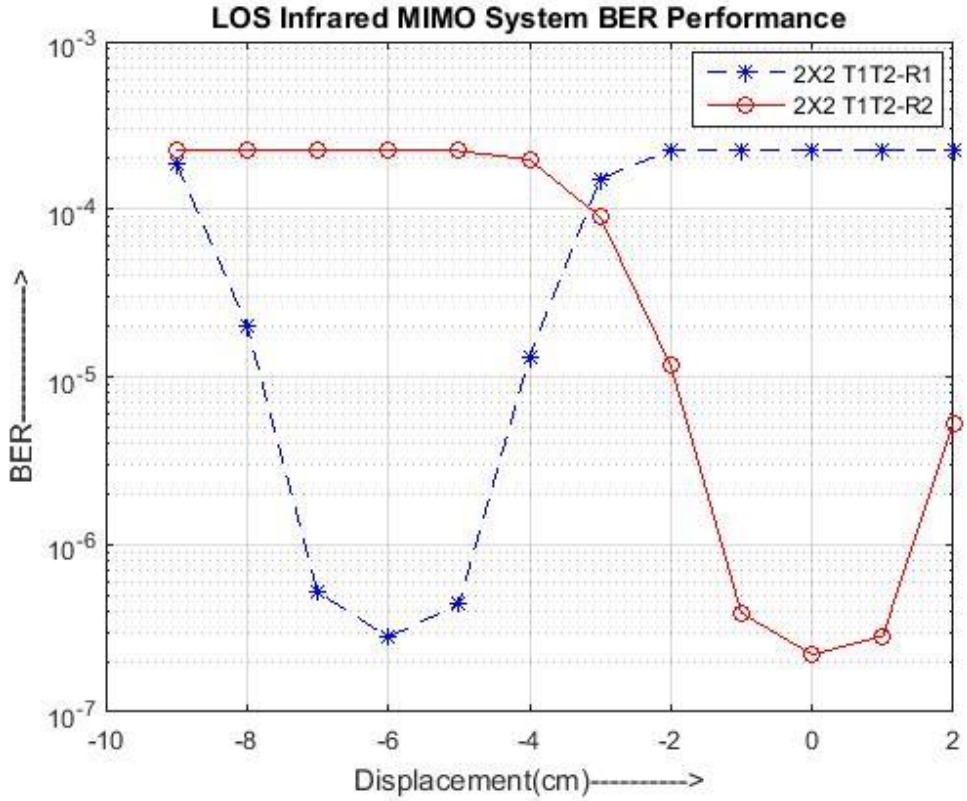

Figure 6-7 Distance = 60cm

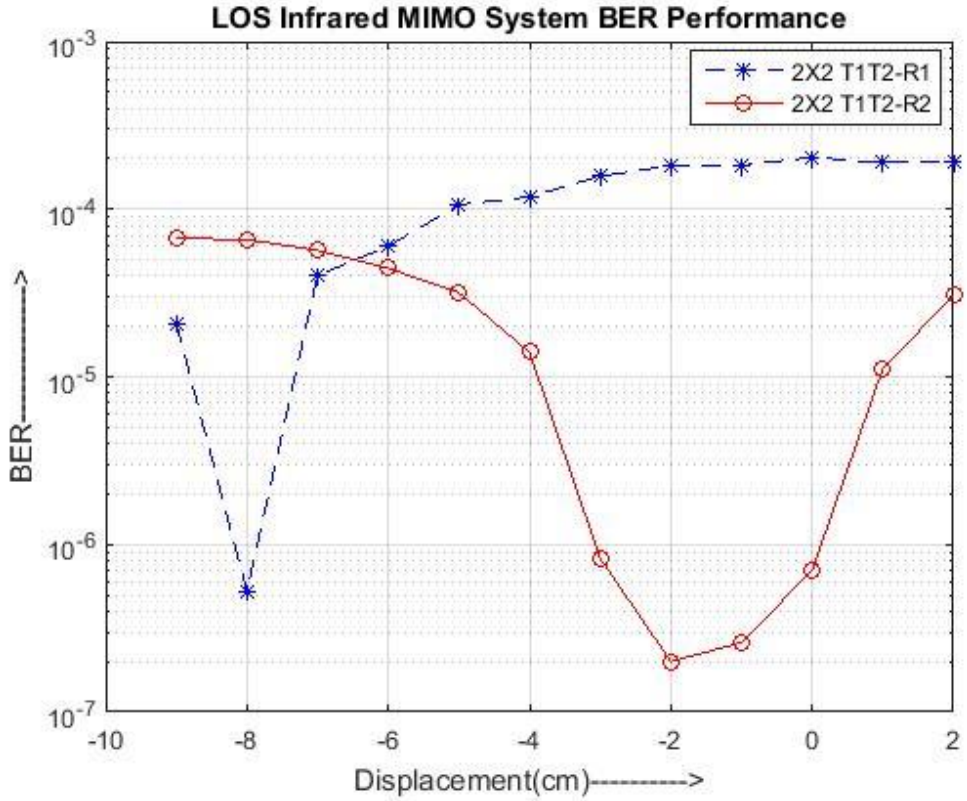

Figure 6-8 Distance = 140cm

In Figures of 6-6 to 6-8, the BER performance of the OOK system is shown when the bandwidth is of 1MHz, whereas the distance varies from 20cm to 140cm.

It is noticed that Receiver R1 and R2 demonstrates different distribution patterns, which have resulted from the differences in the receiver soldering angles, and the errors occurred during the installation and measurement process, which is considered to be acceptable from the viewpoint of the circuit designs.

It is clearly shown that the general performance trend of BER values received from 1MHz and 100kHz bandwidth are similar. However, the error rate occurred at R1 increases when the angle is moved into the middle ranges, whereas the error rate of

R2 shows exactly the opposite behaviour. It is also worth noticing that the interference from the background lighting conditions and path loss from the system at 1 MHz is more significant than that from the system of 100kHz. This is probably due to the differing noise bandwidths implied by the differing signal bandwidths necessary.

6.2.3 OOK Modulation in the Dark at 100kHz

It is worth noticing that experimental progress has been achieved by varying displacement from central axis of receivers each 1cm from 0cm to 11cm, but only 0cm, 3cm, 7cm and 10cm were illustrated in this thesis.

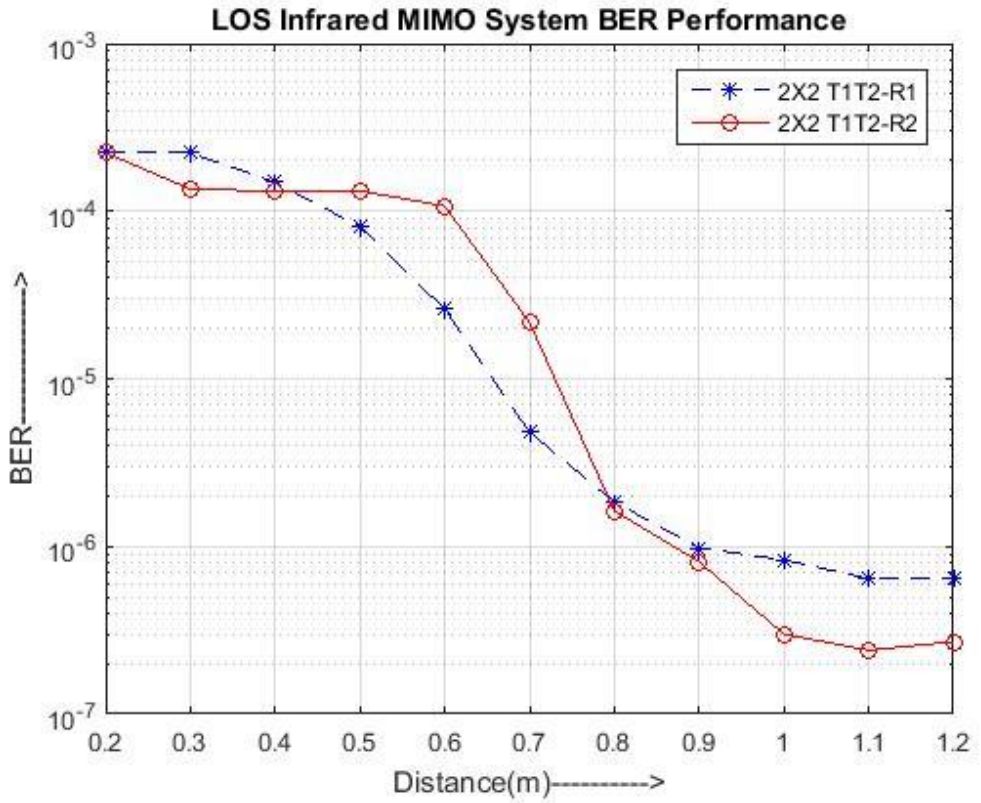

Figure 6-9 Displacement = 0cm

In Figure 6-9, the BER values of R1 declines more sharply than those of R2, because the distance between Receiver 1 and the centre axis of the transmitter box is shorter. When the displacement increases, the effect of the displacement values becomes weaker, consequently, the BER values from both R1 and R2 decline less.

The range with the angle value of 0-3cm is considered as the centre area, where the infrared power is considered to be most concentrated. The x-axis represents the distance apart, whereas the y axis represents the BER performance of the two receivers.

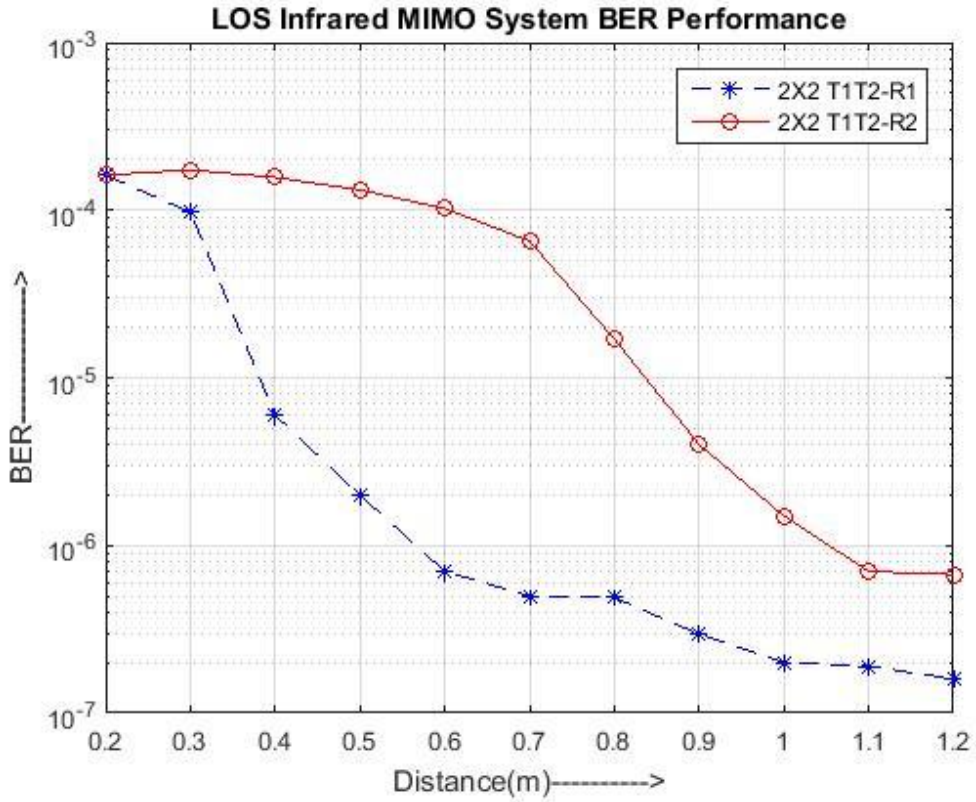

Figure 6-10 Displacement = 3cm

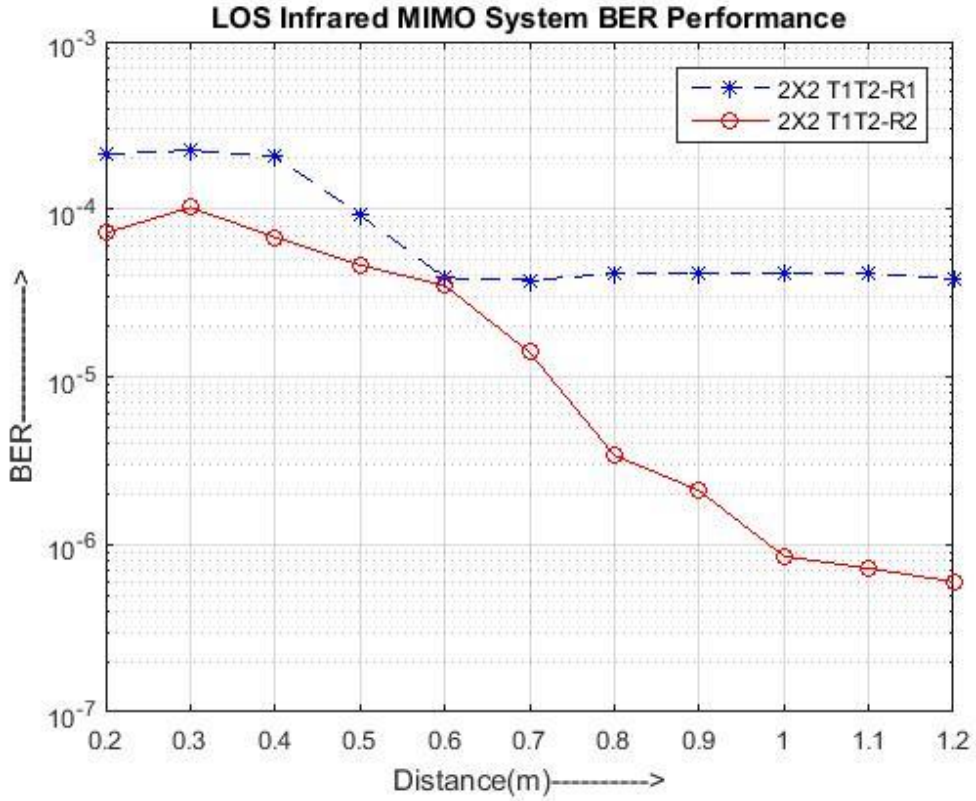

Figure 6-11 Displacement = 7cm

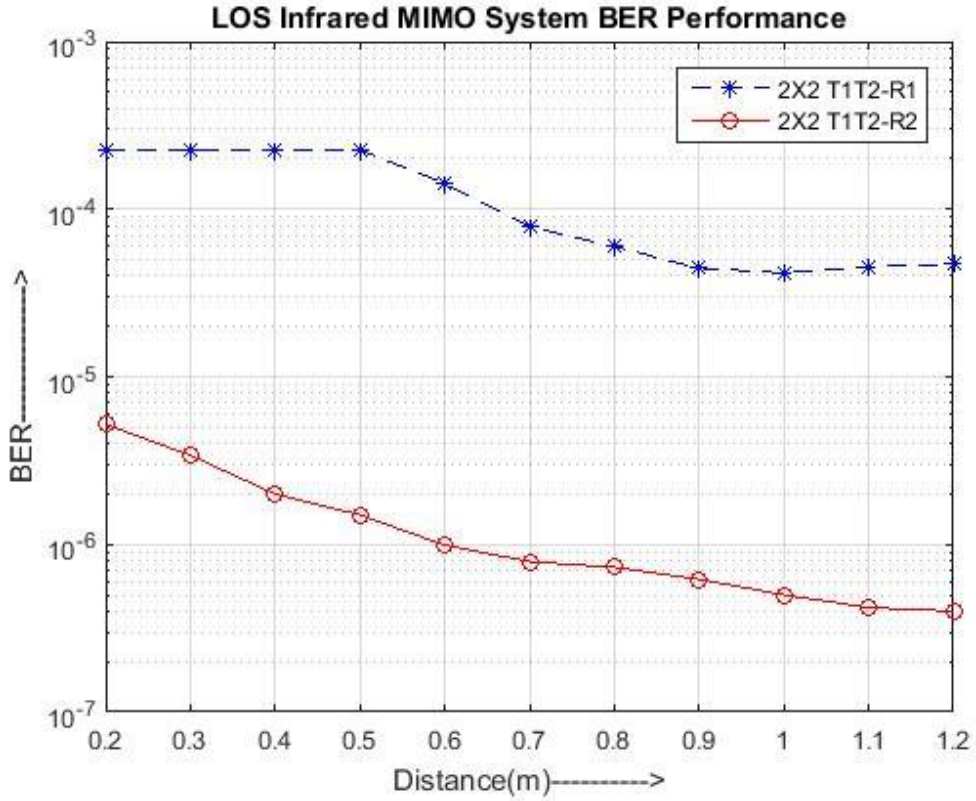

Figure 6-12 Displacement = 10cm

In this section, discussions and analysis are focused on the experiments conducted in a darkroom when all room lights are kept turned off, and the experiments are performed during the night time. It is concluded that the outcomes of the system performed in the darkroom are better than those conducted under normal daylight conditions, when the error rate is 3 times lower than the level of the latter, because of the reduced noise and other interferences.

In Figures of 6-10 to 6-12, the BER values are displayed with the plotted curves when both angle and distance are changed. The first group of experiments are conducted with results plotted with the varied distances as the abscissa. With the distance varied within the short and middle ranges, the BER value decreases when the receiving angle increases, which is observed for both Receiver R1 and R2. However, the BER value shows a stabilized flat shoulder when the displacement exceeds 8cm, and the performance of R1 is much worse than that of R2 due to a longer placed distance, which results an error rate nearly 100 times higher.

6.2.4 OOK Modulation in the Dark at 1MHz

It is worth noticing that experimental progress has been achieved by varying the displacement from central axis of receivers each 1cm from 0cm to 11cm, but only 0cm, 2cm, 4cm, 6cm 8cm and 10cm were illustrated in this thesis.

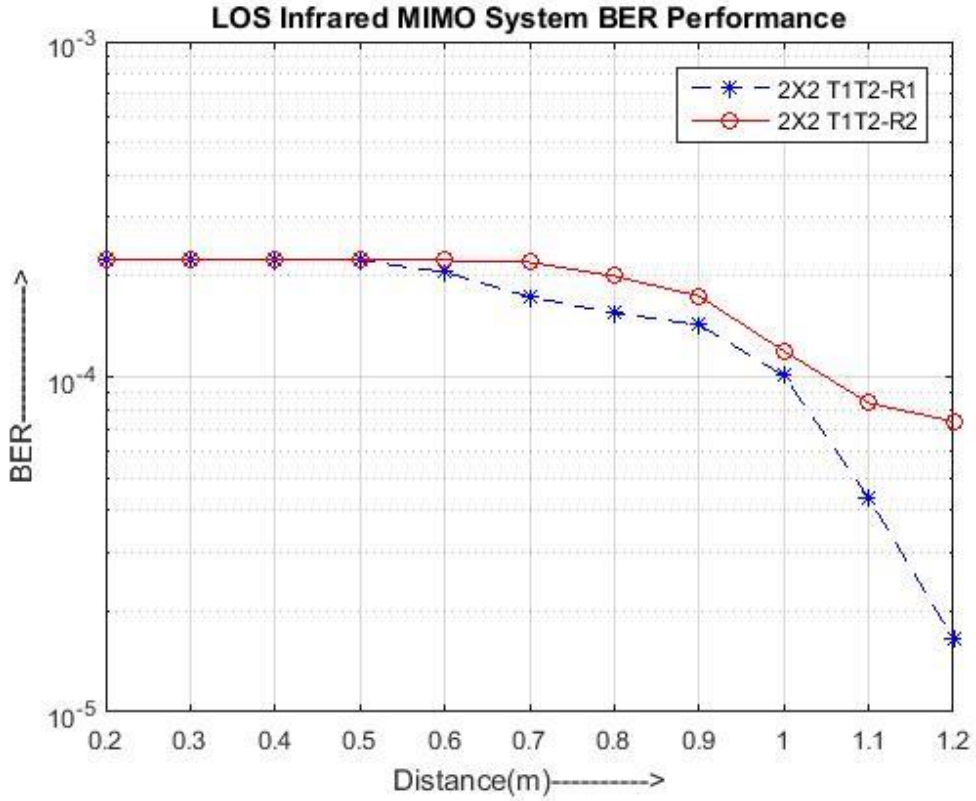

Figure 6-13 Displacement = 0cm

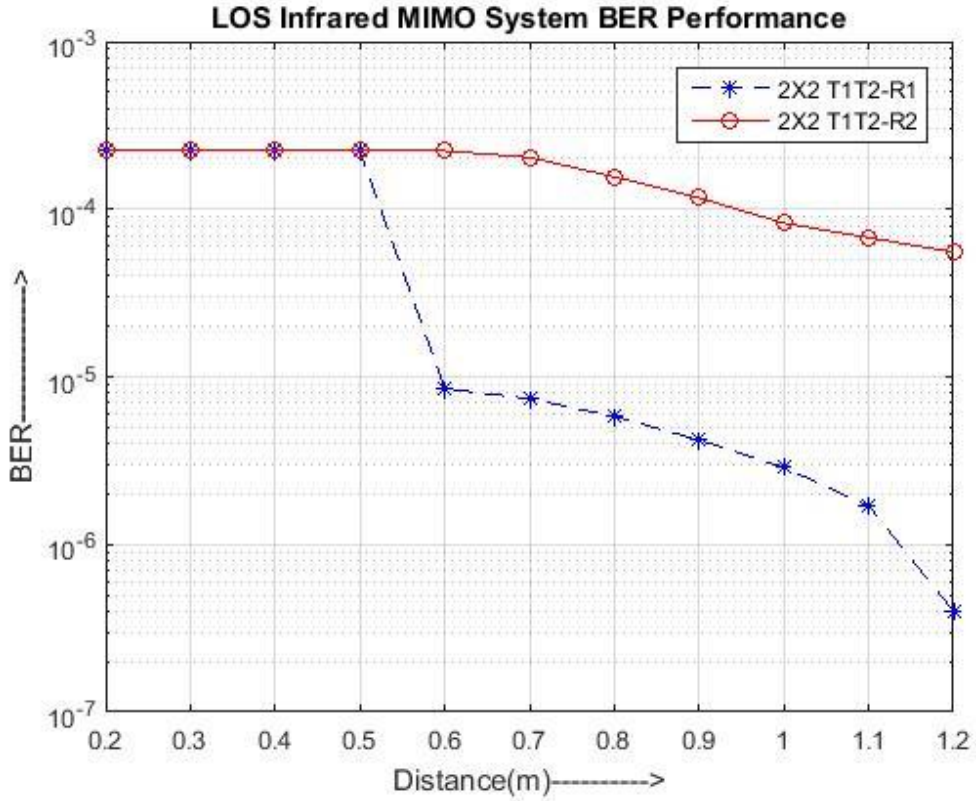

Figure 6-14 Displacement = 2cm

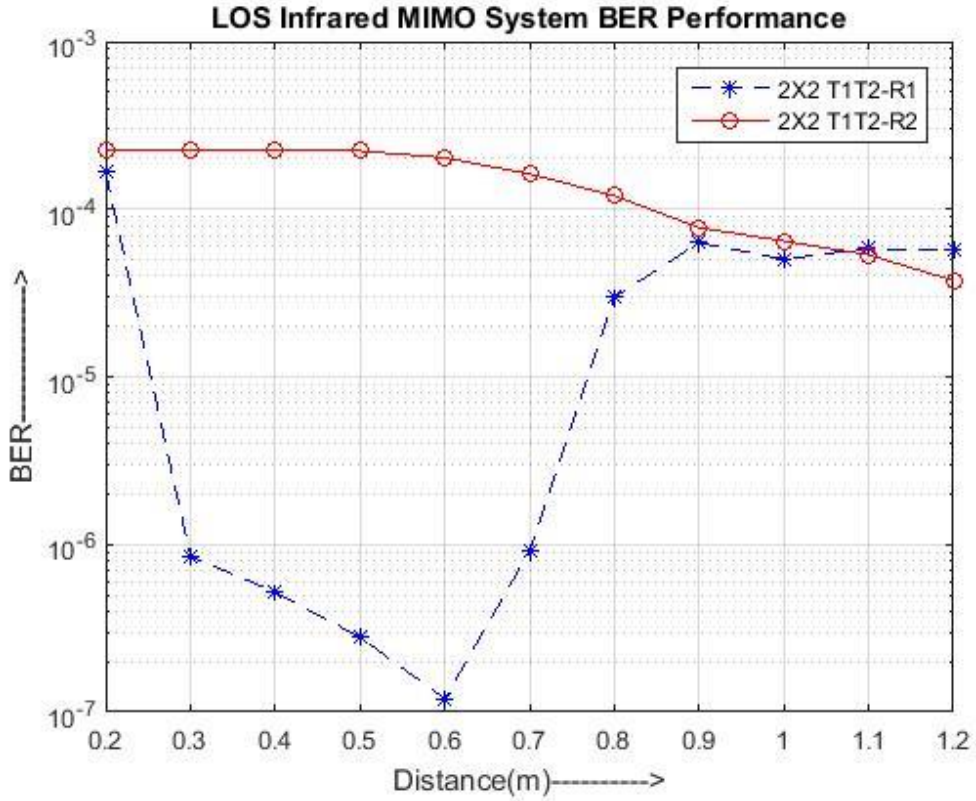

Figure 6-15 Displacement = 4cm

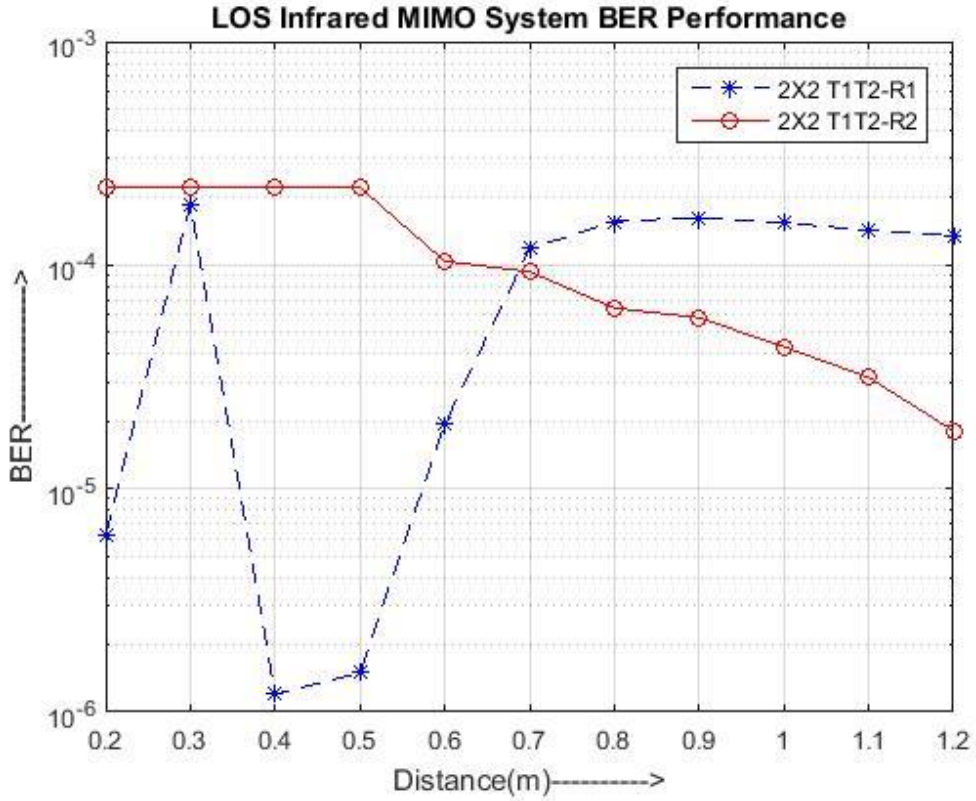

Figure 6-16 Displacement = 6cm

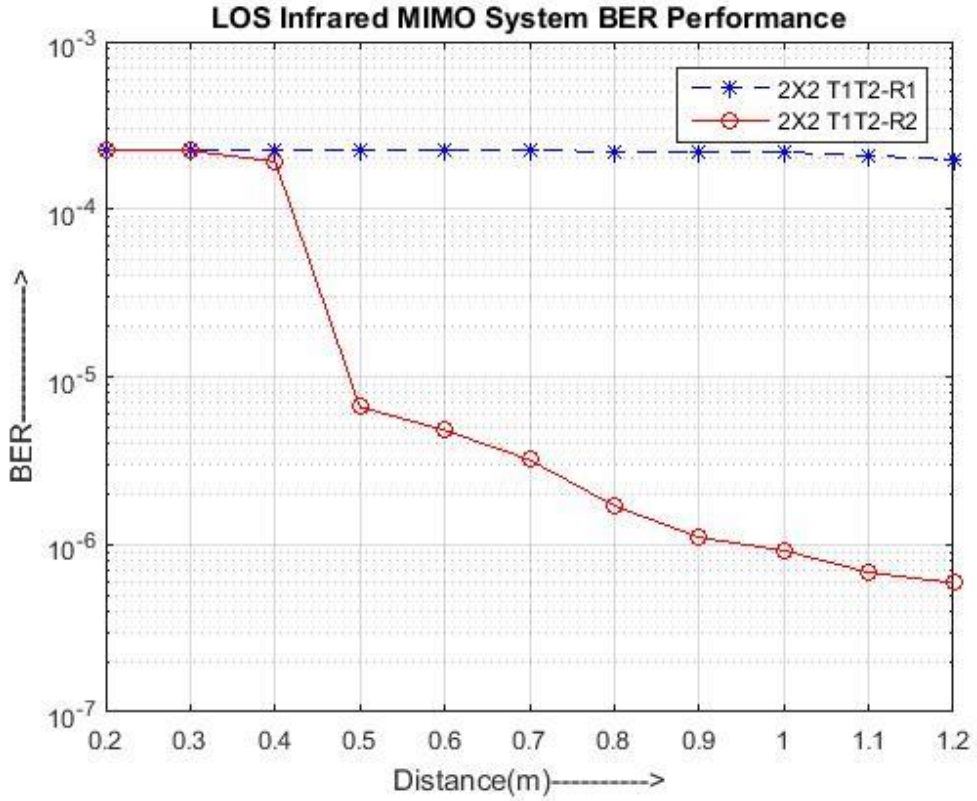

Figure 6-17 Displacement = 8cm

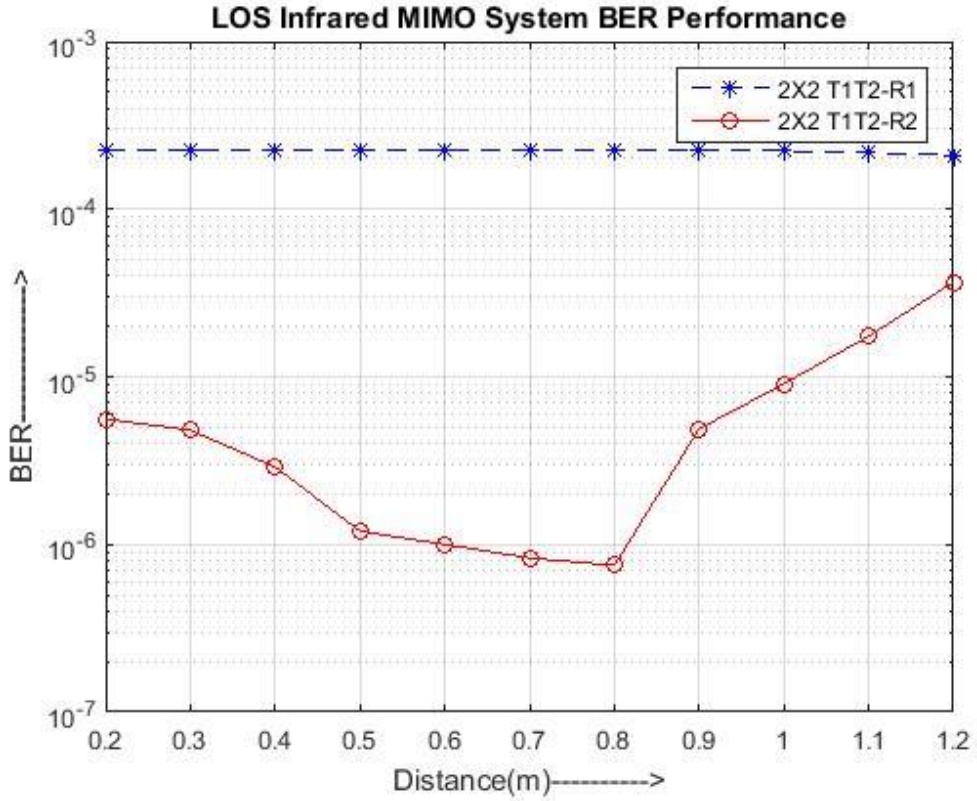

Figure 6-18 Displacement = 10cm

Unlike the smooth curve as having demonstrated from the experiment results by using the OOK modulation with a bandwidth of 100kHz, and which are conducted in a darkroom, the results of these particular experiments show severe fluctuations in the plotted curves. There are several reasons contributed to such behaviours, including:-

1. In comparison with those conducted with 100kHz bandwidth signals, the experiments performed at a higher frequency are more susceptible to errors because the BER value of 1MHz system are higher and easier to be affected by background light and other noise sources. In Figure 6-15, the BER value dips when the distance varies from 20cm to 60cm, and climbs back when the distance exceeds 60cm. Such behaviour can be best explained when the coverage increases with the distance, the BER values decline, however, when the distance reaches at a certain point, the path loss become more dominant than the other factors, which leads to the increases of BER values with distances, consequently. In Figures 6-16, the BER of R1 increases when the distance increases from 20cm to 30cm, due to the low coverage at 30cm and high interference due to background lighting within the corresponding range.

2. When the horizontal displacement is over 7cm, the receiver placed at the far side, R1, moves out of the coverage, which results in the BER tending to become a constant value.

6.2.5 SIR-RZI Modulation

The following section focuses mainly on the review and evaluation of the correlation and differences between the SISO and MIMO approaches. Three groups of independent experiments have been conducted, including the SISO, the 2X4 MIMO, and the 4X4 MIMO SIR-DZI systems. The X-coordinate represents the displacement and the Y-coordinate represents the BER value.

1. SISO SIR-RZI Modulation based system

It is worth noticing that experimental progress has been achieved by varying the distance between transmitters and receivers each 10cm from 20cm to 150cm, but only 20cm, 80cm and 150cm were illustrated in this thesis.

2. 2X4 SIR-RIZ Modulation based system:

It is worth noticing that experimental progress has been achieved by varying the distance between transmitters and receivers each 10cm from 20cm to 150cm, but only 20cm, 80cm and 150cm were illustrated in this thesis.

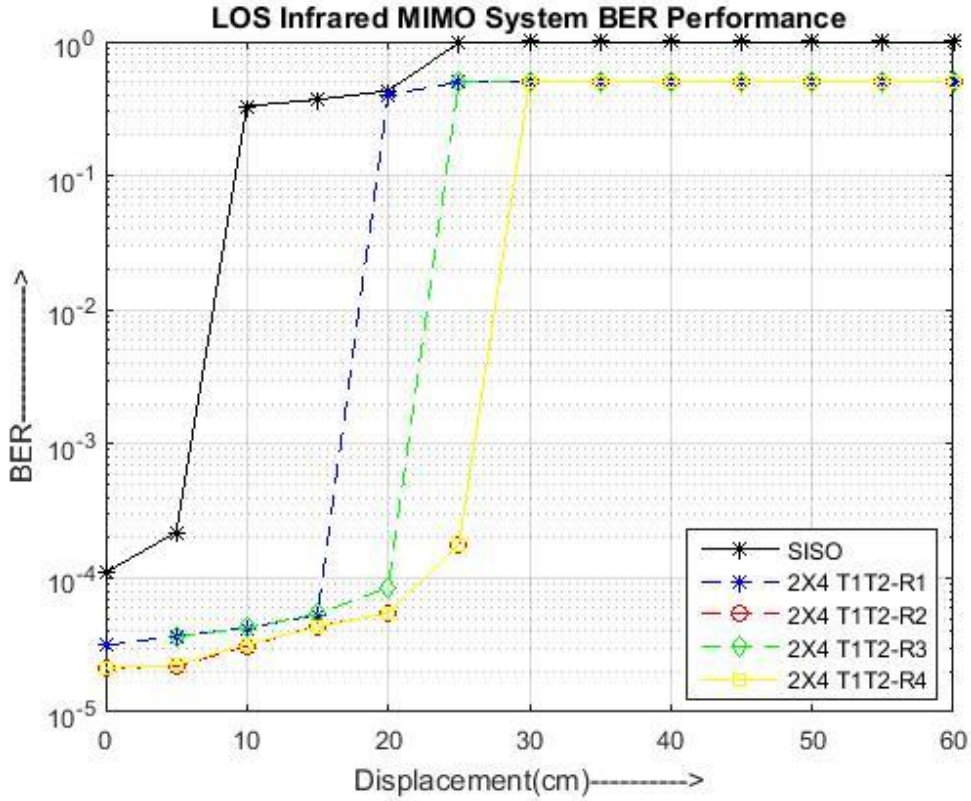

Figure 6-19 Distance = 20cm

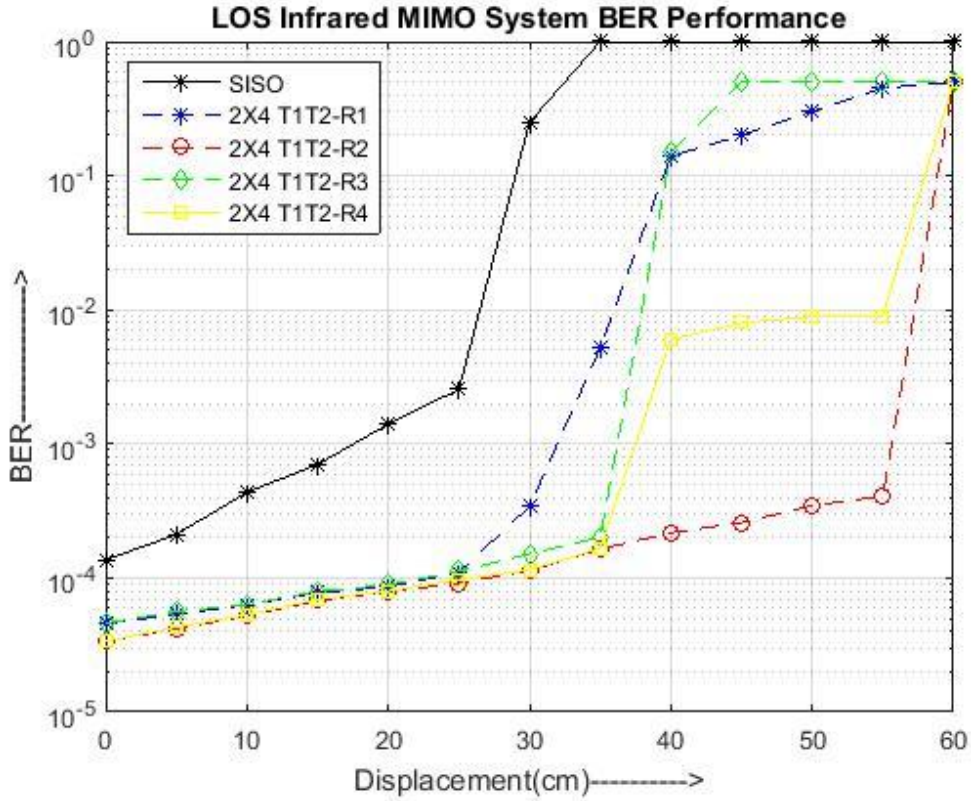

Figure 6-20 Distance = 80cm

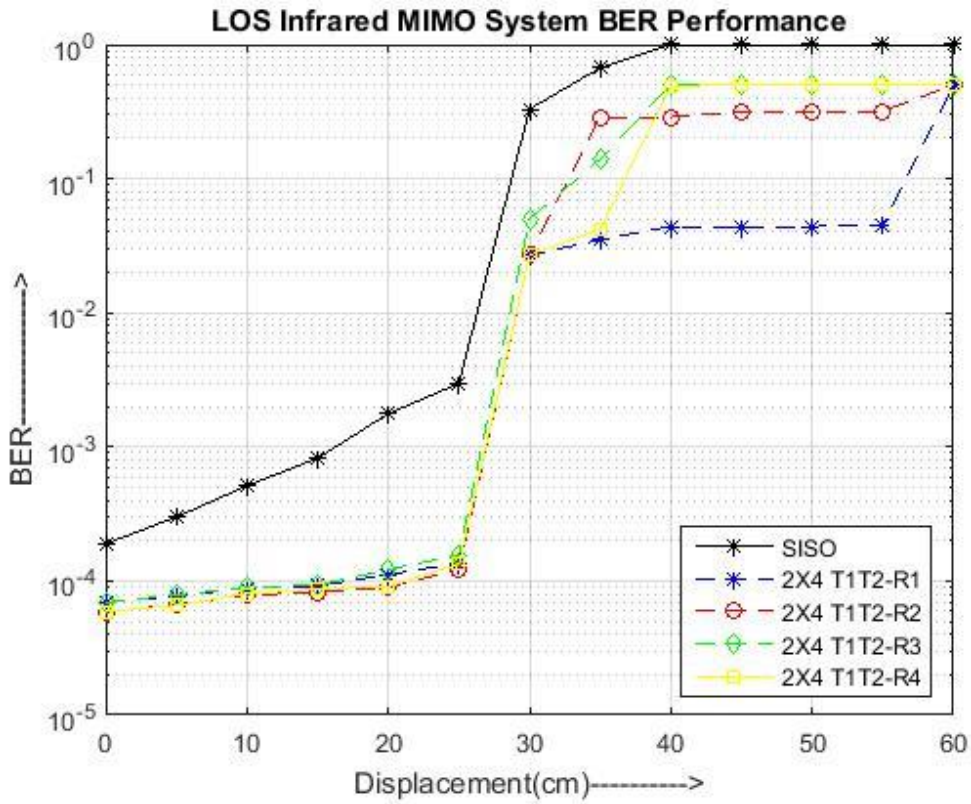

Figure 6-21 Distance = 150cm

3. 4X4 SIR-RZI Modulation based system:

It is worth noticing that experimental progress has been achieved by varying the distance between transmitters and receivers each 10cm from 20cm to 150cm, but only 20cm, 80cm and 150cm were illustrated in this thesis.

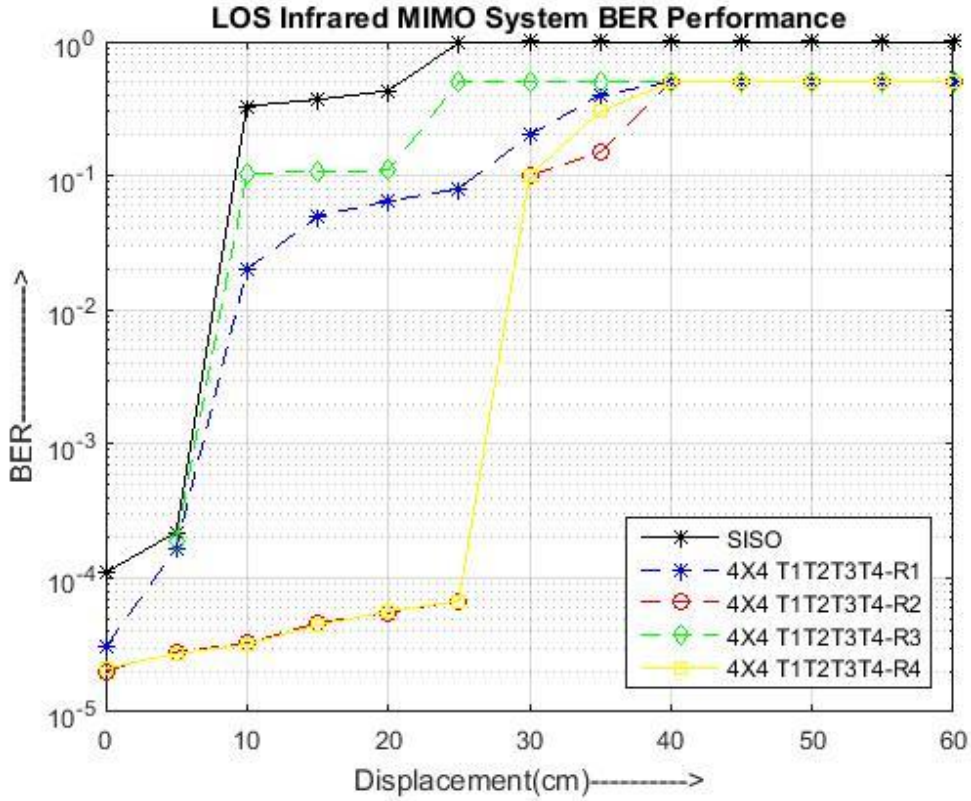

Figure 6-22 Distance = 20cm

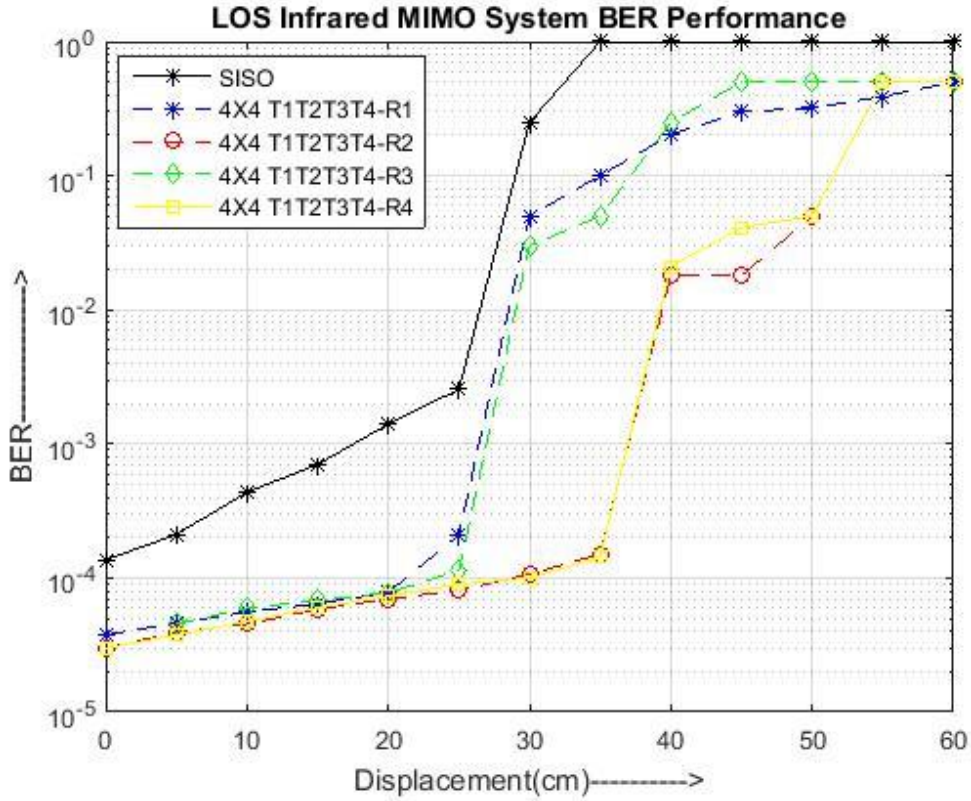

Figure 6-23 Distance = 80cm

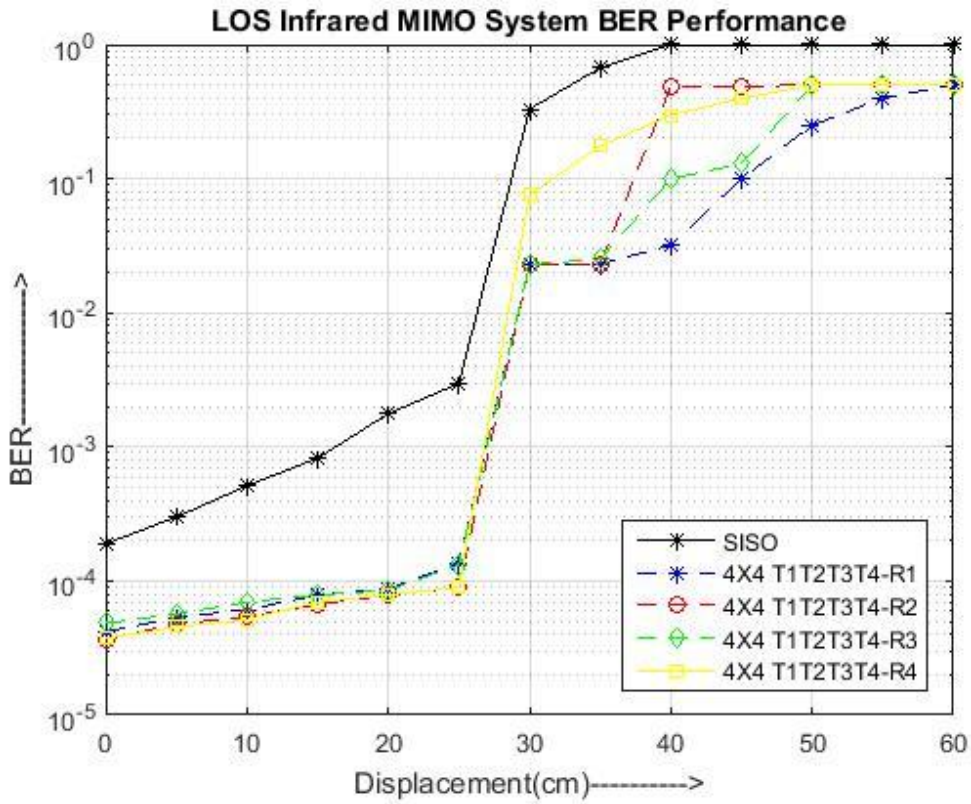

Figure 6-24 Distance = 150cm

This section covers the review and discussion on three groups of empirical data, amongst which two groups come from the application of MIMO technology, and one comes from the reference data of a SISO system. All of the experiments are conducted by using SIR-RZI modulation in accordance with the MIMO system.

It can be clearly observed that, within the effective range of the coverage and distance, both the 2X4 and the 4X4 MIMO systems present superior results in comparison with those from the SISO system. However, within the middle displacement values (0 – 20cm), the 2X4 MIMO system demonstrate better performance than that of the 4X4 system, which results from more concentration and faster signal allocation and transmission. In the 2X4 system, the controller only needs to allocate the transmitting signal between two LEDs, which functions as the

switch to be turned on and off. However, in the 4X4 system, the controller has to allocate the data into 4 channels, which results in a longer response time and higher possibility of data error. On the other hand, the 4X4 system has demonstrated far better performance in the displacement coverage, whereas the system proves to work effectively when the displacement exceeds 30cm.

It is well recognized that in the 4X4 MIMO system, the effect of displacement plays a more important role than in SISO-based 2X4 MIMO systems. It is also recognized that the BER performance illustrated in this section shows that the SIR-RZI system has better stability, broader coverage and has increased resistance to interferences, but however, it is more difficult to implement for application purposes.

6.2.6 PPM Modulation 1MHz

It may be seen that the experimental proceeded by varying the displacement from central axis of receivers each 5cm from 0cm to 60cm, but only 0cm, 25cm, 40cm and 60cm were illustrated in this thesis. SISO experimental result of displacement 0cm was used as the reference data.

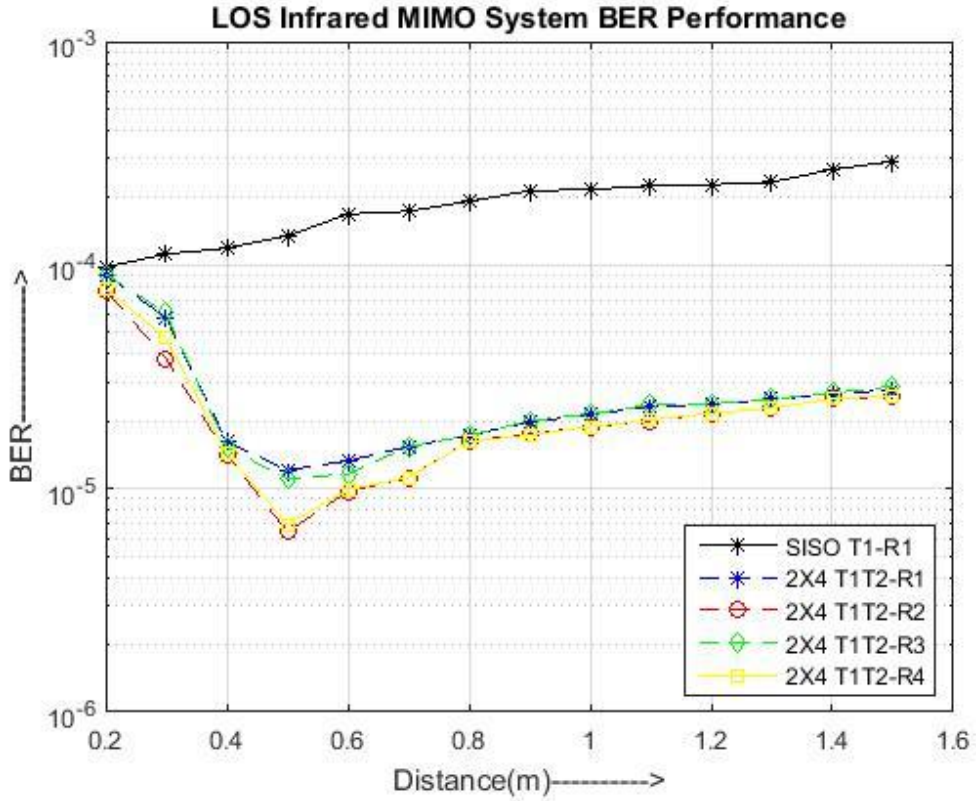

Figure 6-25 Displacement = 0cm 2X4

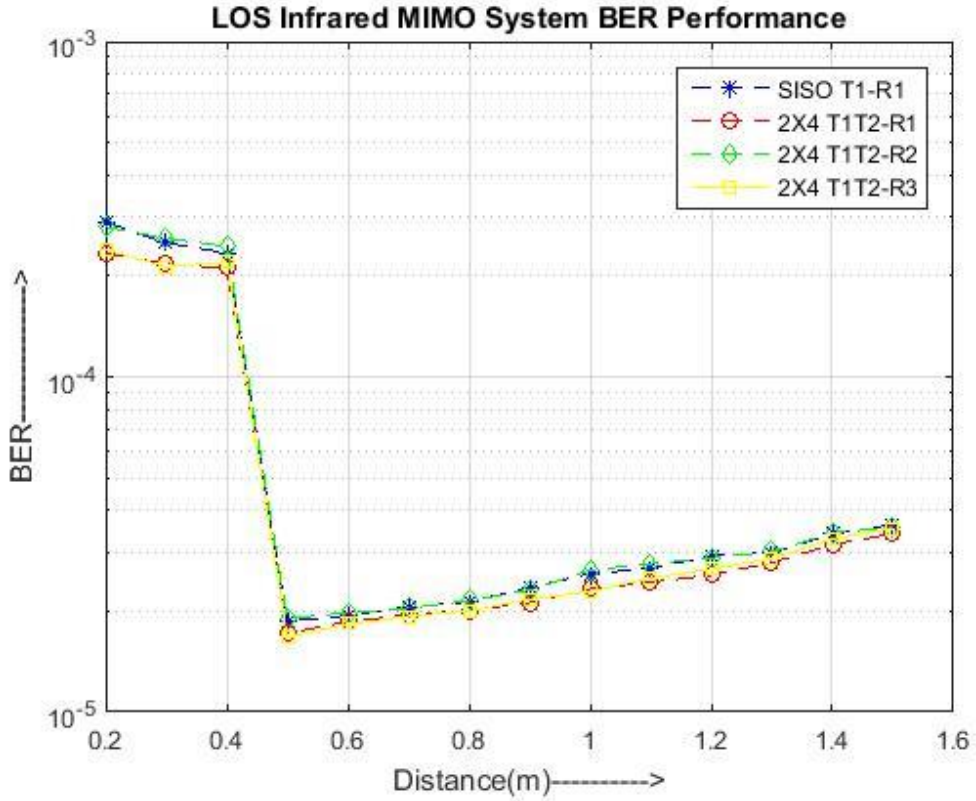

Figure 6-26 Displacement = 25cm 2X4

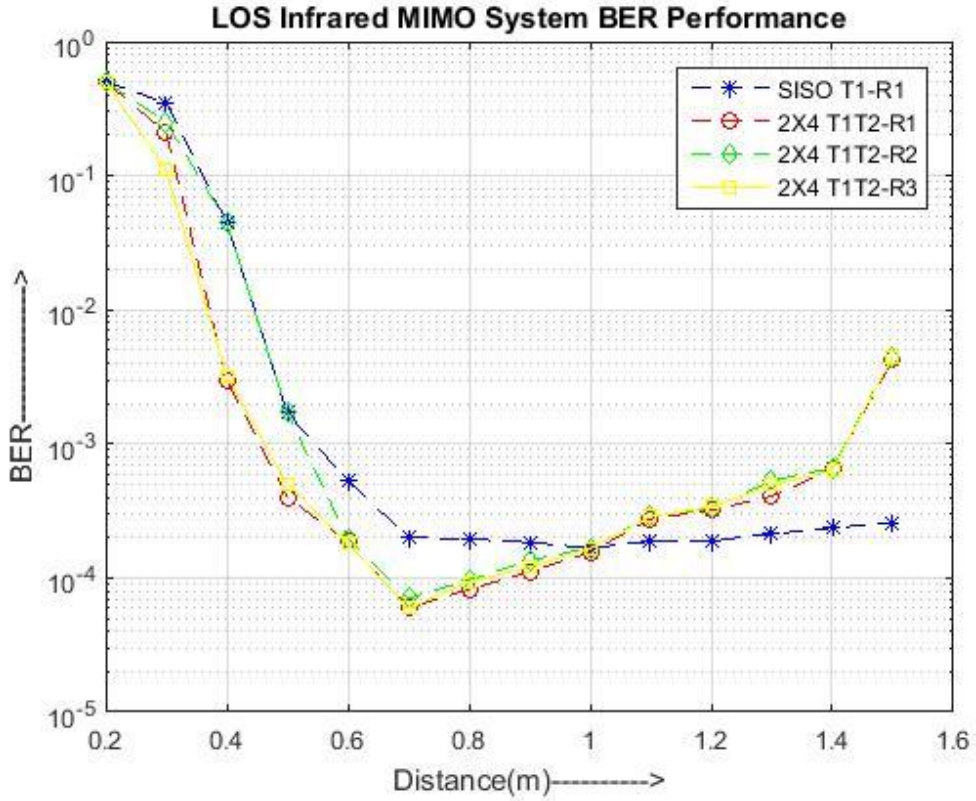

Figure 6-27 Displacement = 40cm 2X4

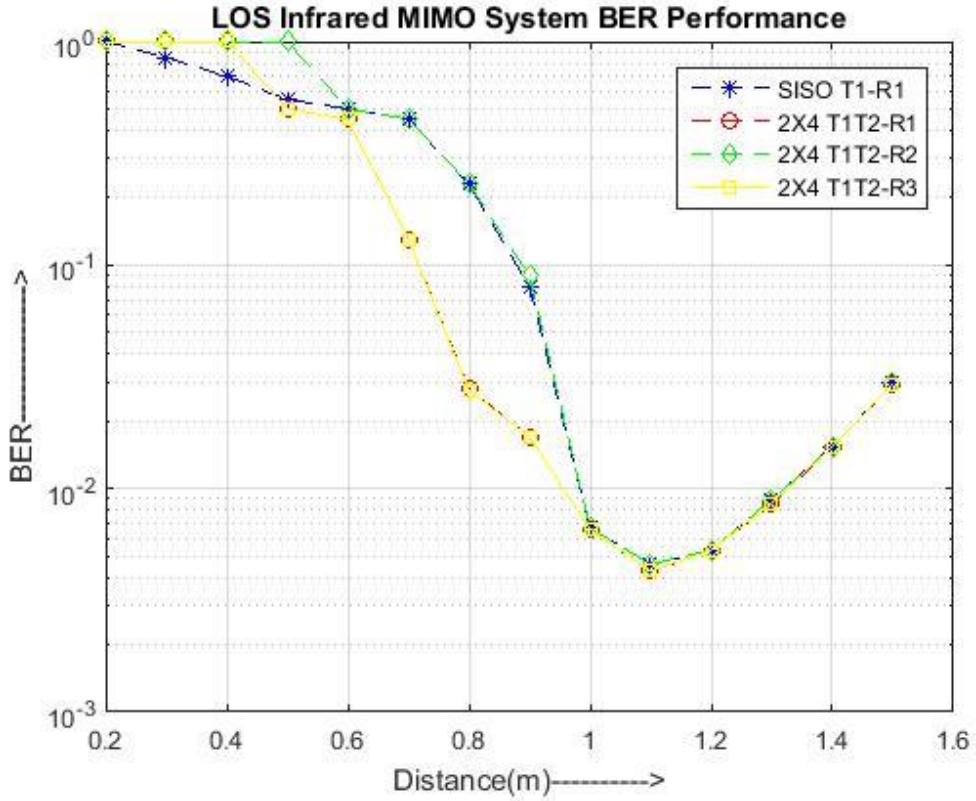

Figure 6-28 Displacement = 60cm 2X4

The distance between the transmitter box and receiver box is the lateral coordinate, and the vertical coordinate is the BER performance value.

In the 4PPM MIMO system with a frequency of 1 MHz, one group of SISO data was recorded for reference only. In comparison with the SISO system, it is clearly observed that the BER performance based on the MIMO system is 10 times better (as shown in Figure 6-25). By taking the same emitter angle and radiant intensity of LEDs, and also by choosing a similar sensitivity of photodiode at 20MHz and 30MHz respectively, the PPM system shows better performance in comparison with the OOK system, which shows a broader coverage, i.e., the PPM transceiver box is 1.235 times larger in size than the OOK Transmitter box, but the displacement is capable of reaching 60cm. Moreover, the signals with lower bit errors can be transmitted along the same transmission distance.

6.3 Summary

Chapter 6 covers the comprehensive analyses on the experimental results obtained from three measuring systems have been presented. The results from the SISO system designed with the OOK modulation has also been used for comparison. In comparison with the 1MHz OOK MIMO system, the PPM system has been shown to demonstrate superior performances, although it requires a more complex design.

The next chapter presents the extension of this chapter, in which the experimental results are further fitted by curve-fitting. In the next chapter, part of the experimental results are selected as training data for the curve fitting, and then the rest are selected for verification of the accuracy of the model. Their matching indicates a sufficient accuracy of the fitted model, which could be considered in the following research. The function *f(A,D)* is used in the following chapter, where *f(A,D)* are the BER values. As is introduced in Chapter 4, *A* is the displacement, *D* is the distance. These functions are generated by using displacement/distance values and corresponding measured BER values in the Matlab curve fitting model. Each section would introduce different fitted model by using different modulations.

Chapter 7 BER Curve-Fitting

7.1 Introduction

In Chapter 6, a comprehensive review and discussion has been accomplished about the experiments conducted using MIMO modulations, and the data received from the experiments were plotted for analysis purposes. Chapter 7 is presented as the extension of the previous chapter, in which the empirical results are further analysed not only by using graphic displays, but also by curve-fitting. Curve fitting is a mathematical approximation using continuous functions to describe a set of discrete points. It is an approximate analytical expression method with discrete data. Many engineering problems can only get a number of discrete data by sampling or experimental methods. Based on these data, one can find a continuous function/curve, which makes the experimental data coincide with the equations and which can be calculated based on the fitted equation to analyze and estimate the experimental results.

Based on the BER value in association with the defined Distance / Displacement, the mathematical model of BER in relation to the Distance / Displacement is developed. The evaluated model is verified by making comparative matches between the empirical and the evaluated results, which leads to the finalization of the evaluated model. Some empirical data points are randomly selected to match with the

evaluated plot for verification purposes only, and the matching indicates a sufficient accuracy for the fitted model.

As discussed, the main objective of this chapter is to find out the correlation between the BER, distance and displacement, then conclude the evaluated models which help calculating the BER value by given distance and displacement in the following research. In this chapter, using curve fitting tool in Matlab, the experimental results are evaluated.

Firstly, *A* represents displacement and *D* represents distance. Fixing displacement / distance, and changing distance/displacement would generate BER-distance / displacement curve in Matlab.

Secondly, using curve fitting tool to evaluate the fitting equation of BER-distance/displacement, then choosing the one with the highest overlapping rate by considering the real correlation between BER and distance/displacement.

Thirdly, in order to derivate the final equations for the relationship between distance / displacement of specific BER and the corresponding displacement / distance, the parameters of the evaluated equations on last step are considered. For example, assuming $f(D) = a\exp(bD)$ is the evaluated BER-distance equation, in the view of the fact that parameters a and b are in changed behaviour with displacement A, the

correlation equation between parameters and displacement A could be generate by curve fitting. Similarly, if the $f(A) = a\exp(bA)$ is the evaluated BER-displacement equation, in the view of the fact that parameters *a* and *b* are in changed behaviour with distance, the correlation equation between parameters and distance *D* could be generate by curve fitting.

Finally, the parameters in BER-distance equations are substituted by displacement using parameter-displacement equations. In each part of the following sections, different functions were generated, because for different modulations, displacement, distance, and background light the BER will change in different ways, which lead to the different relationships between parameters and BER values.

7.2 OOK Modulation

7.2.1 OOK 100kHz 70 – 140cm Distance

In an OOK 100kHz MIMO system, the relationship between the distance of a specific BER value and the corresponding displacement can be described by the equation shown as $f(A) = a\exp(bA)$, in which *f(A)* is BER and *A* represents the displacement, from the central axis of the Receivers. When the distance varies from 70 to 140 cm, the BER value of OOK 100kHz at 1 cm of Displacement is plotted to verify the evaluated model.

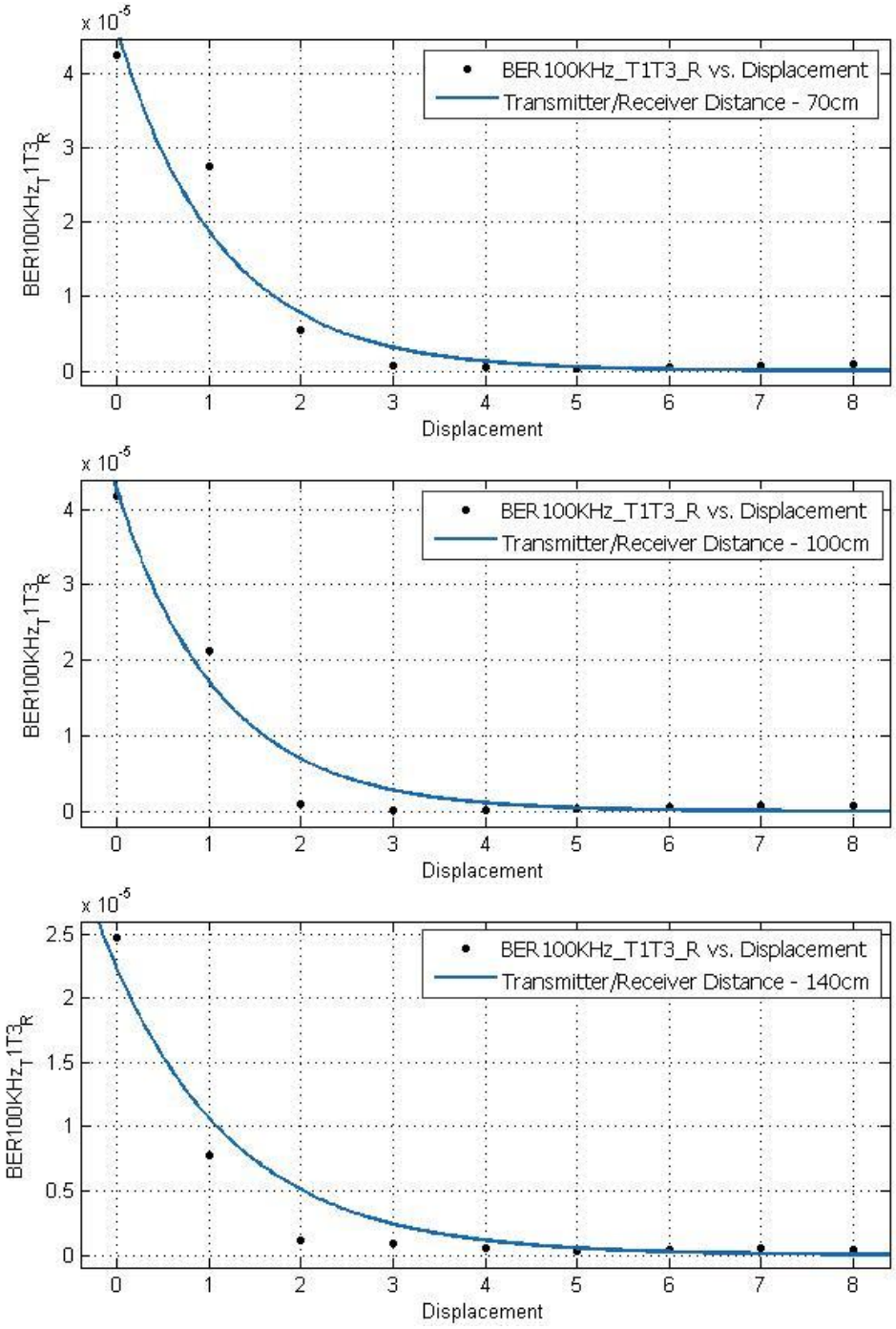

Figure 7-1 Fitting Distance 70cm – 140cm

Figure 7-1 illustrates the graphical coordination of the BER versus Displacement at various distances between transmitters and receivers, in which the plotted curve represents the theoretical results, and the scattered data points are the results received from the measurements. It can be clearly observed that the theoretical projection follows the same trends as the experimental data. It is clearly shown the BER value

at the displacement of 1cm matches closely with the plotted curve of the empirical model. In order to find the values of *a* and *b* in this case, curve-fitting is performed to fit the data using the logarithm of BER. As is explained in Section 7.1, considering *a* and *b* are in changed behaviour with distance *D*, the fitted equations were given as:

$$\begin{aligned} a = & -0.0005851 - 0.0009876\cos(2.992D) + 9.492\times10^{-5}\sin(2.992D) \\ & -0.004654\cos(5.984D) + 8.232\times10^{-5}\sin(5.984D) \\ & +0.0001072\cos(8.976D) + 2.979\times10^{-5}\sin(8.976D) \end{aligned} \tag{7.1}$$

$$b = -0.9517\exp(-(\frac{D-0.9031}{0.7695}))^2 - 0.3056\exp(-(\frac{D-1.295}{0.1058}))^2 \tag{7.2}$$

In Figure 7-2, the values of *a* and *b* at a distance of 120cm are randomly selected as the verification data point, which are used to evaluate the accuracy of the model. The matching of the empirical data and mathematical model appear to correspond reasonably well.

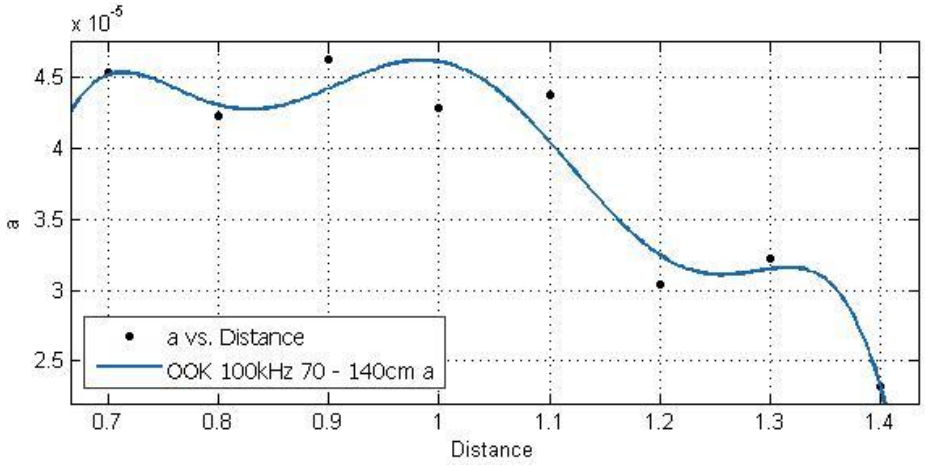

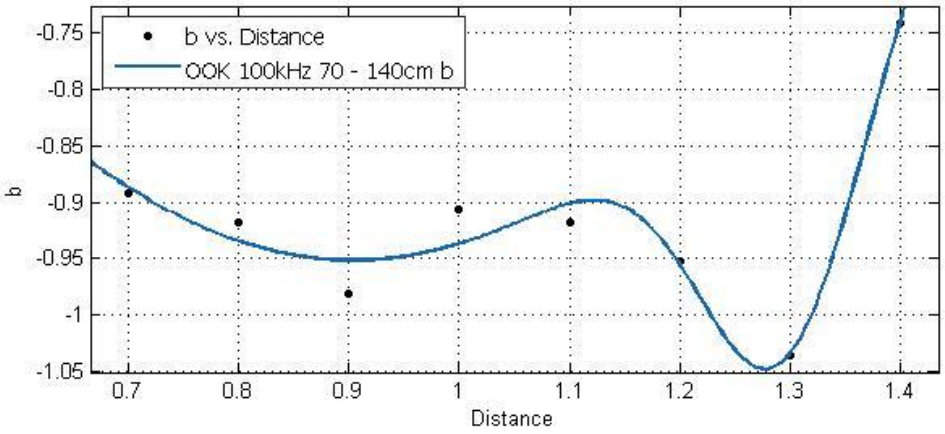

Figure 7-2 Estimated values of a and b

7.2.2 OOK 1MHz 70 – 110cm Distance

When the distance varies between 70cm and 110cm, the following mathematical model can be used to describe the behaviour of the data as required, $f(A) = a_0 + a_1 \cos(Aw) + b_1 \sin(Aw)$, in which *f(A)* is BER and *A* represents the displacement as shown in the previous section. The BER value at the displacement of 7cm is selected to verify the empirical model, whereas the values of *a0*, *a1* and *b1* at a distance of 100cm are used to verify the empirical projections.

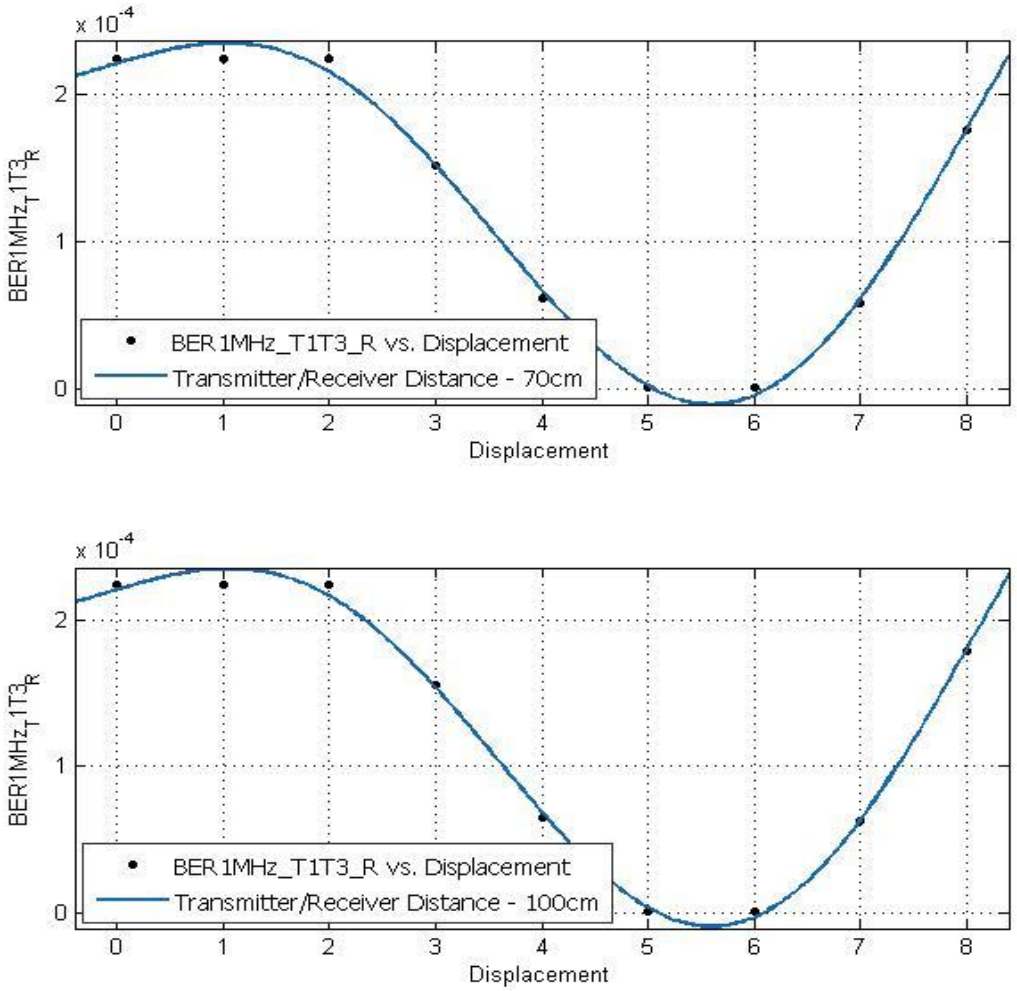

Figure 7-3 Fitting Distance 70cm – 110cm

In the above illustrated model, similarly with Section 7.2.1, *D* stands for the distance as defined, and in order to find the values of *a0*, *a1* and *b1* in this case, curve-fitting is performed to fit the data using the logarithm of BER. This gives:

$$a_0 = 10^{-6.533D^4+23.97D^3-32.7D^2+19.66D-8.322} \tag{7.3}$$

$$a_1 = 10^{-4.206-0.002532\cos(22.44D)-0.003079\sin(22.44D)} \tag{7.4}$$

$$b_1 = 10^{-3.954-0.005228\cos(12.38D)+0.001202\sin(12.38D)} \tag{7.5}$$

$$w = 0.7854 \tag{7.6}$$

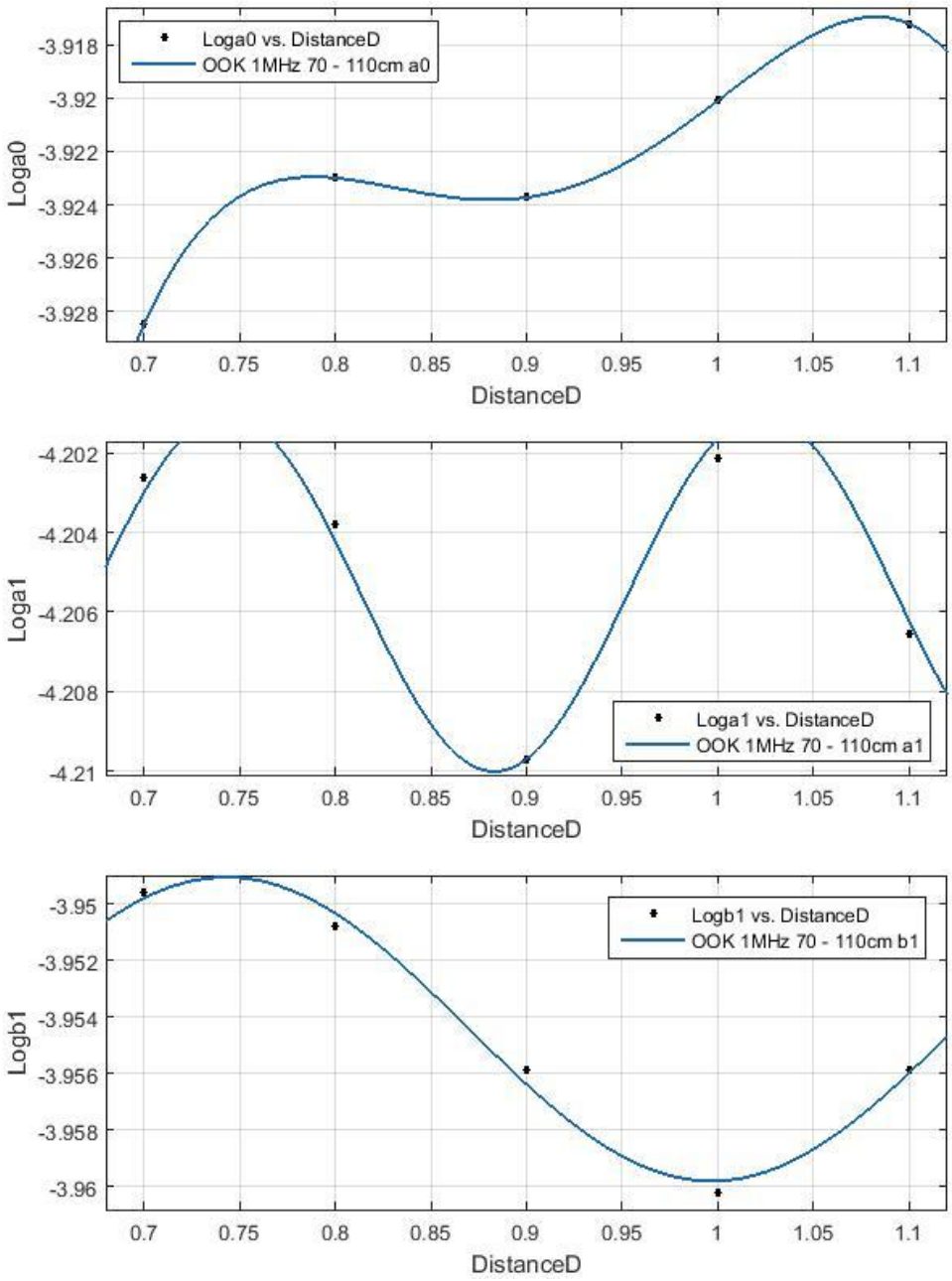

Figure 7-4 Estimated values of *a0*, *a1* and *b1*

Figure 7-3 and 7-4 confirm that the mathematical model shows a fairly good match with the empirical data, and therefore can be used for the data analysis in the research following.

7.2.3 OOK 1MHz 120 – 140cm Distance

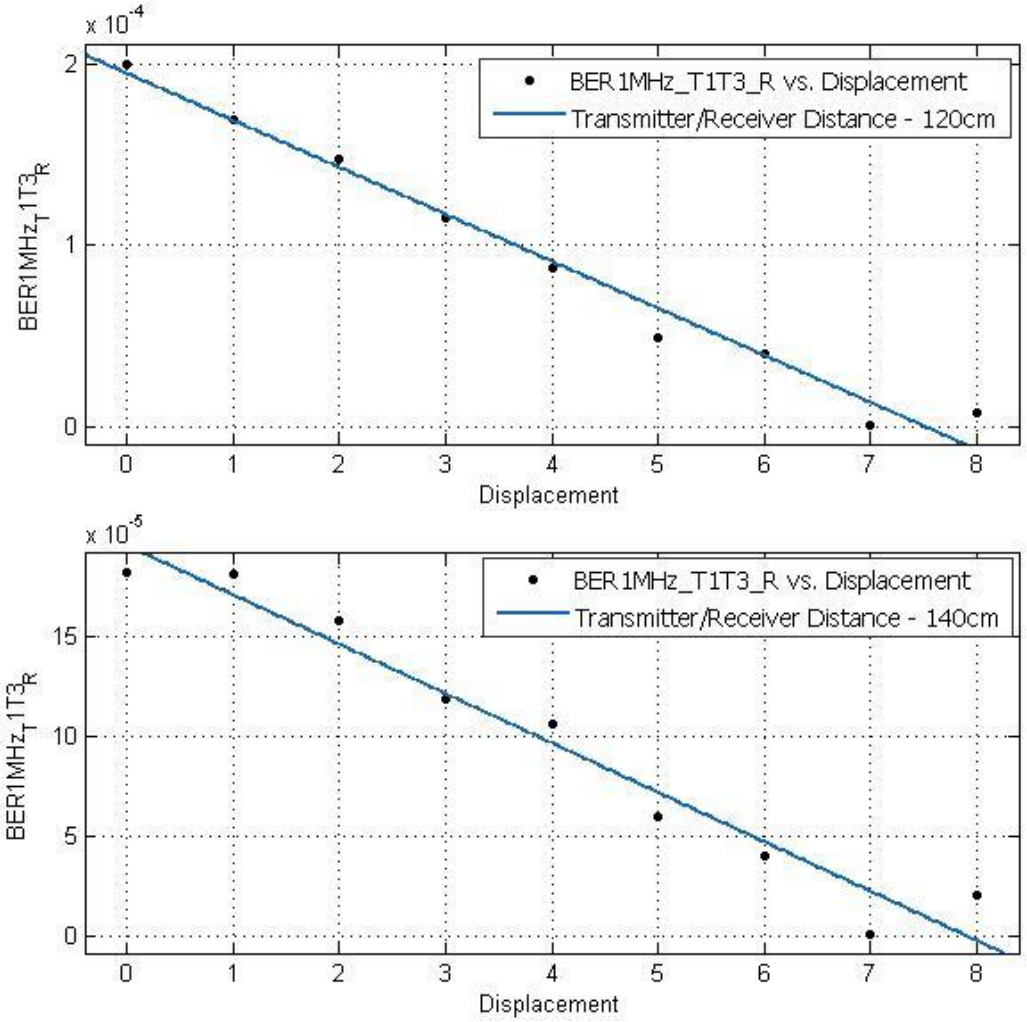

Figure 7-5 Fitting Distance 120cm – 140cm

Between the distance of 120cm and 140cm, the evaluated model can be described as $f(A) = p_1 A + p_2$, in which A represents the displacement. In order to find the values of *p1* and *p2* in this case, similarly with Section 7.2.1, curve-fitting is performed to fit the data using the logarithm of BER. This gives:

$$p_1 = 10^{-4.61\exp(-(\frac{D-1.312}{1.075})^2)} \tag{7.7}$$

$$p_2 = 10^{-3.744\exp(-(\frac{D-1.296}{1.021})^2)} \tag{7.8}$$

D represents the distance as defined in the experiments. The BER at a displacement of 5cm is selected to verify the empirical model. It should be stated that due to insufficient data available from the experiments, no matching comparison was completed.

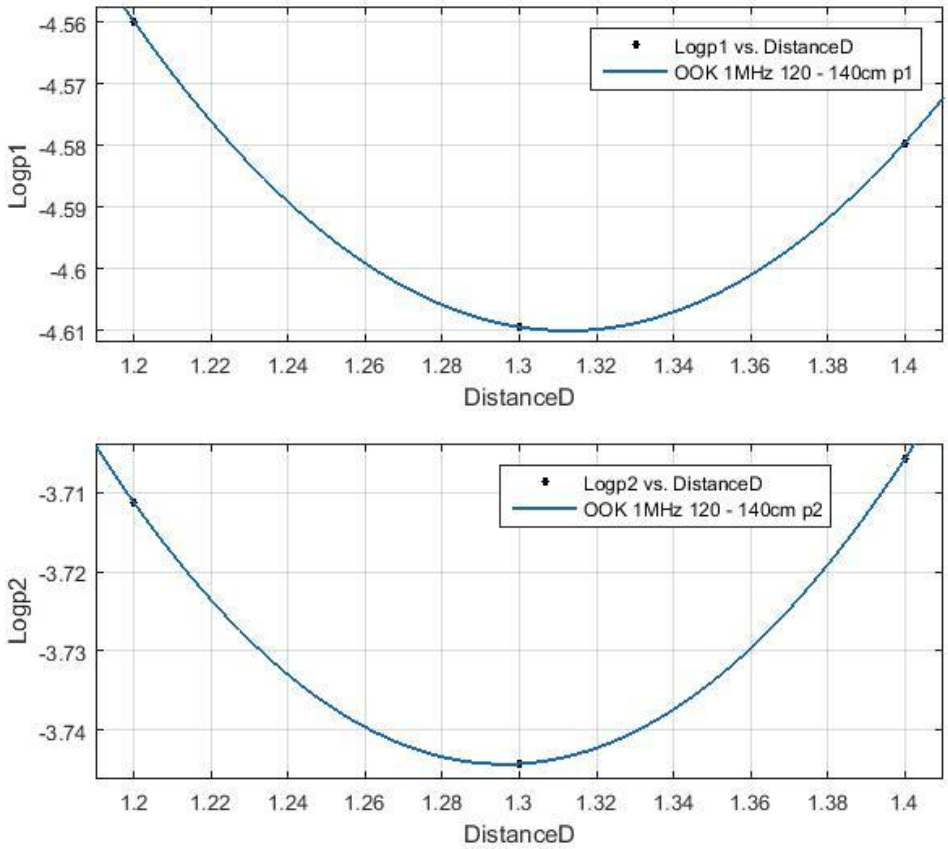

Figure 7-6 Estimated values of *p1* and *p2*

It is clearly shown that the BER values and other relevant parameters show a fairly good agreement with the mathematical projection, and the deviation of the two appears to correspond reasonably.

7.2.4 OOK 100kHz Darkroom 0-9cm Displacement

When the experiments by using the OOK 100kHz system are performed in a darkroom, the mathematical model can be modified as: $f(D) = a\exp(bD)$ in which *f(D)* is BER and D represents the distance between the receivers and the transmitters. The BER value at the distance of 80cm is selected to verify the empirical model, and values of *a* and *b* at the displacement of 5cm are selected to verify the parameters fitted from the model.

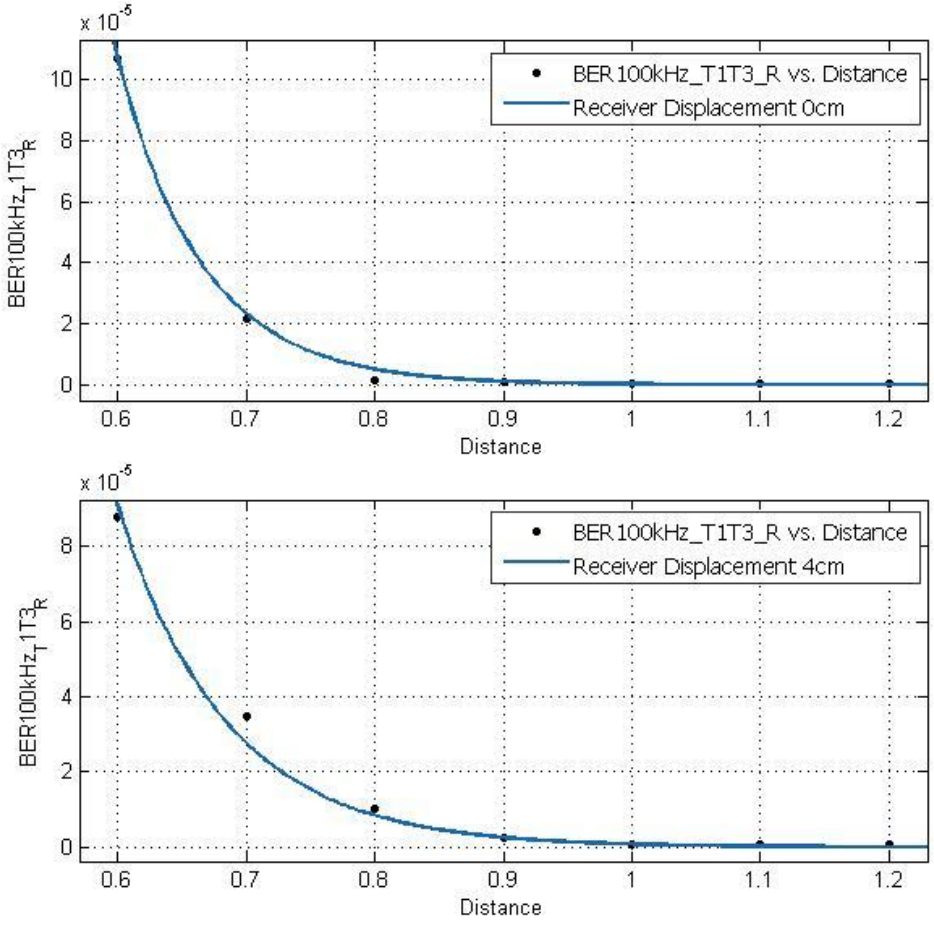

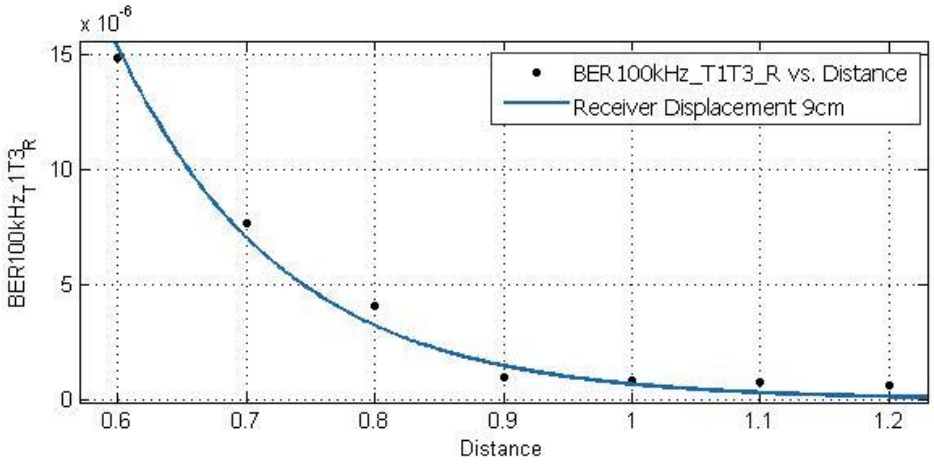

Figure 7-7 Fitting 0 – 9cm Displacement

It is worth noticing that in the darkroom, the differences between the theoretical model and the experimental results are less obvious than those obtained under normal lab conditions, which can be interpreted as the system having experienced less interference from other signals and background lighting conditions. In order to find the values of *a* and *b* in this case, considering a and b are in changed behaviour with displacement A, curve-fitting is performed to fit the data using the logarithm of BER. This gives:

$$a = 10^{4.162\times10^{10}-5.549\times10^{10}\cos(0.001005A)-2.576\times10^{8}\sin(0.001005A)+1.387\times10^{10}\cos(0.00201A)+1.288\times10^{8}\sin(0.00201A)} \quad (7.9)$$

$$b = -6.161\times10^{10} + 8.214\times10^{10}\cos(0.001252A) + 4.826\times10^{10}\sin(0.001252A) - 2.053\times10^{10}\cos(0.002504A) - 2.413\times10^{8}\sin(0.002504A) \quad (7.10)$$

A stands for the Displacement.

Figure 7-8 illustrates the comparison of the empirical results and the logarithm value of evaluated results. By making comparison with the data selected for verification, the fitted model appears to correspond reasonably clearly.

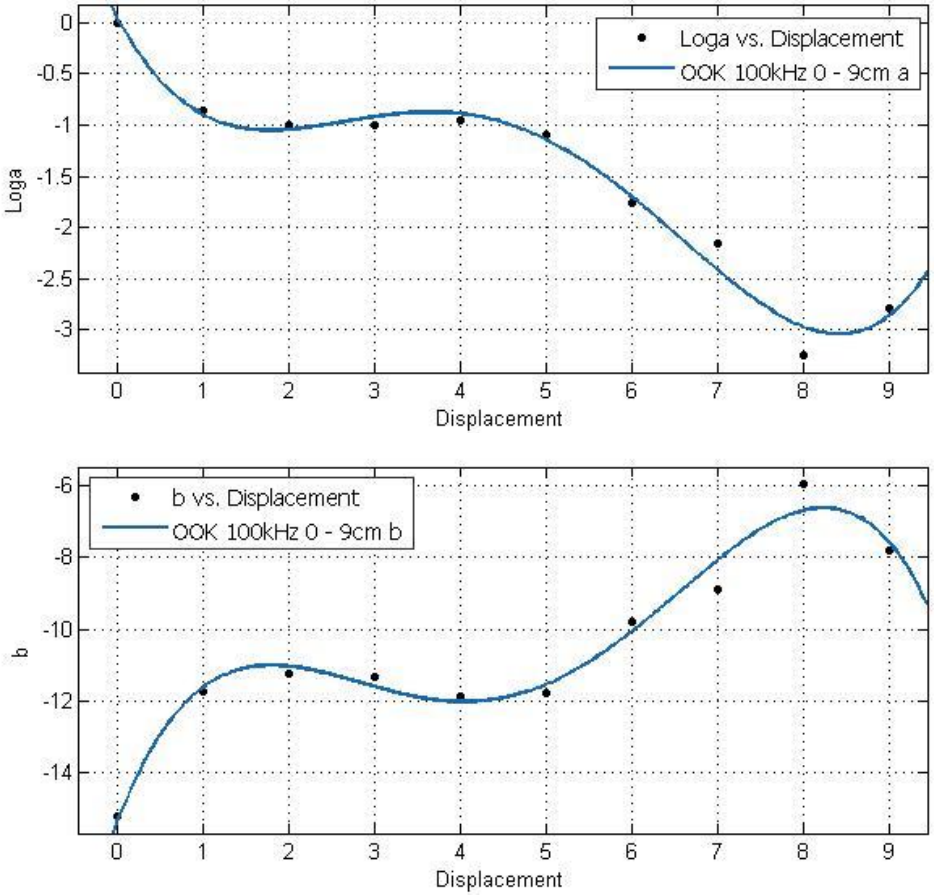

Figure 7-8 Estimated value of *a* and *b*

7.2.5 OOK 1MHz Darkroom 0 – 6cm Displacement

Between the displacement range of 0 and 6cm, the model can be described as $f(D) = 10^{a_0 + a_1 \cos(Dw) + b_1 \sin(Dw)}$, in which D represents the distance between the transmitters and the receivers. The BER value at the distance of 0.5m and 0.9m is selected to verify the empirical projection, and the values of *a0*, *a1*, *b1* and *w* at the displacement of 5 cm are selected to verify the evaluated model as fitted.

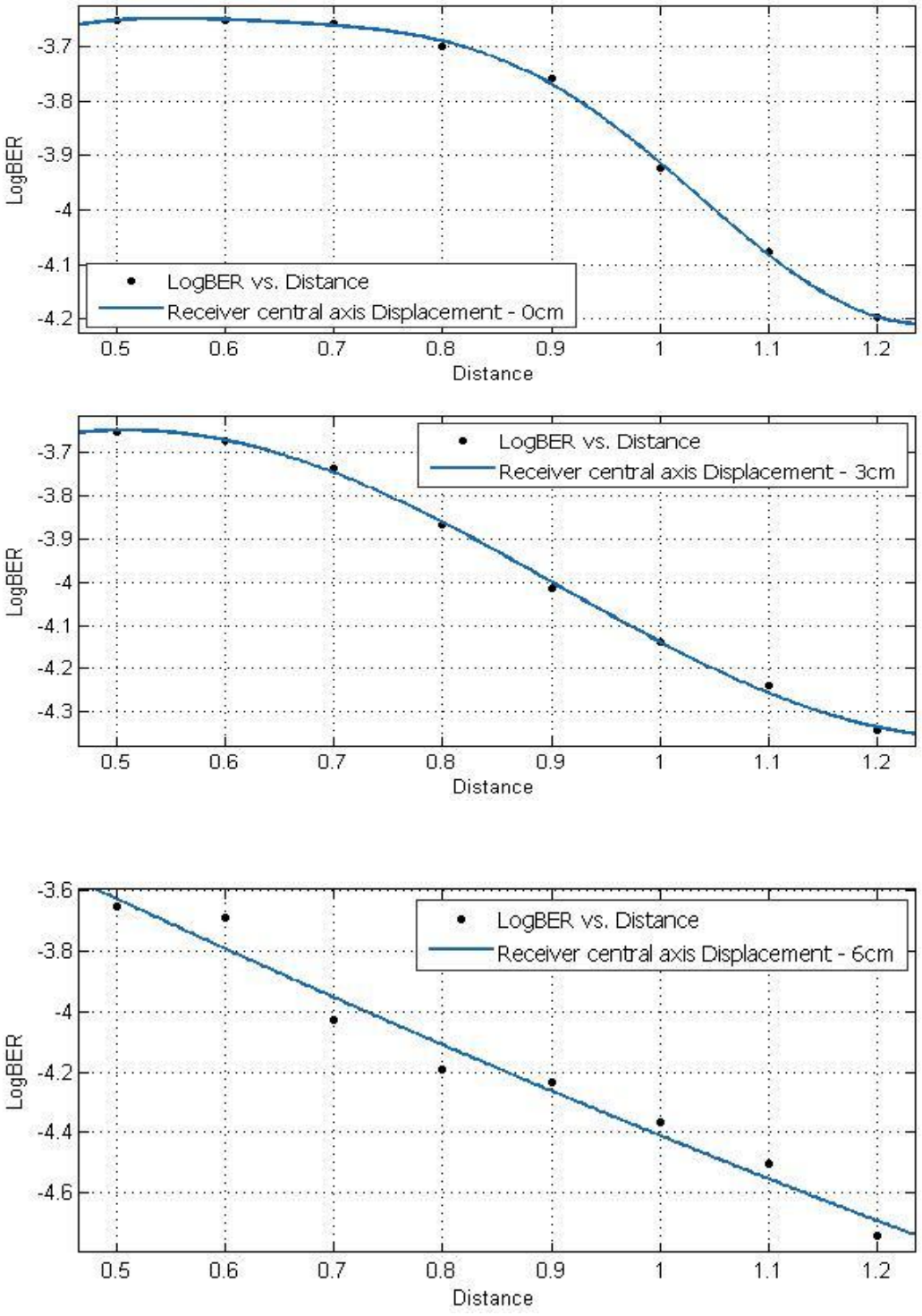

Figure 7-9 Fitting Angle 0cm – 6cm

In order to find the values of *a0*, *a1*, *b1* and *w* in this case, similarly with Section 7.2.4, curve-fitting is performed to fit the data using the logarithm of BER. This gives

$$a_0 = -4.071 + 0.06375\cos(0.7085A) + 0.1687\sin(0.7085A) + 0.06411\cos(1.417A) + 0.02181\sin(1.417A) \quad (7.11)$$

$$a_1 = 0.952 - 1.305\cos(0.3862A) - 0.9249\sin(0.3862A) + 0.1038\cos(0.7724A) + 0.4067\sin(0.7724A) \quad (7.12)$$

$$b_1 = 0.2782 - 0.09799\cos(0.938A) - 0.1547\sin(0.938A) \quad (7.13)$$

$$w = 2.763 + 0.7336\cos(0.5569A) + 2.143\sin(0.5569A) + 0.5149\cos(1.1138A) - 0.1613\sin(1.1138A) \quad (7.14)$$

A stands for the Displacement.

In comparison with the experimental results received under normal lighting conditions, the model developed to describe the experimental data received under darkroom conditions demonstrates closer correspondence. In addition, the results from the OOK 100kHz systems prove to show better stability, and better resistance to interference. Moreover, the continuity and the level of engagement also shows better performance than those conducted at a higher frequency.

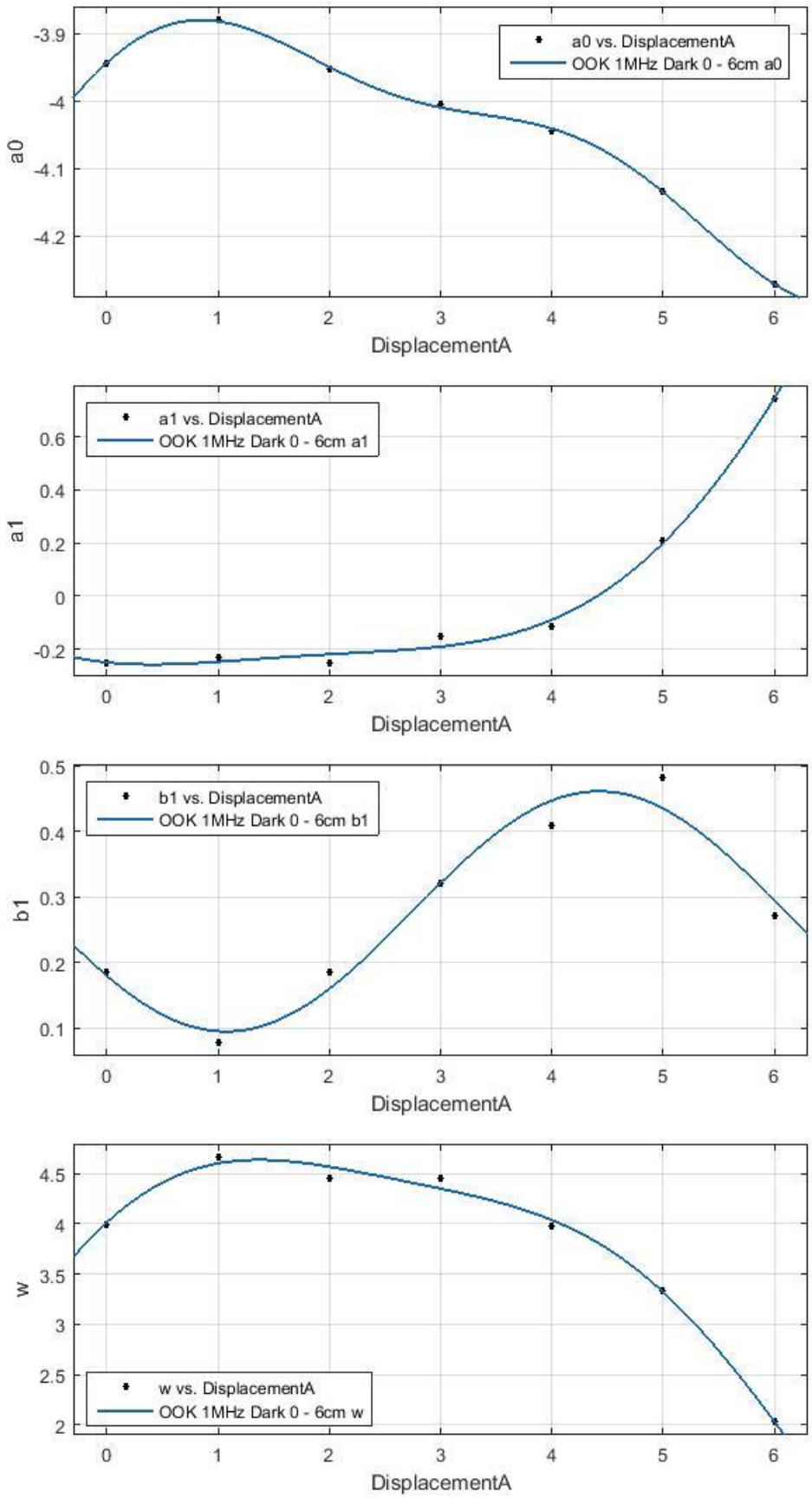

Figure 7-10 Estimated values of *a0*, *a1*, *b1* and *w*

7.2.6 OOK 1MHz Darkroom 7 – 10cm Displacement

When the angle is increased to 7cm, the following model can be used $f(D) = a\exp(bD)$, in which *f(D)* is BER and *D* represents the distance. The value BER at the distance of 0.6m and 0.8m are selected to verify the empirical model, however, due to insufficient experimental data, the verification of the evaluated model was not completed. Unlike the BER in displacement 7cm, 8cm and 9cm, when the distance increase, the BER in displacement 10cm continues to grow.

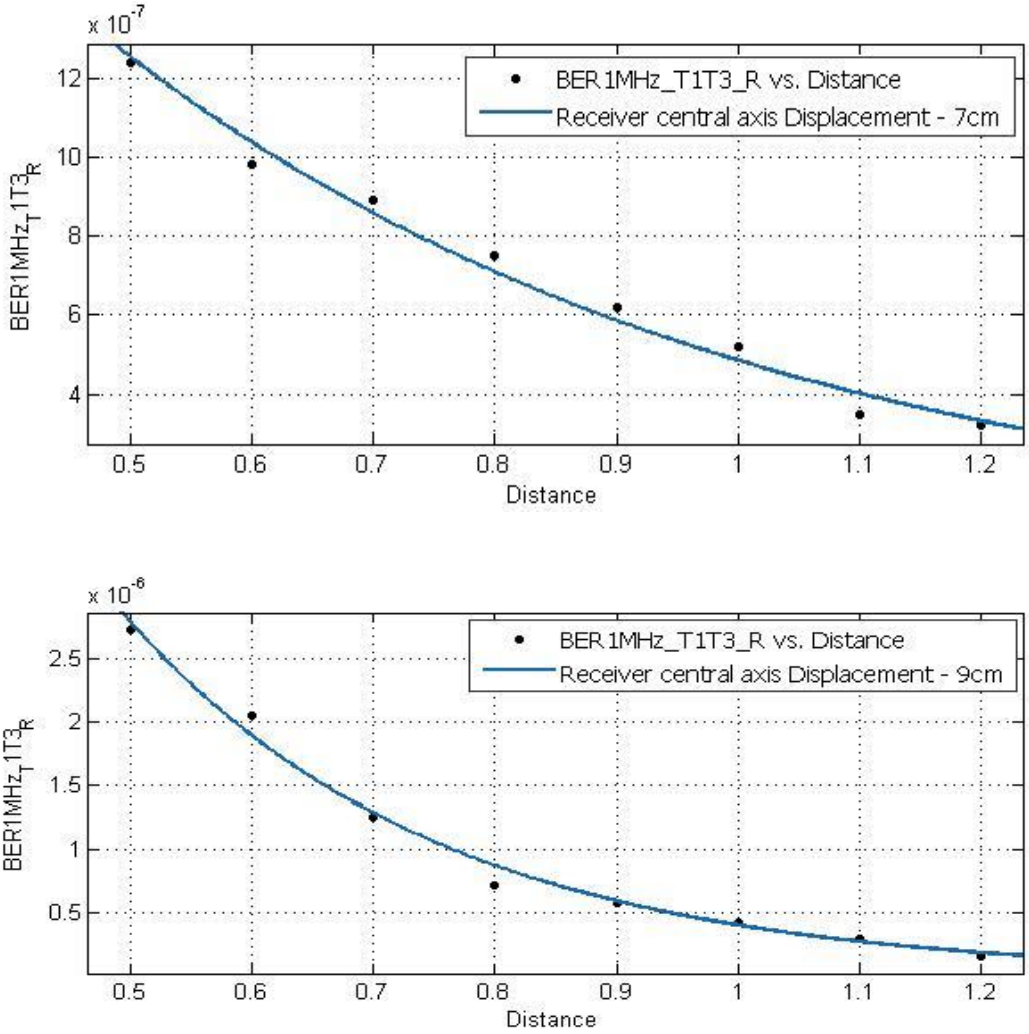

Figure 7-11 Fitting Displacement 7cm – 10cm

In order to find the values of a and b in this case, similarly with Section 7.2.4, curve-fitting is performed to fit the data using the logarithm of BER. This gives:

$$a = 2.357\times10^{-5} - 4.275\times10^{-5}\cos(2.094A) - 2.781\times10^{-5}\sin(2.094A) \quad (7.15)$$

$$b = 1.458A^3 - 33.78A^2 + 259.6A - 659.4 \quad (7.16)$$

A represents the Displacement.

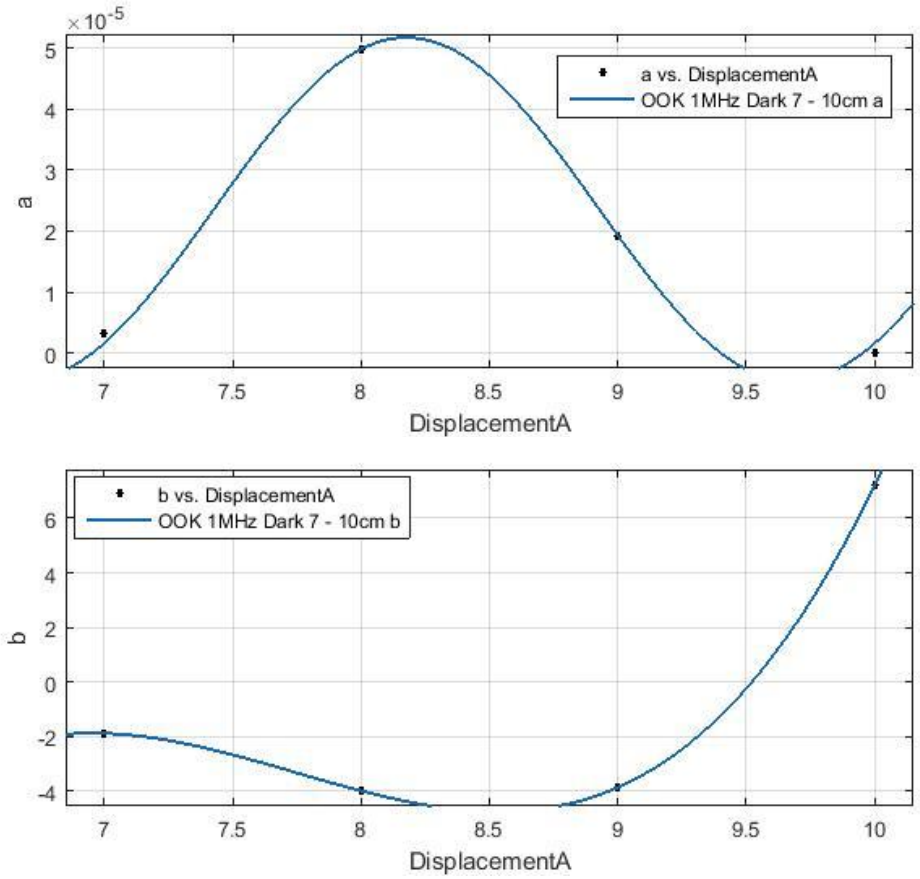

Figure 7-12 Estimated values of *a* and *b*

As shown in Figure 7-11 and 7-12, both BER values received from the experiments and the empirical results demonstrate a fairly good match. However, due to the limitations of the displacement when the receivers can't receive any signals at the distance exceeding 11cm, the data received from the distance ranging from 7 cm to 10 cm can only be derived with three empirical points, which is considered to be insufficient for making comparisons.

7.3 PPM and SZI Modulation

7.3.1 PPM 1MHz 0 – 25cm Displacement

When the displacement ranges from 0 to 25cm, the model can be described by $f(D) = p_1 D + p_2$ in which D represents the distance.

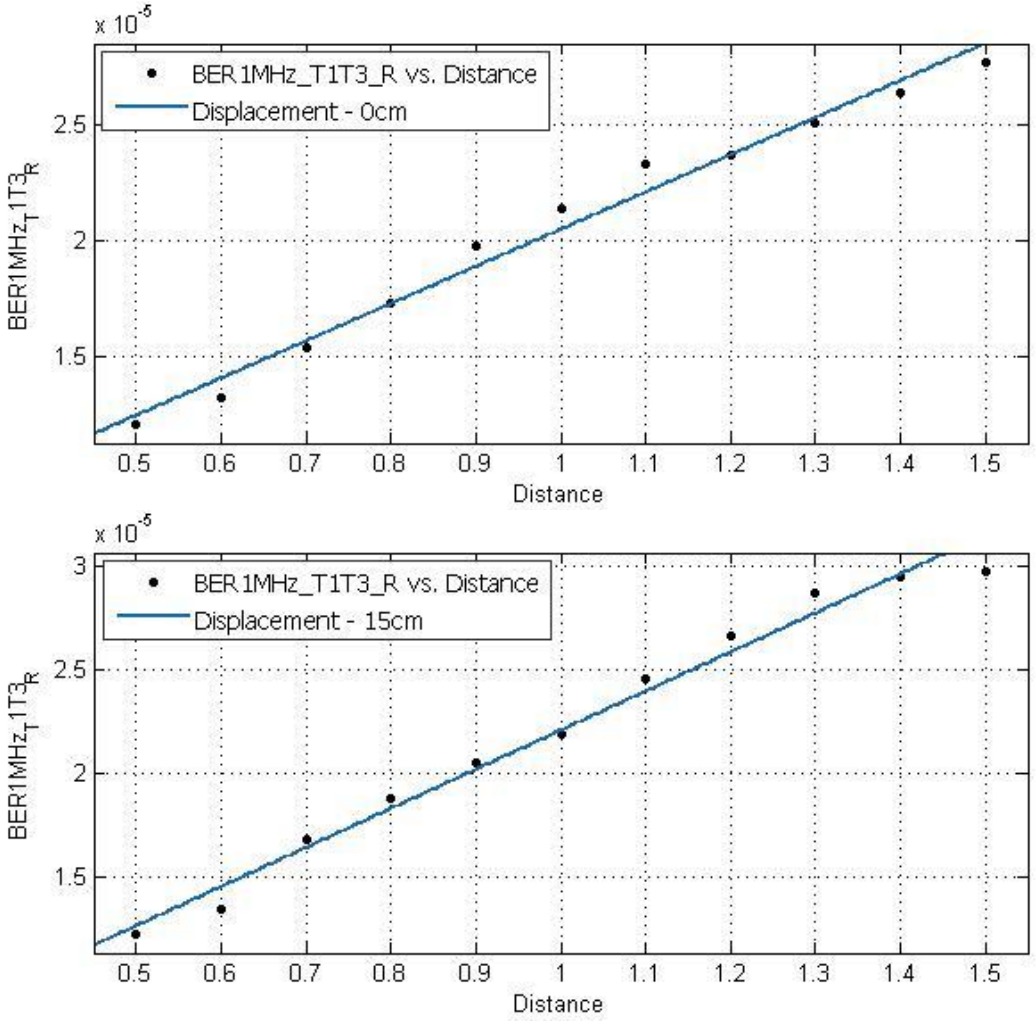

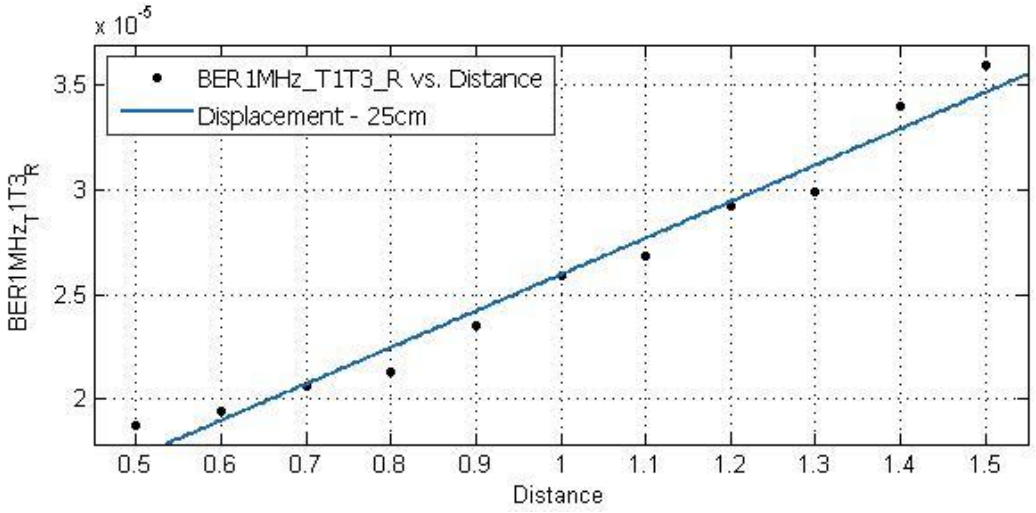

Figure 7-13 Fitting 0 – 25cm Displacement

In order to find the values of *p1* and *p2* in this case, similarly with section 7.2.4, curve-fitting is performed to fit the data using the logarithm of BER. This gives

$$p_1 = 10^{-4.768-0.03139\cos(0.4546A)-0.05391\sin(0.4546A)} \tag{7.17}$$

$$p_2 = 10^{-5.464+0.1697\cos(0.3703A)+0.2502\sin(0.3703A)} \tag{7.18}$$

A represents the Displacement. In the above described model, the BER value at the distance of 0.7 m and 1.1 m are selected to verify the empirical model, and *p1* and *p2* at the displacement of 5 cm are used for verifications.

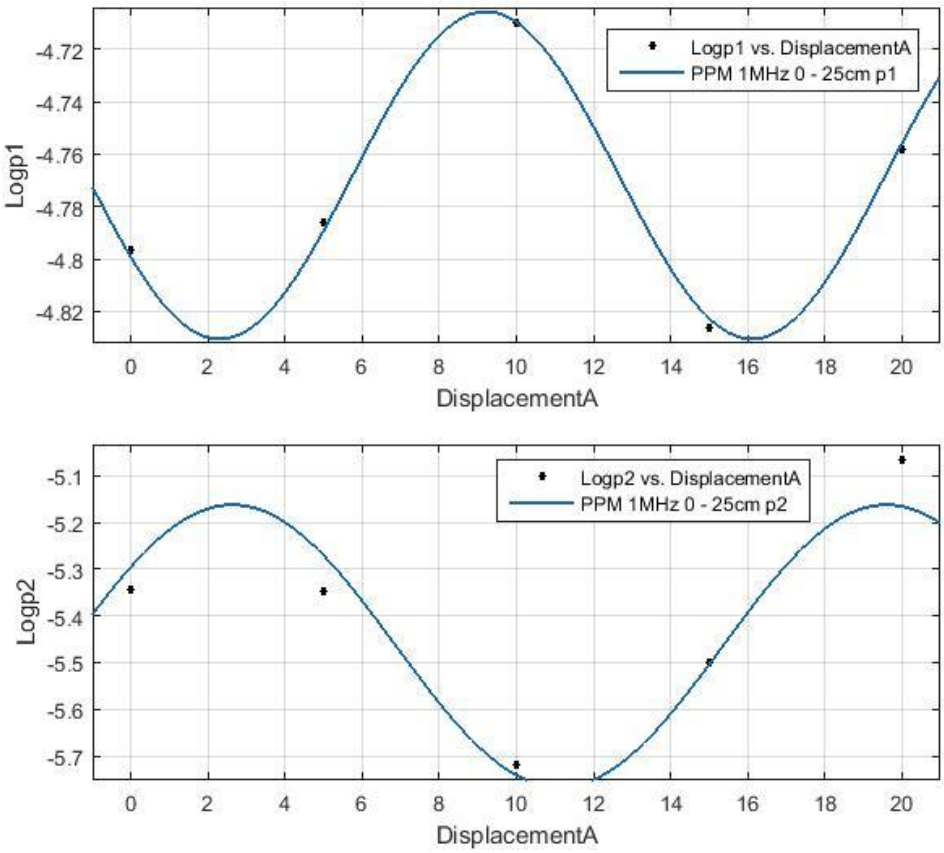

Figure 7-14 Estimated values of *p1* and *p2*

Figure 7-13 shows the comparison between the empirical results and evaluated BER value, whereas Figure 7-14 illustrates the comparisons between parameters derived from the model and the evaluated values. It has been clearly demonstrated that the empirical results match with the data distribution of the experiments when the distance varies between 0.5 to 1.5m.

7.3.2 PPM 1MHz 30 – 60cm Displacement

When the displacement is increased to 30cm, the model can be described by $f(D) = a\exp(bD)$ in which D represents the distance between the transmitters and the receivers. It should be noticed that when distance increases, the BER comes down and up because when distance is close, the coverage is quite low. Increasing distance improves the coverage, and as a result, the BER performance becomes better. But as the distance continues to grow over 1.4m, the signal power decays, the SNR becomes the primary factor and BER performance becomes worse even coverage is improved; this is the reason BER increases when distance is over 1.4m.

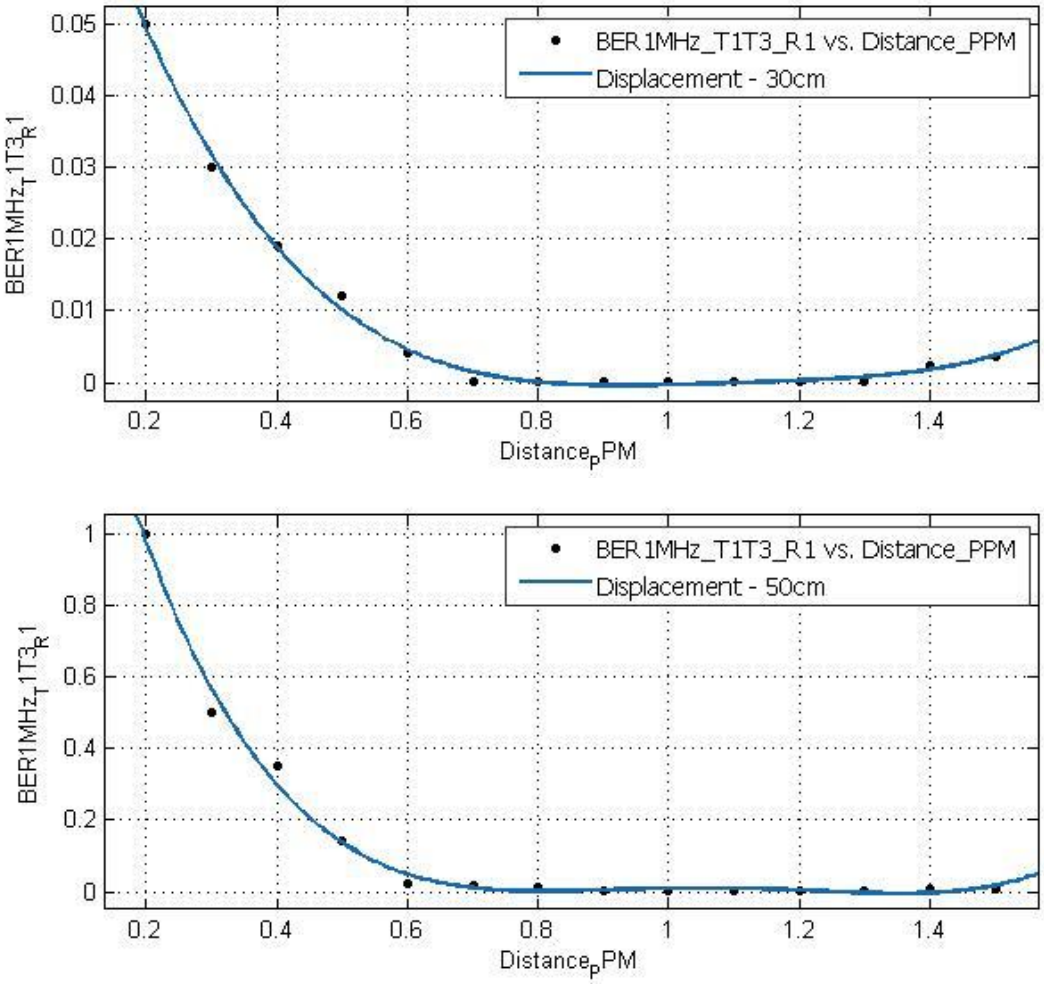

Figure 7-15 Fitting 30 – 60cm Displacement

In order to find the values of *a* and *b* in this case, similarly with section 7.2.4, curve-fitting is performed to fit the data using the logarithm of BER. This gives:

$$a = 10^{0.1091 - 0.1929\cos(0.1549A) + 0.6677\sin(0.1549A) + 0.2653\cos(0.3098A) + 0.03859\sin(0.3098A)} \tag{7.19}$$

$$b = -0.0001502A^4 + 0.02689A^3 - 1.75A^2 + 49.01A - 504.6 \tag{7.20}$$

A represents the Displacement between 30 and 60cm. The BER value at the distance of 0.5m and 0.7m are selected to verify the empirical model, and *a* and *b* at the displacement of 35cm are used for verifications.

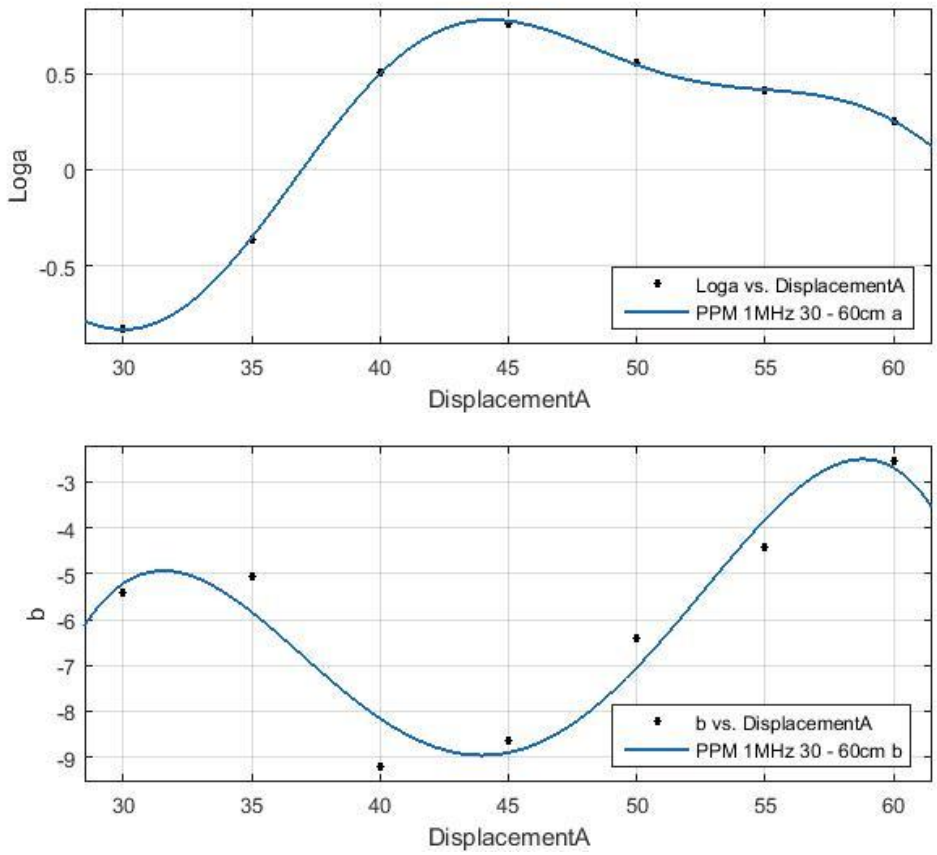

Figure 7-16 Estimated values of *a* and *b*

As shown in Figure 7-15 and 7-16, both BER values and the data distribution derived from the empirical model demonstrate fluctuations. However, from the view point of the curve fitting approach, the percentage of overlapped data is over 95%, which confirms the fact that the experiment results are in good correlation with the theoretical projections.

7.3.3 SIR-RZI 100kHz 2X4 50 – 130cm Distance

In the SIR-RZI 2X4 MIMO system, the data shows a high level of continuity, which can be described with the same distribution: $f(A) = a_1 \exp(-(\frac{A-b_1}{c_1})^2)$ whereas the distance varies between 50 and 130cm, in which *A* represents the displacement, and in order to find the values of *a1*, *b1*, and *c1* in this case, curve-fitting is performed to fit the data using the logarithm of BER. This gives:

$$a_1 = -0.2944 + 0.003317\cos(5.236D) + 0.008324\sin(5.236D) - 0.01036\cos(10.472D) + 0.004108\sin(10.472D) - 6.58110^{-5}\cos(15.708D) - 0.01099\sin(15.708D) \quad (7.21)$$

$$b_1 = 1.787 + 0.00398\cos(8.49D) - 0.002125\sin(8.49D) + 0.002417\cos(16.98D) - 0.001706\sin(16.98D) - 0.0003012\cos(25.47D) - 0.002682\sin(25.47D) \quad (7.22)$$

$$c_1 = 13.95 - 2.055\cos(4.245D) + 2.554\sin(4.245D) \quad (7.23)$$

D represents the distance.

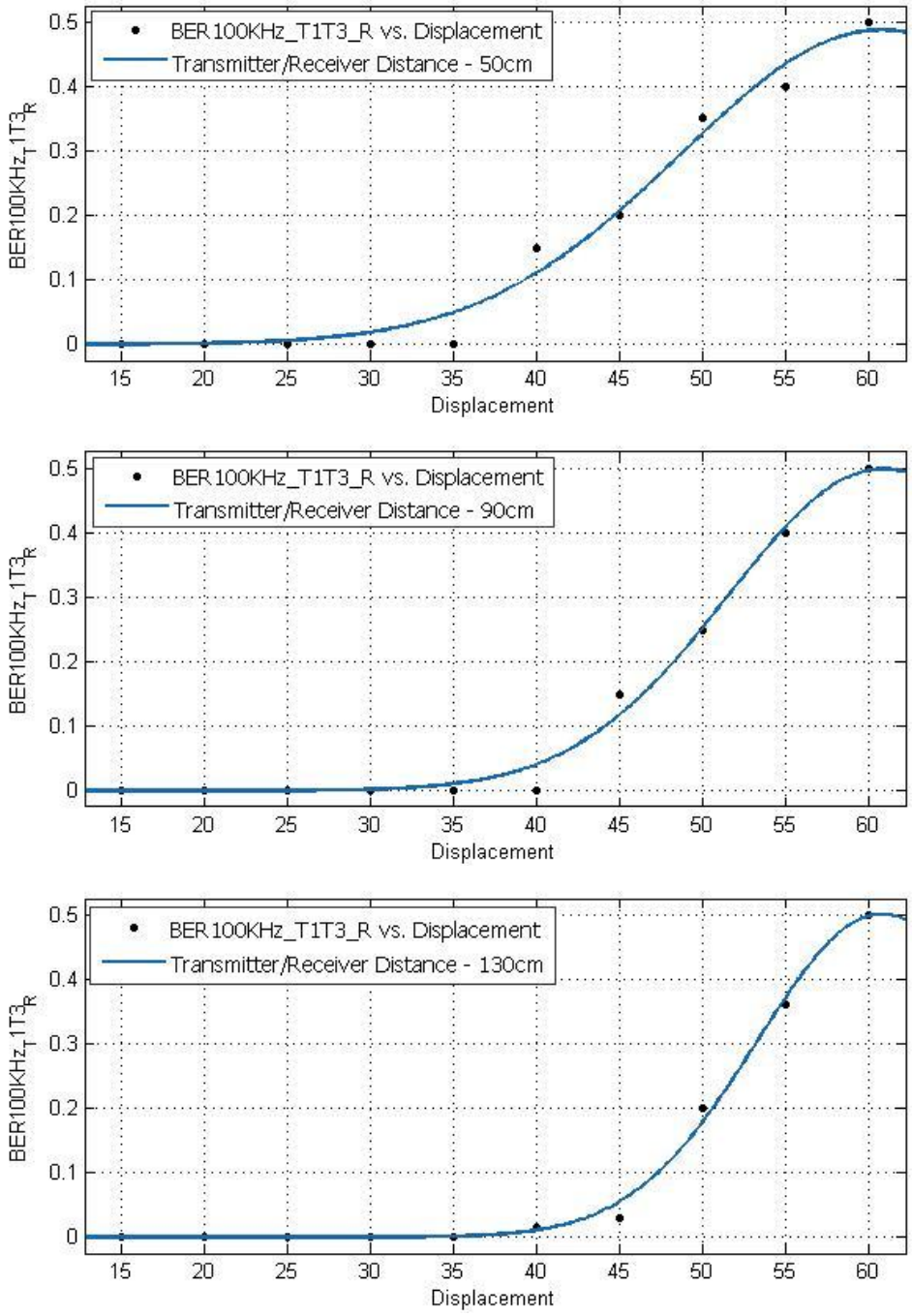

Figure 7-17 Fitting 50 – 130cm Distance

It is worth noticing that when the displacement increases, the empirical BER value becomes unchanged at 1 , which indicates the fact that the receivers are moved out of the coverage range. However, due to the high level of overlapping percentage at 94.6%, the model is considered as valid with acceptable deviations. In Figure 7-17

and 7-18, it illustrates the theoretical data distribution derived from the model are in fairly good match with the experiment data. The BER value at the angle of 30cm and 50cm are selected to verify the empirical model, and *a1*, *b1* and *c1* at the distances of 0.8m and 1m are used for respective verifications.

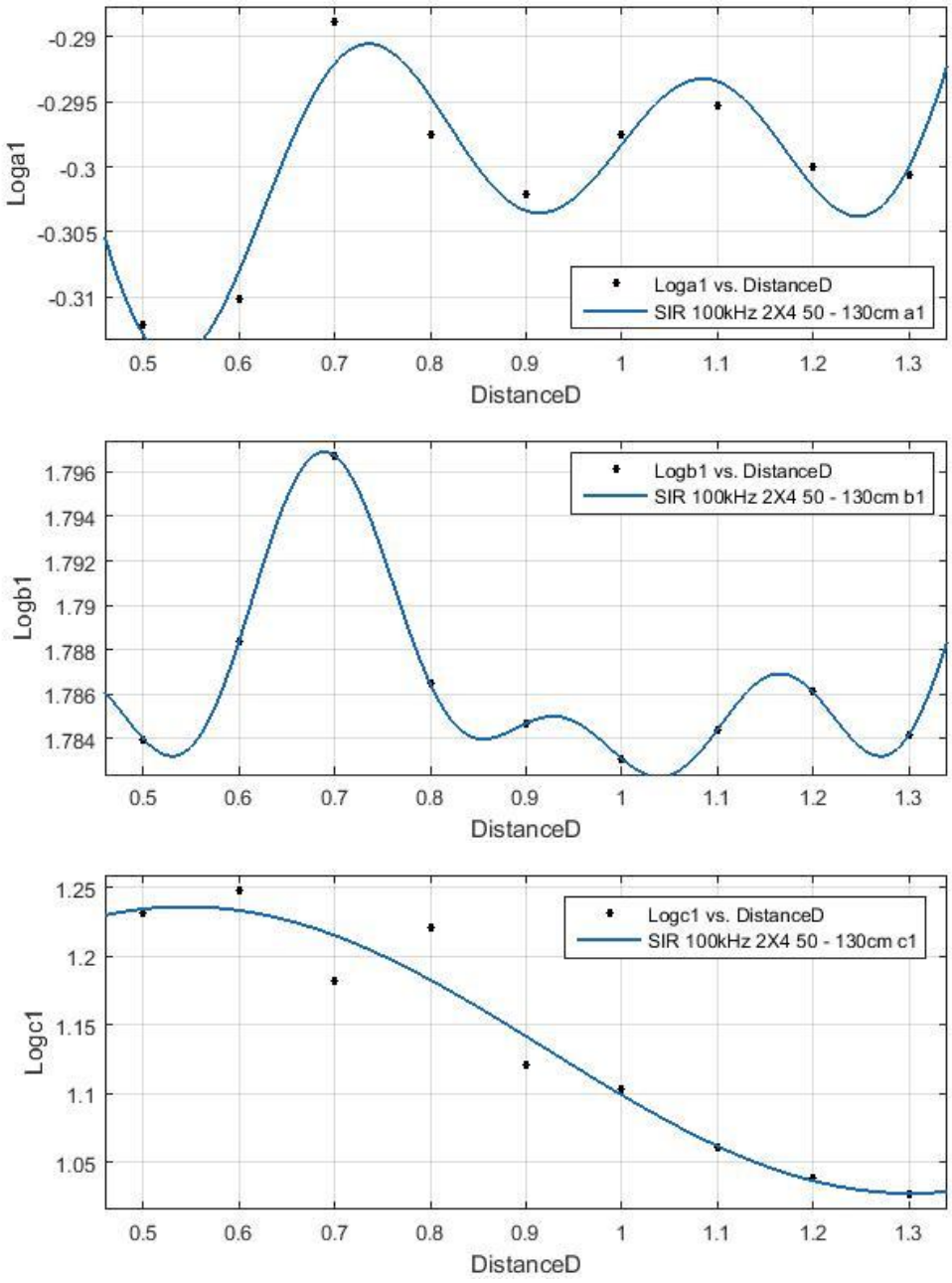

Figure 7-18 Estimated values of *a1*, *b1* and *c1*

7.3.4 SIR-RZI 100kHz 4X4 20 -60cm Distance

The model of 4X4 RZI system can be described by $f(A)=10^{a\exp(bA)}$ in which A represents the displacement between 20 and 60cm. In order to find the values of a and b in this case, curve-fitting is performed to fit the data using the logarithm of BER. This gives:

$$a=-4.906\exp(-(\frac{D-0.6687}{1.395})^2) \tag{7.24}$$

$$b=-0.07002\exp(-(\frac{D-0.3466}{0.4284})^2) \tag{7.25}$$

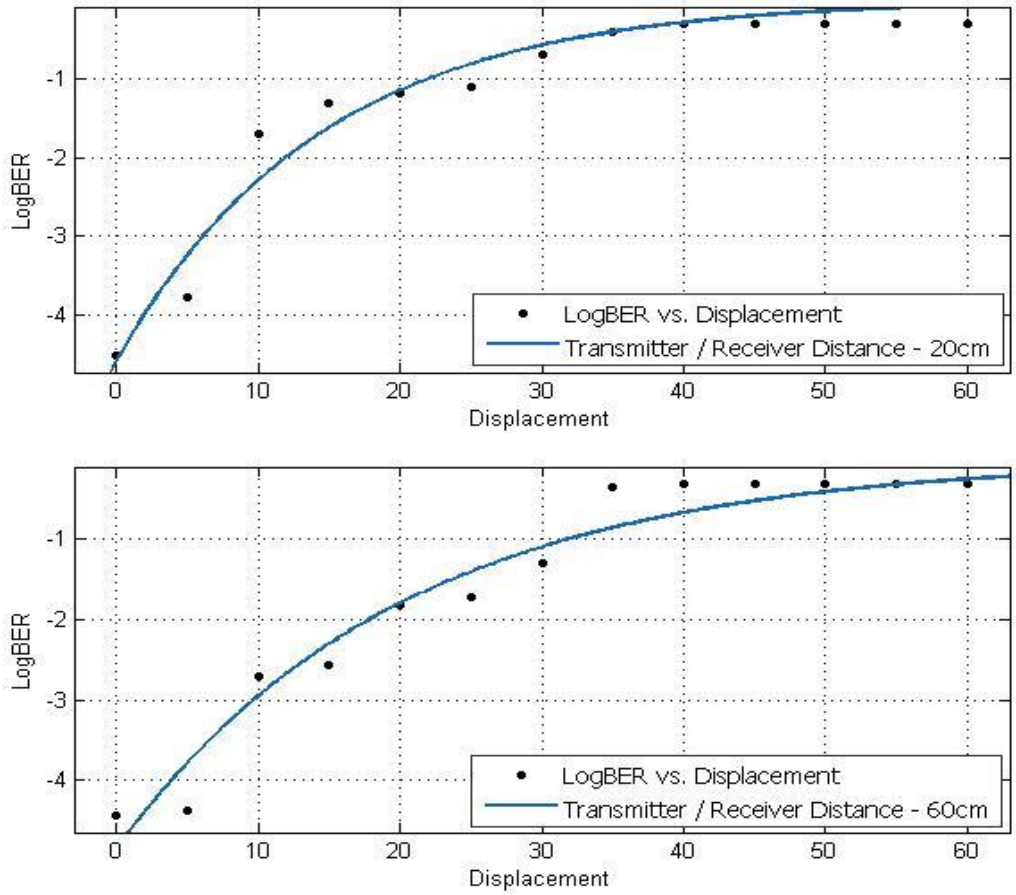

Figure 7-19 Fitting 20 – 60cm Distance

D represents the distance between the transmitter and the receiver box. As shown in Figure 7-19, the curve reflects the theoretical result whereas the scattered data points

represent the empirical results of BER value. In comparison with those received from the experiments using the 2X4 system, the percentage of overlapping is at 93.41%, although lower that expectations but may be considered as acceptable.

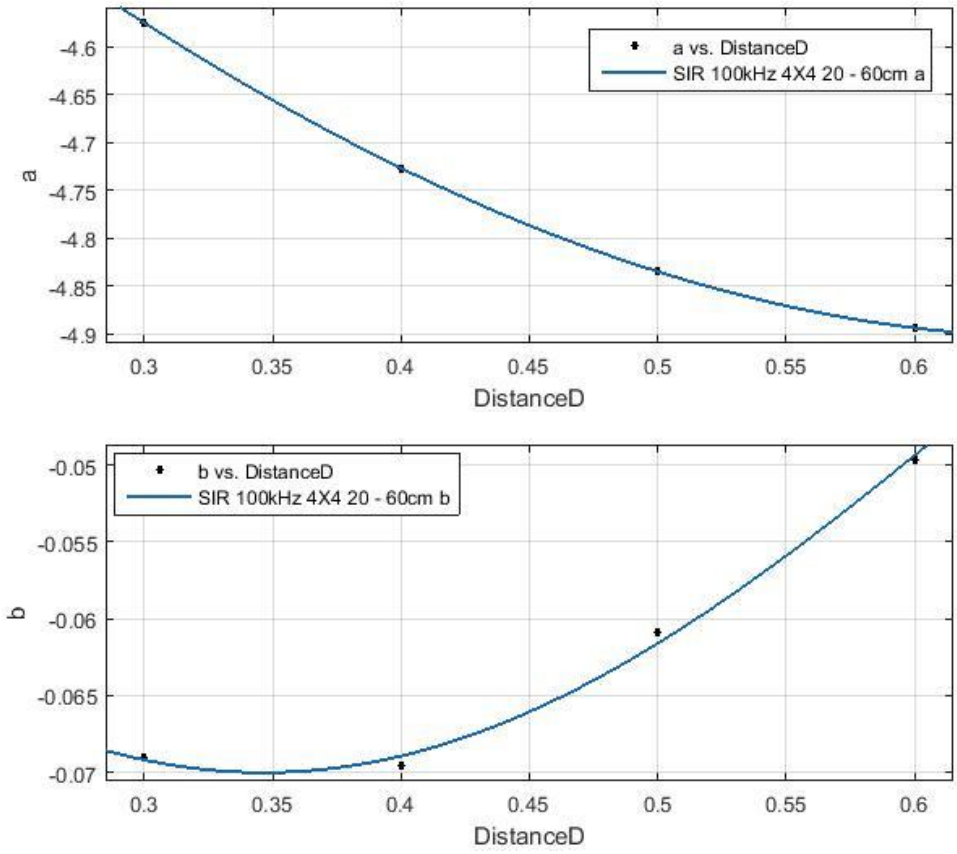

Figure 7-20 Estimated values of *a* and *b*

The BER values at the displacement 15cm and 30cm are selected to verify the empirical model, and a1, b1 and c1 at the distance of 0.5m are used for verifications.

7.3.5 SIR-RZI 100kHz 4X4 70 – 150cm Distance

The model for distance between 70 cm and 150 cm can be described by $f(A) = a_1 \exp(-(\frac{A-b_1}{c_1})^2)$, in which A represents the displacement,

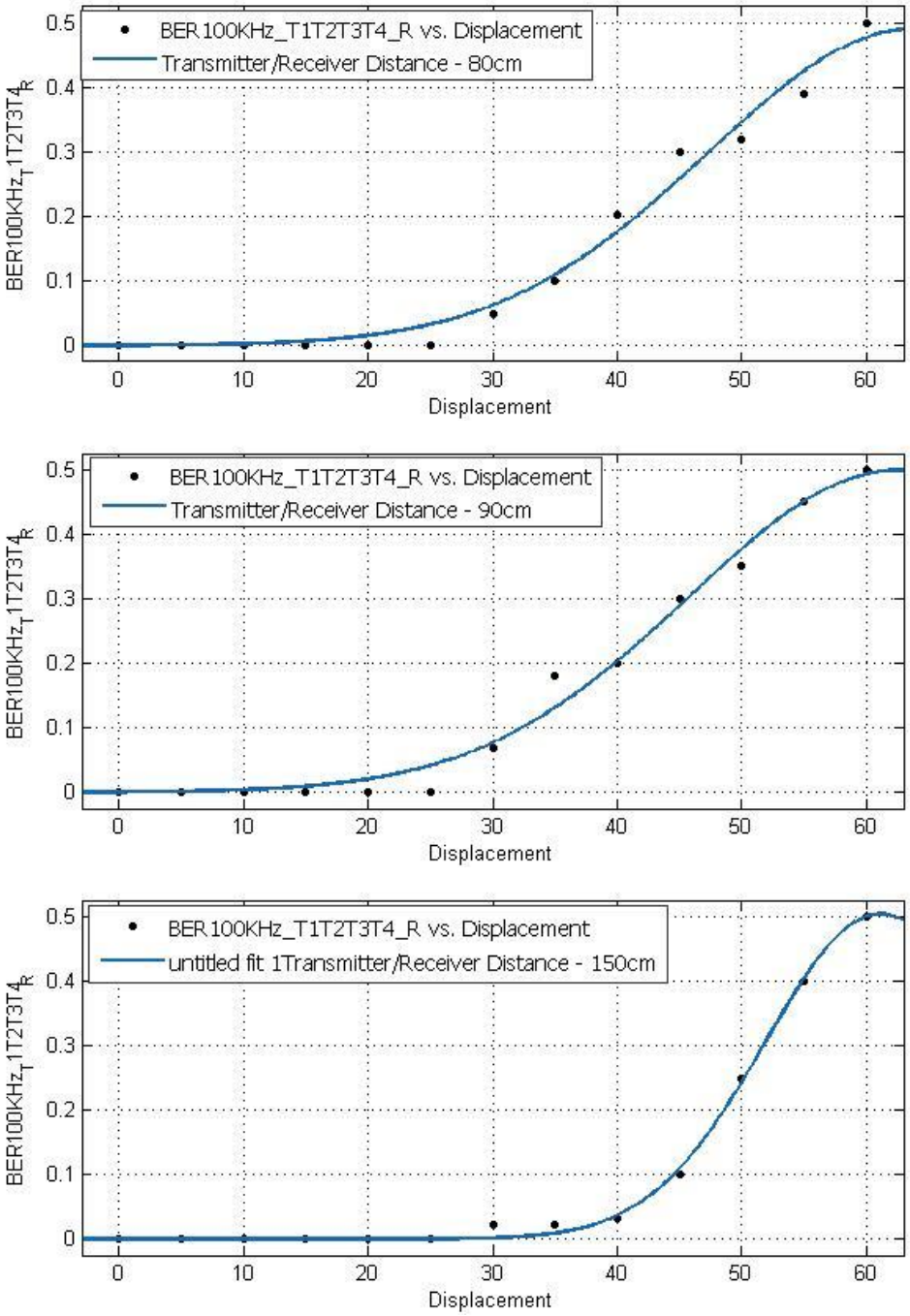

Figure 7-21 Fitting 70 – 150cm Distance

In order to find the values of *a1*, *b1* and *c1* in this case, curve-fitting is performed to fit the data using the logarithm of BER. This gives:

$$a_1 = 0.5031 + 0.003371\cos(6.052D) + 0.0124\sin(6.052D) \tag{7.26}$$

$$\begin{aligned} b_1 = {} & 61.64 + 0.8606\cos(14.15D) - 0.7794\sin(14.15D) - 0.2057\cos(28.3D) \\ & -0.1954\sin(28.3D) - 0.339\cos(52.45D) + 1.32\sin(52.45D) \end{aligned} \tag{7.27}$$

$$\begin{aligned} c_1 = {} & 15.75 + 3.128\cos(6.518D) - 5.406\sin(6.518D) - 1.429\cos(13.036D) \\ & -2.15\sin(13.036D) - 0.2845\cos(19.554D) - 1.344\sin(19.554D) \end{aligned} \tag{7.28}$$

D represents the distance between the transmitter box and the receiver box. The BER value at the displacement 40cm and 50cm are selected to verify the empirical model, and the *a1*, *b1* and *c1* at the distance of 1.1m are used for verifications.

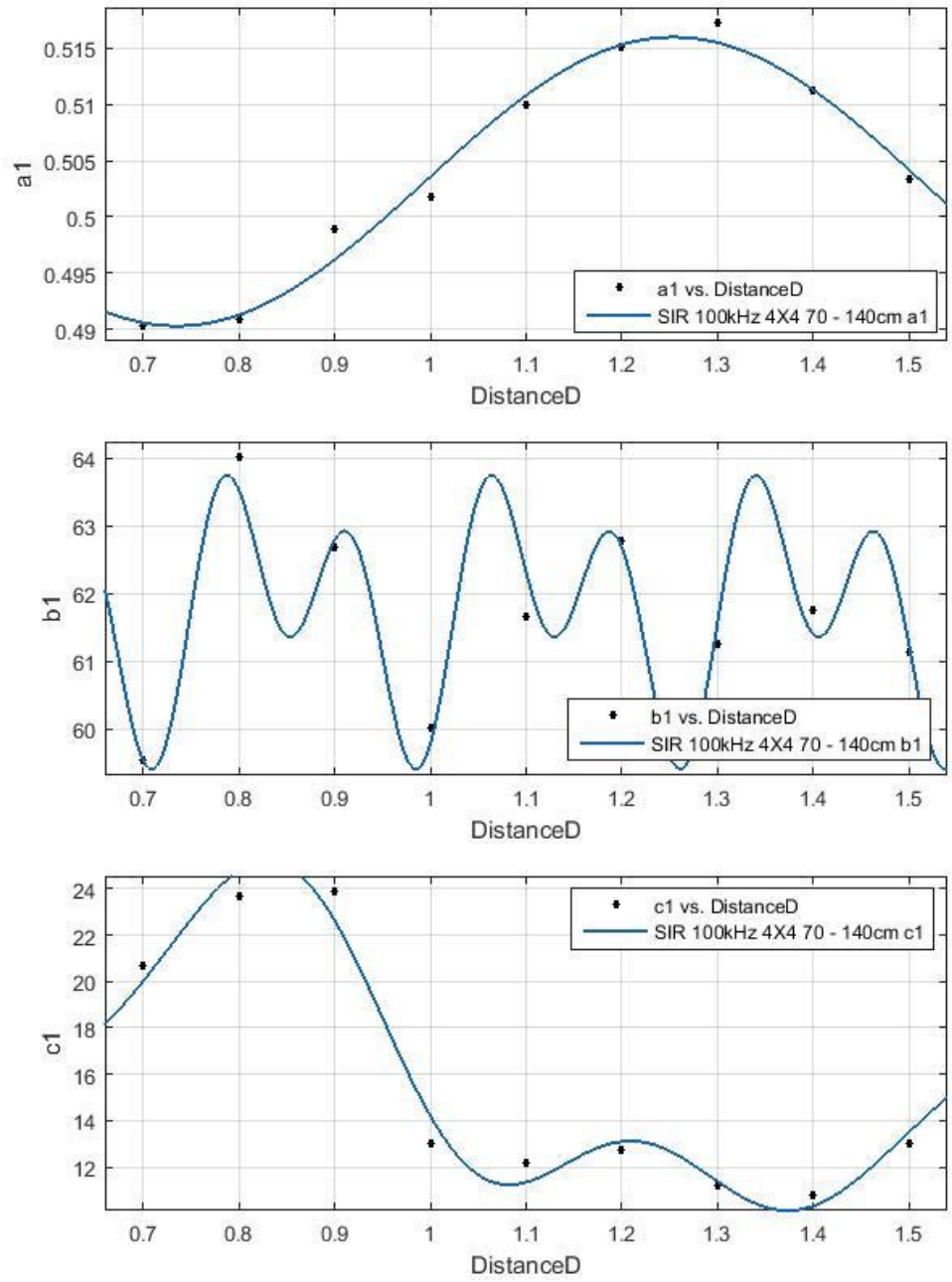

Figure 7-22 Estimated value of *a1*, *b1* and *c1*

It can be clearly observed that when the distance increases, the overlapping percentage of the data from the BER value and those derived from the empirical model increases.

7.4 Summary

Chapter 7 covered the theoretical approach in evaluated models used in describing BER values in correlation with the distances and displacements applied to the MIMO systems, which were verified by a high level of matching with data distribution fitted from the empirical results. It is worth noticing that, although some points were observed with clear fitted from the evaluated projected data distributions, such evaluation may be considered acceptable by making comparison with the results obtained experimentally. Moreover, the percentage of the overlapped data between the empirical results and evaluated projections is considered at a fairly high level of 93%. It can be concluded that the evaluated models developed from this research can be applied for future development, including the performance evaluations of the BER value in multi-dimensions, or a wireless MIMO system with more transmitters and receivers.

Chapter 8 Conclusion

8.1 Summary

This research proposes that optical wireless MIMO systems can be considered as one of the alternative technologies that can be applied in high-speed wireless communications, and the work covers a comprehensive review and evaluation of experimental observations, and theoretical analysis of both optical wireless and MIMO technology. As described in Chapter 1, a SISO system can only send or receive a single signal-stream, whereas, by using appropriate processing, a MIMO system is capable of sending and receiving multiple signals, and hence is able to differentiate signals sent from various transceivers. Due to the fact that the MIMO system allows more data to be transmitted, it is possible to be able to solve problems associated with channel fading, therefore minimizing the occurrence of errors. In a MIMO system, the diversity gain can reach a high magnitude, which increases both transmission distances and the coverage of transmitter arrays. Another MIMO technology as proposed is the multiplexing technology, which uses space and time coding to achieve signals with a much lower bit error rate in the entire system. It is confirmed that, by using optical wireless MIMO technology, it can benefit from cost saving, unrestricted bandwidths, high quality data-transmissions, zero interference with RF-based communication signals, and highly-secure transmissions.

Chapter 2 covers a review of previous research conducted by using optical wireless and MIMO technology. In this chapter, the Alamouti space time coding, background knowledge of infrared communication technology, receivers for optical wireless communication systems, and MIMO antenna/transceiver selection technology were all presented, in order to be able to build experimental optical wireless MIMO systems.

In Chapter 3, it has provided analyses of important OW configurations using APD receivers. First, the WMC model was employed to analyse the SISO configuration using a large deviations approach. Second, in the comparison with a Gaussian approximation showed that the latter was reasonable for the parameters considered, and made for a more tractable approach. Thus, an analytical expression for 2-1 MISO was successfully developed. Third, simulation was used, which was implemented via using importance sampling and successfully compared to the analytical results. To complete the results for SIMO and MIMO, upper and lower bounds were introduced and the corresponding BER curves obtained from importance sampling. This chapter also illustrates the coding gains possible using diversity schemes for APD OW systems. In the presence of strong fading, the SISO approach is rendered virtually useless, whereas diversity offers acceptable BER values. The results underpin the approach of this thesis, where indoor PIN diode based experimental measurements confirm the gains offered by diversity.

Chapter 4 and 5 describe a detailed process and experimental methodology for

developing circuit designs for three infrared MIMO systems using different modulation, including OOK PPM, and SIR-DZI modulation. A detailed description on the research methodology is also presented within Chapter 4. A group of experiments were systematically designed and performed for evaluating the technical features and application potential of multiplexing and diversity technology. Three infrared MIMO systems were designed for the purpose of laboratory experiments, including a 100kHz -10MHz OOK modulation system, an SIR-DZI system, and a 1MHz PPM modulation system. During the experiments, several factors were taken into consideration as causing interference and degradation in evaluations, including the distance between the transmitter and receiver boxes, the distance of the angle opening stretched between the receiving point and the centre axis of the Transmitter-Receiver boxes, and the background lighting conditions when the experiments using the OOK system were conducted in a darkroom during the night time. It was also included in Chapter 2 that the BER is considered to be a standard indicator to evaluate the physical performance of the experimental work. The results received from the specified experiments indicate that the systems prove to be viable for conducting the designed experiments, as the agreement between them and measurements seems relatively acceptable, i.e., the bit error rate of a square wave modulation is lower than10^{-5}.

Chapter 6 presents comprehensive analyses on the experimental results received from the above-mentioned three systems. The results from the SISO system designed using OOK modulation and SIR-DZI modulation were presented for comparison references. In comparison with the 1MHz/ OOK/ MIMO system, the PPM system was shown to provide superior characteristics, even if the design was more complex.

In comparison with the OOK 100kHz system, the SIR-DZI system was able to perform better over a greater distance, but shows poorer ability in minimizing the effect of interference.

Chapter 7 describes the process of curve fitting used for evaluating the BER performance of the MIMO system versus the variations in specified distances (the distance between the transmitter and receiver boxes), and the specified displacements, which is defined as the displacement from the central axis of the receiver boxes. The results demonstrate that a high level of matching between the results derived from the evaluated model, and the results derived from the empirical data distribution were verified at 93%. It is worth noticing that, although some points are observed with obvious deviations from the evaluated data distributions, such deviations are considered acceptable, as the agreement between them and result seems relatively good. It can be further concluded that the fitted models used for the specified evaluation appear to correspond reasonably well, and so therefore can be applied in the future research development.

8.2 Recommendations for future research.

Firstly, several mathematical models have been evaluated in this research, based on which further research and experiments can be conducted to evaluate the BER performance in multi-dimensional systems, and to verify the matching level of the theoretical and empirical results for a wireless MIMO system by using more transmitters and receivers, including for {4 x 4}, {4 x 8}, {8 x 8} and even for {16 x

16} MIMO modulation. Different modulations, such as DPPM and others, could also be considered in future work.

Secondly, based on the same methodology and experiment process, further research and experiments can be carried out on the MIMO system integrated with an APD receiver. Although the system is not desirable to be considered as a potential indoor optical system because of the eye safety concerns due to the high infrared power, and the high noise gain, it has clearly been demonstrated that such a system could be considered as a potential application for outdoor communications.

Thirdly, in this thesis, mathematical models have been evaluated based on the experimental results, and the theoretical models could be considered as a comparison method for empirical results, which should refer to existing optical wireless MIMO theory and be derived from the corresponding MIMO system model. Moreover, the experimental environment (background noise and other parameters) should be considered. Using these theoretical models, the accuracy of empirical models could be evaluated fully.

Fourthly, new optical wireless MIMO systems could be designed to operate in different experimental environments, such as rainfall/snowfall, underwater, and other situations, where more parameters which complicate impact factors should be considered. Meanwhile, numerical analysis and empirical analysis could be conducted in corresponding situations.

Finally, as is mentioned in Chapter 2, Section 5, a candidate application of optical wireless MIMO technology – the Optical Wireless Network (OWN) - was introduced, and using existing research results, an optical wireless network with multiple layers could be conducted.

Appendix I: Circuit Component Value of OOK based MIMO System

Comment	Description	Designator	Footprint	LibRef	Quantity
47pF	Capacitor	C0, C7	R38	Cap	2
0.1uF	Capacitor	C1, C4, C6	R38	Cap	3
10uf	Capacitor	C2, C3, C5	CAPPR5-5x5	Cap2	3
220nF	Capacitor	C10	R38	CAP	1
10u	Capacitor	C11, C13, C21, C23, C31	CAPPR5-5x5	CAP	5
0.1u	Capacitor	C12, C14, C22, C24, C32	R38	CAP	5
302pF	Capacitor	C25	R38	CAP	1
177pF	Capacitor	C26	R38	CAP	1
33pF	Capacitor	C27	R38	CAP	1
20pF	Capacitor	C33	R38	CAP	1
SFH4350	Typical RED GaAs LED	D0	LED-1	LED1	1
S1223	Photosensitive Diode	D1	CAPPR5-5x5	Photo Sen	1
Photo Sen	Photosensitive Diode	D2	CAPPR5-5x5	Photo Sen	1
Diode 1N4149	Computer Diode	D3	DO-35A	Diode 1N4149	1
Power&Control_Signal	Header, 4-Pin	J1	HDR1X4	Header 4	1
POWER	Header, 4-Pin	J2	HDR1X4	Header 4	1
Header 6	Header, 6-Pin	J3	HDR1X6	Header 6	1
Header 2	Header, 2-Pin	J5	HDR1X2	Header 2	1
ZTX320	NPN Bipolar Transistor	Q0, Q1	TO-226	NPN	2
NPN	NPN Bipolar Transistor	Q2	TO-226	NPN	1
1k		R00, R3, R4, R10, R11, R31	AXIAL-0.3	MINIRES2	6
33		R1	AXIAL-0.3	MINIRES2	1
100		R01	AXIAL-0.3	MINIRES2	1
5.6k		R2	AXIAL-0.3	MINIRES2	1
10k		R02, R12	AXIAL-0.3	MINIRES2	2
330		R21, R22, R23, R24	AXIAL-0.3	MINIRES2	4
2.97K		R25	AXIAL-0.3	MINIRES2	1

5k		R32, R33, R34, R35, R36	AXIAL-0.3	MINIRES2	5
AD8055		U1	DIP-8	OP193ES-REEL7	1
AD8055		U2	DIP8	OP193ES-REEL7	1
AD8561	Ultrafast TTL Compa	U3	Q-8	AD9696TQ	1

Table A-1 System Components

Appendix II: Circuit Design for PPM/RZI based MIMO System

1. IrDA Higher speed (1.1-1.3, FIR-4PPM)

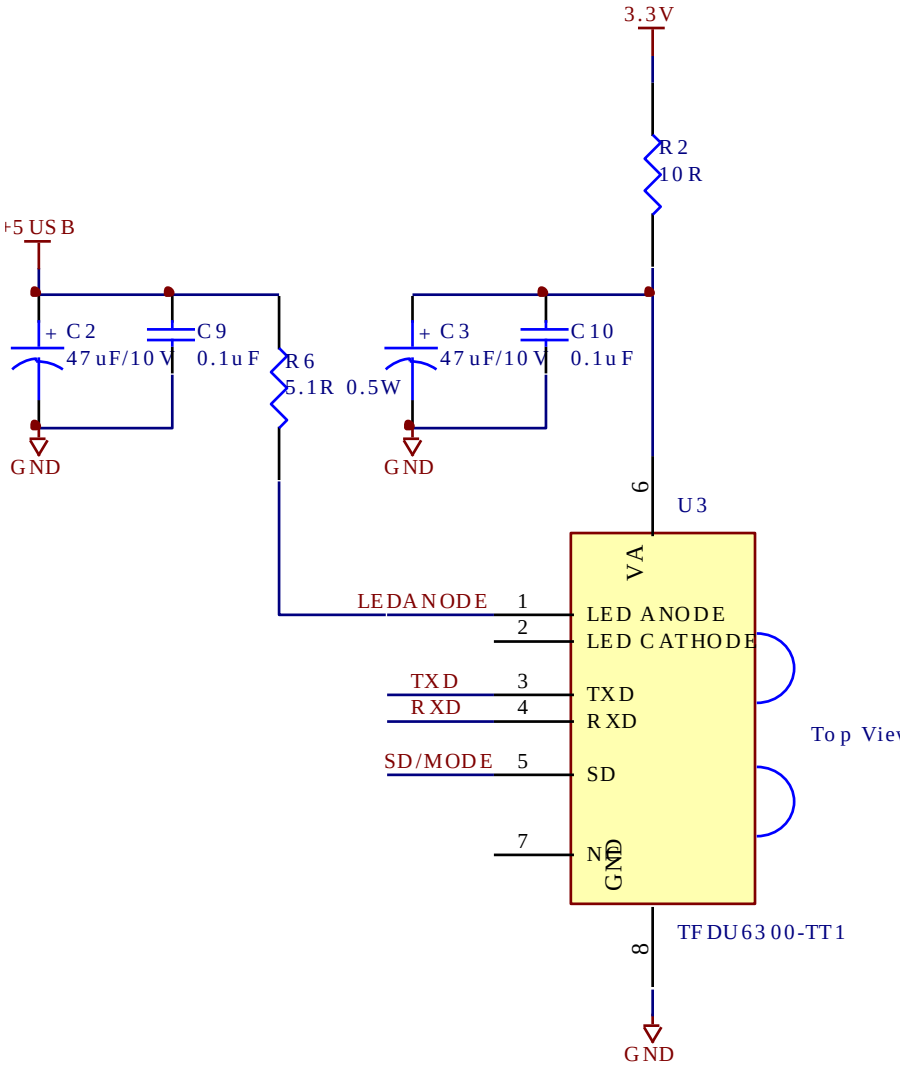

Figure A-1

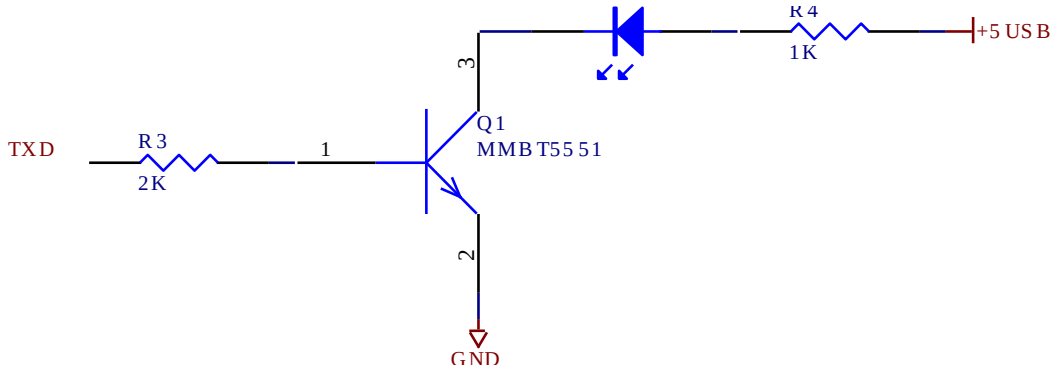

Figure A-2

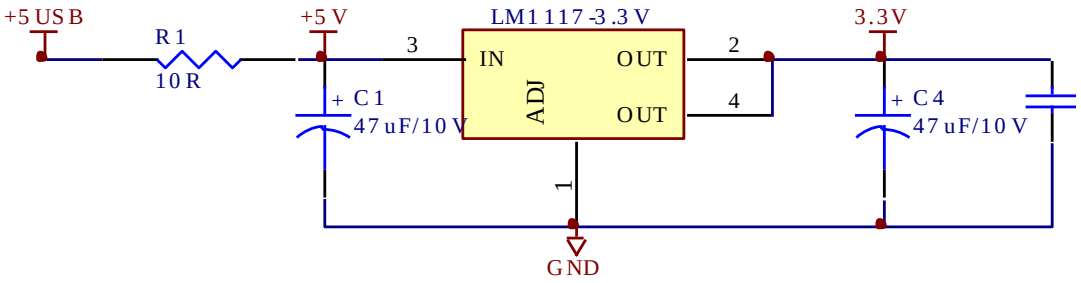

Figure A-3

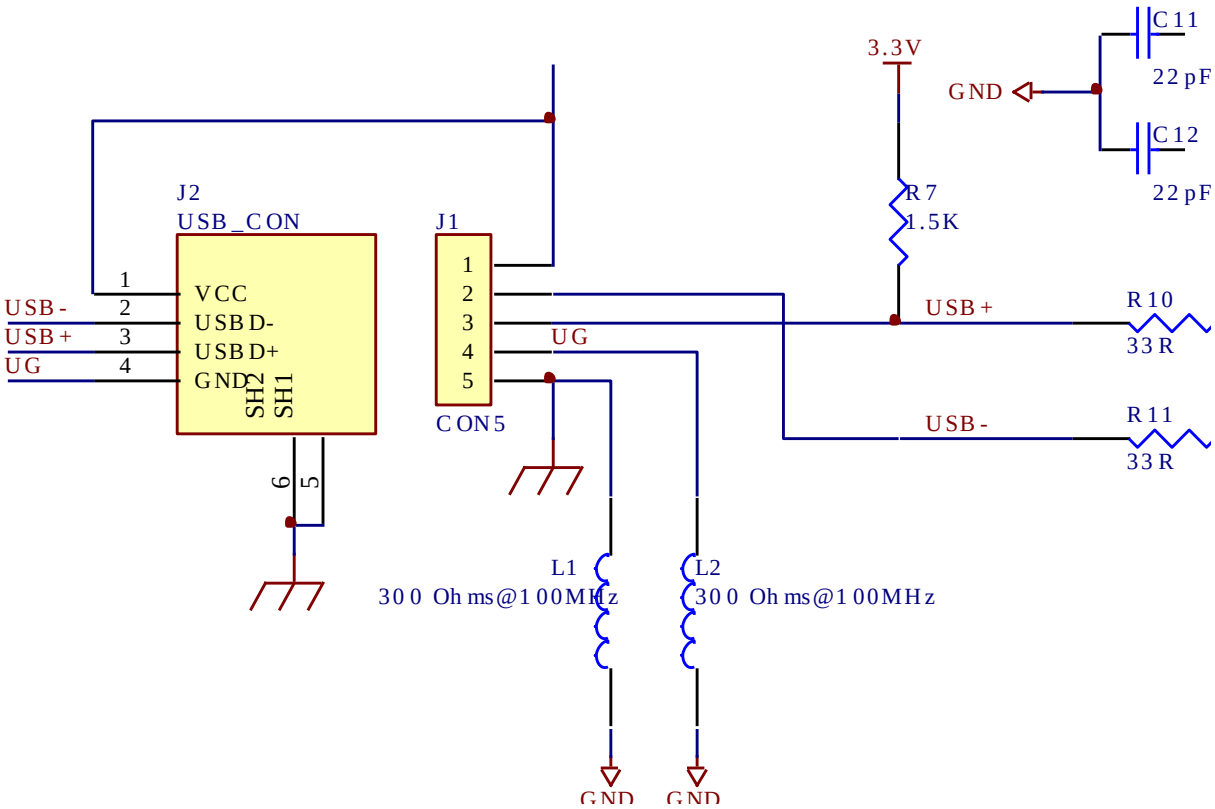

Figure A-4

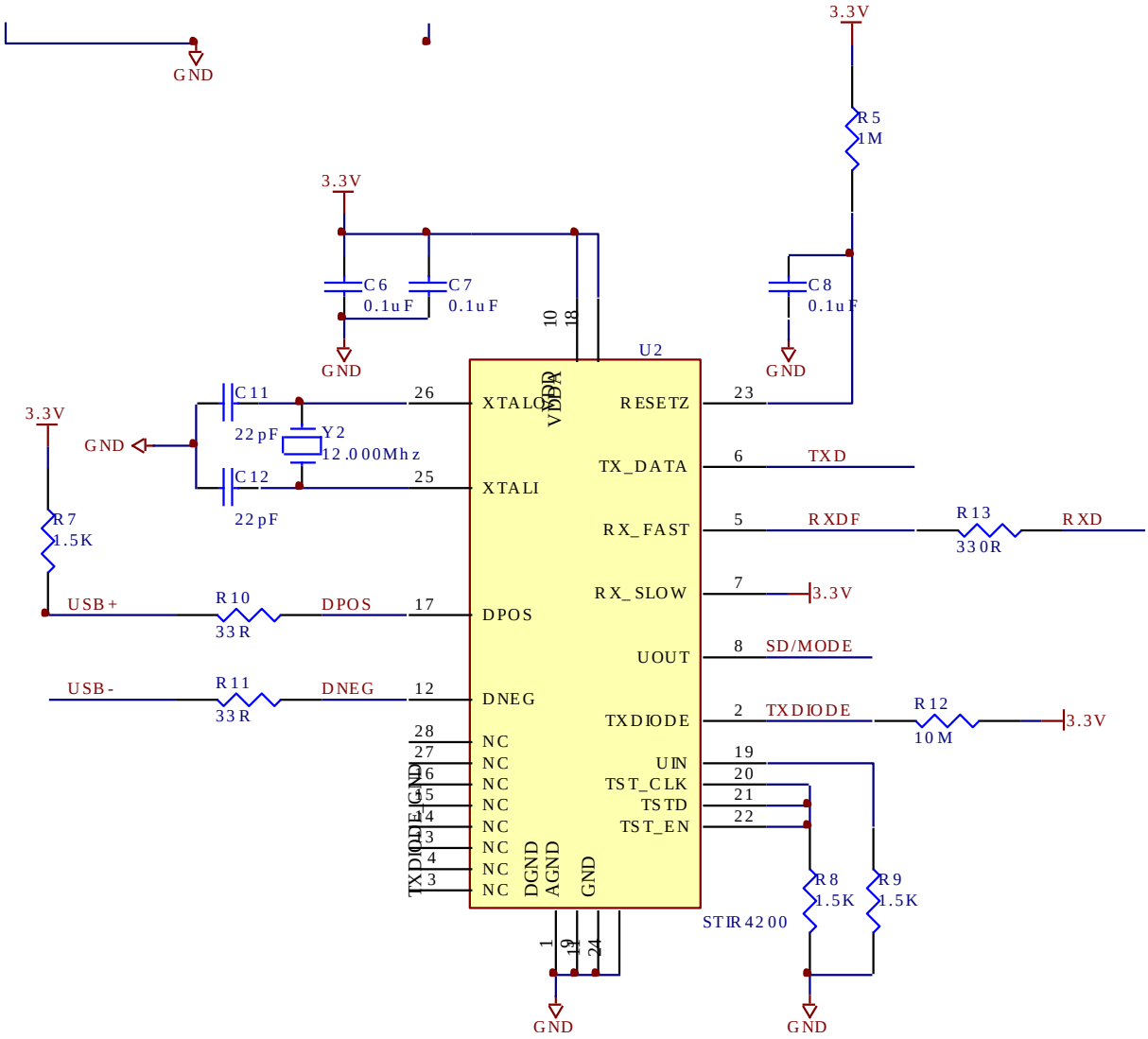

Figure A-5

2. IrDA 1.0 (SIR-Pulse Modulation)

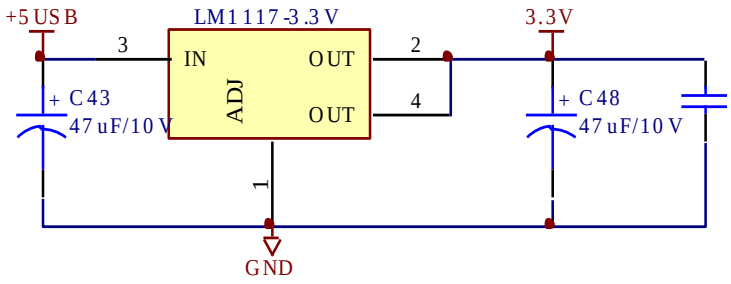

Figure A-6

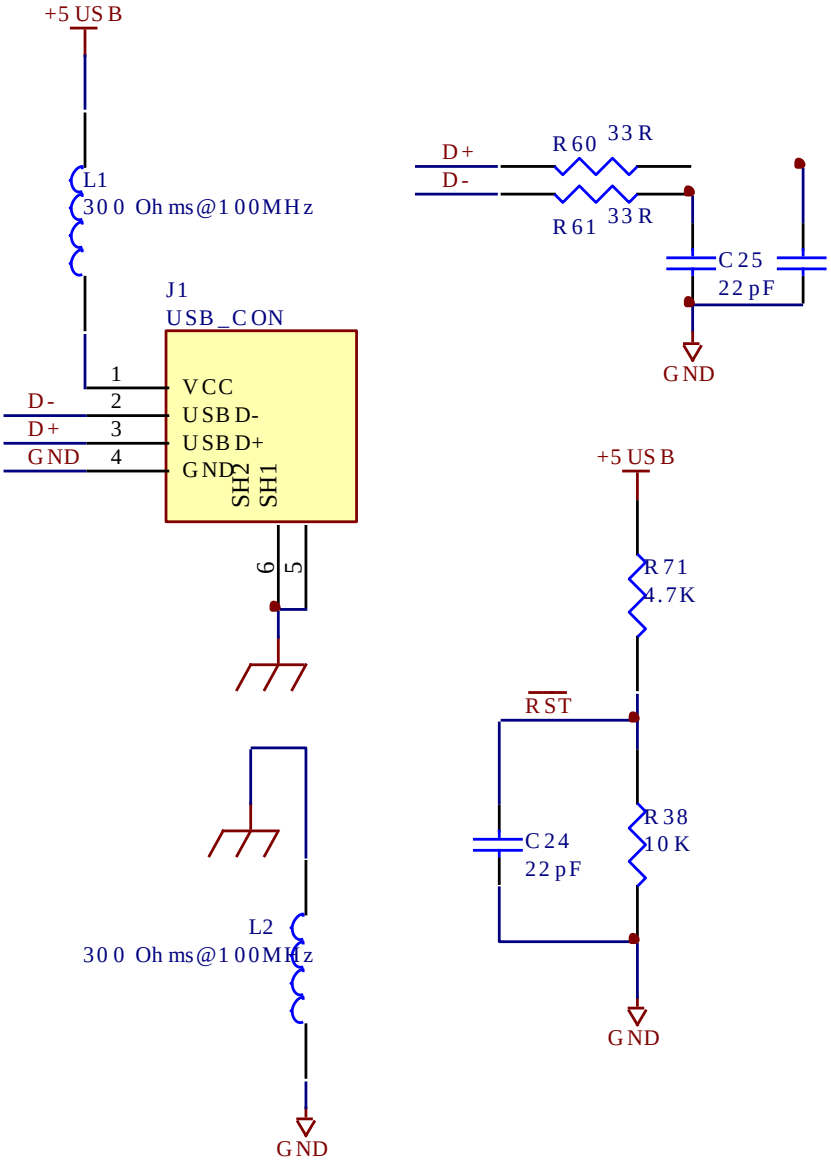

Figure A-7

TUSB2046B	4 port USB HUB, which extends the one PC I/O port to four
USB – RS232 Bridge	FT232RL, which could connect and transfer between USB port and 232 serial port
MCP2120	SIR Encoder

TFDU6300	Infrared Transceiver

Table A-2 Device in SIR System

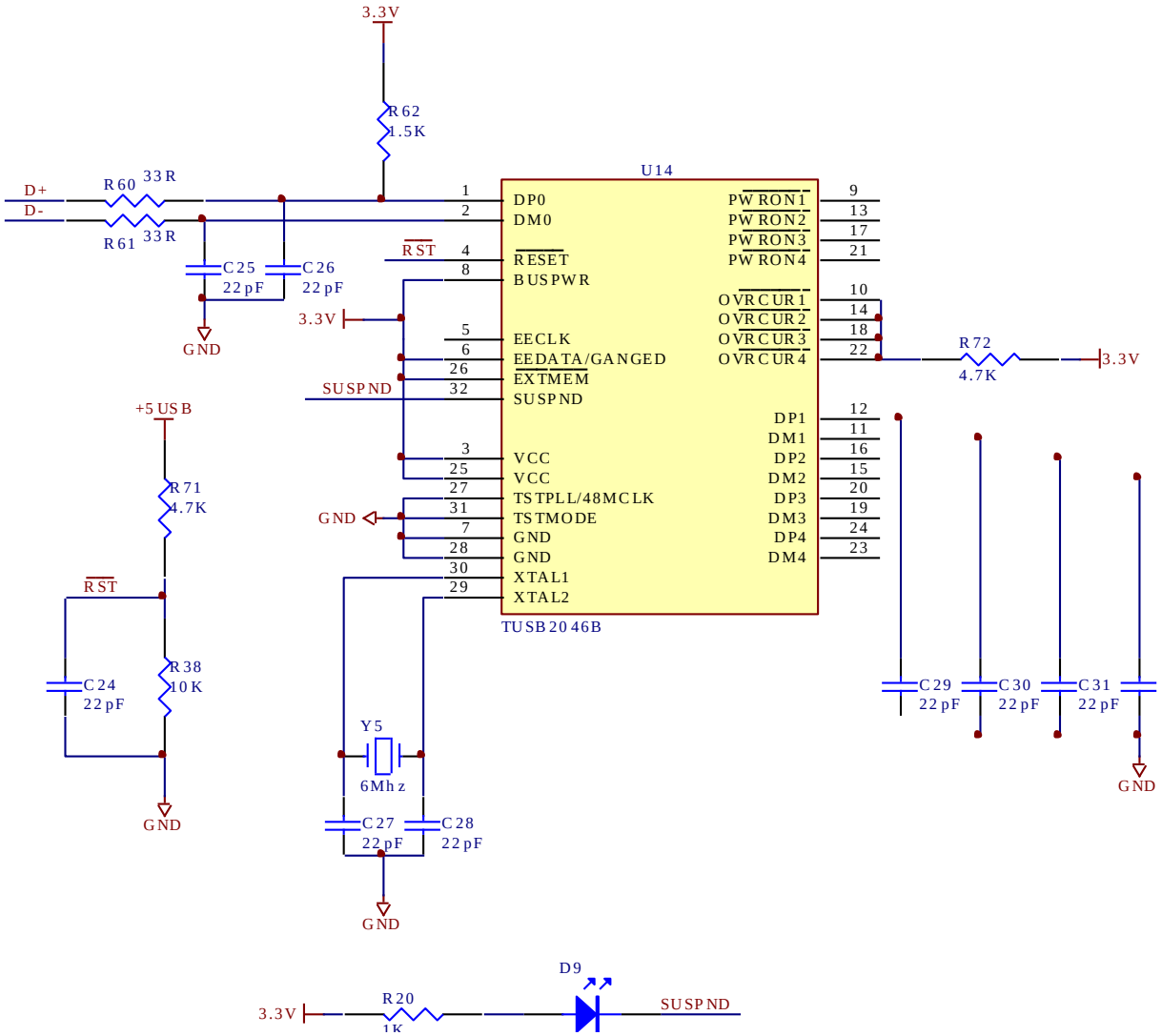

Figure A-8

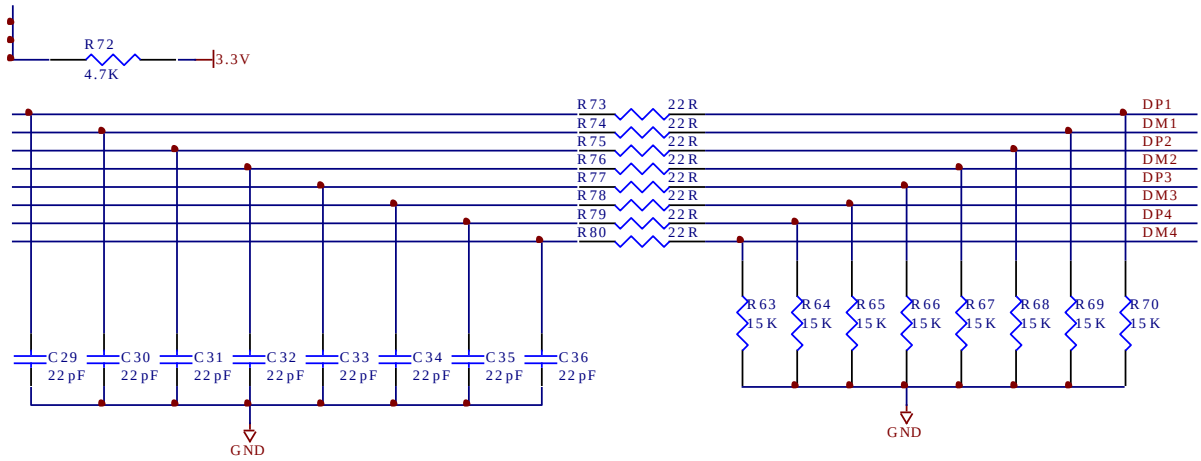

Figure A-9

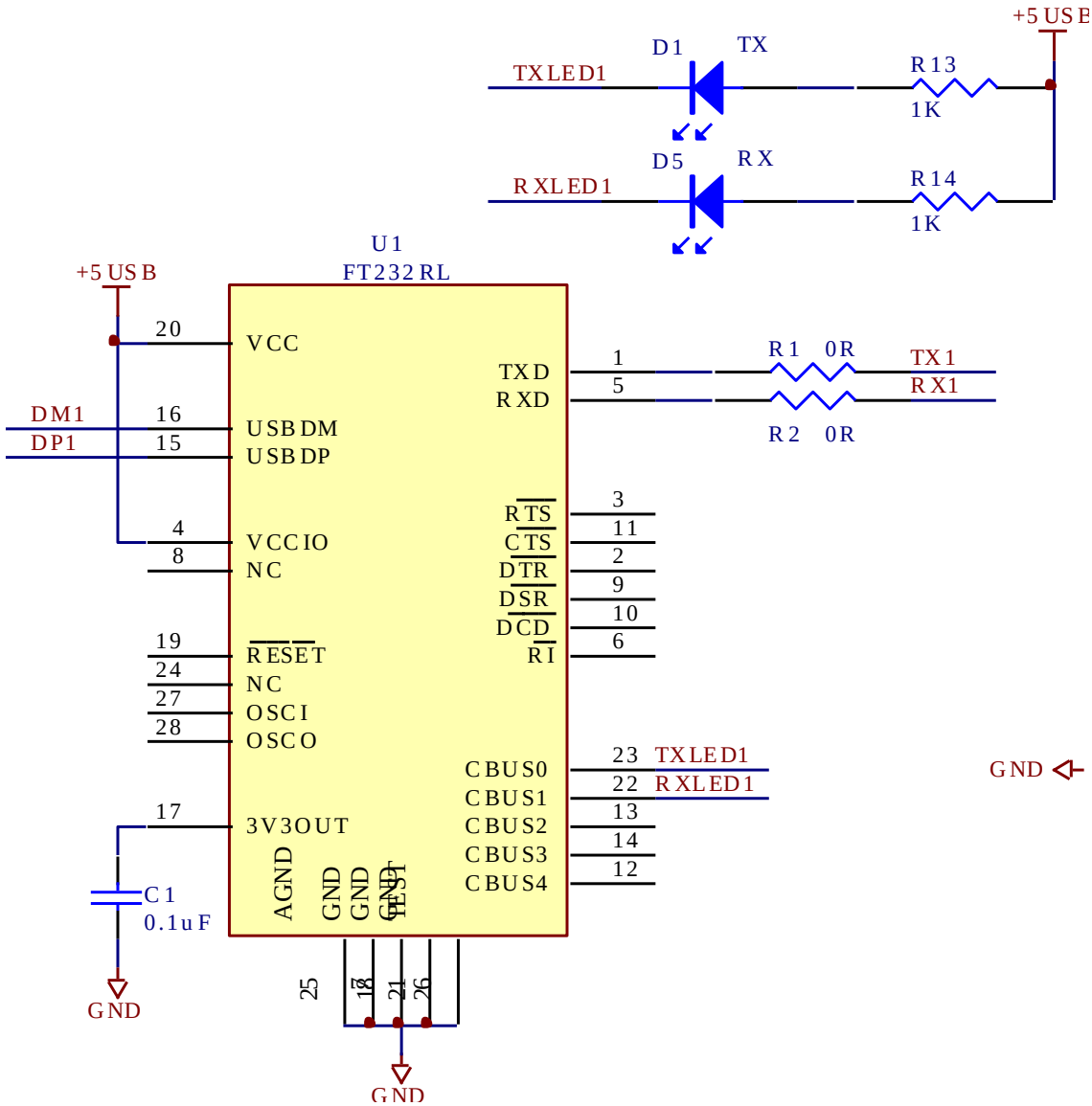

Figure A-10

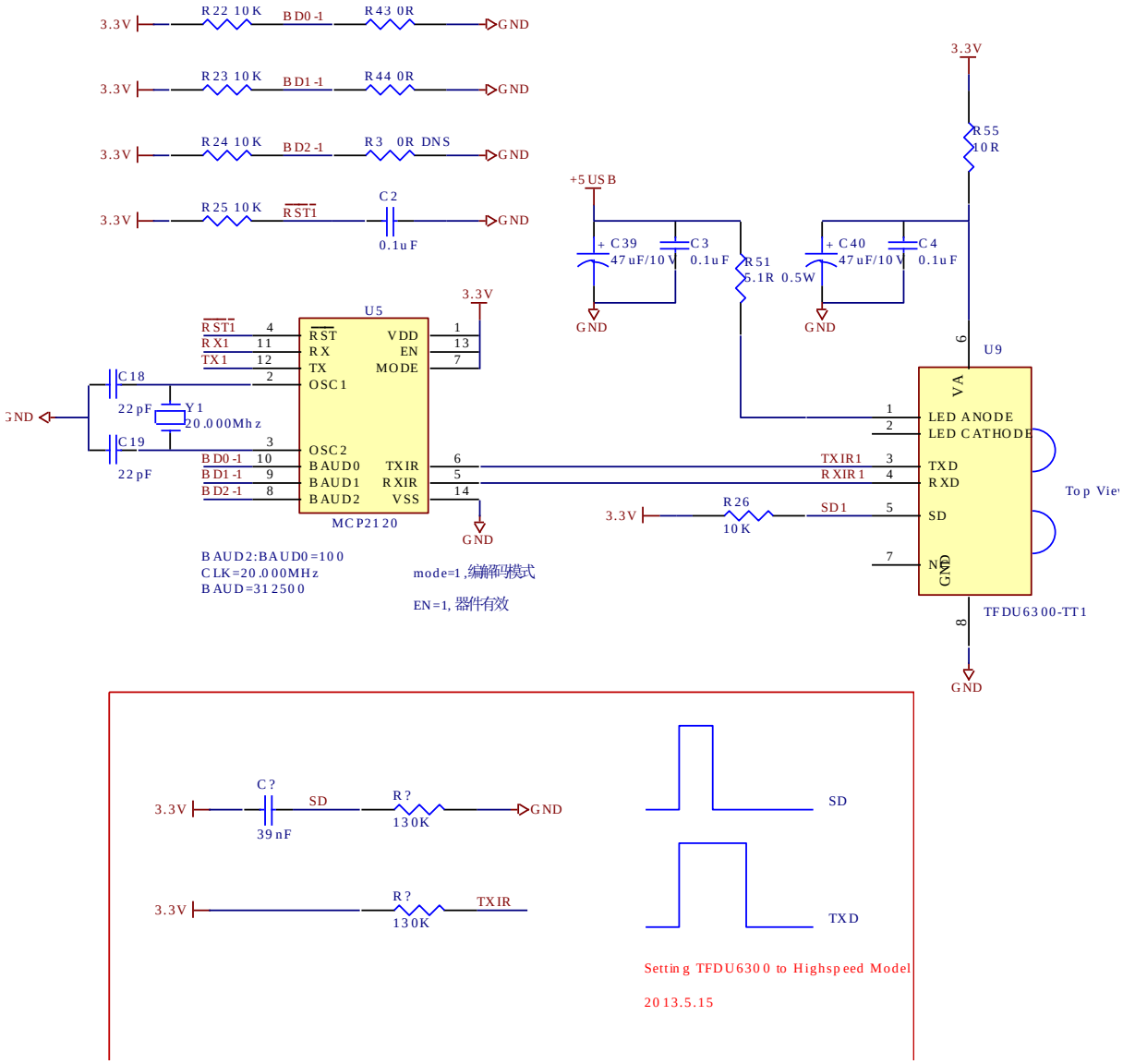
3.3V
R22 10K
BD0-1
R43 0R
GND
R23 10K
BD1-1
R44 0R
R24 10K
BD2-1
R3 0R DNS
R25 10K
RST1
C2
0.1uF
+5USB
C39
47uF/10V
C3
0.1uF
R51
5.1R 0.5W
C40
C4
R55
10R
U5
U9
RST
RX
TX
OSC1
OSC2
BAUD0
BAUD1
BAUD2
VDD
EN
MODE
TXIR
RXIR
VSS
MCP2120
C18
22pF
Y1
20.000Mhz
C19
BAUD2:BAUD0=100
CLK=20.000MHz
BAUD=312500
mode=1,編輯狀態式
EN=1, 器件有效
R26
10K
SD1
TXIR1
RXIR1
LED ANODE
LED CATHODE
TXD
RXD
SD
TFDU6300-TT1
C?
39nF
R?
130K
Setting TFDU6300 to Highspeed Model
2013.5.15

Figure A-11

Bibliography

[1] J. Grubor, S. Randel, K. D. Langer, J. W. Walewski, "Broadband Information Broadcasting Using LED-Based Interior Lighting", IEEE Journal of Lightwave Technology, vol. 26, no. 24, 2008.

[2] H. Le Minh, Z. Ghassemlooy, D. O'Brien, G. Faulkner, "Indoor Gigabit Optical Wireless Communications - Challenges and Possibilities", *Proc. 12th IEEE Conference on Transparent Optical Networks (ICTON),* 2010 [6 pages].

[3] H. Le Minh, D. O'Brien, G. Faulkner, L. Zeng, K. Lee, D. Jung, and Y. Oh, "High-speed visible light communications using multiple-resonant equalization", *IEEE Photonics Technology Letters,* vol. 20, no. 14, pp. 1243-1245, 2008.

[4] J. Grubor, K. D. Langer, S. C. J. Lee, T. Koonen, and J. W. Walewski, "Wireless high-speed data transmission with phosphorescent white-light LEDs", *Proc. 23rd European Conference and Exhibition of Optical Communication (ECOC),* 2007 [2 page post deadline paper].

[5] G. Nykolak, P. F. Szajowski, G. Tourgee, and H. Presby, "2.5 Gbit/s free space optical link over 4.4 km", *Electronics Letters,* vol.35, pp. 578-579, 1999.

[6] J. R. Barry, Wireless Infrared Communications, *Kluwer,* 1994.

[7] F. E. Alsaadi, J. M. H. Elmirghani, "Performance evaluation of 2.5Gbit/s and 5Gbit/s Optical wirelesssystems employing a two dimensional adaptive beam clustering method and imaging diversity detection", IEEE Journal on Selected Areas in Communications, vol. 27, no. 8, pp. 1507-1519, 2009.

[8] G. Ntogari, T. Kamalakis, T. Sphicopoulos, "Performance analysis of space time block codingtechniques for indoor optical wireless systems", IEEE

Journal on Selected Areas in Communications, vol. 27, no. 9, pp. 1545-1552, 2009.

[9] S. Haykin, "Neural networks expand SP's horizons", IEEE Signal Processing Magazine, vol. 13, no. 2, pp. 24-49, 1996.

[10] A. Hussain, J. J. Soraghan, T. S. Durrani, "A new adaptive functional-link neural-network-based DFEfor overcoming co-channel interference", IEEE Transactions on Communications, vol. 45, no. 11, pp. 1358-1362, 1997.

[11] S. Rajbhandari, Z. Ghassemlooy, M. Angelova, "Bit error performance of diffuse indoor optical wireless channel pulse position modulation system employing artificial neural networks for channel equalisation", IET Optoelectronics, vol. 3, no. 4, pp. 169-179, 2009.

[12] D. Takase, T. Ohtsuki, "Optical Wireless MIMO Communications", *Proc. IEEE Grobal Telecommunications Conference (GLOBECOM),* vol. 2, pp. 928-932, 2004 [5 pages].

[13] D. Takase, T. Ohtsuki, "Optical Wireless MIMO (OMIMO) with Backward Spatial Filter (BSF) in Diffuse Channels", *Proc. IEEE International Conference on Communications (ICC),* vol. 2, pp. 954-958, 2007 [5 pages].

[14] R. Mesleh, R. Mehmood, H. Elgala, H. Haas, "Indoor MIMO Optical Wireless Communication Using Spatial Modulation", *Proc. IEEE International Conference on Communications (ICC),* pp. 1-5, 2010 [5 pages].

[15] D. O'Brien, "Multi-Input Multi-Output (MIMO) Indoor Optical Wireless Communications", *Proc. 2009 Conference Record of the Forty-Third Asilomar Conference on Signals, Systems and Computers,* pp. 1636-1639. 2009 [4 pages].

[16] R. Otte, Low-Power Wireless Infrared Communications, *Springer,* 2010.

[17] American National Standards Institute, American National Standard for the Safe Use of Lasers Z136.l-1993 (ANSI Z136.1-1993), pp. 31,32,41,42, 1993.

[18] Infrared Data Association, Infrared Data Association Serial Infrared Physical Layer Link Specification, Version 1.0, November, 1994.

[19] Infrared Data Association, Infrared Data Association Serial Infrared Physical Layer Link Specification, Version 1.1, November, 1995.

[20] Infrared Data Association, Infrared Data Association Serial Infrared Physical Layer Link Specification, Version 1.2, November, 1997.

[21] C. Zhang, R. R. Bitmead, "State space modeling for MIMO wireless channels", *Proc. IEEE International Conference on Communications (ICC)*, vol.2, pp. 2297-2301, 2005 [5 pages].

[22] S. M. Alamouti, "A simple transmit diversity technique for wireless communications", IEEE Journal on Select Areas in Communications, vol. 16, no. 8, pp. 1451-1458, 1998.

[23] J. B. Carruthers, J. M. Kahn, "Angle diversity for nondirected wireless infrared communication", IEEE Transactions on Communications, vol. 48, no. 6, pp. 960-969, 2000.

[24] H. Joshi, R. J. Green, M. S. Leeson, "Channel Models for Optical Wireless Communication Systems", Proc. 11th International Conference on Transparent Optical Networks (ICTON), pp. 1, 2009 [1 page].

[25] K. Jastrowa, R. Miintera, R. Piesiewiczb, T. Kiimer, M. Kochd and T.Kleine-Ostmanna, "300 GHz Channel Measurement and Transmission System", *Proc. IEEE Infrared Millimeter and Terahertz Waves International Conference*, pp. 1-2, 2008 [2 pages].

[26] A. Sivabalan, J John, "Modeling and simulation of indoor optical wireless

channels: a review", *Proc. TENCON 2003 Conference on Convergent Technologies for the Asia-Pacific Region*, Vol.3, pp. 1082-1085, 2003 [4 pages].

[27] S. Hranilovic, Wireless Optical Communication Systems, *Springer*, 2004.

[28] T. Koonen, "Fiber to the home/fiber to the premises: What, where and when?", Proceedings of the IEEE, vol. 94, no. 5, pp. 911–934, 2006.

[29] G. Ntogari, T. Kamalakis, T. Sphicopoulos, "Analysis of Indoor Multiple-Input Multiple-Output Coherent Optical Wireless Systems", IEEE Journal of Lightwave Technology, vol. 30, no. 3, pp. 317-324, 2012.

[30] O. Bouchet, M. Wolf, M. E. Tabach, T. Kamalakis, F. Grahame, J. Walewski, S. Nerreter, M. Franke, J. Grubor, D. O'Brien, and K. D. Langer, "Hybrid Wireless Optics (HWO): Building the Next-Generation Home Network," *Proc. 6th International Symposium on Communication Systems, Networks and Digital Signal Processing (CNSDSP)*, pp. 283-287, 2008 [5 pages].

[31] D. O'Brien, S. Quasem, S. Zikic, and G. Faulkner, "Multiple input multiple output systems for optical wireless; challenges and possibilities," Proc. SPIE 6304, Free-Space Laser Communications VI, vol. 6304, pp. 630416.1–630416.7, 2006.

[32] R. Heath, Jr. A. Paulraj, "Switching between multiplexing and diversity based on constellation distance," IEEE Transactions on Communications, vol. 53, no. 6, pp. 962-968, 2005.

[33] L. Zheng, D. N. C. Tse, "Diversity and Multiplexing: A Fundamental Tradeoff in Multiple-Antenna Channels," IEEE Transactions on Information Theory, vol. 49, no. 5, pp. 1073-1096, 2003.

[34] I. Mansour, J. S. Rahhal, H. Farahneh, "Two Slot MIMO Configuration for

Cooperative Sensor Network", International Journal of Communications, Network and System Science, vol. 3, no. 9, pp. 750-754, 2010.

[35] V. W. S. Chan , "Free-space optical communications", IEEE/OSA Journal of Lightwave Technology, vol. 24, no. 12, pp. 4750-4762, 2006

[36] J. Grubor, S. Randel, K. Dieter Langer, and J.W. Walewski, "Broadband Information Broadcasting Using LED-Based Interior Lighting", IEEE Journal of Lightwave Technology, vol. 26, no. 24, pp. 3883-3892, 2008.

[37] D. Gesbert, M. Shafi, D.Shiu, P. J. Smith, and A. Naguib, "From theory to practice: an overview of MIMO space-time coded wireless systems," IEEE Journal on Selected Areas in Communications, vol. 21, no. 3, pp. 281-302, 2003.

[38] M. A. Khalighi and M. Uysal, "Survey on Free Space Optical Communication: A Communication Theory Perspective", IEEE Communications Surveys and Tutorials, vol. 16, no. 4, pp. 2231-2258, 2014.

[39] T. Fath and H. Haas, "Performance Comparison of MIMO Techniques for Optical Wireless Communications in Indoor Environments", IEEE Transactions on Communications, vol. 61, no. 2, pp. 733- 742, 2013.

[40] P. P. Webb, R. J. McIntyre and J. Conradi, "Properties of Avalanche Photodiodes", RCA Review, vol. 35, pp. 234-278, 1974.

[41] J. Grubor, K.-D. Langer, S. C. J. Lee, T. Koonen, and J. W. Walewski, "Wireless high-speed data transmission with phosphorescent white-light LEDs", *Proc. 23rd European Conference and Exhibition of Optical Communication (ECOC)*, 2007 [2 page post deadline paper].

[42] C. H. Yeh, Y. L. Liu and C. W. Chow, "Real-time white-light phosphor-LED visible light communication (VLC) with compact size", Optics Express, vol.

21, no. 22, pp. 26192-26197, 2013.

[43] J.-Y.Sung, C.-W. Chow and C.-H.Yeh, "Is blue optical filter necessary in high speed phosphor-based white light LED visible light communications?", Optics Express, vol. 22, no. 17, pp. 20646-20651, 2014.

[44] S.G. Wilson, M. Brandt-Pearce, Q. Cao and J. Leveque, "Free-space optical MIMO transmission with Q-ary PPM." IEEE Transactions on Communications, vol. 53, no. 8, pp. 1402-1412, 2005.

[45] R. J. McIntyre, "The distribution of gains in uniformly multiplying avalanche photodiodes: Theory," IEEE Transactions on Electron Devices, vol. 19, no. 6, pp. 703–713, 1972.

[46] J. J. Conradi, "The distribution of gains in uniformly multiplying avalanche photodiodes: Experimental," IEEE Transactions on Electron Devices, vol. 19, no. 6, pp. 714–718, June 1972.

[47] K. R. Baker, "On the WMC density as an inverse Gaussian probability density," IEEE Transactions on Communications, vol. 44, no. 1, pp. 15–17, Jan. 1996.

[48] J. T. K. Tang and K. B. Letaief, "The use of WMC distribution for performance evaluation of APD optical communication systems", IEEE Transactions on Communications, vol. 46, no. 2, 279-285, 1998.

[49] K. B. Letaief and J. S. Sadowsky, "Computing bit-error probabilities for avalanche photodiode receivers by large deviations theory," IEEE Transactions on Information Theory, vol. 38, no. 3, pp. 1162–1168, 1992.

[50] J. R. F. Da Rocha and J. J. O'Reilly, "Modified Chernoff bound for binary optical communication," *Electronics Letters*, vol. 18, no. 16, pp. 708–710, 1982.

[51] F. M. Davidson and X. Sun, "Gaussian approximation versus nearly exact performance analysis of optical communication systems with PPM signalling and APD receivers", IEEE Transactions on Communications, vol. 36, no. 11, pp.1185 -1191, 1988.

[52] N. Cvijetic, N., S. G. Wilson and M. Brandt-Pearce, "Performance Bounds for Free-Space Optical MIMO Systems with APD Receivers in Atmospheric Turbulence", IEEE Journal on Selected Areas in Communications, vol. 26, no. 3, pp. 3-12, 2008.

[53] I. A. Glover and P. M. Grant, Digital Communications, *Prentice-Hall*, 2004

[54] G. Einarsson, Principles of Lightwave Communications, *Wiley*, 1996.

[55] H.E. Nistazakis, V.D. Assimakopoulos , G.S. Tombras, "Performance estimation of free space optical links over negative exponential atmospheric turbulence channels", Optik, vol. 122, no. 24, pp. 2191–2194, 2011.

[56] J. He, R. A. Norwood, M. Brandt-Pearce, I. B. Djordjevic, M. Cvijetic, , S. Subramaniam, R. Himmelhuber, C. Reynolds, P. Blanche, B. Lynn and N. Peyghambarian, "A survey on recent advances in optical communications", Computers & Electrical Engineering, vol. 40, no. 1, pp. 216–240, 2014.

[57] E. J. Lee and V. W. S. Chan, "Part 1: optical communication over the clear turbulent atmospheric channel using diversity", IEEE Journal on Selected Areas in Communications, vol. 22, no. 9, pp. 1896-1906, 2004.

[58] S. M. Navidpour, M. Uysal, and M. Kavehrad, "BER performance of free-space optical transmission with spatial diversity," IEEE Transactions on Wireless Communications, vol. 6, no. 8, p. 2813-2819, 2007

[59] M. Safari and M. Uysal, "Do We Really Need OSTBCs for Free-Space Optical Communication with Direct Detection?", IEEE Transactions on Wireless

Communications, vol. 7, no. 11, pp. 4445-4448, 2008.

[60] M. K. Simon and V. A. Vilnrotter, "Alamouti-type space-time coding for free-space optical communication with direct detection," IEEE Transactions on Wireless Communications., vol. 4, no. 1, pp. 35–39, 2005.

[61] L. M. Delves and J. L. Mohamed, Computational Methods for Integral Equations, *Cambridge University Press*, 1985.

[62] P. Brandimarte, Numerical methods in finance and economics: a MATLAB-based introduction, Hoboken, *Wiley Interscience*, 2006.

[63] D. J. C. MacKay, Information Theory, Inference, and Learning Algorithms, *Cambridge University Press*, 2003.

[64] R. R.-Iniguez, S. M. Idrus, Z. Sun, Optical wireless communications: IR for wireless connectivity, *CRC Press*, 2008.

[65] R. J. Green, M. Higgins, H. Joshi, M. Leeson, ''Bandwidth Extension for Optical Wireless Receiver-Amplifiers'', *Proc. 10th IEEE Conference on Transparent Optical Networks (ICTON)*, pp. 201-204, 2008 [4 pages].

[66] Z. Ghassemlooy, S. Rajbhandari, "Performance of diffused indoor optical wireless links employing neural and adaptive linear equalizers", *Proc. IEEE 6th conference on Information, Communications and Signal Processing*, pp. 1-6, 2007 [6 pages].

[67] T. Fath, H. Haas, "Performance Comparison of MIMO Techniques for Optical Wireless Communications in Indoor Environments", IEEE Transactions on Communications, vol. 61, no. 2, pp. 733-742, 2013.

[68] S. G. Wilson, M. Brandt-Pearce, Q. Cao, and M. Baedke, "Optical repetition MIMO transmission with multipulse PPM," IEEE Journal on Select Areas in Communications, vol. 23, no. 9, pp. 1901–1910, 2005.

[69] S. Navidpour, M. Uysal, and M. Kavehrad, "BER performance of freespace optical transmission with spatial diversity," IEEE Transactions on Wireless Communication, vol. 6, no. 8, pp. 2813–2819, 2007.

[70] L. Zeng, D. O'Brien, H. Minh, G. Faulkner, K. Lee, D. Jung, Y. Oh, and E. T. Won, "High data rate multiple input multiple output (MIMO) optical wireless communications using white LED lighting," IEEE Journal on Select Areas in Communications, vol. 27, no. 9, pp. 1654–1662, 2009.